Philipps Universität Marburg

Roles of the second messenger cyclic di-GMP in environmental adaptation of *Sinorhizobium meliloti*

Dissertation

zur Erlangung des Doktorgrades

der Naturwissenschaften

(Dr. rer. nat.)

dem Fachbereich Biologie

der Philipps-Universität Marburg

vorgelegt von

Simon Schäper

geboren in Lünen

Marburg an der Lahn, Juni 2017

Die Untersuchungen zur vorliegenden Arbeit wurden von März 2013 bis Juni 2017 am LOEWE-Zentrum für Synthetische Mikrobiologie (SYNMIKRO) in Marburg unter der Leitung von Frau Prof. Dr. Anke Becker durchgeführt.

Vom Fachbereich Biologie der Philipps-Universität Marburg als Dissertation angenommen am: 03.10.2017

1. Gutachterin: Prof. Dr. Anke Becker
2. Gutachter: Prof. Dr. Erhard Bremer

Weitere Mitglieder der Prüfungskommission:

Prof. Dr. Hans-Ulrich Mösch
Dr. Gert Bange
Prof. Dr. Martin Thanbichler

Tag der mündlichen Prüfung: 19.10.2017

Die während der Promotion erzielten Ergebnisse sind zum Teil in folgenden Original-publikationen veröffentlicht worden:

Schäper S, Krol E, Skotnicka D, Kaever V, Hilker R, Søgaard-Andersen L, Becker A. 2016. Cyclic di-GMP regulates multiple cellular functions in the symbiotic alphaproteobacterium *Sinorhizobium meliloti*. J Bacteriol 198(3):521-535.

Schäper S*, Steinchen W*, Krol E, Altegoer F, Skotnicka D, Søgaard-Andersen L, Bange G, Becker A. 2017. AraC-like transcriptional activator CuxR binds c-di-GMP by a PilZ-like mechanism to regulate extracellular polysaccharide production. Proc Natl Acad Sci U S A 114(24):E4822-E4831.
*Co-first author

Schäper S, Yau H, Krol E, Skotnicka D, Kaever V, Søgaard-Andersen L, Vollmer W, Becker A. A dynamic c-di-GMP phosphodiesterase is linked to alpha-rhizobial cell growth and division. Manuscript in preparation.

Table of contents

Abbreviations

µM	micromolar
µm	micrometer
7TMR-DISMED2	seven-transmembrane receptor with diverse intracellular signaling modules extracellular domain 2
A	alanine
A site	active site
AHLs	*N*-acyl homoserine lactones
BCIP	5-bromo-4-chloro-3-indolylphosphate
bi-HTH	bi-partite helix-turn-helix
bp	base pairs
$CaCl_2$	calcium chloride
c-di-GMP	bis-(3′,5′)-cyclic dimeric guanosine monophosphate
CF	Calcofluor
Ch	chapter
CoIP	co-immunoprecipitation
CPRG	chlorophenol red-β-D-galactopyranoside
CR	Congo red
C-terminus	carboxyl-terminus
CTH	C-terminal helix
CUP	c-di-GMP-regulated uncharacterized polysaccharide
CuxR	c-di-GMP-responsive UDP-xylose regulator
DGC	diguanylate cyclase
DNA	deoxyribonucleic acid
dpi	days post inoculation
DRaCALA	differential radial capillary action of ligand assay
E	glutamate
EAL	characteristic domain of PDEs
EGFP	enhanced green fluorescent protein
EMSA	electrophoretic mobility shift assay
EPS	exopolysaccharide
EPS I	exopolysaccharide I/succinoglycan
EPS II	exopolysaccharide II/galactoglucan
et al.	lat., and others
Fig	figure
fl-WGA	fluorescently-labeled wheat germ-agglutinin
GdcP	growth zone dynamic c-di-GMP phosphodiesterase
GdpM	growth zone dynamic putative metallopeptidase
GGDEF	characteristic domain of DGCs
GTase	glycosyltransferase
GTP/GDP/GMP	guanosine tri-/di-/monophosphate
h	hour
HADA	blue-fluorescent D-amino acid
HD	helical hairpin
HD-GYP	characteristic domain of PDEs
HDX-MS	hydrogen-deuterium-exchange mass spectrometry
HMW	high molecular weight
I site	inhibitory site
IPTG	isopropyl β-D-1-thiogalactopyranoside
$IR_{cuxR\text{-}uxs1}$	*cuxR-uxs1* intergenic region
kb	kilo base pairs
K_d	dissociation constant
LB	lysogeny broth

LMW	low molecular weight
LPS	lipopolysaccharide
Mb	mega base pairs
McrA	motility-associated c-di-GMP receptor A
$MgCl_2$	magnesium chloride
min	minute
mL	milliliter
ML	mixed-linkage
mM	millimolar
MM	MOPS-buffered minimal medium
MOPS	3-(N-morpholino) propanesulfonic acid
NaCl	sodium chloride
N-terminus	amino-terminus
OD	optical density
PAS	PAS protein domain named after the proteins Per/Arnt/Sim
PDE	c-di-GMP phosphodiesterase
PG	peptidoglycan
pGpG	5′-phosphoguanylyl
PilZ	protein domain named after the type IV pilus control protein first identified in *Pseudomonas aeruginosa*
R	arginine
rdar	red, dry and rough
REC	receiver domain
rpm	rounds per minute
s	second
SDS	sodium dodecyl sulfate
Tab	table
TM	transmembrane
TY	tryptone yeast
UDP	uridine diphosphate
Wt	wild-type

Chapter 1: Summary

Bacteria have evolved various systems for the integration of environmental signals to rapidly coordinate cellular pathways and adapt to changes in their environment. In the quickly advancing field of nucleotide-based second messengers, cyclic dimeric guanosine monophosphate (c-di-GMP) has emerged as a key regulatory player whose underlying signaling networks control major adaptational and lifestyle changes. Enzymes that catalyze synthesis and degradation of c-di-GMP, named diguanylate cylases (DGCs) and phosphodiesterases (PDEs), respectively, are near-ubiquitous in the bacterial kingdom. Despite the numerous studies aiming to better understand the role of c-di-GMP in bacteria, knowledge on integration of c-di-GMP networks into other regulatory networks, the molecular inventory of c-di-GMP receptors and molecular mechanisms underlying c-di-GMP-dependent regulation is limited.

This study investigated roles of c-di-GMP in environmental adaptation of soil-dwelling *Sinorhizobium meliloti*, a rod-shaped alphaproteobacterium from the order Rhizobiales that exists either in free-living states or in symbiosis with leguminous plant hosts. The *S. meliloti* genome encodes 22 proteins putatively involved in synthesis, degradation and binding of c-di-GMP. Single mutations in 21 of these genes did not cause evident changes in surface attachment, swimming motility or exopolysaccharide (EPS) production. Moreover, screening the different phenotypes of *S. meliloti* c-di-GMP^0 mutants revealed no defects in cell viability and symbiotic potency. In contrast, artificially increasing c-di-GMP levels by overproduction of several DGCs promoted production of extracellular matrix components and surface attachment, whereas swimming motility and extracellular accumulation of *N*-Acyl-homoserine lactones (AHLs) was reduced.

The identification of genetic determinants responsible for observed phenotypic changes at elevated c-di-GMP levels proved c-di-GMP-dependent regulation at both transcriptional and post-translational levels. The *SMc01790-SMc01796* locus, homologous to the *Agrobacterium tumefaciens uppABCDEF* cluster governing biosynthesis of a unipolar polysaccharide (UPP), was required for c-di-GMP-stimulated surface attachment, while the stand-alone PilZ domain protein SMc00507 (renamed McrA) acted as c-di-GMP receptor protein involved in regulation of swimming motility. Transcriptome profiling of *S. meliloti* at elevated c-di-GMP levels revealed upregulation of the *uxs1-SMb20463* gene cluster governing biosynthesis of an extracellular

polysaccharide (referred to as CUP). Resulting from this finding, AraC-like transcriptional activator SMb20457 (renamed CuxR) was shown to bind c-di-GMP by a mechanism similar to that of PilZ domains, which provided an example of convergent evolution in two distinct protein families.

This study demonstrates that the c-di-GMP network in *S. meliloti* is integrated into other cellular systems, particularly the well-characterized regulatory network for opposing control of EPS biosynthesis and motility. For instance, CuxR-mediated activation of CUP production was counteracted by the global repressor MucR, while both MucR and the AHL-sensitive master regulator ExpR reduced UPP-mediated surface attachment at elevated c-di-GMP levels. Moreover, a new cellular function was assigned to the essential PDE SMc00074 (renamed GdcP), which is linked to cell envelope biogenesis in alpha-rhizobial species.

Overall, c-di-GMP-dependent regulation of multiple cellular functions indicated that high c-di-GMP levels favor a sedentary lifestyle of free-living *S. meliloti*. The switch of single motile bacteria from a planktonic state to a structured community of cells might contribute to environmental adaptation and long-term survival of *S. meliloti* in its natural soil habitat.

Zusammenfassung

Bakterien haben diverse Systeme zur Verarbeitung von Umweltsignalen entwickelt, um zelluläre Signalwege unmittelbar aufeinander abstimmen und sich an wechselnde Umweltbedingungen anpassen zu können. Auf dem fortschreitenden Gebiet der Nukleotid-basierten sekundären Botenstoffe stellte sich zyklisches dimeres Guanosinmonophosphat (c-di-GMP) als ein regulatorisches Schlüsselmolekül heraus, dessen zugrunde liegende Signalnetzwerke Veränderungen in Anpassungsformen und Lebensweisen steuern. Enzyme, welche die Reaktionen zur Synthese (Diguanylatzyklasen, DGCs) und zum Abbau (Phosphodiesterasen, PDEs) von c-di-GMP katalysieren, sind nahezu allgegenwärtig im Reich der Bakterien. Trotz der zahlreichen Untersuchungen zum besseren Verständnis der Funktion von c-di-GMP in Bakterien ist das Wissen über die Integration c-di-GMP-basierter Signalnetzwerke in andere regulatorische Netzwerke, das molekulare Inventar von c-di-GMP-Rezeptoren und die molekularen Mechanismen, welche der c-di-GMP-abhängigen Regulation zugrunde liegen, begrenzt.

In dieser Arbeit wurde die Funktion von c-di-GMP bei der Umweltanpassung des bodenbewohnenden Bakteriums *Sinorhizobium meliloti* untersucht, einem stäbchenförmigen Alphaproteobakterium der Ordnung Rhizobiales, welches entweder in freilebenden Stadien oder in Symbiose mit hülsenfruchtartigen Wirtspflanzen vorkommt. Das Genom von *S. meliloti* kodiert für 22 Proteine, welche potenziell an der Synthese, dem Abbau und der Perzeption von c-di-GMP beteiligt sind. Einfachmutanten für 21 der kodierenden Gene wiesen keine deutlichen Veränderungen der Oberflächenanheftung, der Flagellen-basierten Motilität oder der Biosynthese von Exopolysacchariden (EPSs) auf. Darüber hinaus zeigten die phänotypischen Tests für *S. meliloti* c-di-GMP^0 Mutanten weder eine Beeinträchtigung in der Lebensfähigkeit noch einen Effekt in ihrer symbiontischen Wirksamkeit auf. Die durch Überproduktion verschiedener DGCs erzeugten Anstiege der intrazellulären c-di-GMP-Konzentration bewirkten hingegen eine vermehrte Produktion von Bestandteilen der extrazellulären Matrix, eine verstärkte Oberflächenanheftung der Bakterien, eine verringerte Flagellen-basierte Motilität sowie eine reduzierte Akkumulation von extrazellulären *N*-Acyl-Homoserin-Laktonen (AHLs).

Die Identifizierung von genetischen Faktoren, welche für die beobachteten phänotypischen Veränderungen verantwortlich waren, offenbarte eine c-di-GMP-abhängige Regulation auf transkriptioneller sowie posttranslationaler Ebene. Der

SMc01790-SMc01796 Locus, welcher homolog zum *uppABCDEF* Gen-Cluster in *Agrobacterium tumefaciens* ist und hier zur Biosynthese eines unipolaren Polysaccharids (UPP) benötigt wird, stellte sich als verantwortlich für die c-di-GMP-abhängige Oberflächenanheftung heraus, wohingegen das einzelne PilZ Domäne-Protein SMc00507 (umbenannt zu McrA) als c-di-GMP-Rezeptor in der Regulation der Flagellen-basierten Motilität fungierte. Eine Transkriptomanalyse für *S. meliloti* mit erhöhten c-di-GMP-Konzentrationen deckte eine Hochregulierung des *uxs1-SMb20463* Gen-Clusters auf, welches für die Biosynthese eines extrazellulären Polysaccharids (benannt als CUP) benötigt wird. Infolge dieser Entdeckung wurde für den AraC-ähnlichen Transkriptionsaktivator SMb20457 (umbenannt zu CuxR) ein Bindungsmechanismus für c-di-GMP aufgedeckt, welcher demjenigen von PilZ-Proteinen ähnelt und somit ein Beispiel für konvergente Evolution in zwei unterschiedlichen Proteinfamilien lieferte.

Die während dieser Arbeit erzielten Ergebnisse zeigen, dass das c-di-GMP-Netzwerk von *S. meliloti* in andere zelluläre Systeme, im Speziellen in das regulatorische Netzwerk für die gegenläufige Kontrolle der EPS-Biosynthese und Motilität, eingegliedert ist. Beispielhaft dafür war die entgegenwirkende Regulation der CuxR-vermittelten Aktivierung der CUP-Produktion durch den globalen Repressor MucR. Darüber hinaus bewirkten MucR sowie der AHL-sensitive Masterregulator ExpR eine Reduktion der UPP-vermittelten Oberflächenanheftung bei erhöhten c-di-GMP-Konzentrationen. Außerdem wurde der essenziellen PDE SMc00074 (umbenannt zu GdcP) eine neue zelluläre Funktion zugeordnet, welche im Zusammenhang mit der Biogenese der Zellhülle von Alpharhizobien steht.

Insgesamt zeigte die c-di-GMP-abhängige Regulation mehrerer zellulärer Funktionen, dass erhöhte c-di-GMP-Konzentrationen eine sessile Lebensweise von freilebenden *S. meliloti* begünstigt. Die Umstellung motiler Bakterien von einer planktonischen Lebensweise zu einer strukturierten Gemeinschaft von Zellen könnte daher zur Anpassung und zum Überleben von *S. meliloti* in dessen natürlichem Lebensraum beitragen.

Chapter 2: Introduction

Bacteria constantly face changes of environmental conditions in their natural habitats. Perception and integration of signals from various environmental factors are necessary for generating physiological, genetic and cellular adaptational responses that contribute to long-term survival. Bacteria have evolved various signal transduction systems including transfer of phosphate groups between two conserved components, a histidine kinase and a response regulator protein (Stock *et al.*, 2000). Another strategy for environmental adaptation includes second messenger-based systems sensing environmental signals (first messenger) followed by metabolization of a small soluble molecule (second messenger) that regulates cellular processes. Nucleotide-based second messenger signaling in bacteria is essential for bacterial survival under changing environmental conditions. Among the best known as well as recently discovered nucleotides with signaling function are 3′,5′-cyclic guanosine monophosphate (cGMP), 3′,5′-cyclic adenosine monophosphate (cAMP), guanosine-3′,5′-bis-pyrophosphate (ppGpp), bis-(3′,5′)-cyclic dimeric guanosine monophosphate (c-di-GMP), cyclic di-3′,5′-adenosine monophosphate (c-di-AMP) and cyclic 3′,3′-AMP-GMP (cGAMP) (Gomelsky, 2011; Gründling & Lee, 2016; Krasteva & Sondermann, 2017). This study places special focus on environmental adaptation of bacteria through signaling based on the second messenger c-di-GMP.

2.1 c-di-GMP signaling in bacteria

c-di-GMP has emerged as one of the most common and important bacterial second messengers in the large prokaryotic domain Bacteria. 30 years of research on c-di-GMP have revealed key regulatory roles in lifestyle changes of many bacteria, including regulation of a plethora of cellular processes such as biofilm formation and dispersal, motility, virulence, cell cycle and differentiation (Römling *et al.*, 2013). The ubiquitousness of enzymes related to c-di-GMP synthesis and turnover in all major bacterial phyla made c-di-GMP being recognized as a universal bacterial second messenger. Regulation based on c-di-GMP signaling takes place at transcriptional, post-transcriptional and post-translational levels. The number of identified targets and mechanisms of c-di-GMP-mediated regulation is constantly increasing. For instance, recent research revealed new types of c-di-GMP receptors and c-di-GMP-regulated

cellular functions, such as bacterial cell growth and division (Tschowri *et al.*, 2014; Gupta *et al.*, 2016; Kim & Harshey, 2016; Sprecher *et al.*, 2017).

2.1.1 c-di-GMP metabolism

The biochemical and structural characterization of proteins involved in synthesis, degradation and binding of c-di-GMP provided deep mechanistic insights into the metabolism of the second messenger (Schirmer & Jenal, 2009). c-di-GMP is synthesized by diguanylate cyclases (DGCs) containing a GGDEF domain with a GG(D/E)EF signature motif constituting the active site (A site). The A site is required for specific binding of a GTP molecule (glycine residues), coordination of Mg^{2+} or Mn^{2+} (glutamate in the fourth position) and formation of a phosphodiester bond (aspartate/glutamate in position three) (Chan *et al.*, 2004; Wassmann *et al.*, 2007). For DGC activity, GGDEF domains have to form a catalytically competent homodimer in which physical contact of two A sites is generated. This change in oligomeric state favors condensation of two GTP molecules resulting in production of one c-di-GMP molecule (Fig. 1). Biochemical studies of primary signals affecting dimerization of GGDEF domains and therefore regulating DGC activity revealed negative feedback regulation by c-di-GMP binding to a RxxD motif constituting the inhibitory site (I site) (Chan *et al.*, 2004; Christen *et al.*, 2006). The I site is positioned five amino acids upstream of the GG(D/E)EF motif but spatially distal from the A site. It is present in about half of all annotated GGDEF domains and can be also involved in protein-protein interactions (Seshasayee *et al.*, 2010; Dahlstrom *et al.*, 2016).

c-di-GMP hydrolysis is catalyzed by EAL and HD-GYP domains, the former contains an EAL signature motif in the active site. EAL domains have c-di-GMP-specific phosphodiesterase (PDE) activity, which results in the formation of the linear nucleotide pGpG (Fig. 1). pGpG is further degraded to GMP by oligoribonucleases representing another central feature of c-di-GMP signaling (Cohen *et al.*, 2015; Orr *et al.*, 2015). c-di-GMP-specific PDE activity requires either Mg^{2+} or Mn^{2+}, whereas presence of Ca^{2+} strongly inhibits PDE activity (Schmidt *et al.*, 2005). Crystal structures of EAL domains revealed c-di-GMP binding through two metal cations. The glutamate residue of the active site is directly involved in coordination of one of two metal ions and conserved in all active enzymes (Tchigvintsev *et al.*, 2010). The vast majority of EAL domains form homodimers or higher-order oligomers *in vitro*, and a dimer is the most probable functional unit of the EAL domain *in vivo* (Barends *et al.*, 2009; Sundriyal *et al.*, 2014;

Bellini *et al.*, 2017). A further reaction for c-di-GMP degradation is catalyzed by HD-GYP domains possessing hydrolytic activities towards diverse substrates (Galperin *et al.*, 1999; Ryan *et al.*, 2006). Different to EAL domains, HD-GYP domains degrade c-di-GMP in a one-step reaction that yields to two molecules of GMP (Bellini *et al.*, 2014) (Fig. 1).

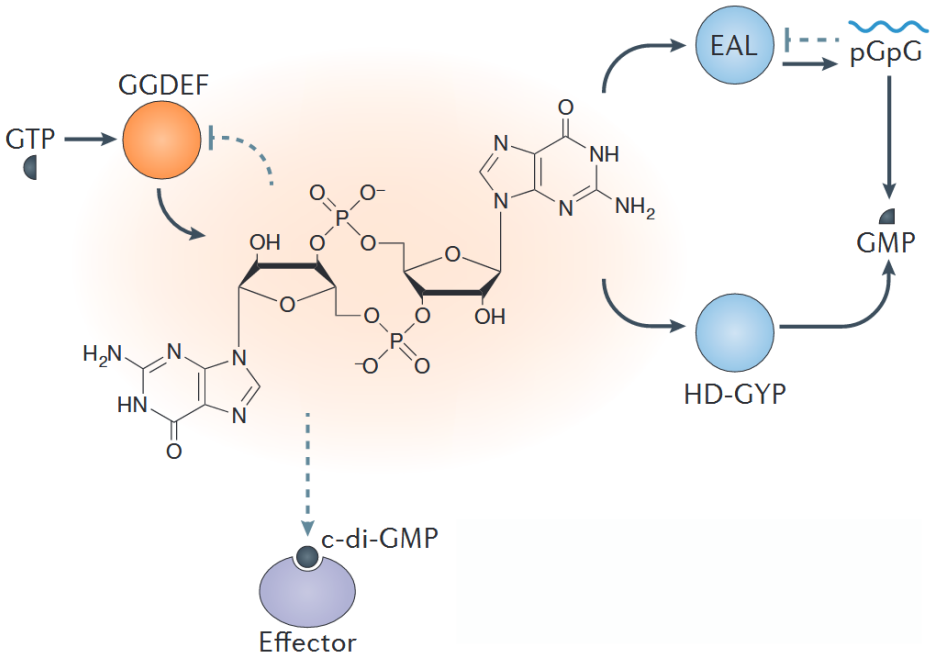

Figure 1. Synthesis, degradation and perception of intracellular c-di-GMP. c-di-GMP is synthesized from two GTP molecules by diguanylate cyclases containing a GGDEF domain. Phosphodiesterases, containing either an EAL or HD-GYP domain, degrade c-di-GMP to pGpG or GMP, respectively. c-di-GMP binding to the I site of GGDEF domains provides a negative feedback mechanism. c-di-GMP is perceived by various effectors, such as PilZ domains, transcription factors and riboswitches, to initiate downstream signaling events. Adapted from Jenal *et al.* (2017).

GGDEF and EAL domains are often arranged in tandem, as ca. 1/3 of all GGDEF domains and ca. 2/3 of all EAL domains are present in the same multidomain proteins (Römling *et al.*, 2013). The controversy of two domains with antagonistic functions in the same protein may be explained by either differential regulation for each domain or enzymatic incompetence of one of the domains. For instance, in *Agrobacterium tumefaciens*, enzymatic activity of the dually functional GGDEF-EAL domain protein DcpA is shifted from a DGC to PDE activity in presence of the pteridine reductase PruA (Feirer *et al.*, 2015). In *Vibrio parahaemolyticus*, the membrane-standing GGDEF-EAL domain protein ScrC switches from the DGC mode to the PDE mode in response to autoinducer molecules at high cell densities (Trimble & McCarter, 2011). The PAS-GGDEF-EAL domain protein PdeA from *Caulobacter crescentus* contains a degenerate A site (GEDEF) and has no DGC activity, but the GGDEF domain is able to

bind GTP and thus to regulate the PDE activity of the covalently linked EAL domain (Christen *et al.*, 2005). Hence, catalytically inactive domains may have evolved different functions and serve as receptors for their substrates or participate in protein-protein interactions.

Genomic analyses predicting GGDEF, EAL and HD-GYP domains as well as experimental evidence revealed a broad distribution of c-di-GMP signaling proteins among the major phylogenetic branches of bacteria, such as Proteobacteria, Spirochetes, Cyanobacteria, Actinobacteria and Firmicutes (Galperin *et al.*, 2001). Genes encoding these protein domains are present in multiple copies per genome and their number can vary significantly even between species from the same genus (Bobrov *et al.*, 2011). Comparative genomic analyses indicated that free-living bacteria with complex environmental lifestyles carry far more c-di-GMP-metabolizing enzymes than obligate parasites (Galperin, 2005). Moreover, GGDEF and EAL proteins were also found in plants and lower eukaryotes, such as poplar, hydra and sea anemone (Römling *et al.*, 2013). In the social amoeba *Dictyostelium discoideum*, c-di-GMP is used as an extracellular signal and acts as a developmental regulator (Chen & Schaap, 2012).

GGDEF and EAL domains are often coupled to diverse sensory input domains and are therefore part of the cellular signal transduction machinery. Cytoplasmic proteins containing GGDEF, EAL and HD-GYP domains are most commonly combined with signal receiver (REC) and Per-Arnt-Sim (PAS) domains, which modulate enzymatic activities of the covalently attached effector domains (Römling *et al.*, 2013). Several DGCs and PDEs were characterized that directly link perception of environmental signals to the activation of c-di-GMP-dependent signaling pathways, such as the O_2-sensing DGC AxDGC2 from *Acetobacter xylinum* or the light-regulated PDE BlrP1 from *Klebsiella pneumoniae* (Barends *et al.*, 2009; Qi *et al.*, 2009). A powerful mechanism for GGDEF domain activation is based on phosphorylation of the REC domain, which was demonstrated for the DGCs PleD from *C. crescentus* and WspR from *Pseudomonas aeruginosa* (Hickman *et al.*, 2005; Paul *et al.*, 2007; Wassmann *et al.*, 2007). Membrane-standing sensors that combine cytoplasmic GGDEF, EAL and HD-GYP domains with periplasmic or extracellular sensory domains form another important group of signaling proteins (Galperin, 2005). NicD from *P. aeruginosa* binds glutamate in the periplasmic space resulting in increased DGC activity of its cytoplasmic GGDEF domain (Basu Roy & Sauer, 2014). Similarly, binding of arginine supposedly modulates DGC activity of CdgH from *Vibrio cholerae* (Xu *et al.*, 2017).

2.1.2 c-di-GMP receptors

Proteins that bind the second messenger c-di-GMP are key components for orchestrating signals generated by c-di-GMP-metabolizing enzymes (Fig. 1). c-di-GMP receptors from a broad range of protein families have emerged and regulate target processes at transcriptional, post-transcriptional and post-translational levels (Römling *et al.*, 2013).

Proteins containing a PilZ domain (named after the type IV pilus control protein *P. aeruginosa* PA2960) are the most common c-di-GMP receptors. Based on comparative sequence analysis, the PilZ domain was first described by Amikam & Galperin (2006). These authors defined an approximately 100 amino acid C-terminus of the glycosyltransferase (GTase) BcsA of the *Gluconacetobacter xylinus* cellulose synthase complex as a separate protein domain. PilZ domains occur also as single-domain proteins or can be found covalently linked to EAL or GGDEF-EAL domains. First experimental evidence for c-di-GMP binding to the PilZ domain was provided for BcsA from *G. xylinus* and YcgR from *Escherichia coli* (Ryjenkov *et al.*, 2006). Lately, more PilZ domain proteins have been shown to specifically bind c-di-GMP and regulate various cellular functions, such as DgrA and DgrB from *C. crescentus* (Christen *et al.*, 2007), Alg44 and MapZ from *P. aeruginosa* (Merighi *et al.*, 2007; Whitney *et al.*, 2015; Xu *et al.*, 2016), as well as PlzC and PlzD from *V. cholerae* (Pratt *et al.*, 2007). PilZ domains have different binding affinities for c-di-GMP in the submicromolar range, which basically corresponds with physiological concentrations measured for intracellular c-di-GMP (Christen *et al.*, 2007; Christen *et al.*, 2010; Pultz *et al.*, 2012). Structural characterization of PilZ domains provided evidence for substantial structural changes upon c-di-GMP binding and confirmed the two conserved motifs RxxxR and (D/N)x(S/A)xG as the c-di-GMP binding sites (Benach *et al.*, 2007; Ramelot *et al.*, 2007). c-di-GMP functions as an interdomain or intermolecular linker bringing together two protomers and initiating downstream signaling events. Thereby, c-di-GMP in different oligomeric forms and conformational states can bind to the PilZ domain (Benach *et al.*, 2007; Ramelot *et al.*, 2007; Gentner *et al.*, 2012; Krasteva & Sondermann, 2017), which in turn can form different oligomeric states (Ko *et al.*, 2010; Li *et al.*, 2011). These molecular mechanisms indicate increased complexity and different modes of PilZ domain-derived downstream signaling.

GGDEF and EAL domains that lost their enzymatic functions can also serve as c-di-GMP receptors. Catalytically inactive GGDEF domains with retained I site can

bind c-di-GMP, which was shown for PopA promoting cell cycle progression in *C. crescentus* (Duerig *et al.*, 2009). Similarly, spatial localization of hybrid histidine kinase SgmT from *Myxococcus xanthus* is dependent on c-di-GMP binding to the intact I site (Petters *et al.*, 2012). In *P. aeruginosa,* c-di-GMP binding to the degenerate GGDEF domain of PelD regulates polysaccharide biosynthesis (Lee *et al.*, 2007). Additionally, enzymatically inactive EAL domains can also function as c-di-GMP receptors as demonstrated for *P. aeruginosa* FimX involved in type IV pilus-based motility (Navarro *et al.*, 2009) and for *Pseudomonas fluorescens* LapD involved in regulation of surface attachment (Newell *et al.*, 2009).

Further domains that facilitate c-di-GMP binding have been identified. c-di-GMP binding is facilitated by the I site-like motif RxGD of the GIL domain (previously referred to as domain of unknown function, DUF2819) present in beta- and gammaproteobacterial species (Fang *et al.*, 2014). A unique c-di-GMP binding mode was identified for the widespread MshEN domain involving a conserved 24 amino acid stretch that facilitates hydrophobic interactions (Wang *et al.*, 2016). A recent study described acetyltransferase HfsK from *C. crescentus* as a potent c-di-GMP-binding protein (Sprecher *et al.*, 2017). Moreover, two types of c-di-GMP-specific mRNA riboswitches were identified in eubacteria enabling regulation of gene expression at post-transcriptional level (Sudarsan *et al.*, 2008; Lee *et al.*, 2010).

An increasing number of c-di-GMP-responsive transcription factors from various protein families provide an additional level for c-di-GMP-dependent regulation of multiple cellular functions. c-di-GMP was shown to bind to transcriptional activators, including CRP/FNR-type Clp from *Xanthomonas campestris* (Chin *et al.*, 2010) and TetR-like LtmA from *Mycobacterium smegmatis* (Li & He, 2012), as well as transcriptional repressors, such as developmental master regulator BldD from *Streptomyces venezuelae* (Tschowri *et al.*, 2014). In *P. aeruginosa* and *V. cholerae*, polysaccharide production is regulated at transcriptional level by c-di-GMP binding to NtrC-type FleQ and VpsT from the FixJ-LuxR-CsgD family of response regulators, respectively (Hickman & Hardwood, 2008; Krasteva *et al.*, 2010). The number of proteins allosterically regulated by c-di-GMP is continuously growing.

2.1.3 Target processes regulated by c-di-GMP

The pleiotropic effects of c-di-GMP on numerous target processes have been subject of intense research during the last 30 years. As a first step towards functional

characterization of this second messenger, c-di-GMP was identified in *G. xylinus* (at that time referred to as *Acetobacter xylinum*) as an allosteric activator of cellulose biosynthesis (Ross *et al.*, 1987). Subsequent research revealed a key regulatory function of c-di-GMP in the motility-to-sessility transition of free-living bacteria. Depending on environmental stimuli, single motile bacteria switch from a planktonic state to a community-based lifestyle including multicellular growth in a colony or biofilm. This drastic lifestyle change is dependent on tightly controlled, temporally coordinated and c-di-GMP-regulated complex processes, such as motility, (initial) attachment, and production of extracellular matrix components (Monds & O'Toole, 2009). As a general rule, high intracellular c-di-GMP levels negatively affect motility and virulence, while promoting adherence, biofilm formation, cell cycle progression and development (Römling *et al.*, 2013; Jenal *et al.*, 2017) (Fig. 2).

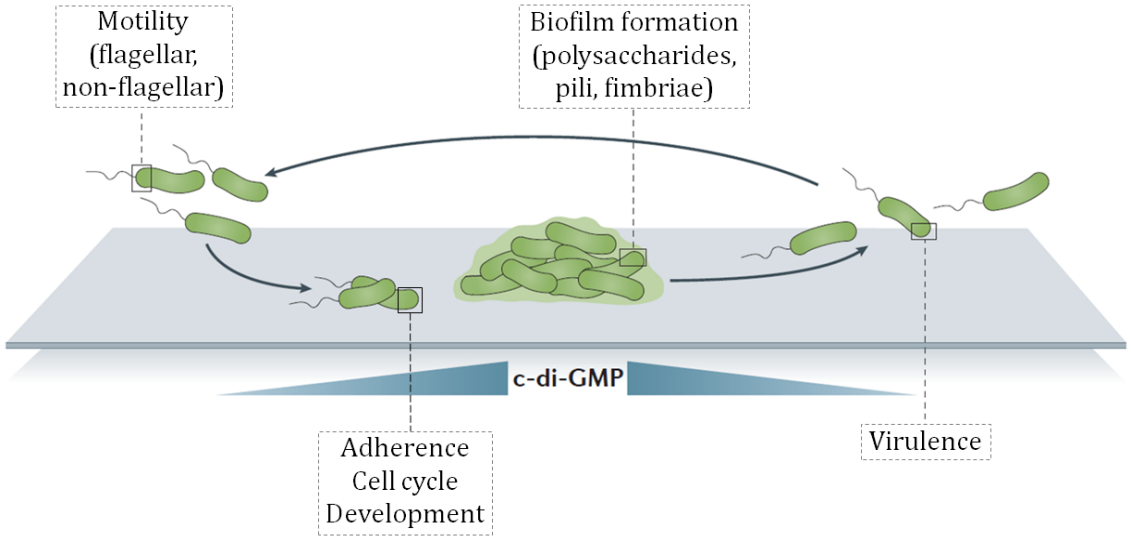

Figure 2. c-di-GMP regulates multiple cellular functions and controls the motile-to-sessile switch of bacteria. Bacterial surface attachment, biofilm formation and dispersal are shown schematically. Various cellular functions that are either activated or inhibited depending on the levels of intracellular c-di-GMP have been identified in several bacterial species, such as *Escherichia coli*, *Caulobacter crescentus*, *Pseudomonas aeruginosa*, *Salmonella* Enteritidis and *Streptomyces venezuelae*. Modified after Jenal *et al.* (2017).

Mechanistic insights into c-di-GMP-dependent regulation of motility on a small time scale were obtained for several flagellated bacterial species. In the enteric bacterium *E. coli*, the PilZ domain protein YcgR slows down flagellar rotation upon interaction with the flagellar motor protein MotA and controls flagellar motor direction upon interaction with the flagellum switch complex FliGMN (Boehm *et al.*, 2010; Paul *et al.*, 2010). Similarly, the YcgR homolog YpfA inhibits motility in *Bacillis subtilis* upon direct interaction with MotA (Chen *et al.*, 2012), while the two stand-alone PilZ domain

proteins DgrA and DgrB from *C. crescentus* mediate c-di-GMP-dependent motility control through a yet unknown mechanism (Christen *et al.*, 2007). In *P. aeruginosa*, the single-domain PilZ protein MapZ interacts with chemotaxis methyltransferase CheR1 to control methylation of chemoreceptors and therefore flagellar motor switching (Xu *et al.*, 2016). Additional regulation of flagellar motility is based on c-di-GMP heterogeneity, which is generated upon interaction between the PDE Pch and CheA of the chemotaxis machinery (Kulasekara *et al.*, 2013). In the same bacterium, flagellar motility is regulated on a larger time scale by the transcriptional regulator FleQ, repressing flagellar gene expression in a c-di-GMP-dependent manner (Hickman & Harwood, 2008). c-di-GMP also regulates non-flagellar motility, such as type IV pilus-mediated twitching motility via c-di-GMP receptor FimX from *P. aeruginosa* (Kazmierczak *et al.*, 2006).

Many bacteria form biofilms upon production of compounds such as diverse exopolysaccharides (EPSs), adhesive pili, non-fimbrial adhesins and extracellular DNA. These can serve as structural components of the extracellular polymeric matrix and promote multicellular morphotypes or cooperative bacterial movements (Zogaj *et al.*, 2001; Whitchurch *et al.*, 2002; Gao *et al.*, 2012; Serra *et al.*, 2013). c-di-GMP-dependent regulation of EPS biosynthesis in various bacteria is a conserved mechanism for the formation of extracellular matrix-encased biofilms (McDougald *et al.*, 2012; Liang, 2015). Cellulose biosynthesis is allosterically controlled by c-di-GMP binding to the PilZ domain of the bacterial cellulose synthase BcsA and GIL domain protein BcsE from *E. coli* (Ryjenkov *et al.*, 2006; Fang *et al.*, 2014). In the same organism, production of biofilm matrix component poly-β-1,6-*N*-acetylglucosamine (PNAG) is facilitated by direct c-di-GMP binding to inner membrane components of the biosynthetic machinery, thereby promoting protein-protein interactions and stimulating GTase activity of PgaCD (Steiner *et al.*, 2013). Production of alginate in mucoid *P. aeruginosa* is dependent on c-di-GMP binding to PilZ domain-containing Alg44, which is part of a large inner membrane-located alginate synthase complex (Merighi *et al.*, 2007). Pel production in non-mucoid *P. aeruginosa* biofilms is modulated by c-di-GMP binding to the I site of c-di-GMP receptor PelD, which activates the associated GTase PelF (Lee *et al.*, 2007; Whitney *et al.*, 2012). In *K. pneumoniae*, type 3 fimbriae-mediated biofilm formation is stimulated upon c-di-GMP binding to PilZ domain transcriptional activator MrkH (Wilksch *et al.*, 2011; Schumacher & Zeng, 2016). Interestingly, c-di-GMP-dependent regulation of biofilm formation takes place in

a non-uniform distribution across the biofilm and follows a defined spatiotemporal pattern during colony maturation (Nair *et al.*, 2017).

c-di-GMP-dependent signaling pathways control morphogenesis and developmental transitions in several bacterial species. Quantification of c-di-GMP at single-cell level in *Caulobacter, Pseudomonas, Salmonella* and *Klebsiella* species revealed an asymmetric distribution of the second messenger upon cell division (Christen *et al.*, 2010). The bimodal distribution of c-di-GMP during the swarmer-to-stalked cell transition in dimorphic *C. crescentus* is dependent on the polarly localized DGC PleD, which contributes to polar differentiation and stalk biogenesis (Aldridge *et al.*, 2003; Paul *et al.*, 2004; Christen *et al.*, 2010). In *C. crescentus*, c-di-GMP levels oscillate in a cell cycle-dependent manner, whereas cells unable to produce c-di-GMP display an altered morphology and loose their polar appendages (Abel *et al.*, 2013). In-depth analysis revealed c-di-GMP binding to the essential cell cycle kinase CckA that coordinates chromosome replication with cell morphogenesis in *C. crescentus* (Lori *et al.*, 2015). c-di-GMP-dependent regulation of development was shown for *S. venezuelae* and the social bacterium *M. xanthus* (Tschowri *et al.*, 2014; Skotnicka *et al.*, 2016a), while c-di-GMP signaling pathways related to cell growth and division were identified in *E. coli* and *M. smegmatis* (Gupta *et al.*, 2016; Kim & Harshey, 2016).

Virulence of animal and plant pathogens, including processes such as host adherence, secretion of virulence factors, cytotoxicity and resistance to oxidative stress, is controlled by c-di-GMP (Römling *et al.*, 2013). In the phytopathogen *Xanthomonas campestris*, c-di-GMP contributes to synthesis of virulence factors (Ryan *et al.*, 2007). Upon removal of all DGCs, *Salmonella* Enteritidis virulence decreased in a mouse model of systemic infection, whereas virulence increased in a mouse model of *Brucella melitensis* infection (Solano *et al.*, 2009; Petersen *et al.*, 2011). Efficient regulation of virulence by c-di-GMP was exemplified by an outbreak of enterohaemorrhagic *E. coli* that caused high incidence of life-threatening haemolytic uraemic syndrome in Germany in 2011 (Richter *et al.*, 2014). Finally, importance of c-di-GMP in bacterial virulence is further indicated by specific recognition of the second messenger by the STING (Stimulator of Interferon Genes) protein of the host innate immune system (Karaolis *et al.*, 2007; Burdette *et al.*, 2011).

2.2 Model organism *Sinorhizobium meliloti*

Sinorhizobium meliloti is a well-studied Gram-negative bacterium from the

alphaproteobacterial family Rhizobiaceae. In its natural soil habitat, *S. meliloti* occurs either in free-living states or in symbiosis with leguminous plant hosts from the genera *Medicago*, *Melilotus* and *Trigonella* (Fig. 3). The establishment of an efficient symbiosis requires an exchange of signaling molecules ('molecular dialogue'; Dénarié *et al.*, 1993) including the secretion of plant flavonoids and rhizobial lipochitin oligosaccharides (Nod factors). In the early stage of infection, a microcolony of bacteria is trapped inside a curled root hair and individual cells enter the plant cell within tubular structures called infection threads (Jones *et al.*, 2007) (Fig. 3b). A complex and spatiotemporally coordinated infection process results in the development of root nodules (Fig. 3c). Under micro-oxic conditions inside the plant cells, *S. meliloti* differentiates into morphologically distinctive and polyploid bacteroids (Fig. 3d), which convert atmospheric nitrogen to biologically available ammonium (Vasse *et al.*, 1990). Ammonium is utilized by the plant, which in turn delivers carbon sources to the benefit of the bacteria (Oldroyd *et al.*, 2011). Considering the suppression of a plant defense response by *S. meliloti* as well as its close relation to plant and animal pathogens from the genera *Agrobacterium* and *Brucella*, it is discussed whether the symbiotic association of rhizobial bacteria with leguminous plant hosts has evolved from a pathogenic relationship ('intelligent pathogens'; Deakin & Broughton, 2009).

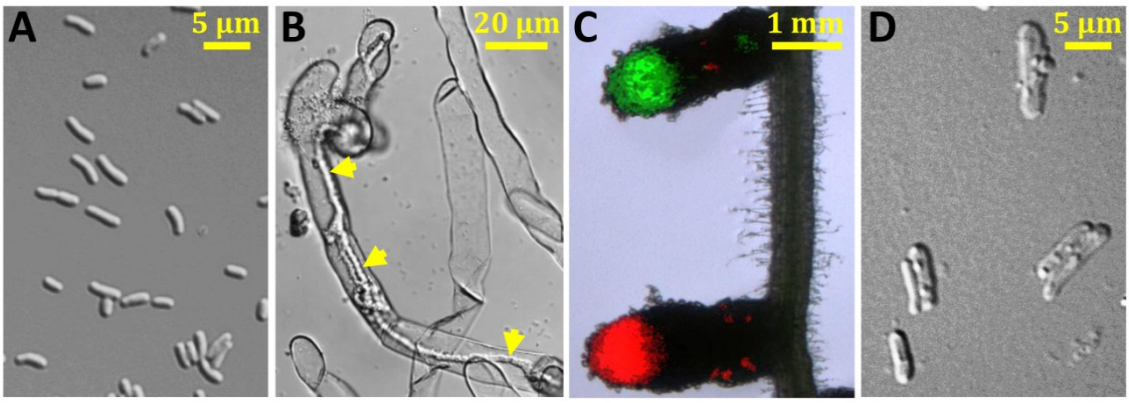

Figure 3. *S. meliloti* in the free-living state and in symbiosis with *Medicago sativa*. (A) Free-living *S. meliloti* cells taken from liquid culture. **(B)** Infection thread (indicated by yellow arrows) initiated by *S. meliloti* inside a root hair of *M. sativa* (7 dpi). **(C)** *M. sativa* root with nodules containing green- and red-fluorescent *S. meliloti* (21 dpi). **(D)** *S. meliloti* differentiated into bacteroids isolated from *M. sativa* root nodules (28 dpi). Microscopic image in panel D was provided by Alexandra Peregrina Lavín, Estación Experimental del Zaidín CSIC (Granada). dpi, days post inoculation.

Rod-shaped *S. meliloti* proliferates by asymmetric cell division that features synthesis of new cell wall material at one cell pole and chromosome segregation towards the growing cell pole (Brown *et al.*, 2012; Frage *et al.*, 2016). The bacteria form

peritrichous flagella enabling swimming motility, which is restricted to exponential growth and allows *S. meliloti* to actively move towards chemotactic attractants (Sourjik *et al.*, 2000; Schmitt, 2002; Rotter *et al.*, 2006). The *S. meliloti* genome consists of three replicons including the chromosome (3.65 Mb) and the two megaplasmids pSymA (1.35 Mb) and pSymB (1.68 Mb). Genomic sequence data for *S. meliloti* strain Rm1021 is available since 2001 (Finan *et al.*, 2001; Galibert *et al.*, 2001). The two closely related and commonly used reference strains Rm1021 and Rm2011 are spontaneous streptomycin-resistant derivatives of the natural isolate and parent strain SU47.

The ability of rhizobia to produce a complex array of glucidic molecules, such as EPSs, lipopolysaccharide (LPS), capsular polysaccharide, K-antigen polysaccharide, cyclic glucans, glucomannan and gel-forming polysaccharide (Fraysse *et al.*, 2003; Laus *et al.*, 2006), creates an excellent basis for studying regulation of polysaccharide biosynthesis in these organisms. Rhizobial surface polysaccharides are important during the infection process and function as signaling molecules, which are perceived by the host plant. EPSs also contribute to nutrient gathering, protection against environmental stress and antimicrobial compounds, attachment to surfaces and biofilm formation (Skorupska *et al.*, 2006; Downie, 2010). *S. meliloti* produces the two major and symbiotically active EPSs succinoglycan (EPS I) and galactoglucan (EPS II). EPS I is an acidic heteropolymer consisting of repeating octasaccharide subunits, each of them containing seven D-glucose molecules and one D-galactose molecule substituted with acetyl, succinyl and pyruvyl groups (Reinhold *et al.*, 1994). Its biosynthesis is governed by an approximately 35 kb gene cluster located on the pSymB megaplasmid and containing 28 *exo/exs* genes (Reuber & Walker, 1993). EPS II consists of disaccharide repeating units containing D-glucose and D-galactose substituted with acetyl and pyruvyl groups. Its biosynthesis is governed by an approximately 27 kb gene cluster on the pSymB megaplasmid and containing 22 genes (formerly named *exp*) organized in the five transcription units *wga, wgcA, wggR, wgd* and *wge* (Becker *et al.*, 1997; Bahlawane *et al.*, 2008a). EPS I is produced in high molecular weight (HMW) and low molecular weight (LMW) forms, the latter thought to be involved in suppressing the plant defense response (Niehaus *et al.*, 1993). A *S. meliloti exoY* mutant, unable to produce EPS I, fails to initiate the formation of an infection thread at early stages of infection (Cheng & Walker, 1998). Either supplementation of LMW EPS I (Battisti *et al.*, 1992; Urzainqui & Walker, 1992) or transcriptional activation of EPS II production (González *et al.*, 1996) can suppress the phenotype of EPS I-deficient *S. meliloti* strain Rm1021.

A complex regulatory network with crosstalk between its different components controls the process of EPS biosynthesis in *S. meliloti* (Janczarek, 2011). Environmental conditions, such as limitations of nitrogen and sulphur, high phosphate concentrations and hyperosmotic stress, stimulate EPS I production, while EPS II production is upregulated under phosphate starvation (Doherty *et al.*, 1988; Zhan *et al.*, 1991; Mendryhal & González, 2000). Numerous genes involved in regulation of EPS I and EPS II biosynthesis have been identified including *mucR*, *expR* and *phoB*. MucR is a zinc-finger transcriptional regulator and binds to promoter regions in the two gene clusters governing EPS I and EPS II biosynthesis. It is transcriptionally autoregulated and couples both biosynthetic pathways by positive regulation of EPS I production and negative regulation of EPS II production (Bertram-Drogatz *et al.*, 1998; Rüberg *et al.*, 1999). MucR also modulates swimming motility of *S. meliloti* by repressing the transcription of flagellar gene regulator *rem*, therefore regulating EPS biosynthesis and motility in an opposing manner (Rotter *et al.*, 2006; Bahlawane *et al.*, 2008b). Expression of EPS II biosynthesis genes is stimulated by PhoB, the response regulator of the PhoR-PhoB two-component system, when concentrations of inorganic phosphate are low (Krol & Becker, 2004). Moreover, the Sin/ExpR quorum-sensing system, including autoinducer synthase SinI and LuxR-type regulator ExpR that binds long-chain *N*-acyl-homoserine lactones (AHLs), regulates various target processes at the level of transcription (Charoenpanich *et al.*, 2013). Mutation of either *expR* or *sinI* in *S. meliloti* Rm1021 results in a dry colony phenotype due to downregulated EPS II production (Pellock *et al.*, 2002; Marketon *et al.*, 2003). Noteworthy, the commonly used laboratory strains Rm1021 and Rm2011 carry a mutation at the *expR* locus (Pellock *et al.*, 2002).

2.3 c-di-GMP signaling in the order Rhizobiales

Although c-di-GMP signaling has been studied extensively in various bacterial linages and species since its discovery 30 years ago, regulatory functions of the second messenger in the order Rhizobiales remain largely unknown. Some studies have characterized genes related to c-di-GMP and the analysis of phenotypic effects of artificially altered c-di-GMP levels. Among bacteria from the order Rhizobiales, c-di-GMP was first detected in *A. tumefaciens* cell extracts, and addition of c-di-GMP to membrane preparations stimulated cellulose production (Amikam & Benziman, 1989). Further evidence for c-di-GMP to be involved in regulation of cellular functions in

alpha-rhizobia was obtained for *Rhizobium leguminosarum* bv. *trifolii*, in which c-di-GMP-stimulated cellulose production is mediated by *divK* and *celR* (an ortholog of DGC-encoding *pleD* from *C. crescentus*) (Ausmees *et al.*, 1999). Mutation and overexpression of *celR* in *A. tumefaciens* revealed a function of c-di-GMP related to biofilm formation, production of a polar adhesion structure, plant surface attachment, and virulence (Barnhart *et al.*, 2013, 2014). Formation of aggregates and rosettes by *A. tumefaciens* overproducing c-di-GMP is dependent on the *uppABCDEF* gene cluster governing biosynthesis of a lectin-binding unipolar polysaccharide (UPP) (Xu *et al.*, 2013). Recently, a pterin-mediated signaling pathway was identified that modulates enzymatic activity of the dually functional GGDEF-EAL domain protein DcpA regulating UPP and cellulose production in *A. tumefaciens* (Feirer *et al.*, 2015).

In *R. leguminosarum* and *Rhizobium etli*, overexpression of a constitutively active *pleD* variant, used to artificially increase intracellular c-di-GMP levels, resulted in enhanced EPS production, biofilm formation and adhesion to plant roots, while symbiotic efficiency and swimming motility were decreased (Pérez-Mendoza *et al.*, 2014). When the c-di-GMP-binding protein BdcA from *E. coli* was overproduced in *S. meliloti* 102F34, biofilm dispersal and enhanced motility was observed, presumably as a consequence of lowered concentrations of free c-di-GMP inside the cells (Ma *et al.*, 2011). Phenotypic analysis of *E. coli* overexpressing *cdgA* and *cdgB*, both encoding GGDEF-EAL domain proteins from *R. etli*, suggested dual enzymatic activities of both proteins. In addition, stimulated *cdgB* promoter activity in *R. etli* indicated a putative role of c-di-GMP during plant infection (Gao *et al.*, 2014).

In *S. meliloti*, an initial incomplete screen of 14 Rm1021 mutants for genes related to c-di-GMP metabolism identified eleven mutants as weakly affected in growth rate, motility, EPS production and nodule occupancy (Wang *et al.*, 2010). Recently, elevated levels of c-di-GMP were shown to induce production of a novel mixed-linkage (ML) β-glucan in *S. meliloti* Rm8530, supposedly by activation of the membrane-standing GTase BgsA upon binding of c-di-GMP to its C-terminal portion (Pérez-Mendoza *et al.*, 2015). Moreover, ML β-glucan biosynthesis is subject to transcriptional regulation by ExpR (Pérez-Mendoza *et al.*, 2015). c-di-GMP binding to *S. meliloti* flagellar export ATPase FliI was demonstrated by Trampari *et al.* (2015), who suggested a mechanism for c-di-GMP-mediated regulation of swimming motility at post-translational level.

In sum, past studies on c-di-GMP regulating behavior and cellular functions in bacteria from the order Rhizobiales generated incomplete knowledge on the roles of c-di-GMP

in the physiology and environmental adaptation of these bacteria. For instance, it is poorly understood how c-di-GMP signaling is integrated into other cellular networks of alpha-rhizobial species. Particularly, genetic determinants, c-di-GMP effectors and the underlying molecular mechanisms responsible for observed phenotypic changes upon artificially altered c-di-GMP levels remain largely unknown. c-di-GMP signaling pathways and mechanisms that contribute to environmental adaptation are therefore subjects to current research.

2.4 Scope of this study

The aim of this study was to answer if and how c-di-GMP signaling contributes to viability and switches between different lifestyles in the framework of environmental adaptation of *S. meliloti.* The first part of this study focused on systematic analysis of genes encoding putative c-di-GMP-metabolizing and -binding proteins. Based on the observed phenotypic changes upon overproduction of several DGCs, genetic determinants for c-di-GMP-dependent regulation of motility, surface attachment and production of extracellular matrix components have been identified (Schäper *et al.*, 2016; Chs. 3.1 & 6). In the second part, transcriptional activator SMb20457 (renamed CuxR) was genetically and biochemically characterized in the light of c-di-GMP-dependent regulation of a new extracellular polysaccharide in *S. meliloti* (Schäper *et al.*, 2017; Chs. 3.2 & 7). The third part dealed with membrane-standing c-di-GMP PDE SMc00074 (renamed GdcP) and its functional characterization, which highlighted an essential function related to alpha-rhizobial cell growth and division (Schäper *et al.*, in preparation; Chs. 3.3 & 8).

Chapter 3: Results and Discussion

3.1 c-di-GMP regulates multiple cellular functions in *S. meliloti*

To elucidate the role of c-di-GMP in environmental adaptation of *S. meliloti*, the genome of strain Rm2011 was subjected to bioinformatic analysis revealing 22 putative c-di-GMP-metabolizing and -binding proteins (Ch. 6, Fig. 2). 18 proteins contained a GGDEF domain with weakly or highly conserved GGDEF domain motifs, and in twelve of these proteins the GGDEF domain was arranged in tandem with an EAL domain. Two putative c-di-GMP binding stand-alone PilZ domain proteins and no proteins containing a HD-HYP domain could be identified. Predicted transmembrane (TM) α-helices indicated association with the membrane for nearly half of the identified proteins. Most of the c-di-GMP-related domains were fused to other signaling domains including REC, PAS, GAF, HAMP, CHASE, MHYT, 7TMR-DISM_7TM and 7TMR-DISMED2 (Ch. 6, Fig. 2). Depending on the adaptability of an organism in changing environmental conditions, the total number of DGC- and PDE-encoding genes (*e.g.*, zero in *Streptococcus pneumoniae*, six in *B. subtilis*, 14 in *C. crescentus*, 29 in *E. coli*, and 62 in *V. cholerae*) and the complexity of downstream signaling networks can vary considerably among bacterial species (Galperin, 2005; Römling *et al*., 2013). The total number of 20 putative c-di-GMP-metabolizing enzymes in *S. meliloti* might be in line with this trend since these soil-dwelling bacteria are facultative symbionts, which occur either in free-living states or in association with leguminous plant hosts.

3.1.1 c-di-GMP is not essential in *S. meliloti*

As a first step towards functional characterization of c-di-GMP, the ability of *S. meliloti* strain Rm2011 to produce this second messenger was tested by direct quantification of c-di-GMP. LC-MS/MS-based quantification revealed intracellular c-di-GMP levels of 2-6 pmol/mg protein in Rm2011 grown in liquid culture, which was comparable to c-di-GMP concentrations that have been determined for other bacterial species, such as *E. coli* and *M. xanthus* (Spangler *et al.*, 2010; Skotnicka *et al.*, 2016b). Exponentially growing cells had a 10-30-fold higher c-di-GMP content than cells in the stationary growth phase (Ch. 6, Fig. 1). Moreover, intracellular c-di-GMP levels of exponential-phase cells approximately correlated with growth rate, as cells grown in TY medium or phosphate-sufficient MOPS-buffered minimal medium (MM) had about two-fold shorter doubling times and two- to four-fold higher c-di-GMP levels than phosphate-

limited cells (Ch. 6, Fig. 1). Growth-dependent alterations in c-di-GMP concentrations were also reported for *E. coli* showing higher levels of c-di-GMP at the transition to stationary phase than in the exponential and stationary phases (Spangler *et al.*, 2010). The detection of c-di-GMP in *S. meliloti* indicated activities of c-di-GMP-metabolizing enzymes and existence of dedicated signaling pathways.

In order to functionally characterize components of the c-di-GMP network, loss-of-function mutants for 21 genes encoding putative c-di-GMP-metabolizing and -binding proteins in Rm2011 were constructed and assayed for phenotypic changes in production of extracellular matrix components, swimming motility, surface attachment and symbiosis with *Medicago sativa*. Mutation of the *SMc00074* gene, previously identified as possibly essential (Cowie *et al.*, 2006), appeared to be lethal, therefore this gene was characterized further (Chs. 3.3 & 8). None of the single c-di-GMP-related gene mutants were notably affected in swimming motility, attachment to abiotic surface, binding of hydrophobic dye Congo red (CR) or production of EPS I and EPS II (Ch. 6, Fig. S1). Besides, all mutants were able to establish symbiosis with *M. sativa*. Due to possible redundancy of c-di-GMP-metabolizing enzymes, c-di-GMP-depleted (c-di-GMP^0) strains were constructed by stepwise deletion of 16 GGDEF domain-encoding genes in Rm2011 and Rm2011 *expR*$^+$. For both c-di-GMP^0 strains the concentration of c-di-GMP extracted from exponentially growing cells was below the lower limit of detection (<3.3 nM). These strains showed slightly increased sensitivity to acid stress, whereas no or weak changes in production of EPS I and EPS II, CR binding, swimming motility, surface attachment or root nodule symbiosis with *M. sativa* were observed (Ch. 6, Figs. S3-5). The c-di-GMP^0 strains were viable, with growth rate and microscopic appearance similar to the c-di-GMP-sufficient parent strains.

Systematic mutational analysis of GGDEF-, EAL-, and PilZ-domain-encoding genes signified differences of c-di-GMP function in *S. meliloti* compared to that in other bacteria. Most unexpectedly, the *S. meliloti* c-di-GMP^0 strains did not show salient phenotypes in the physiological processes tested, except for increased sensitivity to acid stress. This was in contrast to removal of all c-di-GMP-producing enzymes in dimorphic alphaproteobacterium *C. crescentus*, which was non-motile due to lack of flagella, affected in surface attachment and impaired in cell differentiation, the latter impairment resulting in aberrant cell morphology (Abel *et al.*, 2013). Deletion of all GGDEF domain-encoding genes in *Salmonella* Enteritidis resulted in abrogation of typically c-di-GMP-regulated cellular functions such as motility, cellulose and fimbriae

production, while growth and resistance to acid, salt, or starvation stress were unaffected (Solano *et al.*, 2009). In the case of *S. meliloti*, the phenotypic neutrality of the c-di-GMP^0 strains is unlikely to be due to low abundance or absence of c-di-GMP in the wild-type under the growth conditions applied in this study, since the c-di-GMP content was in a similar range compared to other bacteria studied. However, it cannot be excluded that the Rm2011 laboratory strain has lost sensory and regulatory pathways that stimulate enhanced c-di-GMP production.

3.1.2 Elevated levels of c-di-GMP promote sessility of *S. meliloti*

The results of phenotypic screening of c-di-GMP-related gene mutants indicated that c-di-GMP is not essential for free-living and plant-associated *S. meliloti* under laboratory conditions. As an alternative approach, c-di-GMP-related genes were overexpressed for altering intracellular c-di-GMP levels, aiming for their functional characterization. Heterologous expression of the DGC gene *dgcA* from *C. crescentus* in Rm2011 resulted in inhibited swimming motility and reduced EPS II production, whereas CR staining and surface attachment were enhanced. By contrast, heterologous expression of PDE-encoding *yhjH* from *E. coli* reduced surface attachment by circa two-fold but did not affect other phenotypes (Ch. 6, Fig. 3). Similar to heterologous expression of *dgcA*, overexpression of endogenous *pleD*, *SMb20523*, *SMb20447*, *SMc01464* and *SMc03178* resulted in inhibition of swimming motility and EPS II production as well as increased surface attachment and CR staining (Ch. 6, Fig. 3). Exchange of PleD A site motif GGEEF to GGAAF abolished the effects of *pleD* overexpression, supporting DGC activity of PleD and a c-di-GMP-dependent nature of the observed phenotypic changes (Ch. 6, Fig. 3). Further evidence for PleD, SMb20523, SMb20447, SMc01464 and SMc03178 representing functional DGCs was provided by an approximately 200- to 2,500-fold increase in c-di-GMP content of Rm2011 overproducing these proteins (Ch. 6, Fig. 4a). Four of these proteins possess a canonical GG(D/E)EF motif, whereas SMb20447 has an AGDEF motif (Ch. 6, Fig. 2), as has been reported for the functional DGC VCA0965 from *V. cholerae* (Hunter *et al.*, 2014). SMb20447 and SMc03178 have both complete GGDEF and EAL domains, suggesting that DGC activity of these proteins is dominant under the conditions of overproduction. Control of the catalytic activities of such dual-function enzymes can be a key point of regulation. A regulatory control of both enzymatic functions has been reported for *A. tumefaciens* DcpA, *P. aeruginosa* MucR and RmcA, *V. parahaemolyticus* ScrC,

Rhodobacter sphaeroides BphG1, and *Legionella pneumophila* Lpl0329 (Tarutina *et al.*, 2006; Ferreira *et al.*, 2008; Levet-Paulo *et al.*, 2011; Li *et al.*, 2013; Feirer *et al.*, 2015; Okegbe *et al.*, 2017). Unexpectedly, overproduction of the predicted PDE SMb21517, a stand-alone EAL domain protein, resulted in a moderate increase in c-di-GMP content, reduced biofilm formation by circa two-fold and inhibited motility (Ch. 6, Figs. 3 & 4a). Similar effects were observed upon overproduction of EAL or HD-GYP domain proteins in *L. pneumophila* or *Pectobacterium atrosepticum* (Levi *et al.*, 2011; Tan *et al.*, 2014), indicating indirect effects on other DGCs or PDEs.

Overexpression of *SMb20447* and *SMc03178,* both generating higher c-di-GMP levels compared to *pleD* and *SMb20523* overexpression, resulted in inhibited growth and aberrant cell elongation, indicating interference of very high c-di-GMP with cell cycle control (Ch. 6, Fig. 4). Exchange of SMc03178 A site motif GGDEF to GGAAF abolished the effects of *SMc03178* overexpression on cell morphology (Ch. 8, Fig. S5). *S. meliloti* cell elongation provoked at very high c-di-GMP levels might have been directly caused by this second messenger or indirectly by exhausting the GTP pool. In *C. crescentus*, c-di-GMP and the single-domain response regulator DivK convergently regulate cell cycle progression. In this regulation, c-di-GMP-induced phosphatase activity of the cell cycle kinase CckA promotes replication initiation and cell cycle progression. The C-terminal part of the *S. meliloti* CckA, which contains the catalytic and REC domains, shares 47 % identity with its *C. crescentus* ortholog, including residue Y514, shown to be important for binding of c-di-GMP (Lori *et al.*, 2015). Thus, it is tempting to speculate that, at least at very high c-di-GMP concentrations, binding of c-di-GMP to CckA possibly also impacts the *S. meliloti* cell cycle.

Based on the observation that c-di-GMP regulates a multitude of cellular processes in *S. meliloti*, gene mutants were screened to identify targets regulated by c-di-GMP and genetic determinants that were responsible for observed phenotypic changes. Overexpression of *SMc01464*, *SMb20447* and *SMc03178,* which resulted in higher c-di-GMP levels compared to *pleD* and *SMb20523*, was accompanied by increased EPS I production indicated by staining with the fluorescent dye Calcofluor (CF) (Ch. 6, Fig. 3). Increased CF brightness of Rm2011 overexpressing *SMb20447* was abolished upon deletion of *exoY*, encoding a key enzyme of the EPS I biosynthesis pathway, while no change in *exoY* promoter activity was detected (Ch. 6, Fig. 5a-b). This suggested c-di-GMP-dependent regulation of EPS I biosynthesis at post-translational level. Reduced EPS II production at elevated c-di-GMP levels was likely the result of

inhibited promoter activity of EPS II biosynthesis gene *wgeA*, indicating regulation by c-di-GMP at the level of transcription (Ch. 6, Fig. 5b-c). Search for genetic factors involved in c-di-GMP-mediated surface attachment in *S. melioti* revealed gene cluster *SMc01790-SMc01796*, which is homologous to *A. tumefaciens uppABCDEF* (Ch. 6, Fig. S8a). In this organism, the gene cluster governs biosynthesis of a unipolar polysaccharide (UPP) required for c-di-GMP-dependent attachment and cell aggregation (Xu *et al.*, 2013). Integration of a mutagenic plasmid into *SMc01792* abolished surface attachment by Rm2011 overexpressing *pleD* (Ch. 6, Fig. 8a), suggesting that *S. meliloti* could utilize UPP for surface attachment and employ similar mechanisms of c-di-GMP-stimulated UPP production as *A. tumefaciens*. Determination of promoter activities in the *SMc01790-SMc01796* gene cluster revealed no changes upon overexpression of *pleD*, suggesting c-di-GMP-dependent regulation at post-translational level. In *A. tumefaciens*, UPP biosynthesis is controlled by a pterin-mediated signaling pathway regulating dual-function DGC-PDE DcpA (Feirer *et al.*, 2015). Evidences for surface attachment regulated by c-di-GMP at post-translational level have also been obtained in other bacterial species. Surface attachment of *C. crescentus* is facilitated by the holdfast adhesin, whose biosynthesis is subject to regulation by c-di-GMP effector protein HfsK (Sprecher *et al.*, 2017). In *P. fluorescens*, function of surface adhesin LapA is regulated by c-di-GMP binding to membrane-standing LapD, thus preventing periplasmic proteolysis of LapA (Newell *et al.*, 2009).

Evidence for global repressor MucR being involved in regulation of UPP biosynthesis in *S. meliloti* was provided, as Rm2011 lacking MucR and overexpressing *pleD* showed cell aggregation and staining with fluorescently-labeled wheat germ-agglutinin (fl-WGA) (Ch. 6, Fig. 8a). In the case of *A. tumefaciens*, fl-WGA has been used for probing UPP in single cells (Xu *et al.*, 2013). Moreover, strains with restored *expR* and overexpressing *pleD* showed attenuated attachment to an abiotic surface, irrespective of EPS I and EPS II production (Ch. 6, Fig. 8a). These data suggested that MucR and ExpR, both members of the regulatory network for opposing control of EPS biosynthesis and motility, may add another layer to the regulation of UPP biosynthesis in *S. meliloti*.

c-di-GMP signaling was previously reported to interfere with quorum sensing in several bacterial species (Srivastava & Waters, 2012). The quorum sensing system in *S. meliloti* employs *N*-acyl homoserine lactones (AHLs) produced by the autoinducer synthase SinI and recognized by the transcriptional master regulator ExpR (Hoang *et al.*, 2004).

Knowing that c-di-GMP and ExpR regulate similar cellular functions such as EPS production and swimming motility, interference of both signaling modules was analyzed by determining relative amounts of AHLs secreted by Rm2011 at various c-di-GMP levels. Overproduction of different DGCs resulted in reduced accumulation of AHLs in the culture supernatant. The concomitant inhibition of *sinI* promoter activity most likely accounted for this phenotypic change (Ch. 6, Fig. 7). Thus, elevated c-di-GMP levels negatively affected AHL production at the level of *sinI* transcription. A drop in c-di-GMP levels during the transition from exponential to stationary growth phase of *S. meliloti* (Ch. 6, Fig. 1) may serve as a fine-tuning mechanism attenuating AHL accumulation in rapidly growing cells and contribute to ExpR-dependent regulation of gene expression at high cell densitites.

In *C. crescentus*, evidence for c-di-GMP gradients inside bacterial cells was provided based on specific subcellular localizations of DGCs and PDEs, which restrict signaling events to specific sites of the cell (Huitema *et al.*, 2006; Christen *et al.*, 2010; Abel *et al*., 2011; Lori *et al.*, 2015). Localization of PleD, SMb20523, SMb20447, SMc01464, SMc03178 and SMb21517 was analyzed in *S. meliloti* by replacing the encoding genes with *egfp* fusion constructs at their native genomic loci. Fluorescence signals were detected in Rm2011 producing PleD-EGFP, SMb20447-EGFP and SMc01464-EGFP indicating expression of the corresponding genes in laboratory conditions (Ch. 6, Fig. S6). In the case of PleD-EGFP, exponentially growing cells displayed one focus at one cell pole. Time-lapse microscopy revealed PleD-EGFP localization to the newly developed cell pole (Ch. 6, Fig. 6b). In contrast, *C. crescentus* PleD localizes in its active form to the stalked cell pole where it acts in polar differentitation and stalk biogenesis (Paul *et al.*, 2004). Although the *C. crescentus* and *S. meliloti* PleD proteins share 51 % identity, their modes of regulation and roles in the cell cycle may be different. This notion was supported by different phenotypes of the mutant strains, as the *S. meliloti pleD* mutant did not differ from the wild-type in motility (Ch. 6, Fig. S1), while the *C. crescentus pleD* mutant was shown to be hypermotile due to defects in flagellum ejection and stalk morphogenesis (Hecht & Newton, 1995). Similarly to the *S. meliloti pleD* mutant, an *A. tumefaciens pleD* deletion mutant was unaffected in motility and showed no obvious developmental defects (Kim *et al.*, 2013). PleD could therefore have evolved different cellular functions in *C. crescentus* and *S. meliloti.*

Summarizing, c-di-GMP was found to regulate multiple cellular functions in *S. meliloti* since artificially increased c-di-GMP levels promoted production of surface

polysaccharides and attachment, whereas motility and accumulation of AHLs were attenuated. In this context, c-di-GMP-dependent regulation appeared to take place at both transcriptional and post-translational levels. This was consistent with observations made for other bacterial species in which c-di-GMP was described as a key regulatory player in the motility-to-sessility transition (Römling *et al.*, 2013). Environmental conditions triggering increases in intracellular c-di-GMP levels may therefore favor a sedentary lifestyle of free-living *S. meliloti* in its natural soil habitat.

3.1.3 c-di-GMP binds to the single-domain PilZ protein McrA to regulate swimming motility

PilZ domain proteins are known to be involved in regulation of motility in various bacterial species, as they either repress motility in *C. crescentus*, *E. coli* and *B. subtilis* (Christen *et al.*, 2007; Boehm *et al.*, 2010; Chen *et al.*, 2012) or stimulate it in *Azospirillum brasilense*, *Borrelia burgdorferi* and *Treponema denticola* (Pitzer *et al.*, 2011; Bian *et al.*, 2013; Russell *et al.*, 2013). For instance, YcgR from *E. coli* interacts with flagellar motor proteins to reduce flagellar rotation speed (Boehm *et al.*, 2010; Paul *et al.*, 2010) and *P. aeruginosa* MapZ interacts with a chemotaxis methyltransferase to control flagellar motor switching (Xu *et al.*, 2016).

To functionally characterize the two single-domain PilZ proteins SMc00507 and SMc00999 from *S. meliloti*, loss-of-function mutants were analyzed for their ability to retain c-di-GMP-associated phenotypic changes. Overexpression of *pleD* in strains lacking SMc00507 (renamed McrA, for motility-associated c-di-GMP receptor A) did not result in repressed swimming motility, whereas strains lacking SMc00999 were not considerably affected in any of the analyzed phenotypes (Ch. 6, Fig. S11). Furthermore, Rm2011 simultaneously overexpressing *pleD* and *mcrA* was non-motile and affected in surface attachment compared to a strain overexpressing only *pleD* (Ch. 6, Fig. 3). Reduced surface attachment upon *pleD-mcrA* overexpression was a result of strongly repressed swimming motility, because different flagellar mutants overexpressing *pleD* were also impaired in adherence (Ch. 6, Fig. S9). This finding indicated that flagellar motility is important for c-di-GMP-mediated surface attachment of *S. meliloti*, which is in agreement with the observation that flagellar motility accelerates surface adhesion of various bacteria (Karatan & Watnick, 2009). The phenotype of Rm2011 Δ*mcrA* overexpressing *pleD* was complemented by additional overexpression of *mcrA*, whereas $mcrA_{\mathrm{AxxxA}}$ encoding a protein variant containing mutations in the conserved RxxxR

motif of PilZ domains was unable to further repress motility (Ch. 6, Fig. 9d). This result suggested that McrA may bind c-di-GMP *in vivo* and is involved in regulation of swimming motility in *S. meliloti*.

Direct interaction between McrA and c-di-GMP was confirmed by differential radial capillary action of ligand assay (DRaCALA; Roelofs *et al.*, 2011) (performed by Dr. Dorota Skotnicka). Spotting purified His_6-McrA preincubated with [α-^{32}P]-labeled c-di-GMP on a nitrocellulose membrane allowed detection of an intense signal in the centre of the spot indicating positive interaction (Ch. 6, Fig. 9b). This pattern was not observed when either unlabeled c-di-GMP was added to the reaction or His_6-$McrA_{AxxxA}$ instead of the wild-type variant was used, further suggesting direct interaction between McrA and c-di-GMP (Ch. 6, Fig. 9b). Evidence for conformational changes of McrA upon c-di-GMP binding was provided by an increase in relative fluorescence of Rm2011 expressing *mcrA* fused to *cypet* and *ypet* at both termini (Ch. 6, Fig. 9c). This result indicated that in a c-di-GMP-bound state both McrA termini get in close proximity. In the case of *Salmonella* PilZ domain proteins YcgR and BcsA, tested in a similar experimental setup, c-di-GMP binding triggers conformational changes that result in increased distance between the termini (Pultz *et al.*, 2012). This discrepancy may exemplify increased complexity and different modes of PilZ domain-derived downstream signaling.

McrA is a small protein of 101 amino acids solely comprising a PilZ domain. Such architecture is not uncommon. However, not much is known about the functions of these proteins. DgrA and DgrB are stand-alone PilZ domain proteins involved in c-di-GMP-dependent repression of motility in *C. crescentus*. DgrA binds c-di-GMP *in vitro*, and its overexpression results in decreased abundance of the flagellar rotation protein FliL via an unknown mechanism (Christen *et al.*, 2007). Although no significant homology exists between McrA and DgrA, the congruent architecture comprising just a PilZ domain implies that their function likely relies on interactions with other proteins. Thus, it is tempting to speculate that McrA intramolecular structural rearrangements upon c-di-GMP binding facilitate protein-protein interactions to initiate downstream signaling events.

The functional redundancy of DGCs in repression of Rm2011 swimming motility raised the question if numerous c-di-GMP signaling pathways are integrated by McrA. To address this question, swimming motility of Rm2011 and Rm2011 Δ*mcrA*, both overexpressing either *pleD, SMb20523, SMb20447, SMc01464* or *SMc03178*, was

compared (performed by Vincent Franz). Motility was repressed in both strains upon overexpression of *SMb20523, SMb20447, SMc01464* and *SMc03178*, whereas inhibiton of motility upon *pleD* overexpression was observed only in the wild-type strain (Fig. 4). This data suggested McrA being a c-di-GMP receptor that specifically responds to signals from the DGC PleD, which might include a direct interaction between both proteins. By contrast, c-di-GMP-dependent repression of motility irrespective of McrA regulatory function may include a mechanism for blocking secretion of flagellar proteins. c-di-GMP binding to *S. meliloti* FliI was previously shown to inhibit its flagellar export ATPase activity (Trampari *et al.,* 2015), whereas c-di-GMP binding to the C-terminus of FliF, resembling the PilZ domain in size and signature motif RxxxRx$_{21}$DxSxxG, remains to be investigated.

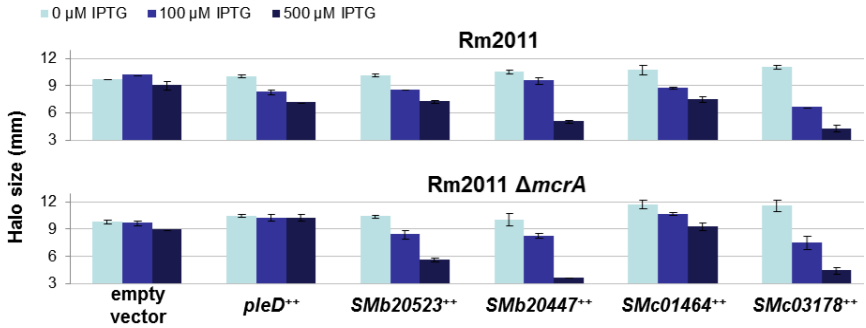

Figure 4. McrA-mediated repression of motility is specific to PleD-derived signaling. Liquid cultures of Rm2011 wild-type and Rm2011 Δ*mcrA,* both harboring either IPTG-inducible expression vector pWBT (provided by M. McIntosh) or pWBT carrying indicated DGC-encoding genes, were spotted on semi-solid TY agar supplemented with the indicated IPTG concentrations. Swimming motility was assessed by measuring the halo diameter after incubation for three days at 30 °C. Error bars represent the standard deviation of three biological replicates. Adapted from Vincent Franz (2015).

Involvement of McrA in regulation of swimming motility was elucidated by recording trajectories of actively moving *S. meliloti* cells. Overexpression of *pleD-mcrA* abolished swimming in a medium containing 20 % Ficoll, whereas cells harboring the empty vector control were still motile (Fig. 5a). To get a hint whether McrA function is related to flagellar assembly or to rotation, flagellar basal body protein FliG was fused to EGFP in order to study its localization in Rm2011. Fluorescence signals were detected in the majority of exponentially growing cells and indistinguishable for cells either haboring the empty vector control or overexpressing *pleD-mcrA* (Fig. 5b). This result suggested presence of functional flagellar basal bodies in the non-motile cells. Unlike *E. coli* and *P. aeruginosa*, flagella of motile *S. meliloti* cells rotate only clockwise, while rotary speed can be modulated by slowing flagellar rotation (Attmannspacher *et al.*, 2005). McrA-mediated regulation of swimming motility may therefore slow down flagellar rotation speed.

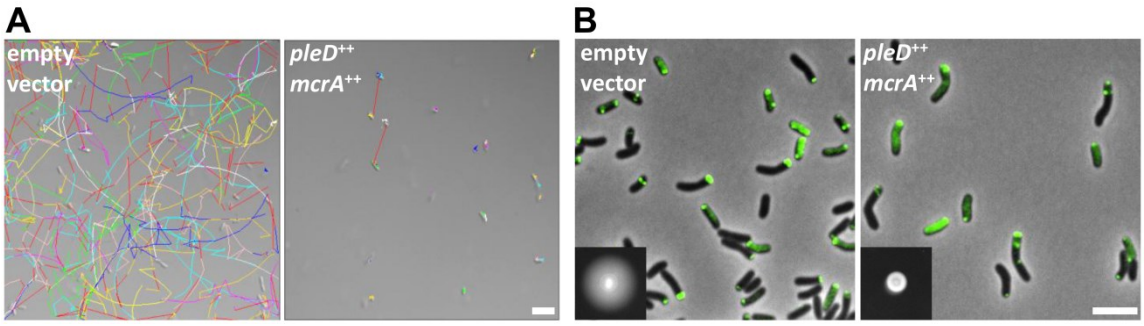

Figure 5. McrA slows down swimming speed, but does not affect presence of flagellar motor switch protein FliG. (A) Rm2011 wild-type, harboring either empty vector pWBT (provided by M. McIntosh) or pWBT carrying *pleD* and *mcrA*, was grown in liquid TY medium supplemented with 0.5 mM IPTG. Exponentially growing cells were collected by centrifugation and resuspended in medium containing 20 % Ficoll. Videos were recorded for a 10 s time period using DIC microscopy. Trajectories of single cells were calculated using ImageJ plugin Particle Tracker. Bar, 5 µm. **(B)** Rm2011 *fliG-egfp*, expressing *egfp*-tagged *fliG* from the native genomic location and harboring either empty vector pWBT or pWBT carrying *pleD* and *mcrA*, was grown to exponential growth phase in liquid TY medium containing 0.5 mM IPTG and cells were analyzed by fluorescence microscopy. Insets show halos indicating swimming motility of the respective strains. Bar, 5 µm.

3.2 CuxR is a new type of c-di-GMP-responsive transcription factor and regulates extracellular polysaccharide production

3.2.1 c-di-GMP, CuxR and MucR regulate transcription of a gene cluster governing biosynthesis of a new extracellular polysaccharide

Gene expression controlled by c-di-GMP at the level of transcription was examined by transcriptome profiling of Rm2011 at elevated c-di-GMP levels. Expression of five genes, namely *uxs1*, *SMb20460, SMb20462, SMb20463* and *hemK1,* was significantly upregulated upon overexpression of *pleD* (Ch. 7, Tab. S1). The first four of these genes clustered together with *uxe* and *SMb20461* on megaplasmid pSymB forming the putative six-gene operon *uxs1-SMb20463* (Fig. 6a). Transcriptional activation of *uxs1-SMb20463* was confirmed by stimulated EGFP production in Rm2011 carrying *uxs1* promoter (P*uxs1*)-*egfp* fusion at elevated c-di-GMP levels. Overproduction of several DGCs in Rm2011 increased fluorescence signals by about 16-fold compared to non-induced conditions, whereas $PleD_{GGAAF}$ was unable to stimulate EGFP production (Ch. 7, Fig. 2a). This result indicated regulation of P*uxs1* activity by c-di-GMP.

Enzymatic activities of Uxs1 and Uxe as UDP-xylose synthase and UDP-xylose 4′-epimerase, respectively, were experimentally verified by Gu *et al.* (2011). SMb20460 was annotated as family 2 GTase with eight predicted TM α-helices facilitating localization to the cytoplasmic membrane. The central GTase domain, flanked by two TM α-helices on the N-terminal side and six TM α-helices on the C-terminal side, is

likely located in the cytoplasm. SMb20461, SMb20462 and SMb20463 were annotated as signal peptide proteins and predicted to localize to the periplasmic space without a membrane-anchoring α-helix. SMb20462 was annotated as a member of glycosylhydrolase family 26 involved in endohydrolysis of glucosidic linkages. SMb20461 and SMb20463 both contain a domain of unknown function (DUF995) and share 38 % amino acid sequence identity, while SMb20463 is shorter by approximately 20 amino acids at both termini. Secondary structure analysis of both hypothetical proteins revealed presence of eight sequential β-strands that might form a β-barrel and facilitate localization to the outer membrane. Taken together, bioinformatic analyses indicated that the gene products of *uxs1-SMb20463* could be involved in biosynthesis of a polysaccharide compound (further referred to as c-di-GMP-regulated uncharacterized polysaccharide, CUP).

The ability of Rm2011 to produce CUP was assayed by growing wild-type and mutant strains on solid medium containing CR. Strains with interrupted *uxs1-SMb20463* and producing c-di-GMP at elevated levels were unable to bind CR indicating a lack of CUP production (Ch. 7, Fig. 1a & c). In addition, ectopic expression of the complete *uxs1-SMb20463* gene cluster under the control of an IPTG-inducible promoter in Rm2011 resulted in increased CR staining (Ch. 7, Fig. 1d). These results strongly suggested that transcriptional activation of *uxs1-SMb20463* governing CUP biosynthesis was responsible for enhanced CR binding by Rm2011 at elevated c-di-GMP levels. Phylogenetic analysis suggested that other species from the Rhizobiaceae could also be able to produce CUP, as the complete putative *uxs1-SMb20463* operon was conserved in *Sinorhizobium medicae*, while sequences homologous to the *uxs1-SMb20460* portion were found in *Sinorhizobium fredii* NGR234, *Sinorhizobium americanum, Rhizobium* sp. NGR234 and *R. leguminosarum*.

Closer inspection of the genomic context in Rm2011 identified a gene encoding a putative transcriptional regulator from the AraC family (*SMb20457*) upstream of the *uxs1-SMb20463* gene cluster (Fig. 6a). To test whether this protein was involved in c-di-GMP-mediated transcriptional activation of *uxs1-SMb20463*, P*uxs1* activity was measured in strains containing a mutagenic plasmid in *SMb20457*. Rm2011 lacking SMb20457 and overexpressing *pleD* did not display activation of P*uxs1* (Ch. 7, Fig. 2b). Likewise, overexpression of *SMb20457* in c-di-GMP-depleted strain Rm2011 c-di-GMP^0 did not result in P*uxs1* activation (Ch. 7, Fig. 2c). Overexpression of both *pleD* and *SMb20457* resulted in a 50-fold or 23-fold higher fluorescence signal than

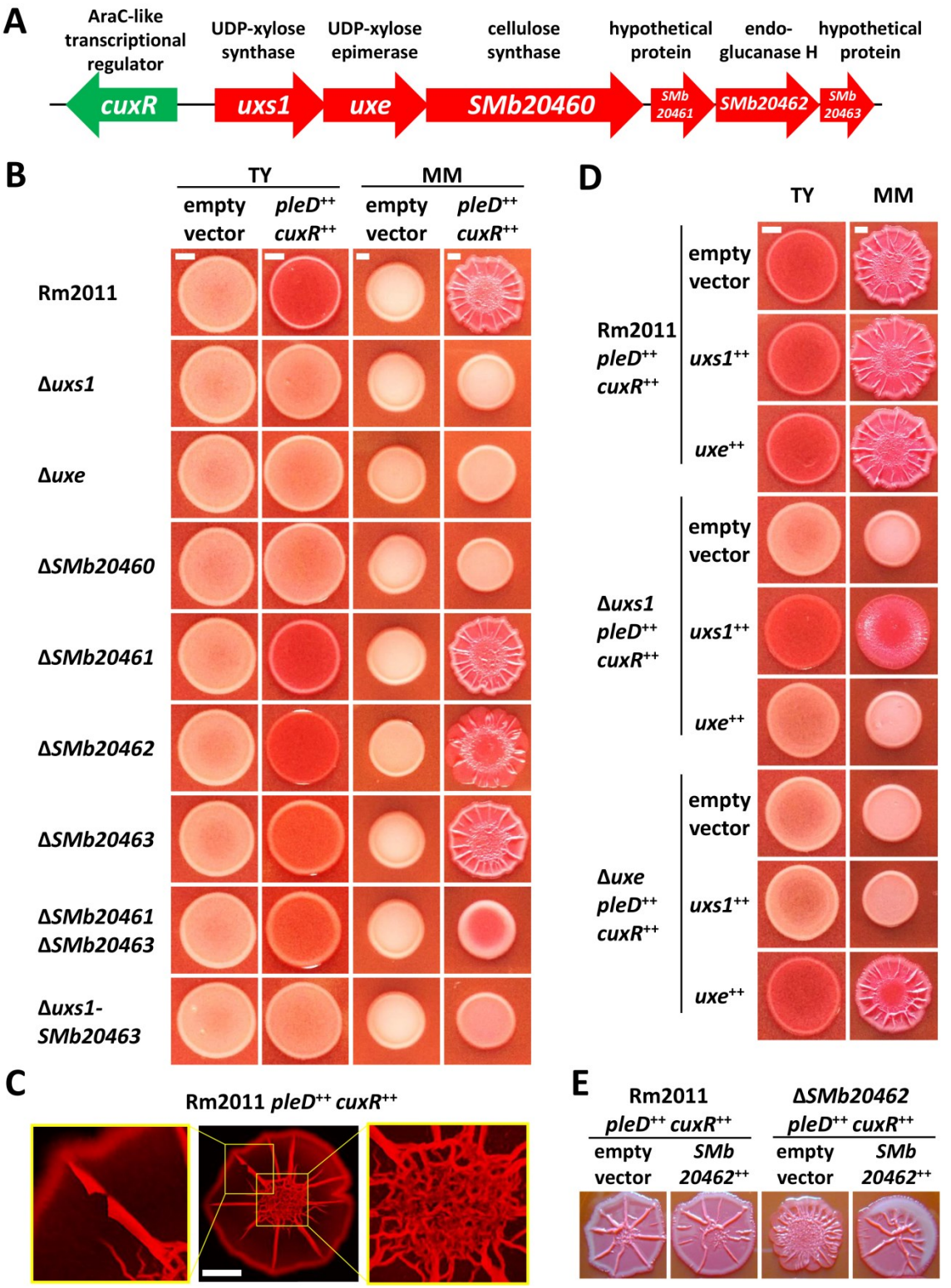

Figure 6. *uxs1*, *uxe* and *SMb20460* are essential for CUP biosynthesis in *S. meliloti* Rm2011. **(A)** Schematic representation of the *uxs1-SMb20463* gene cluster and upstream located *cuxR* (*SMb20457*) with indicated gene annotations. **(B)** Rm2011 wild-type and mutant strains, each harboring either medium-copy number plasmid pWBT (provided by M. McIntosh) or pWBT carrying *pleD* and *cuxR*, grown on TY and MM agar supplemented with CR and 0.5 mM IPTG. Bars, 2 mm. **(C)** Macro-colony of Rm2011 wild-type, harboring pWBT-*pleD-cuxR* and constitutively expressing *mCherry in trans*, grown on MM agar supplemented with CR and 0.1 mM IPTG for three days at 30 °C. Images were acquired with a binocular using the red fluorescence channel. Bar, 5 mm. **(D)** Rm2011 wild-type, Rm2011 Δ*uxs1* and Rm2011 Δ*uxe,* each harboring pWBT-*pleD-cuxR* and either low-copy number plasmid pR_EGFP (Torres-Quesada *et al.*, 2013), pR-*uxs1* or pR-*uxe*, grown on TY and MM agar supplemented with CR and 0.5 mM IPTG. Bars, 2 mm. **(E)** Rm2011 wild-type and Rm2011 Δ*SMb20462*, both harboring pWBT-*pleD-cuxR* and either pR_EGFP or pR-*SMb20462*, grown on MM agar supplemented with CR and 0.5 mM IPTG.

single *pleD* and *SMb20457* overexpressions, respectively (Ch. 7, Fig. 2c). Thus, *SMb20457* (renamed c-di-GMP-responsive UDP-xylose regulator, *cuxR*) was required for c-di-GMP-dependent activation of P*uxs1*.

In order to functionally characterize single genes of the putative operon *uxs1-SMb20463*, Rm2011 deletion mutants were tested for their ability to retain the CR phenotype. The wild-type strain overexpressing *pleD-cuxR* formed red colored macro-colonies upon growth on TY and MM agar, while growth on the latter medium promoted vigorous colony expansion and formation of wrinkles (Fig. 6b). Closer inspection at higher magnification and resolution revealed a symmetric architecture and the formation of 3D structures within such a macro-colony, suggesting a multicellular-like behavior (Fig. 6c). Noteworthy, removal of CR from the medium abolished the colony expansion and formation of wrinkles indicating that CR is required for expression of this phenotype. Deletion of *uxs1*, *uxe* or *SMb20460* resulted in a loss of the CR phenotype similar to strains lacking the complete *uxs1-SMb20463* gene cluster or harboring the empty vector control (Fig. 6b). The CR phenotype was restored by ectopic expression of *uxs1* and *uxe* in the respective mutants, while no cross-complementation was observed (Fig. 6d). Strains containing single gene deletions of *SMb20461, SMb20462* and *SMb20463* were not notably affected in their ability to bind CR (Fig. 6b). However, macro-colonies of Rm2011 lacking *SMb20462* and grown on MM displayed a pronounced wrinkling phenotype, which was complemented with plasmid-borne *SMb20462* (Fig. 6b & e). Moreover, Rm2011 lacking both *SMb20461* and *SMb20463* showed reduced colony expansion and diminished formation of wrinkles upon growth on MM (Fig. 6b). Summarizing, *uxs1*, *uxe* and *SMb20460* were considered as essential for CUP production, whereas *SMb20461, SMb20462* and *SMb20463* likely encode proteins with accessory functions. SMb20462 may determine the molecular weight of CUP, while functionally redundant SMb20461 and SMb20463 may be involved in modification of CUP.

In enterobacteria *E. coli* and *Salmonella* Typhimurium, a multicellular and aggregative behavior on plates, designated as rdar (red, dry and rough) morphotype, has been described (Zogaj *et al.*, 2001). Enhanced production of the two extracellular components cellulose and aggregative fimbriae accounts for the expression of the rdar morphotype, which has been linked to survival in nutrient-limited environments. Based on the striking similarity of the rdar morphotype and colony morphology of Rm2011 producing CUP, it is tempting to speculate that CUP biosynthesis is part of a survival

strategy of soil-dwelling *S. meliloti.*

This notion was tested by evaluating the potency of CUP-producing Rm2011 for the formation of biofilms on hydrophobic and hydrophilic abiotic surfaces. Rm2011 wild-type and EPS I/EPS II-deficient Rm2011 Δ*exoP-Z wgeB*$^-$, both ectopically expressing *uxs1-SMb20463*, attached to polystyrene two- to three-fold more efficient than strains harboring the empty vector control (Fig. 7a). Overexpression of *pleD-cuxR* in Rm2011 resulted in strong adherence to glass irrespective of EPS I and EPS II production, while strongly dependent on presence of the *uxs1-SMb20463* gene cluster. The glass surface-attached cells were strikingly resilient, because neither addition of organic solvents nor heat treatment was sufficient to disperse these biofilms (Fig. 7b). These data suggested binding capacity of CUP to diverse substrates, thus broadening the spectrum of biotic and abiotic surfaces potentially colonized by *S. meliloti* in the rhizosphere.

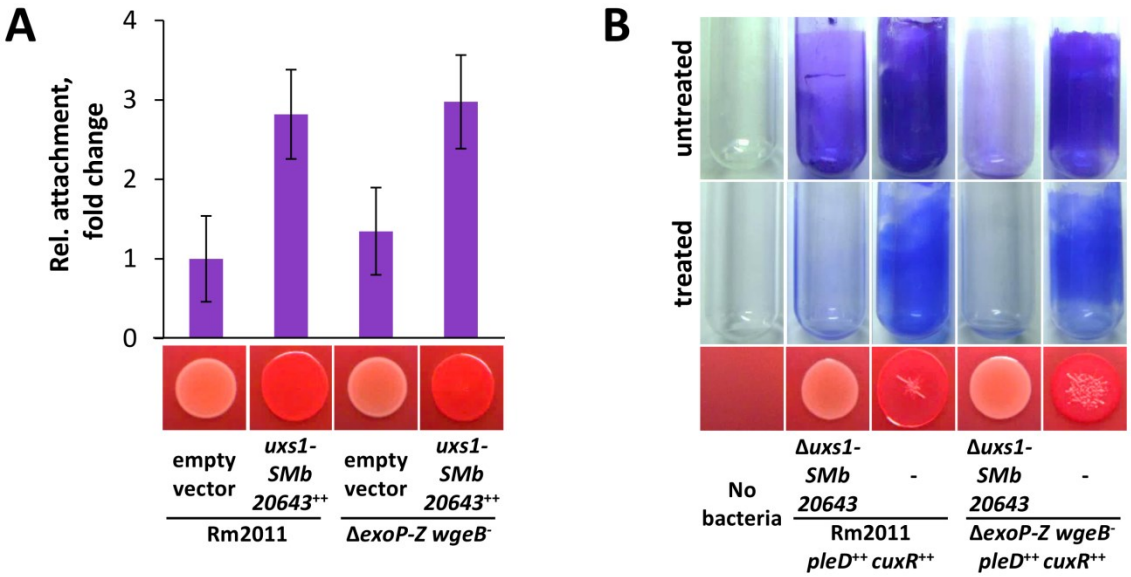

Figure 7. CUP biosynthesis governed by the *uxs1-SMb20463* gene cluster facilitates surface attachment of *S. meliloti* Rm2011. (A) Rm2011 wild-type and EPS I/EPS II-deficient Rm2011 Δ*exoP-Z wgeB*$^-$, both harboring either medium-copy number plasmid pSRKGm (Khan *et al.*, 2008) or pSRKGm carrying the *uxs1-SMb20463* gene cluster, grown on TY agar supplemented with CR and 0.5 mM IPTG. The indicated strains were tested for attachment to polystyrene as described in Chapter 6. Attachment is shown relative to that of Rm2011 harboring pSRKGm. Error bars represent the standard deviation of six biological replicates. **(B)** Rm2011 wild-type and mutant strains, each harboring pWBT-*pleD-cuxR*, were tested for CR binding as described in panel A and attachment to glass surface. The latter was assayed by growing the strains in MM supplemented with 0.5 mM IPTG in glass tubes for two days at 30 °C with shaking at 200 rpm. Bacterial cultures (with similar OD_{600} values) were removed from the tubes, which were then washed with distilled water, filled with 0.1 % (w/v) Crystal violet solution, washed two additional times, and dried ('untreated'). Cell material attached to the glass tubes was additionally incubated in detaching solution (80 % acetone, 20 % ethanol) for one hour at 60 °C and tubes were rigorously vortexed. The liquid was removed from the tubes prior to imaging ('treated').

Besides *uxs1-SMb20463*, *exoP-Z* and *wgeB,* the gene *exoB* was deleted and tested for its relevance to CUP production. UDP-glucose 4′-epimerase activity of ExoB in *S. meliloti*

is important for EPS I and EPS II biosynthesis, LPS composition, and nitrogen fixation during symbiosis with the host plant (Putnoky *et al.*, 1990; Williams *et al.*, 1990; Buendia *et al.*, 1991; Reuhs *et al.*, 1995). The CR phenotype of Rm2011 Δ*exoB* overexpressing *pleD-cuxR* was similar to that of the wild-type strain, indicating this gene not to be essential for CUP biosynthesis. Nevertheless, comparative sequence analysis revealed 52 % amino acid sequence identity between ExoB and Uxe. Functional redundancy of both proteins was tested by a complementation experiment using Rm2011 Δ*exoB* overexpressing either *dgcA-cuxR* (stimulation of CUP production by transcriptional activation of *uxs1-SMb20463*; Fig. 8a) or *uxe*. In both cases, Rm2011 Δ*exoB* macro-colonies were stained with CF and displayed a mucoid phenotype, indicating reconstituted EPS I and EPS II production in this strain, respectively (Fig. 8b-c). Moreover, cell extracts of Rm2011 Δ*exoB* overexpressing *uxe* revealed upper LPS-1 and fast-migrating LPS-2 (considered as smooth and rough LPS, respectively; Sharypova *et al.*, 2003), whereas the empty vector control displayed no smooth LPS and only LPS with high SDS-PAGE mobility (Fig. 8d). Accordingly, delayed nodulation and formation of pseudonodules on *M. sativa* roots by Rm2011 Δ*exoB* was suppressed upon *uxe* overexpression (Fig. 8e-f). Thus, *uxe* was sufficient to complement the pleiotropic phenotype of Rm2011 Δ*exoB*. These data strongly suggested that Uxe functions as dually active nucleotide sugar epimerase and is able to convert UDP-glucose to UDP-galactose besides its UDP-xylose 4′-epimerase activity.

Since UDP-glucose 4′-epimerase activity conferred by ExoB in *S. meliloti* and other alpha-rhizobial species is important for symbiosis with host plants, factors that control expression of functionally redundant *uxe* might be of special interest. c-di-GMP-mediated CUP production was more pronounced in a strain lacking global repressor MucR (Ch. 7, Fig. 1a). In agreement with this observation, P*uxs1* activity was strongly increased in Rm2011 Δ*mucR* compared to the wild-type strain (Fig. 9a). The increase in fluorescence signal was mainly dependent on both the presence of functional *cuxR* and native c-di-GMP levels (Fig. 9a). In addition, *cuxR* promoter (P*cuxR*) activity was about four-fold increased in Rm2011 Δ*mucR*, but not altered in strains lacking CuxR (Fig. 9a). Absence of MucR might therefore contribute to higher abundance of CuxR, which is not transcriptionally autoregulated. Taken together, these results suggested that *cuxR* and the *uxs1-SMb20463* gene cluster are part of the *mucR* regulon. In this context, MucR likely prevents c-di-GMP-bound CuxR from activating P*uxs1* and therefore controls expression of *uxe* with potential relevance to symbiosis.

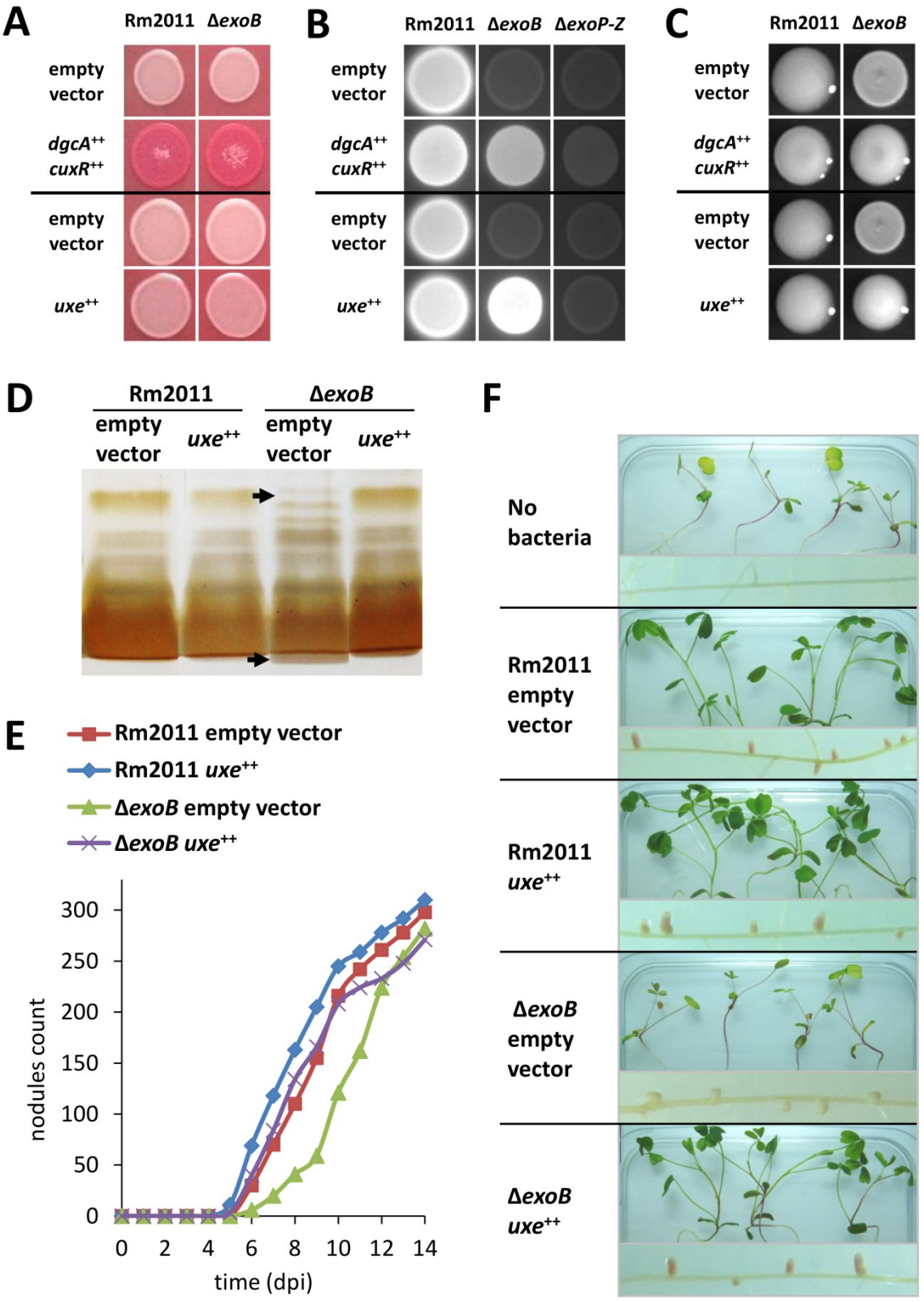

Figure 8. *uxe* complements pleiotropic *S. meliloti* Rm2011 *exoB* mutant phenotype. (A-C) Rm2011 wild-type and Rm2011 Δ*exoB*, both harboring either integrative plasmid pSM10 (Selbitschka *et al.*, 1995), pSM10 carrying *dgcA* and *cuxR,* medium-copy number plasmid pSRK (Torres-Quesada *et al.*, 2013) or pSRK carrying *uxe*, grown on (A) TY agar supplemented with CR, (B) LB agar supplemented with CF (UV-illuminated for image acquisition) or (C) phosphate-limiting MM agar. **(D)** Silver-stained SDS gel (16 %) with proteinase K-treated EDTA-TEA extracts obtained from the indicated *S. meliloti* strains. Arrows indicate upper LPS-1 and fast-migrating LPS-2. **(E)** Nodulation kinetics determined for 48 plants per strain. **(F)** Plant shoots and roots of *M. sativa* inoculated with the indicated *S. meliloti* strains (21 dpi). Experiments were performed with supporting help from Heiko Wendt. dpi, days post inoculation.

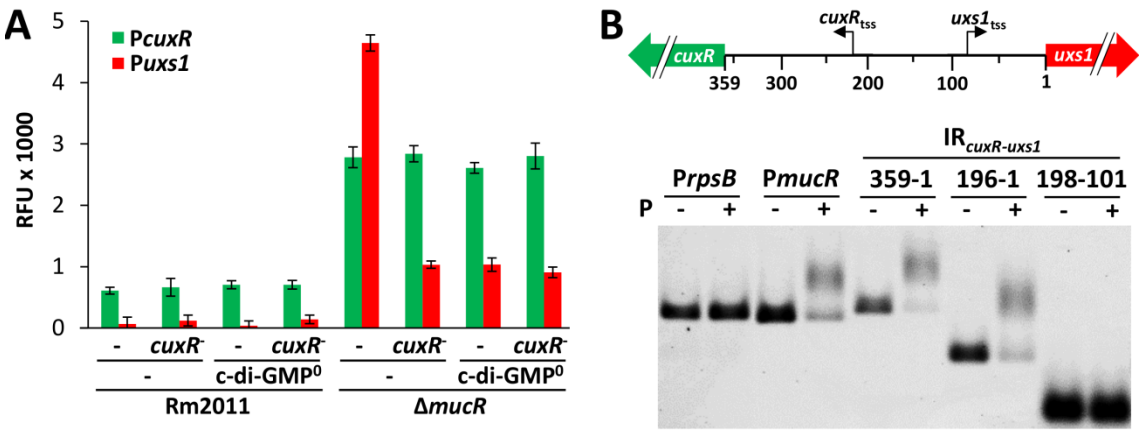

Figure 9. MucR regulates CUP production upon direct interaction with the *cuxR-uxs1* intergenic region. (A) Promoter activities of *cuxR* ('P*cuxR*') and *uxs1* ('P*uxs1*') measured using promoter-*egfp* fusions. Rm2011 wild-type and mutant strains, each harboring medium-copy number plasmid pSRKGm (Khan *et al.*, 2008) carrying promoterless *egfp*, P*cuxR-egfp* or P*uxs1-egfp*, were grown in TY medium to exponential growth phase. Fluorescence was normalized to the OD_{600} of the cultures ('RFU') and values obtained for promoterless *egfp* controls were subtracted. Error bars represent the standard deviation of four biological replicates. **(B)** His_6-MucR (P) interaction with DNA was assayed in an EMSA using fragments containing either the *rpsB* promoter region ('P*rpsB*'; negative control), the *mucR* promoter region ('P*mucR*'; positive control) or (portions of) the *cuxR-uxs1* intergenic region ('$IR_{cuxR\text{-}uxs1}$'). Numbers refer to nucleotides within the $IR_{cuxR\text{-}uxs1}$. Putative transcription start sites ('tss') are indicated (Sallet *et al.,* 2013).

Direct interaction between MucR and DNA containing the *cuxR-uxs1* intergenic region ($IR_{cuxR\text{-}uxs1}$) was probed by electrophoretic mobility shift assay (EMSA). Functionality of purified His_6-MucR protein was verified using DNA fragments upstream of ribosomal protein-encoding *rpsB* and autoregulated *mucR* as negative and positive controls, respectively. A shift of the DNA containing the $IR_{cuxR\text{-}uxs1}$ was observed after pre-incubation with His_6-MucR indicating protein binding (Fig. 9b). Using truncated variants of the $IR_{cuxR\text{-}uxs1}$ suggested the presence of a MucR binding site within the 100 bp region upstream of the *uxs1* start codon (Fig. 9b). Binding of both MucR and CuxR to the $IR_{cuxR\text{-}uxs1}$ might imply a mechanism for antagonistic regulation of *uxs1-SMb20463* transcription and CUP biosynthesis.

Collectively, c-di-GMP-, CuxR- and MucR-dependent regulation of CUP production provided an example for the integration of the c-di-GMP network into the regulatory network for opposing control of EPS biosynthesis and motility in *S. meliloti*. Another example for crosstalk between these two cellular networks was provided by Pérez-Mendoza *et al.* (2015), who demonstrated that biosynthesis of a mixed-linkage (ML) β-glucan is regulated at transcriptional and post-translational levels by the ExpR/SinI system and c-di-GMP, respectively. High complexity in the regulation of extracellular matrix components might imply integration of multiple environmental stimuli and therefore contribute to high adaptability of *S. meliloti* under changing environmental conditions.

3.2.2 CuxR binds c-di-GMP by a PilZ-like mechanism, forms homodimers, and interacts with the *uxs1* promoter region

Activation of the *uxs1* promoter *in vivo* required both elevated c-di-GMP levels and *cuxR* suggesting a direct interaction between CuxR and c-di-GMP. This notion was tested by subjecting purified His_6-CuxR protein to DRaCALA using radiolabeled c-di-GMP (performed by Dr. Dorota Skotnicka). The increased signal density in the centre of the spotting area was not affected upon addition of unlabeled GTP, whereas detection of a diffuse signal upon addition of unlabeled c-di-GMP evidenced specific competition with its labeled counterpart (Ch. 7, Fig. 3a). In addition, biolayer interferometry (BLI) analysis using His_6-CuxR and biotinylated c-di-GMP (performed by Dr. Magdalena Polatynska) confirmed interaction with a dissociation constant (K_d) of 6.7 µM (Ch. 7, Fig. S1). These results indicated AraC-like transcriptional regulator CuxR to represent a new type of c-di-GMP receptor. Noteworthy, CuxR bound to c-di-GMP with a lower affinity compared to most other c-di-GMP effectors either without (*e.g.*, *C. crescentus* HfsK K_d=0.724 µM, Sprecher *et al.*, 2017; *V. cholerae* MshEN K_d=0.5 µM, Wang *et al.*, 2016; *S. venezuelae* BldD K_d=1.8 µM, Schumacher *et al.*, 2017; *E. coli* BcsE K_d=2.42 µM, Fang *et al.*, 2014; *P. aeruginosa* FleQ K_d=4.1 µM, Matsuyama *et al.*, 2016) or with a PilZ domain (*e.g.*, *C. crescentus* DgrA K_d<0.05 µM, Christen *et al.*, 2007; *K. pneumoniae* MrkH K_d=0.107 µM, Schumacher & Zeng, 2016; *E. coli* YcgR K_d=0.191 µM and BcsA K_d=8.24 µM, Pultz *et al.*, 2012).

Binding of CuxR to a DNA fragment containing the $IR_{cuxR\text{-}uxs1}$ was probed by EMSA. In the absence of c-di-GMP, no binding of CuxR to the $IR_{cuxR\text{-}uxs1}$ was observed. However, in the presence of c-di-GMP, but not GTP, a clear band shift was observed demonstrating c-di-GMP-dependent binding of CuxR to the $IR_{cuxR\text{-}uxs1}$ (Ch. 7, Fig. 3b). To define the CuxR binding site, the $IR_{cuxR\text{-}uxs1}$ was systematically shortened and tested by EMSA. A fragment containing 186 bp upstream of the *uxs1* start codon did not bind CuxR in the presence of c-di-GMP, while a fragment containing 196 bp did (Ch. 7, Fig. 3c). This result showed that sequences crucial for binding of CuxR localized between position 186 and 196 upstream of the *uxs1* start codon. Closer inspection of this region revealed the presence of a direct repeat motif CGGGAT-N_6-CGGGAT that partially overlapped with a palindromic sequence CAATC-N_2-GATTG (Ch. 7, Fig. 3d). P*uxs1*$_{166\text{-}195}$ containing both motifs was sufficient for c-di-GMP-dependent CuxR-binding of the DNA (Ch. 7, Fig. 3e). To further dissect the c-di-GMP-dependent binding of CuxR to P*uxs1*$_{166\text{-}195}$, nucleotides within the direct repeat and the palindromic

region were systematically exchanged. Mutating the direct repeat resulted in a complete loss of DNA binding by CuxR in presence of c-di-GMP, whereas mutating the palindrome did not notably affect the binding (Ch. 7, Fig. 3d & f). The same mutations were introduced in P*uxs1* fused to *egfp* for testing c-di-GMP-dependent stimulation of P*uxs1* activity by CuxR *in vivo*. In agreement with the *in vitro* data, only those promoter mutants that showed a c-di-GMP-dependent binding of CuxR in the EMSAs stimulated c-di-GMP-dependent fluorescence (Ch. 7, Fig. 3f & g). This identified the direct repeat CGGGAT-N_6-CGGGAT as the primary DNA binding site of CuxR within the *uxs1* promoter region.

To gain mechanistic insights into CuxR function, the crystal structure of CuxR was solved (by Dr. Wieland Steinchen) revealing a protein architecture that can be divided into a Cupin-like domain, a helical hairpin (HP), a bi-partite helix-turn-helix (bi-HTH) domain, and a C-terminal helix (CTH) connected to the bi-HTH through a disordered linker of approximately 15 amino acids (Ch. 7, Fig. 4a). The Cupin-like domain was reminiscent of the arabinose-binding domain of AraC from *E. coli* (Soisson *et al.*, 1997), although both domains significantly differed in size and topology (Ch. 7, Fig. S2). Investigation of crystallographic contacts showed that the HP of one CuxR interacted with a symmetry-related HP (Ch. 7, Fig. 4b). In this regard, CuxR was similar to transcriptional regulator AraC, which homodimerizes mediated by α2 of the HP, albeit differences between both proteins were apparent (Ch. 7, Fig. 4c).

To investigate whether homodimerization of CuxR via its HPs is a prerequisite for its c-di-GMP-dependent DNA binding, residues in this putative dimerization interface were exchanged to glutamate and the corresponding protein variants were tested by EMSA. While variant R222E was still able to bind to P*uxs1* in the presence of c-di-GMP, the L200E and N203E variants were not (Ch. 7, Fig. 5a). To consolidate that the inability to bind to DNA was indeed caused by a defect in homodimerization of CuxR, cross-linking experiments with purified His_6-CuxR protein and its variants were performed in the absence and presence of c-di-GMP (by Dr. Wieland Steinchen). While wild-type CuxR and the R222E variants showed a protein band corresponding to a homodimer in the presence of c-di-GMP, the L200E and N203E variants did not (Ch. 7, Fig. 5b). To exclude that the inability of the L200E and N203E variants to homodimerize was caused by impaired c-di-GMP binding, DRaCALAs with CuxR and the three variants were performed confirming c-di-GMP binding (Ch. 7, Fig. 5c). *In vitro* data were in agreement with CR binding and P*uxs1* activation assays employing the overproduced

CuxR variants in a *cuxR* mutant strain also overproducing PleD. In these assays, the R222E variant behaved like native CuxR, while the L200E and N203E variants showed decreased CR staining and P*uxs1* activation (Ch. 7, Fig. 5d). Taken together, these results suggested that the HP of CuxR is important for the c-di-GMP-dependent homodimerization, which is in turn required for DNA binding and stimulation of P*uxs1* activity.

To identify the c-di-GMP binding site of CuxR, hydrogen-deuterium-exchange mass spectrometry (HDX-MS) was employed, a method that allows determination of conformational changes within proteins upon their interaction with ligands (Marciano *et al.*, 2014; Steinchen *et al.*, 2015) (performed by Dr. Wieland Steinchen). Four regions of CuxR (named as R1 to R4) displayed significant differences in deuterium incorporation upon addition of c-di-GMP (Ch. 7, Fig. 6a-b). The HDX-MS results substantiated that c-di-GMP mediates homodimerization of CuxR as shown by the strong stabilization of the R3 region. However, they did not discriminate whether R1, R2 or R4 contained the c-di-GMP binding site. To elucidate which of these regions contributes to c-di-GMP binding, c-di-GMP binding of a CuxR variant lacking the CTH (CuxR-ΔCTH) was probed by DRaCALA. This variant did not show any alteration in c-di-GMP binding suggesting that R4 is not involved in c-di-GMP binding (Ch. 7, Fig. 6c). Multi-sequence alignments of the N-termini of CuxR proteins from various rhizobial species revealed a conserved RxxxR motif in the N-terminal region of the protein. The presence of this motif seemed to be restricted to rhizobial species and resembled the RxxxR motif found in PilZ domain proteins involved in c-di-GMP binding (Amikam & Galperin, 2006; Ryjenkov *et al.*, 2006) (Ch. 7, Fig. S4). Substitution of both arginines with alanine (*i.e.*, R24A and R28A) eliminated c-di-GMP binding to CuxR in the DRaCALA (Ch. 7, Fig. 6c). Additionally, a screen for residues located in region R2 and its close proximity revealed that R162 is critical for c-di-GMP-dependent binding of CuxR to DNA (Ch. 7, Fig. S5). This R162A variant showed impaired c-di-GMP binding in the DRaCALA (Ch. 7, Fig. 6c). Both R162A and R24-R28 variants were unable to form homodimers and did not bind to DNA in the presence of c-di-GMP (Ch. 7, Fig. 6d-e). *In vivo*, these CuxR variants failed to stimulate P*uxs1* activity and showed reduced CR staining (Ch. 7, Fig. 6f).

Conclusively, the CuxR mode of c-di-GMP binding was highly reminiscent to that of PilZ domains (Ch. 7, Fig. 7). In the PilZ domain, two intercalated c-di-GMP molecules primarily interact with the two arginines present within the conserved RxxxR motif of

the disordered N-terminus. Additionally, one of the two intercalated c-di-GMP molecules interacts with amino acid side chains at the outer surface of the β-barrel of PilZ through a (D/N)x(S/A)xxG motif (Amikam & Galperin, 2006; Ryjenkov *et al.*, 2006; Römling *et al.*, 2013). A conserved arginine residue (*i.e.*, R95 in *P. aeruginosa* Alg44) provided by the β-barrel establishes further contact to one c-di-GMP molecule and influences the number of c-di-GMP bound to the protein (Whitney *et al.*, 2015) (Ch. 7, Fig. 7). In this regard CuxR showed surprising similarities to PilZ. CuxR primarily interacts with c-di-GMP via a conserved RxxxR motif present within its disordered N-terminus. Additionally, the outer surface of the β-barrel of its Cupin-like domain is involved in c-di-GMP binding (Ch. 7, Fig. 7). PilZ and CuxR could therefore provide an example of convergent evolution in which c-di-GMP binding sites of similar topology have evolved independently in two distinct protein families. Considering that c-di-GMP often binds to the surface of protein domains with only a few amino acids (mainly involving arginine residues), a protein needs only small modifications that are sufficient to acquire the ability to sense this signaling molecule (Jenal *et al.*, 2017, Krasteva & Sondermann, 2017). Hence, regulation of CUP biosynthesis by c-di-GMP binding to AraC-like CuxR could be an example for the recruitment of additional cellular processes into an existing c-di-GMP network during the course of evolution.

3.3 GdcP is a dynamic c-di-GMP phosphodiesterase involved in alpha-rhizobial cell growth and division

Systematic mutagenesis of 22 c-di-GMP-related genes in Rm2011 suggested *SMc00074* (renamed growth zone dynamic c-di-GMP phosphodiesterase, *gdcP*) to be essential. GdcP is a seven-TM receptor (7TMR) from the thus far uncharacterized bacterial protein family 7TMR-DISM (7TMR with diverse intracellular signaling modules; Anantharaman & Aravind, 2003). GdcP is composed of an extracellular globular 7TMR-DISMED2 domain, a membrane-standing 7TMR-DISM_7TM domain, and cytoplasmic PAS, GGDEF and EAL domains. In general, PAS domains serve as versatile sensors and interaction modules in signal transduction proteins (Möglich *et al.*, 2009). In agreement with the non-canonical GGDQF motif in the predicted GGDEF domain of GdcP, an initial *in vitro* assay with purified His_6-$GdcP_{PAS\text{-}GGDEF\text{-}EAL}$ did not reveal DGC activity (Ch. 6, Fig. S2). However, the GdcP GGDEF domain contains an intact I site (RxxD), while all residues required for PDE activity were conserved in the

EAL domain (Ch. 6, Fig. 2). Thus, GdcP might be able to bind and to degrade c-di-GMP.

3.3.1 GdcP primary function

As a first step towards functional characterization of GdcP, a GdcP depletion strain (Rm2011 GdcP^{dep}) was constructed by placing the chromosomally encoded *gdcP* gene under the control of the IPTG-inducible *lac*-T5 tandem promoter and introducing the *lacI* repressor gene *in trans*. Growth of this strain was strongly dependent on the presence of IPTG in the medium (Ch. 8, Fig. 1a). Cells depleted for GdcP displayed altered morphology as they appeared shorter than non-depleted cells (Ch. 8, Fig. 1a). Electron micrographs revealed shorter cells with a wrinkly cell envelope suggesting a loss of cell wall integrity (Ch. 8, Figs. 1b & S14a). In addition, Rm2011 GdcP^{dep} cells were treated with fluorescently-labeled D-amino acid HADA, a substance used for *in situ* probing of cell wall synthesis (Kuru *et al.*, 2012). Upon growth in presence of IPTG, a characteristic HADA staining pattern at the growing cell pole and the prospective division site of pre-divisional cells was observed, whereas only about half of the cells displayed one HADA focus when grown in absence of IPTG (Ch. 8, Fig. 1c). Taken together, these results suggested that *gdcP* is important for cell growth and division by contributing to synthesis of new cell wall material.

To learn about the subcellular localization pattern of GdcP, an in-frame fusion of chromosomal *gdcP* with either *egfp* or *mCherry* was generated at the native genomic location. GdcP-EGFP localized either at one cell pole or the mid-cell region of pre-divisional cells, while HADA and GdcP-EGFP foci showed co-localization (Ch. 8, Fig. 2a). Tracking GdcP-EGFP by time-lapse microscopy revealed a characteristic spatiotemporal subcellular localization pattern of the protein over the cell cycle. The polar fluorescence signal was detected during the entire phase of cell elongation (Ch. 8, Fig. 2b). Fluorescence disappeared from the pole and appeared at the mid-cell region of pre-divisional cells shortly before separation of mother and daughter cells. GdcP-EGFP was detected at both newborn poles after completion of cell division. Time-lapse microscopy at higher time resolution revealed decomposition of the GdcP-mCherry polar focus followed by accumulation of the fluorescence signal at the prospective division site, while no intermediate fluorescent foci were detected along the cell axis (Ch. 8, Fig. 2c). This result pointed either to polar degradation followed by new septal placement of GdcP-mCherry or free diffusion of single GdcP-mCherry molecules that

rendered the fusion non-detectable. Taken together, these data suggested that GdcP cell cylce-dependent localization to the growing pole and the prospective division site correlated with spatiotemporally controlled cell wall synthesis.

To perform functional characterization of GdcP, mutated and truncated (*egfp*-tagged) *gdcP* variants, transcribed with a strength either similar or elevated compared to the native levels, were tested for their ability to restore growth and cell morphology of the GdcP depletion strain. $gdcP_{Wt}$ and $gdcP_{Wt}$-*egfp* fully complemented growth and morphology defects of GdcP depletion strain Rm2011 $GdcP^{dep}$ in medium without IPTG, in contrast to this strain harboring the empty vector controls (Ch. 8, Fig. 3b-c). Mutations in conserved motifs of the GGDEF (RxxD to AxxA, GGDQF to GAAAF) and EAL domains (EAL to AAL) of GdcP did not abolish the complementation of growth and morphology defects of Rm2011 $GdcP^{dep}$ (Ch. 8, Fig. 3b-c). Complete removal of GGDEF or GGDEF-EAL domains in $GdcP_{\Delta GGDEF}$ or $GdcP_{\Delta EAL\Delta GGDEF}$, respectively, resulted in functional but less stable protein variants, as they supported normal proliferation only when produced at elevated levels (Ch. 8, Fig. 3b-c). These results suggested that the essential function of GdcP is probably independent of c-di-GMP and other components of c-di-GMP signaling. Deletion of N-terminal domains 7TMR-DISMED2, 7TMR-DISM_7TM or PAS, alone or in combinations, strongly reduced the ability of GdcP to complement GdcP depletion phenotypes, irrespective of expression levels (Ch. 8, Fig. 3b). Cells expressing these *gdcP* variants were shortened and similar to the empty vector control (Ch. 8, Fig. 3c). Furthermore, these GdcP variants, tagged with EGFP, had lost the characteristic subcellular localization pattern. In the case of $GdcP_{\Delta 7TMR\text{-}DISMED2}$-EGFP and $GdcP_{\Delta 7TMR\text{-}DISMED2\ \Delta 7TMR\text{-}DISM\_7TM}$-EGFP, the fluorescence signal was almost non-detectable, indicating very low protein abundance (Ch. 8, Fig. 3d). These data indicated that the GdcP essentiality resides in its N-terminal part consisting of the periplasmic 7TMR-DISMED2, membrane-incorporated 7TMR-DISM_7TM and cytoplasmic PAS domains. These were required for both the subcellular localization pattern of the protein and culture growth.

This finding has shed new light on the 7TMR-DISM family since, despite the outstanding number of representatives in different bacterial species, only few of them were functionally studied and roles in biofilm formation were supported. The regulatory output can involve either modulation of enzymatic activity of the cytoplasmic part or protein-protein interactions. In *P. aeruginosa*, 7TMR-DISMED2 domain-coupled

histidine kinases RetS and LadS antagonistically regulate sensor histidine kinase GacS, which is central for regulation of biofilm formation (Davies *et al.*, 2007). Whereas RetS inactivates GacS upon heterodimerization of the cytoplasmic domains, LadS activates GacS by phosphorylation (Chambonnier *et al*., 2016). Also in *P. aeruginosa,* the protein NicD contains a 7TMR-DISMED2 domain in tandem with a cytoplasmic GGDEF domain. Binding of glutamate to the 7TMR-DISMED2 domain of NicD promotes both c-di-GMP synthesis and interactions with other proteins, together triggering biofilm dispersal (Basu Roy & Sauer, 2014). GdcP represents the first member of the 7TMR-DISM family with a function related to cell growth and division.

In order to find potential protein interaction partners of GdcP, Rm2011 expressing *gdcP-3xflag* from the native chromosomal location was constructed and subjected to co-immunoprecipitation (CoIP). Among the identified candidate interaction partners of GdcP, the hypothetical TM proteins SMc02432 (renamed growth zone dynamic putative metallopeptidase, GdpM) and SMc00644 were considered promising due to their high abundance and identification with the highest numbers of unique peptides (Ch. 8, Tab. S3). In addition, CoIP with Rm2011 expressing *gdpM-3xflag* identified highly abundant GdcP and SMc00644, further suggesting direct interactions between these proteins (Ch. 8, Tab. S4). Sequences homologous to GdcP and GdpM (and SMc00644) are largely restricted to the Rhizobiales and three unrelated species from the Gammaproteobacteria and Actinobacteria (Ch 8, Fig. S7a). GdpM contains a LytM domain that is characteristic for members from the family of M23 zinc-dependent metallopeptidases (pfam01551). This domain is predicted to have hydrolytic activity with a range of specificities. Closer inspection of the LytM domain of GdpM revealed a conserved HxxxD motif (Ch 8, Fig. S7c), which is known to be required for zinc ion coordination and hydrolysis of glycine-glycine bonds by *Staphylococcus aureus* LytM (Odintsov *et al.*, 2004; Firczuk *et al.*, 2005). Periplasmic localization of GdpM via its N-terminal TM α-helix was experimentally verified by blue staining of agar cultures expressing *gdpM* variants fused to *E. coli phoA* and grown on medium containing alkaline phosphatase substrate BCIP (Ch 8, Fig. S8) (experiment performed by Dr. Elizaveta Krol).

To study GdpM-dependent phenotypes, a GdpM depletion strain (Rm2011 GdpM^{dep}) was constructed by placing the chromosomal *gdpM* under the control of the IPTG-inducible *lac* promoter and introducing the *lacI* repressor gene *in trans,* also because attempts to generate a knockout mutant failed. This strain was strongly impaired in

growth in the absence of IPTG (Ch. 8, Fig. 5a), which further supported essentiality of *gdpM*. Strikingly similar to cells depleted for GdcP, GdpM-depleted cells were shorter than non-depleted cells (Ch. 8, Figs. 5a & 1a). Electron micrographs showed regions of low electron density within the cells which might represent polyhydroxybutyrate (PHB) granules as part of a general stress response (Ch. 8, Figs. 5b & S14b). Moreover, pulse-labeling of GdpM-depleted cells with HADA revealed a fluorescence focus at the prospective division site in only a minority of pre-divisional cells, whereas Rm2011 GdpM^{dep} grown in IPTG-supplemented medium displayed a wild-type like HADA staining pattern (Ch. 8, Fig. 5c). These phenotypic similarities strengthened the hypothesis on a functional relation between GdpM and GdcP.

To study the subcellular localization pattern of GdpM, the chromosomal *gdpM* allele was replaced by a *gdpM-mCherry* fusion at the native genomic location. Microscopy of the resulting strain revealed predominantly diffuse fluorescence, whereas in some cells a GdpM-mCherry focus was detected at one pole and the mid-cell region of pre-divisional cells. Using time-lapse microscopy, a dynamic GdpM-mCherry localization during cell cycle, reminiscent of the GdcP-EGFP pattern, was observed (Ch. 8, Figs. S9a & 2b). Temporary co-localization of both protein fusions over the cell cycle was detected using Rm2011 carrying both *gdcP-egfp* and *gdpM-mCherry* fusions at their native chromosomal locations (Ch. 8, Fig. S9b). Foci formed by both protein fusions at the pole and the prospective division site overlapped with HADA-derived fluorescence signals (Ch. 8, Fig. S9c). The cell cycle-dependent localization of GdcP and GdpM in *S. meliloti* again pointed to a functional relation between both proteins.

As a first step towards functional characterization of GdpM, effects of *gdpM* overexpression were analyzed. In LB medium, growth of GdpM-overproducing Rm2011 was severely impaired and cells appeared enlarged and spheric compared to the empty vector control (Ch. 8, Fig. 6a). Electron microscopy of GdpM-overproducing cells revealed an unusually enlarged periplasm and severe inner membrane invagination (Ch. 8, Figs. 6b & S14c). HADA incorporation by Rm2011 overexpressing *gdpM* was strongly impaired, as only weak and dispersed fluorescence signals were detected (Ch. 8, Fig. 6c). Notably, increasing osmolarity by adjusting the NaCl concentration to 300 mM mitigated the *gdpM* overexpression-associated changes in morphology and growth (Ch. 8, Fig. S11).

To obtain hints towards a putative GdpM metallopeptidase activity conferred by the LytM domain, wild-type *gdpM* and mutant variants were heterologously expressed in

E. coli. GdpM variants with either a single amino acid exchange in the putative zinc ion coordination motif HxxxD ($GdpM_{H510A}$) or a deletion of the complete LytM domain ($GdpM_{\Delta LytM}$) were generated. Leakage of cytoplasmic β-galactosidase from *E. coli* cells was detected, as indicated by purple coloring of agar cultures overexpressing $gdpM_{Wt}$ and grown on medium supplemented with poorly membrane-permeable β-galactosidase substrate CPRG (Ch. 8, Fig. 6d). In line with this, *E. coli* overexpressing $gdpM_{Wt}$ was affected in growth and showed pronounced cell lysis (Ch. 8, Fig. S13). By contrast, *E. coli* overexpressing $gdpM_{H510A}$ and $gdpM_{\Delta LytM}$ showed a negative CPRG phenotype and no cell lysis (Ch. 8, Figs. 6d & S13). These results would be in agreement with metallopeptidase activity of the LytM domain of GdpM targeting cell wall components *in vivo*.

To test whether GdcP and GdpM are involved in cell envelope biogenesis, muropeptides isolated from *S. melioti* Rm2011 depleted for GdcP and GdpM were determined (performed by Hamish Yau). Muropeptide profiles of Rm2011 $GdcP^{dep}$ and Rm2011 $GdpM^{dep}$ grown in presence of IPTG were similar to those obtained for the Rm2011 wild-type (Ch. 8, Fig. 7a). By contrast, depletion of GdcP and GdpM upon growth of the respective strains in absence of IPTG revealed changes in relative abundances of specific muropeptides (Ch. 8, Fig. 7a). Particularly, the accumulation of penta peptides at altered levels of these proteins pointed to impaired incorporation of new material into the growing sacculus and might involve indirect effects. Taken together, these results supported a function of GdcP and GdpM in cell envelope biogenesis.

To gain further mechanistic insights in GdcP and GdpM functions in *S. meliloti*, purified His_6-tagged variants of both proteins were assayed for binding and hydrolysis of peptidoglycan (PG) (performed by Hamish Yau). His_6-$GdpM_{\Delta tm}$ was mixed with *S. meliloti* murein sacculi and sedimented by ultracentrifugation. The protein was exclusively recovered in the pellet fraction, whereas it remained in the supernatant without the addition of sacculi (Ch. 8, Fig. 7b). By contrast, His_6-$GdcP_{7TMR\text{-}DISMED2}$ showed only small binding capacity in the same conditions, as in presence of sacculi the vast majority of protein remained in the supernatant (Ch. 8, Fig. 7b). PG hydrolase activity of His_6-$GdpM_{\Delta tm}$ was assayed by incubation of the protein with various *S. meliloti* murein substrates followed by muropeptide profiling. Presence of His_6-$GdpM_{\Delta tm}$ did not cause evident changes in the muropeptide profiles, which remained also unchanged when His_6-$GdcP_{7TMR\text{-}DISMED2}$ was added to the reaction (Ch. 8,

Fig. S16). Taken together, these results indicated GdpM to be a potent PG-binding protein, whereas hydrolytic activity towards PG was non-detectable *in vitro*. However, it can not be excluded that assay conditions were suboptimal or that an additional factor is required for stimulation of GdpM activity. The latter has been described for *S. aureus* LytM, whose activity is stimulated by proteolytic cleavage (Odintsov *et al.*, 2004; Firczuk *et al.*, 2005).

To test for possible functional conservation of GdcP within the order Rhizobiales, *R. etli* and *A. tumefaciens* homologs were tagged with EGFP and analyzed for their subcellular localization pattern. Localization of these protein fusions to one cell pole and the mid-cell region of pre-divisional cells of the respective hosts, similar to the subcellular localization pattern of *S. meliloti* GdcP-EGFP, was detected (Ch. 8, Fig. 8a). Pulse-labeling of these strains with HADA showed active cell wall synthesis at the sites where GdcP-EGFP foci were observed (Ch. 8, Fig. 8a). Furthermore, *gdcP* and *gdpM* homologs from *R. etli* and *A. tumefaciens* were able to complement growth and morphology phenotypes of Rm2011 GdcP^{dep} and Rm2011 GdpM^{dep}, respectively (Ch. 8, Fig. 8b-c). The similar subcellular localization pattern of GdcP homologs in *S. meliloti*, *R. etli* and *A. tumefaciens* as well as cross-complementation of *gdcP* and *gdpM* between these species provided evidence for a functional conservation of both proteins in the order Rhizobiales.

Members of the order Rhizobiales, including *S. meliloti*, synthesize cell wall at one pole as well as at the mid-cell region of pre-divisional cells (Brown *et al.*, 2012). Coordinating and directing the PG synthesis machinery is a prerequisite for maintaining cell shape after completion of cell division. Cell wall remodeling was studied mostly in rod-shaped *E. coli, B. subtilis* and *C. crescentus,* all utilizing a laterally dispersed mode of PG synthesis. In these organisms, the PG synthesis machinery associates with the cytoplasmic scaffold proteins MreB (elongasome) and FtsZ (divisome), both directing placement and activity of PG synthases from inside the cell. Members of the Rhizobiales lack the lateral PG synthesis scaffold MreB and other related proteins (Margolin *et al.*, 2009), suggesting the presence of alternative factors coordinating PG synthesis and hydrolysis during cell growth and division.

PG synthesis and hydrolysis were proposed to spatially and temporarily correlate in (*E. coli*) cells. The corresponding enzymes are organized in dynamic and variable multi-protein complexes and their enzymatic activities are strictly regulated (Höltje, 1998; Typas *et al.*, 2012; Egan *et al.*, 2017; Pazos *et al.*, 2017). Cell wall hydrolases are

involved in murein growth, maturation, turnover, recycling, and cleavage of the septum at cell division, while uncontrolled activities can cause cell lysis (Vollmer *et al.*, 2008; Lee & Huang, 2013). These enzymes have various cleavage specificities and often require a PG-binding domain for activity (Buist *et al.*, 2008). Periplasmic interaction between GdcP and the murein-binding putative metallopeptidase GdpM may provide a mechanism to control incorporation of new material into the mesh-like PG sacculus of *S. meliloti* cells. In *C. crescentus*, murein-binding endopeptidase DipM functions in PG remodeling upon cell division by localization to the site of constriction, which is dependent on the essential murein-binding protein FtsN (Möll *et al.*, 2010). Genomes of bacteria from the order Rhizobiales do not encode FtsN suggesting alternative mechanisms for directing PG remodeling enzymes to the septum. In the case of *S. meliloti*, GdcP may be a functional homolog of FtsN and regulate GdpM activity at sites of zonal cell wall synthesis.

The mechanistic consequences and direction of signaling mediated by GdcP and GdpM interaction remain to be investigated in more detail. GdcP-GdpM interaction may modulate perception of environmental stimuli by GdcP receptor domains or promote interactions with other proteins, catalytic activity and ligand binding of the intracellular signaling module. Alternatively, perception of signals from the cytoplasm may modulate accessibility of the interaction interface in GdcP receptor domains for either GdpM or ligands such as murein derivatives. Future work may also address the role of probable interaction partner SMc00644, which might form a heterotrimeric complex together with GdcP and GdpM. Conservation of GdcP, GdpM and SMc00644 in the order Rhizobiales suggested a common mechanism for cell envelope biogenesis in these organisms. The importance of the PG layer in alpha-rhizobial species has recently been demonstrated, as it has an essential role in differentiation during symbiosis (Gully *et al.*, 2016). GdcP and GdpM contribution to the interaction of alpha-rhizobia with their leguminous plant hosts remains to be investigated.

3.3.2 GdcP accessory function

To investigate contribution of GdcP to c-di-GMP signaling in *S. meliloti*, enzymatic activities of its GGDEF and EAL domains and their ability to bind c-di-GMP were examined *in vitro* using [α-^{32}P]-labeled substrates (performed by Dr. Dorota Skotnicka). The EAL domain of GdcP was shown to confer PDE activity towards c-di-GMP, whereas the GGDEF domain showed neither DGC activity nor c-di-GMP binding via

the I site (Ch. 8, Figs. 4a & S4). To examine c-di-GMP PDE activity of GdcP *in vivo*, the c-di-GMP content of GdcP-depleted Rm2011, complemented with either $gdcP_{Wt}$, $gdcP_{AAL}$ or $gdcP_{GAAAF}$ ectopically expressed with a transcription strength similar to the native level, was measured. The c-di-GMP content of cells expressing $gdcP_{Wt}$ and $gdcP_{GAAAF}$ was similar, whereas expression of the PDE active site mutant variant $gdcP_{AAL}$ resulted in a two-fold increase in c-di-GMP content (Ch. 8, Fig. 4b). Additionally, cells expressing $gdcP_{AAL}$ were more sensitive to growth inhibition and cell morphology effects upon ectopical expression of DGC-encoding *SMc03178* compared to cell expressing $gdcP_{Wt}$ (Ch. 8, Fig. 4c-d). Taken together, these data provided evidence that GdcP degrades c-di-GMP *in vivo,* which could imply a mechanism for avoiding harmful increases in intracellular c-di-GMP levels.

The relevance of GdcP to cell envelope biogenesis in combination with its ability to degrade c-di-GMP potentially implies a direct connection between cell wall remodeling and intracellular c-di-GMP signaling. In line with this, recent studies have described a link between c-di-GMP signaling and cell growth and division. In polarly growing *M. smegmatis*, a strain lacking dually active DGC/PDE DcpA displayed cell elongation and multi-septation presumably as a result of transcriptional upregulation of genes with functions related to cell wall processes. This suggested a role of c-di-GMP signaling in cell division and morphology (Gupta *et al.*, 2016). A link between c-di-GMP signaling and PG remodeling was also shown for the cell division-related DGC YfiN from *E. coli*. Under envelope stress conditions, YifN binds to the cytoplasmic scaffold proteins FtsZ and ZipA likely in a c-di-GMP-bound state. This results in recruitment of the protein to the future division site and subsequent inhibition of septal PG synthesis (Kim & Harshey, 2016). Inactivation of the EAL domain of polarly localized GdcP from *S. meliloti* neither altered growth and cell morphology nor GdcP localization, indicating its PDE activity not to be important for its primary function. However, GdcP PDE activity counteracted artificially increased c-di-GMP levels by reducing the concomitant cell damage.

Polar and septal placement of c-di-GMP PDEs has previously been shown to serve as a mechanism for restricting signaling events to specific sites of *C. crescentus* cells. PdeA transiently localizes to the stalked cell pole and determines the swarmer cell-specific program (Abel *et al.*, 2011). Flagellum biogenesis at the swarmer cell pole requires dynamically localizing TipF, whose localization to the division plane is dependent on cytokinesis (Huitema *et al.*, 2006). PDE activity of GdcP in *S. meliloti* may provide a

mechanism for decreasing c-di-GMP levels to initiate downstream signaling events at either the growing cell pole or the mid-cell region of pre-divisional cells. Identification of c-di-GMP effectors and their target genes influenced by GdcP PDE activity would allow a better understanding of the c-di-GMP-related function of GdcP.

Deletion of the GGDEF domain of GdcP resulted in a reduced growth rate, although neither catalytic activity nor c-di-GMP binding could be demonstrated. Comparative sequence analysis revealed protein sequences homologous to *S. meliloti* GdcP and containing an intact A site in the GGDEF domain as in the case of *A. tumefaciens* GdcP, whose EAL domain also contains all conserved motifs indicating PDE activity (Ch. 8, Fig. S7b). However, the functional consequences of a DGC activity in addition to the PDE activity of GdcP remain unclear, also because $gdcP_{Sm}$ and $gdcP_{At}$ complemented the phenotypes of GdcP-depleted Rm2011 in a similar manner (Ch. 8, Fig. 8b-c). The GdcP GGDEF domain may modulate PDE activity of the covalently linked EAL domain. Such an example was described for PAS-GGDEF-EAL domain protein PdeA from *C. crescentus*, which contains a degenerate A site (GEDEF) and possesses no DGC activity, while the GGDEF domain is able to bind GTP and thus to regulate the PDE activity of the covalently linked EAL domain (Christen *et al.*, 2005). Moreover, PDE activities of BifA and RmcA from *P. aeruginosa* were shown to be stimulated depending on the A sites of the covalently linked GGDEF domains (Kuchma *et al.*, 2007; Okegbe *et al.*, 2017). Similar to GdcP from *S. meliloti*, DGC activity of BifA containing a GGDEF domain with a GGDQF motif was not detectable (Kuchma *et al.*, 2007).

GdcP PDE activity may also be modulated by the cytoplasmic PAS domain, which generally regulates the activities of covalently attached effector domains (Möglich *et al.*, 2009). Such a mechanism was identified for DosP from *E. coli*, as O_2-binding to a heme cofactor in the PAS domain results in increased PDE activity of the protein (Tanaka *et al.*, 2007). In *A. xylinum*, AxDGC2 regulates cellular c-di-GMP levels depending on the redox state of a flavin cofactor in the PAS domain, while the oxidized state promotes DGC activity (Qi *et al.*, 2009). The FAD-binding PAS domain of dual-function enzyme RmcA from *P. aeruginosa* supposedly influences the stimulating effect that the GGDEF domain has on the covalently linked EAL domain (Okegbe *et al.*, 2017). For the PAS domain of GdcP a putative heme pocket has been predicted suggesting the protein might be able to sense redox states. A link between redox signaling and cell envelope biogenesis has been reported for gammaproteobacterial

species, as the YfiBNR signal transduction system provides a mechanism for inhibiting septal PG synthesis. Under reducing and envelope stress conditions, redox sensor YfiR is released from the periplasmic PAS domain of the membrane-standing DGC YfiN, which acts as a cell division inhibitor (Malone *et al.*, 2012; Kim & Harshey, 2016). Ligands that bind to the PAS domain of GdcP and their possible contribution to the cell cycle-dependent localization of the protein remain thus far unknown.

Chapter 4: Conclusions

Research on mechanistic and functional aspects of c-di-GMP signaling is rapidly advancing and revealing a physiological complexity of the c-di-GMP network in bacteria. However, knowledge on environmental input signals that control c-di-GMP signaling pathways, cellular activities controlled by c-di-GMP networks and their exact architecture, effects on highly dynamic behavior of cells and integration into other signaling networks is incomplete. This study examined the role of the second messenger c-di-GMP in environmental adaptation of symbiotic alphaproteobacterium *S. meliloti,* a member of the order Rhizobiales for which cellular processes and mechanisms involving c-di-GMP had not been examined in depth.

This study unraveled the roles of c-di-GMP signaling in environmental adaptation of *S. meliloti* by genetic and biochemical approaches. This included identification of genetic determinants responsible for c-di-GMP-mediated phenotypic changes, discovery and first description of a new type of c-di-GMP receptor (AraC-like transcription factor CuxR), and functional characterization of an essential c-di-GMP phosphodiesterase (referred to as GdcP) (Fig. 10). Similar to other species from various bacterial lineages, c-di-GMP emerged as an important second messenger for the transition from a motile, planktonic lifestyle to a sessile, biofilm-associated lifestyle of free-living *S. meliloti*. In this bacterium, elevated c-di-GMP levels stimulate production of extracellular matrix components and repress flagellar motility which is accompanied by effective surface attachment. Therefore, c-di-GMP-dependent regulation may play a significant role for environmental adaptation of *S. meliloti* in its natural soil habitat, since the switch of single motile bacteria from a planktonic state to a structural community of cells increases resistance to antimicrobial compounds and gives rise to higher tolerance to environmental stressors. c-di-GMP-stimulated production of adhesive polysaccharides might also contribute to attachment to biotic and abiotic surfaces in the rhizosphere including plant roots.

The results of this work demonstrate that the c-di-GMP network is integrated into the well-studied regulatory network for opposing control of exopolysaccharide (EPS) biosynthesis and motility in *S. meliloti*. In this organism, c-di-GMP signaling is interlinked with cellular processes that are also regulated by global repressor MucR and master regulator ExpR, such as production of EPS I and EPS II, synthesis of autoinducer molecules and flagellar motility (Fig. 10). Furthermore, evidences were

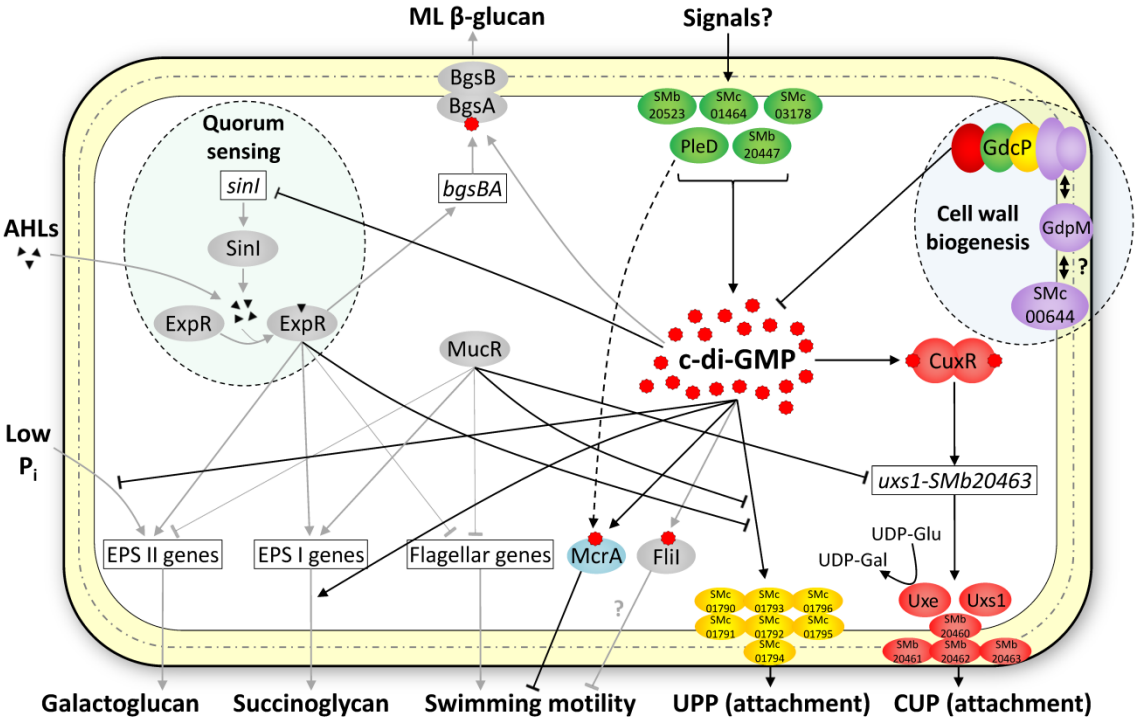

Figure 10. Schematic model of c-di-GMP signaling in *S. meliloti*. Depiction of cellular functions and genetic factors subjected to c-di-GMP-mediated regulation at transcriptional and post-translational levels. In response to environmental or intracellular signals, diguanylate cyclase activities of PleD, SMb20523, SMb20447, SMc01464 and SMc03178 may be stimulated and thus contribute to the intracellular c-di-GMP pool. c-di-GMP degradation is catalyzed by the membrane-standing phosphodiesterase GdcP (SMc00074) with a function related to cell growth and division. Possible protein-protein interactions between GdcP, the putative metallopeptidase GdpM (SMc02432) and the hypothetical transmembrane protein SMc00644, as well as the conservation of these proteins within the order Rhizobiales, suggests a conserved mechanism for cell envelope biogenesis in alpha-rhizobia. c-di-GMP signaling interferes with cell-cell communication ('quorum sensing'), as c-di-GMP represses transcription of autoinducer synthase gene *sinI* and thus inhibits extracellular accumulation of *N*-acyl homoserine lactones ('AHLs'). c-di-GMP regulates the production of multiple polysaccharides, as biosynthesis of a unipolar polysaccharide ('UPP'), succinoglycan ('EPS I'), a Congo red-binding extracellular polysaccharide ('CUP') and a mixed-linkage β-glucan ('ML β-glucan'; Pérez-Mendoza *et al.*, 2015) are stimulated at elevated c-di-GMP levels, whereas galactoglucan ('EPS II') biosynthesis under phosphate-limiting conditions ('low P_i') is negatively regulated at the level of *wgeA* transcription. UPP biosynthesis is governed by the *SMc01790-SMc01796* gene cluster and required for c-di-GMP-mediated surface attachment. c-di-GMP is bound by the newly identified receptors AraC-like transcriptional activator CuxR (SMb20457) and single-domain PilZ protein McrA (SMc00507), as well as previously identified BgsA (Pérez-Mendoza *et al.*, 2015) and FliI (Trampari *et al.*, 2015). c-di-GMP-bound CuxR activates the *uxs1* promoter resulting in upregulated transcription of *uxs1-SMb20463* and CUP production to promote biofilm formation. c-di-GMP binding to McrA results in reduced swimming speed, which might imply a regulatory mechanism that is specific to PleD-derived signaling. Dually functional nucleotide sugar epimerase Uxe converts UDP-glucose ('UDP-Glu') to UDP-galactose ('UDP-Gal'), as it can suppress symbiotic incompetence of *S. meliloti* lacking UDP-glucose 4′-epimerase ExoB. The global repressor MucR counteracts c-di-GMP-mediated activation of CUP biosynthesis at the level of transcription, while both MucR and ExpR attenuate UPP-mediated attachment. Regulatory connections that were identified in previous studies are gray colored.

provided for MucR counteracting c-di-GMP-stimulated production of a new extracellular polysaccharide (referred to as CUP) at the level of transcription, as well as for both ExpR and MucR attenuating surface attachment based on c-di-GMP-mediated production of a unipolar polysaccharide (UPP) (Fig. 10). Besides transcriptional

repression of flagellar genes by MucR and ExpR, signaling based on newly identified c-di-GMP receptor McrA adds another layer to regulation of swimming motility in *S. meliloti*. Altogether, these findings suggest that crosstalk between regulatory networks could enable integration of numerous environmental signals for the regulation of a single target process at multiple levels. Interestingly, interplay between c-di-GMP signaling and another second messenger system has been shown in a recent report, as diguanylate cyclase activity of Lcd1 from pathogenic *Leptospira interrogans* is enhanced upon binding of the widely distributed second messenger cAMP (da Costa Vasconcelos *et al.*, 2017). High complexity in signal transduction pathways for adaptational responses of bacteria might ensure survival in challenging environments.

The identification of the essential c-di-GMP phosphodiesterase GdcP acting in cell envelope biogenesis in polarly growing *S. meliloti* broadens the spectrum of common c-di-GMP-related functions in bacteria (Fig. 10). Considering that modification of the peptidoglycan layer is part of an adaptational response of the murein sacculus to cope with changing conditions (Cava & de Pedro, 2014), it is tempting to speculate that GdcP and functionally related putative peptidoglycan hydrolase GdpM may also contribute to environmental adaptation of *S. meliloti* either in its natural soil habitat or inside host cells. However, evidence for c-di-GMP functions related to cell cycle progression and symbiosis with the host plant *M. sativa* could not be provided for *S. meliloti*. This suggests that the c-di-GMP-related proteins are not active under the conditions tested or that they have a role in processes not assayed in this study. It may also be indicative of overlapping regulatory controls, as has been reported for the regulatory pathway driving cell cycle progression in *C. crescentus* (Lori *et al.*, 2015). Finally, environmental and physiological triggers that modulate c-di-GMP levels to activate distinct signaling pathways in *S. meliloti* remain unknown. Future studies might particularly address molecular mechanisms underlying the regulatory function of c-di-GMP-binding McrA and the regulatory output of c-di-GMP-degrading GdcP.

Chapter 5: Literature

Abel S, Bucher T, Nicollier M, Hug I, Kaever V, Abel Zur Wiesch P, Jenal U. 2013. Bi-modal distribution of the second messenger c-di-GMP controls cell fate and asymmetry during the *Caulobacter* cell cycle. PLoS Genet 9:e1003744.

Abel S, Chien P, Wassmann P, Schirmer T, Kaever V, Laub MT, Baker TA, Jenal U. 2011. Regulatory cohesion of cell cycle and cell differentiation through interlinked phosphorylation and second messenger networks. Mol Cell 43:550-60.

Aldridge P, Paul R, Goymer P, Rainey P, Jenal U. 2003. Role of the GGDEF regulator PleD in polar development of *Caulobacter crescentus*. Mol Microbiol 47:1695-708.

Amikam D, Benziman M. 1989. Cyclic diguanylic acid and cellulose synthesis in *Agrobacterium tumefaciens*. J Bacteriol 171:6649-55.

Amikam D, Galperin MY. 2006. PilZ domain is part of the bacterial c-di-GMP binding protein. Bioinformatics 22:3-6.

Anantharaman V, Aravind L. 2003. Application of comparative genomics in the identification and analysis of novel families of membrane-associated receptors in bacteria. BMC Genomics 4:34.

Attmannspacher U, Scharf B, Schmitt R. 2005. Control of speed modulation (chemokinesis) in the unidirectional rotary motor of *Sinorhizobium meliloti*. Mol Microbiol 56:708-18.

Ausmees N, Jonsson H, Höglund S, Ljunggren H, Lindberg M. 1999. Structural and putative regulatory genes involved in cellulose synthesis in *Rhizobium leguminosarum* bv. *trifolii*. Microbiology 145 (Pt 5):1253-62.

Bahlawane C, Baumgarth B, Serrania J, Rüberg S, Becker A. 2008a. Fine-tuning of galactoglucan biosynthesis in *Sinorhizobium meliloti* by differential WggR (ExpG)-, PhoB-, and MucR-dependent regulation of two promoters. J Bacteriol 190:3456-66.

Bahlawane C, McIntosh M, Krol E, Becker A. 2008b. *Sinorhizobium meliloti* regulator MucR couples exopolysaccharide synthesis and motility. Mol Plant Microbe Interact 21:1498-509.

Barends TR, Hartmann E, Griese JJ, Beitlich T, Kirienko NV, Ryjenkov DA, Reinstein J, Shoeman RL, Gomelsky M, Schlichting I. 2009. Structure and mechanism of a bacterial light-regulated cyclic nucleotide phosphodiesterase. Nature 459:1015-8.

Barnhart DM, Su S, Baccaro BE, Banta LM, Farrand SK. 2013. CelR, an ortholog of the diguanylate cyclase PleD of *Caulobacter*, regulates cellulose synthesis in *Agrobacterium tumefaciens*. Appl Environ Microbiol 79:7188-202.

Barnhart DM, Su S, Farrand SK. 2014. A signaling pathway involving the diguanylate cyclase CelR and the response regulator DivK controls cellulose synthesis in *Agrobacterium tumefaciens*. J Bacteriol 196:1257-74.

Basu Roy A, Sauer K. 2014. Diguanylate cyclase NicD-based signalling mechanism of nutrient-induced dispersion by *Pseudomonas aeruginosa*. Mol Microbiol 94:771-93.

Battisti L, Lara JC, Leigh JA. 1992. Specific oligosaccharide form of the *Rhizobium meliloti* exopolysaccharide promotes nodule invasion in alfalfa. Proc Natl Acad Sci U S A 89:5625-9.

Becker A, Rüberg S, Küster H, Roxlau AA, Keller M, Ivashina T, Cheng HP, Walker GC, Pühler A. 1997. The 32-kilobase *exp* gene cluster of *Rhizobium meliloti* directing the biosynthesis of galactoglucan: genetic organization and properties of the encoded gene products. J Bacteriol 179:1375-84.

Bellini D, Caly DL, McCarthy Y, Bumann M, An SQ, Dow JM, Ryan RP, Walsh MA. 2014. Crystal structure of an HD-GYP domain cyclic-di-GMP phosphodiesterase reveals an enzyme with a novel trinuclear catalytic iron centre. Mol Microbiol

91:26-38.
Bellini D, Horrell S, Hutchin A, Phippen CW, Strange RW, Cai Y, Wagner A, Webb JS, Tews I, Walsh MA. 2017. Dimerisation induced formation of the active site and the identification of three metal sites in EAL-phosphodiesterases. Sci Rep 7:42166.
Benach J, Swaminathan SS, Tamayo R, Handelman SK, Folta-Stogniew E, Ramos JE, Forouhar F, Neely H, Seetharaman J, Camilli A, Hunt JF. 2007. The structural basis of cyclic diguanylate signal transduction by PilZ domains. EMBO J 26:5153-66.
Bertram-Drogatz PA, Quester I, Becker A, Pühler A. 1998. The *Sinorhizobium meliloti* MucR protein, which is essential for the production of high-molecular-weight succinoglycan exopolysaccharide, binds to short DNA regions upstream of *exoH* and *exoY*. Mol Gen Genet 257:433-41.
Bian J, Liu X, Cheng YQ, Li C. 2013. Inactivation of cyclic di-GMP binding protein TDE0214 affects the motility, biofilm formation, and virulence of *Treponema denticola*. J Bacteriol 195:3897-905.
Bobrov AG, Kirillina O, Ryjenkov DA, Waters CM, Price PA, Fetherston JD, Mack D, Goldman WE, Gomelsky M, Perry RD. 2011. Systematic analysis of cyclic di-GMP signalling enzymes and their role in biofilm formation and virulence in *Yersinia pestis*. Mol Microbiol 79:533-51.
Boehm A, Kaiser M, Li H, Spangler C, Kasper CA, Ackermann M, Kaever V, Sourjik V, Roth V, Jenal U. 2010. Second messenger-mediated adjustment of bacterial swimming velocity. Cell 141:107-16.
Brown PJ, de Pedro MA, Kysela DT, Van der Henst C, Kim J, De Bolle X, Fuqua C, Brun YV. 2012. Polar growth in the alphaproteobacterial order Rhizobiales. Proc Natl Acad Sci U S A 109:1697-701.
Buendia AM, Enenkel B, Köplin R, Niehaus K, Arnold W, Pühler A. 1991. The *Rhizobium meliloti exoZl exoB* fragment of megaplasmid 2: ExoB functions as a UDP-glucose 4-epimerase and ExoZ shows homology to NodX of *Rhizobium leguminosarum* biovar *viciae* strain TOM. Mol Microbiol 5:1519-30.
Buist G, Steen A, Kok J, Kuipers OP. 2008. LysM, a widely distributed protein motif for binding to (peptido)glycans. Mol Microbiol 68:838-47.
Burdette DL, Monroe KM, Sotelo-Troha K, Iwig JS, Eckert B, Hyodo M, Hayakawa Y, Vance RE. 2011. STING is a direct innate immune sensor of cyclic di-GMP. Nature 478:515-8.
Cava F, de Pedro MA. 2014. Peptidoglycan plasticity in bacteria: emerging variability of the murein sacculus and their associated biological functions. Curr Opin Microbiol 18:46-53.
Chambonnier G, Roux L, Redelberger D, Fadel F, Filloux A, Sivaneson M, de Bentzmann S, Bordi C. 2016. The Hybrid Histidine Kinase LadS Forms a Multicomponent Signal Transduction System with the GacS/GacA Two-Component System in *Pseudomonas aeruginosa*. PLoS Genet 12:e1006032.
Chan C, Paul R, Samoray D, Amiot NC, Giese B, Jenal U, Schirmer T. 2004. Structural basis of activity and allosteric control of diguanylate cyclase. Proc Natl Acad Sci U S A 101:17084-9.
Charoenpanich P, Meyer S, Becker A, McIntosh M. 2013. Temporal expression program of quorum sensing-based transcription regulation in *Sinorhizobium meliloti*. J Bacteriol 195:3224-36.
Chen Y, Chai Y, Guo JH, Losick R. 2012. Evidence for cyclic di-GMP-mediated signaling in *Bacillus subtilis*. J Bacteriol 194:5080-90.
Chen ZH, Schaap P. 2012. The prokaryote messenger c-di-GMP triggers stalk cell differentiation in *Dictyostelium*. Nature 488:680-3.
Cheng HP, Walker GC. 1998. Succinoglycan is required for initiation and elongation of

infection threads during nodulation of alfalfa by *Rhizobium meliloti*. J Bacteriol 180:5183-91.

Chin KH, Lee YC, Tu ZL, Chen CH, Tseng YH, Yang JM, Ryan RP, McCarthy Y, Dow JM, Wang AH, Chou SH. 2010. The cAMP receptor-like protein CLP is a novel c-di-GMP receptor linking cell-cell signaling to virulence gene expression in *Xanthomonas campestris*. J Mol Biol 396:646-62.

Christen B, Christen M, Paul R, Schmid F, Folcher M, Jenoe P, Meuwly M, Jenal U. 2006. Allosteric control of cyclic di-GMP signaling. J Biol Chem 281:32015-24.

Christen M, Christen B, Allan MG, Folcher M, Jenö P, Grzesiek S, Jenal U. 2007. DgrA is a member of a new family of cyclic diguanosine monophosphate receptors and controls flagellar motor function in *Caulobacter crescentus*. Proc Natl Acad Sci U S A 104:4112-7.

Christen M, Christen B, Folcher M, Schauerte A, Jenal U. 2005. Identification and characterization of a cyclic di-GMP-specific phosphodiesterase and its allosteric control by GTP. J Biol Chem 280:30829-37.

Christen M, Kulasekara HD, Christen B, Kulasekara BR, Hoffman LR, Miller SI. 2010. Asymmetrical distribution of the second messenger c-di-GMP upon bacterial cell division. Science 328:1295-7.

Cohen D, Mechold U, Nevenzal H, Yarmiyhu Y, Randall TE, Bay DC, Rich JD, Parsek MR, Kaever V, Harrison JJ, Banin E. 2015. Oligoribonuclease is a central feature of cyclic diguanylate signaling in *Pseudomonas aeruginosa*. Proc Natl Acad Sci U S A 112:11359-64.

Cowie A, Cheng J, Sibley CD, Fong Y, Zaheer R, Patten CL, Morton RM, Golding GB, Finan TM. 2006. An integrated approach to functional genomics: construction of a novel reporter gene fusion library for *Sinorhizobium meliloti*. Appl Environ Microbiol 72:7156-67.

da Costa Vasconcelos FN, Maciel NK, Favaro DC, de Oliveira LC, Barbosa AS, Salinas RK, de Souza RF, Farah CS, Guzzo CR. 2017. Structural and enzymatic characterization of a cAMP-dependent diguanylate cyclase from pathogenic *Leptospira* species. J Mol Biol doi:10.1016/j.jmb.2017.06.002.

Dahlstrom KM, Giglio KM, Sondermann H, O'Toole GA. 2016. The inhibitory site of a diguanylate cyclase is a necessary element for interaction and signaling with an effector protein. J Bacteriol 198:1595-603.

Davies JA, Harrison JJ, Marques LL, Foglia GR, Stremick CA, Storey DG, Turner RJ, Olson ME, Ceri H. 2007. The GacS sensor kinase controls phenotypic reversion of small colony variants isolated from biofilms of *Pseudomonas aeruginosa* PA14. FEMS Microbiol Ecol 59:32-46.

Deakin WJ, Broughton WJ. 2009. Symbiotic use of pathogenic strategies: rhizobial protein secretion systems. Nat Rev Microbiol 7:312-20.

Dénarié J, Debelle F, Truchet G, Prome JC. 1993. *Rhizobium* and legume nodulation: a molecular dialogue. Current plant science and biotechnology in agriculture, new horizons in nitrogen fixation, Springer International Publishing AG 17:19-30

Doherty D, Leigh JA, Glazebrook J, Walker GC. 1988. *Rhizobium meliloti* mutants that overproduce the *R. meliloti* acidic calcofluor-binding exopolysaccharide. J Bacteriol 170:4249-56.

Downie JA. 2010. The roles of extracellular proteins, polysaccharides and signals in the interactions of rhizobia with legume roots. FEMS Microbiol Rev 34:150-70.

Duerig A, Abel S, Folcher M, Nicollier M, Schwede T, Amiot N, Giese B, Jenal U. 2009. Second messenger-mediated spatiotemporal control of protein degradation regulates bacterial cell cycle progression. Genes Dev 23:93-104.

Egan AJ, Cleverley RM, Peters K, Lewis RJ, Vollmer W. 2017. Regulation of bacterial

cell wall growth. FEBS J 284:851-867.
Fang X, Ahmad I, Blanka A, Schottkowski M, Cimdins A, Galperin MY, Römling U, Gomelsky M. 2014. GIL, a new c-di-GMP-binding protein domain involved in regulation of cellulose synthesis in enterobacteria. Mol Microbiol 93:439-52.
Feirer N, Xu J, Allen KD, Koestler BJ, Bruger EL, Waters CM, White RH, Fuqua C. 2015. A pterin-dependent signaling pathway regulates a dual-function diguanylate cyclase-phosphodiesterase controlling surface attachment in *Agrobacterium tumefaciens*. MBio 6:e00156.
Ferreira RB, Antunes LC, Greenberg EP, McCarter LL. 2008. *Vibrio parahaemolyticus* ScrC modulates cyclic dimeric GMP regulation of gene expression relevant to growth on surfaces. J Bacteriol 190:851-60.
Finan TM, Weidner S, Wong K, Buhrmester J, Chain P, Vorhölter FJ, Hernandez-Lucas I, Becker A, Cowie A, Gouzy J, Golding B, Pühler A. 2001. The complete sequence of the 1,683-kb pSymB megaplasmid from the N_2-fixing endosymbiont *Sinorhizobium meliloti*. Proc Natl Acad Sci U S A 98:9889-94.
Firczuk M, Mucha A, Bochtler M. 2005. Crystal structures of active LytM. J Mol Biol 354:578-90.
Frage B, Döhlemann J, Robledo M, Lucena D, Sobetzko P, Graumann PL, Becker A. 2016. Spatiotemporal choreography of chromosome and megaplasmids in the *Sinorhizobium meliloti* cell cycle. Mol Microbiol 100:808-23.
Franz V. 2015. Untersuchung der Rolle des cyclic-di-GMP Effektors SMc00507 in der Regulation von Motilität in *Sinorhizobium meliloti*. Bachelor thesis, Philipps-Universität Marburg, LOEWE Centre for Synthetic Microbiology, AG Becker.
Fraysse N, Couderc F, Poinsot V. 2003. Surface polysaccharide involvement in establishing the rhizobium-legume symbiosis. Eur J Biochem 270:1365-80.
Galibert F, Finan TM, Long SR, Pühler A, Abola P, Ampe F, Barloy-Hubler F, Barnett MJ, Becker A, Boistard P, Bothe G, Boutry M, Bowser L, Buhrmester J, Cadieu E, Capela D, Chain P, Cowie A, Davis RW, Dréano S, Federspiel NA, Fisher RF, Gloux S, Godrie T, Goffeau A, Golding B, Gouzy J, Gurjal M, Hernandez-Lucas I, Hong A, Huizar L, Hyman RW, Jones T, Kahn D, Kahn ML, Kalman S, Keating DH, Kiss E, Komp C, Lelaure V, Masuy D, Palm C, Peck MC, Pohl TM, Portetelle D, Purnelle B, Ramsperger U, Surzycki R, Thébault P, Vandenbol M, Vorhölter FJ, Weidner S, Wells DH, Wong K, Yeh KC, Batut J. 2001. The composite genome of the legume symbiont *Sinorhizobium meliloti*. Science 293:668-72.
Galperin MY. 2005. A census of membrane-bound and intracellular signal transduction proteins in bacteria: bacterial IQ, extroverts and introverts. BMC Microbiol 5:35.
Galperin MY, Natale DA, Aravind L, Koonin EV. 1999. A specialized version of the HD hydrolase domain implicated in signal transduction. J Mol Microbiol Biotechnol 1:303-5.
Galperin MY, Nikolskaya AN, Koonin EV. 2001. Novel domains of the prokaryotic two-component signal transduction systems. FEMS Microbiol Lett 203:11-21.
Gao M, Coggin A, Yagnik K, Teplitski M. 2012. Role of specific quorum-sensing signals in the regulation of exopolysaccharide II production within *Sinorhizobium meliloti* spreading colonies. PLoS One 7:e42611.
Gao S, Romdhane SB, Beullens S, Kaever V, Lambrichts I, Fauvart M, Michiels J. 2014. Genomic analysis of cyclic-di-GMP-related genes in rhizobial type strains and functional analysis in *Rhizobium etli*. Appl Microbiol Biotechnol 98:4589-602.
Gentner M, Allan MG, Zaehringer F, Schirmer T, Grzesiek S. 2012. Oligomer formation of the bacterial second messenger c-di-GMP: reaction rates and equilibrium constants indicate a monomeric state at physiological concentrations. J Am Chem Soc 134:1019-29.

Gomelsky M. 2011. cAMP, c-di-GMP, c-di-AMP and now cGMP: bacteria use them all!. Mol Microbiol 79:562-5.

González JE, Reuhs BL, Walker GC. 1996. Low molecular weight EPS II of *Rhizobium meliloti* allows nodule invasion in *Medicago sativa*. Proc Natl Acad Sci U S A 93:8636-41.

Gründling A, Lee VT. 2016. Old concepts, new molecules and current approaches applied to the bacterial nucleotide signalling field. Philos Trans R Soc Lond B Biol Sci 371.

Gu X, Lee SG, Bar-Peled M. 2011. Biosynthesis of UDP-xylose and UDP-arabinose in *Sinorhizobium meliloti* 1021: first characterization of a bacterial UDP-xylose synthase, and UDP-xylose 4-epimerase. Microbiology 157:260-9.

Gully D, Gargani D, Bonaldi K, Grangeteau C, Chaintreuil C, Fardoux J, Nguyen P, Marchetti R, Nouwen N, Molinaro A, Mergaert P, Giraud E. 2016. A peptidoglycan-remodeling enzyme is critical for bacteroid differentiation in *Bradyrhizobium* spp. during legume symbiosis. Mol Plant Microbe Interact 29:447-57.

Gupta KR, Baloni P, Indi SS, Chatterji D. 2016. Regulation of growth, cell shape, cell division, and gene expression by second messengers (p)ppGpp and cyclic di-GMP in *Mycobacterium smegmatis*. J Bacteriol 198:1414-22.

Hecht GB, Newton A. 1995. Identification of a novel response regulator required for the swarmer-to-stalked-cell transition in *Caulobacter crescentus*. J Bacteriol 177:6223-9.

Hickman JW, Harwood CS. 2008. Identification of FleQ from *Pseudomonas aeruginosa* as a c-di-GMP-responsive transcription factor. Mol Microbiol 69:376-89.

Hickman JW, Tifrea DF, Harwood CS. 2005. A chemosensory system that regulates biofilm formation through modulation of cyclic diguanylate levels. Proc Natl Acad Sci U S A 102:14422-7.

Hoang HH, Becker A, González JE. 2004. The LuxR homolog ExpR, in combination with the Sin quorum sensing system, plays a central role in *Sinorhizobium meliloti* gene expression. J Bacteriol 186:5460-72.

Höltje JV. 1998. Growth of the stress-bearing and shape-maintaining murein sacculus of *Escherichia coli*. Microbiol Mol Biol Rev 62:181-203.

Huitema E, Pritchard S, Matteson D, Radhakrishnan SK, Viollier PH. 2006. Bacterial birth scar proteins mark future flagellum assembly site. Cell 124:1025-37.

Hunter JL, Severin GB, Koestler BJ, Waters CM. 2014. The *Vibrio cholerae* diguanylate cyclase VCA0965 has an AGDEF active site and synthesizes cyclic di-GMP. BMC Microbiol 14:22.

Janczarek M. 2011. Environmental signals and regulatory pathways that influence exopolysaccharide production in rhizobia. Int J Mol Sci 12:7898-933.

Jenal U, Reinders A, Lori C. 2017. Cyclic di-GMP: second messenger extraordinaire. Nat Rev Microbiol.

Jones KM, Kobayashi H, Davies BW, Taga ME, Walker GC. 2007. How rhizobial symbionts invade plants: the *Sinorhizobium-Medicago* model. Nat Rev Microbiol 5:619-33.

Karaolis DK, Means TK, Yang D, Takahashi M, Yoshimura T, Muraille E, Philpott D, Schroeder JT, Hyodo M, Hayakawa Y, Talbot BG, Brouillette E, Malouin F. 2007. Bacterial c-di-GMP is an immunostimulatory molecule. J Immunol 178:2171-81.

Karatan E, Watnick P. 2009. Signals, regulatory networks, and materials that build and break bacterial biofilms. Microbiol Mol Biol Rev 73:310-47.

Kazmierczak BI, Lebron MB, Murray TS. 2006. Analysis of FimX, a phosphodiesterase that governs twitching motility in *Pseudomonas aeruginosa*. Mol Microbiol 60:1026-43.

Khan SR, Gaines J, Roop RM, Farrand SK. 2008. Broad-host-range expression vectors with tightly regulated promoters and their use to examine the influence of TraR and TraM expression on Ti plasmid quorum sensing. Appl Environ Microbiol 74:5053-62.

Kim HK, Harshey RM. 2016. A diguanylate cyclase acts as a cell division inhibitor in a two-step response to reductive and envelope stresses. MBio 7.

Kim J, Heindl JE, Fuqua C. 2013. Coordination of division and development influences complex multicellular behavior in *Agrobacterium tumefaciens*. PLoS One 8:e56682.

Ko J, Ryu KS, Kim H, Shin JS, Lee JO, Cheong C, Choi BS. 2010. Structure of PP4397 reveals the molecular basis for different c-di-GMP binding modes by PilZ domain proteins. J Mol Biol 398:97-110.

Krasteva PV, Fong JC, Shikuma NJ, Beyhan S, Navarro MV, Yildiz FH, Sondermann H. 2010. *Vibrio cholerae* VpsT regulates matrix production and motility by directly sensing cyclic di-GMP. Science 327:866-8.

Krasteva PV, Sondermann H. 2017. Versatile modes of cellular regulation via cyclic dinucleotides. Nat Chem Biol 13:350-359.

Krol E, Becker A. 2004. Global transcriptional analysis of the phosphate starvation response in *Sinorhizobium meliloti* strains 1021 and 2011. Mol Genet Genomics 272:1-17.

Kuchma SL, Brothers KM, Merritt JH, Liberati NT, Ausubel FM, O'Toole GA. 2007. BifA, a cyclic-Di-GMP phosphodiesterase, inversely regulates biofilm formation and swarming motility by *Pseudomonas aeruginosa* PA14. J Bacteriol 189:8165-78.

Kulasekara BR, Kamischke C, Kulasekara HD, Christen M, Wiggins PA, Miller SI. 2013. c-di-GMP heterogeneity is generated by the chemotaxis machinery to regulate flagellar motility. Elife 2:e01402.

Kuru E, Hughes HV, Brown PJ, Hall E, Tekkam S, Cava F, de Pedro MA, Brun YV, VanNieuwenhze MS. 2012. *In situ* probing of newly synthesized peptidoglycan in live bacteria with fluorescent D-amino acids. Angew Chem Int Ed Engl 51:12519-23.

Laus MC, Logman TJ, Lamers GE, Van Brussel AA, Carlson RW, Kijne JW. 2006. A novel polar surface polysaccharide from *Rhizobium leguminosarum* binds host plant lectin. Mol Microbiol 59:1704-13.

Lee ER, Baker JL, Weinberg Z, Sudarsan N, Breaker RR. 2010. An allosteric self-splicing ribozyme triggered by a bacterial second messenger. Science 329:845-8.

Lee TK, Huang KC. 2013. The role of hydrolases in bacterial cell-wall growth. Curr Opin Microbiol 16:760-6.

Lee VT, Matewish JM, Kessler JL, Hyodo M, Hayakawa Y, Lory S. 2007. A cyclic-di-GMP receptor required for bacterial exopolysaccharide production. Mol Microbiol 65:1474-84.

Levet-Paulo M, Lazzaroni JC, Gilbert C, Atlan D, Doublet P, Vianney A. 2011. The atypical two-component sensor kinase Lpl0330 from *Legionella pneumophila* controls the bifunctional diguanylate cyclase-phosphodiesterase Lpl0329 to modulate bis-(3'-5')-cyclic dimeric GMP synthesis. J Biol Chem 286:31136-44.

Levi A, Folcher M, Jenal U, Shuman HA. 2011. Cyclic diguanylate signaling proteins control intracellular growth of *Legionella pneumophila*. MBio 2:e00316-10.

Li TN, Chin KH, Fung KM, Yang MT, Wang AH, Chou SH. 2011. A novel tetrameric PilZ domain structure from Xanthomonads. PLoS One 6:e22036.

Li W, He ZG. 2012. LtmA, a novel cyclic di-GMP-responsive activator, broadly regulates the expression of lipid transport and metabolism genes in *Mycobacterium smegmatis*. Nucleic Acids Res 40:11292-307.

Li Y, Heine S, Entian M, Sauer K, Frankenberg-Dinkel N. 2013. NO-induced biofilm

dispersion in *Pseudomonas aeruginosa* is mediated by an MHYT domain-coupled phosphodiesterase. J Bacteriol 195:3531-42.
Liang ZX. 2015. The expanding roles of c-di-GMP in the biosynthesis of exopolysaccharides and secondary metabolites. Nat Prod Rep 32:663-83.
Lori C, Ozaki S, Steiner S, Böhm R, Abel S, Dubey BN, Schirmer T, Hiller S, Jenal U. 2015. Cyclic di-GMP acts as a cell cycle oscillator to drive chromosome replication. Nature 523:236-9.
Ma Q, Zhang G, Wood TK. 2011. *Escherichia coli* BdcA controls biofilm dispersal in *Pseudomonas aeruginosa* and *Rhizobium meliloti*. BMC Res Notes 4:447.
Marciano DP, Dharmarajan V, Griffin PR. 2014. HDX-MS guided drug discovery: small molecules and biopharmaceuticals. Curr Opin Struct Biol 28:105-11.
Margolin W. 2009. Sculpting the bacterial cell. Curr Biol 19:R812-22.
Marketon MM, Glenn SA, Eberhard A, González JE. 2003. Quorum sensing controls exopolysaccharide production in *Sinorhizobium meliloti*. J Bacteriol 185:325-31.
Matsuyama BY, Krasteva PV, Baraquet C, Harwood CS, Sondermann H, Navarro MV. 2016. Mechanistic insights into c-di-GMP-dependent control of the biofilm regulator FleQ from *Pseudomonas aeruginosa*. Proc Natl Acad Sci U S A 113:E209-18.
McDougald D, Rice SA, Barraud N, Steinberg PD, Kjelleberg S. 2012. Should we stay or should we go: mechanisms and ecological consequences for biofilm dispersal. Nat Rev Microbiol 10:39-50.
Mendrygal KE, González JE. 2000. Environmental regulation of exopolysaccharide production in *Sinorhizobium meliloti*. J Bacteriol 182:599-606.
Merighi M, Lee VT, Hyodo M, Hayakawa Y, Lory S. 2007. The second messenger bis-(3'-5')-cyclic-GMP and its PilZ domain-containing receptor Alg44 are required for alginate biosynthesis in *Pseudomonas aeruginosa*. Mol Microbiol 65:876-95.
Möglich A, Ayers RA, Moffat K. 2009. Structure and signaling mechanism of Per-ARNT-Sim domains. Structure 17:1282-94.
Möll A, Schlimpert S, Briegel A, Jensen GJ, Thanbichler M. 2010. DipM, a new factor required for peptidoglycan remodelling during cell division in *Caulobacter crescentus*. Mol Microbiol 77:90-107.
Monds RD, O'Toole GA. 2009. The developmental model of microbial biofilms: ten years of a paradigm up for review. Trends Microbiol 17:73-87.
Nair HA, Periasamy S, Yang L, Kjelleberg S, Rice SA. 2017. Real time, spatial, and temporal mapping of the distribution of c-di-GMP during biofilm development. J Biol Chem 292:477-487.
Navarro MV, De N, Bae N, Wang Q, Sondermann H. 2009. Structural analysis of the GGDEF-EAL domain-containing c-di-GMP receptor FimX. Structure 17:1104-16.
Newell PD, Monds RD, O'Toole GA. 2009. LapD is a bis-(3',5')-cyclic dimeric GMP-binding protein that regulates surface attachment by *Pseudomonas fluorescens* Pf0-1. Proc Natl Acad Sci U S A 106:3461-6.
Niehaus K, Kapp D, Pühler A. 1993. Plant defence and delayed infection of alfalfa pseudonodules induced by an exopolysaccharide (EPS I)-deficient *Rhizobium meliloti* mutant. Planta 190:415-425.
Odintsov SG, Sabala I, Marcyjaniak M, Bochtler M. 2004. Latent LytM at 1.3 Å resolution. J Mol Biol 335:775-85.
Okegbe C, Fields BL, Cole SJ, Beierschmitt C, Morgan CJ, Price-Whelan A, Stewart RC, Lee VT, Dietrich LEP. 2017. Electron-shuttling antibiotics structure bacterial communities by modulating cellular levels of c-di-GMP. Proc Natl Acad Sci U S A doi:10.1073/pnas.1700264114.
Oldroyd GE, Murray JD, Poole PS, Downie JA. 2011. The rules of engagement in the

legume-rhizobial symbiosis. Annu Rev Genet 45:119-44.
Orr MW, Donaldson GP, Severin GB, Wang J, Sintim HO, Waters CM, Lee VT. 2015. Oligoribonuclease is the primary degradative enzyme for pGpG in *Pseudomonas aeruginosa* that is required for cyclic-di-GMP turnover. Proc Natl Acad Sci U S A 112:E5048-57.
Paul K, Nieto V, Carlquist WC, Blair DF, Harshey RM. 2010. The c-di-GMP binding protein YcgR controls flagellar motor direction and speed to affect chemotaxis by a "backstop brake" mechanism. Mol Cell 38:128-39.
Paul R, Abel S, Wassmann P, Beck A, Heerklotz H, Jenal U. 2007. Activation of the diguanylate cyclase PleD by phosphorylation-mediated dimerization. J Biol Chem 282:29170-7.
Paul R, Weiser S, Amiot NC, Chan C, Schirmer T, Giese B, Jenal U. 2004. Cell cycle-dependent dynamic localization of a bacterial response regulator with a novel di-guanylate cyclase output domain. Genes Dev 18:715-27.
Pazos M, Peters K, Vollmer W. 2017. Robust peptidoglycan growth by dynamic and variable multi-protein complexes. Curr Opin Microbiol 36:55-61.
Pellock BJ, Teplitski M, Boinay RP, Bauer WD, Walker GC. 2002. A LuxR homolog controls production of symbiotically active extracellular polysaccharide II by *Sinorhizobium meliloti*. J Bacteriol 184:5067-76.
Pérez-Mendoza D, Aragón IM, Prada-Ramírez HA, Romero-Jiménez L, Ramos C, Gallegos MT, Sanjuán J. 2014. Responses to elevated c-di-GMP levels in mutualistic and pathogenic plant-interacting bacteria. PLoS One 9:e91645.
Pérez-Mendoza D, Rodríguez-Carvajal M, Romero-Jiménez L, Farias GeA, Lloret J, Gallegos MT, Sanjuán J. 2015. Novel mixed-linkage β-glucan activated by c-di-GMP in *Sinorhizobium meliloti*. Proc Natl Acad Sci U S A 112:E757-65.
Petersen E, Chaudhuri P, Gourley C, Harms J, Splitter G. 2011. *Brucella melitensis* cyclic di-GMP phosphodiesterase BpdA controls expression of flagellar genes. J Bacteriol 193:5683-91.
Petters T, Zhang X, Nesper J, Treuner-Lange A, Gomez-Santos N, Hoppert M, Jenal U, Søgaard-Andersen L. 2012. The orphan histidine protein kinase SgmT is a c-di-GMP receptor and regulates composition of the extracellular matrix together with the orphan DNA binding response regulator DigR in *Myxococcus xanthus*. Mol Microbiol 84:147-65.
Pitzer JE, Sultan SZ, Hayakawa Y, Hobbs G, Miller MR, Motaleb MA. 2011. Analysis of the *Borrelia burgdorferi* cyclic-di-GMP-binding protein PlzA reveals a role in motility and virulence. Infect Immun 79:1815-25.
Pratt JT, Tamayo R, Tischler AD, Camilli A. 2007. PilZ domain proteins bind cyclic diguanylate and regulate diverse processes in *Vibrio cholerae*. J Biol Chem 282:12860-70.
Pultz IS, Christen M, Kulasekara HD, Kennard A, Kulasekara B, Miller SI. 2012. The response threshold of *Salmonella* PilZ domain proteins is determined by their binding affinities for c-di-GMP. Mol Microbiol 86:1424-40.
Putnoky P, Petrovics G, Kereszt A, Grosskopf E, Ha DT, Bánfalvi Z, Kondorosi A. 1990. *Rhizobium meliloti* lipopolysaccharide and exopolysaccharide can have the same function in the plant-bacterium interaction. J Bacteriol 172:5450-8.
Qi Y, Rao F, Luo Z, Liang ZX. 2009. A flavin cofactor-binding PAS domain regulates c-di-GMP synthesis in AxDGC2 from *Acetobacter xylinum*. Biochemistry 48:10275-85.
Ramelot TA, Yee A, Cort JR, Semesi A, Arrowsmith CH, Kennedy MA. 2007. NMR structure and binding studies confirm that PA4608 from *Pseudomonas aeruginosa* is a PilZ domain and a c-di-GMP binding protein. Proteins 66:266-71.

Reinhold BB, Chan SY, Reuber TL, Marra A, Walker GC, Reinhold VN. 1994. Detailed structural characterization of succinoglycan, the major exopolysaccharide of *Rhizobium meliloti* Rm1021. J Bacteriol 176:1997-2002.

Reuber TL, Walker GC. 1993. Biosynthesis of succinoglycan, a symbiotically important exopolysaccharide of *Rhizobium meliloti*. Cell 74:269-80.

Reuhs BL, Williams MN, Kim JS, Carlson RW, Côté F. 1995. Suppression of the Fix$^-$ phenotype of *Rhizobium meliloti exoB* mutants by *lpsZ* is correlated to a modified expression of the K polysaccharide. J Bacteriol 177:4289-96.

Richter AM, Povolotsky TL, Wieler LH, Hengge R. 2014. Cyclic-di-GMP signalling and biofilm-related properties of the Shiga toxin-producing 2011 German outbreak *Escherichia coli* O104:H4. EMBO Mol Med 6:1622-37.

Roelofs KG, Wang J, Sintim HO, Lee VT. 2011. Differential radial capillary action of ligand assay for high-throughput detection of protein-metabolite interactions. Proc Natl Acad Sci U S A 108:15528-33.

Römling U, Galperin MY, Gomelsky M. 2013. Cyclic di-GMP: the first 25 years of a universal bacterial second messenger. Microbiol Mol Biol Rev 77:1-52.

Ross P, Weinhouse H, Aloni Y, Michaeli D, Weinberger-Ohana P, Mayer R, Braun S, de Vroom E, van der Marel GA, van Boom JH, Benziman M. 1987. Regulation of cellulose synthesis in *Acetobacter xylinum* by cyclic diguanylic acid. Nature 325:279-81.

Rotter C, Mühlbacher S, Salamon D, Schmitt R, Scharf B. 2006. Rem, a new transcriptional activator of motility and chemotaxis in *Sinorhizobium meliloti*. J Bacteriol 188:6932-42.

Rüberg S, Pühler A, Becker A. 1999. Biosynthesis of the exopolysaccharide galactoglucan in *Sinorhizobium meliloti* is subject to a complex control by the phosphate-dependent regulator PhoB and the proteins ExpG and MucR. Microbiology 145 (Pt 3):603-11.

Russell MH, Bible AN, Fang X, Gooding JR, Campagna SR, Gomelsky M, Alexandre G. 2013. Integration of the second messenger c-di-GMP into the chemotactic signaling pathway. MBio 4:e00001-13.

Ryan RP, Fouhy Y, Lucey JF, Crossman LC, Spiro S, He YW, Zhang LH, Heeb S, Cámara M, Williams P, Dow JM. 2006. Cell-cell signaling in *Xanthomonas campestris* involves an HD-GYP domain protein that functions in cyclic di-GMP turnover. Proc Natl Acad Sci U S A 103:6712-7.

Ryan RP, Fouhy Y, Lucey JF, Jiang BL, He YQ, Feng JX, Tang JL, Dow JM. 2007. Cyclic di-GMP signalling in the virulence and environmental adaptation of *Xanthomonas campestris*. Mol Microbiol 63:429-42.

Ryjenkov DA, Simm R, Römling U, Gomelsky M. 2006. The PilZ domain is a receptor for the second messenger c-di-GMP: the PilZ domain protein YcgR controls motility in enterobacteria. J Biol Chem 281:30310-4.

Sallet E, Roux B, Sauviac L, Jardinaud MF, Carrère S, Faraut T, de Carvalho-Niebel F, Gouzy J, Gamas P, Capela D, Bruand C, Schiex T. 2013. Next-generation annotation of prokaryotic genomes with EuGene-P: application to *Sinorhizobium meliloti* 2011. DNA Res 20:339-54.

Schäper S, Krol E, Skotnicka D, Kaever V, Hilker R, Søgaard-Andersen L, Becker A. 2016. Cyclic di-GMP regulates multiple cellular functions in the symbiotic alphaproteobacterium *Sinorhizobium meliloti*. J Bacteriol 198:521-35.

Schäper S, Steinchen W, Krol E, Altegoer F, Skotnicka D, Søgaard-Andersen L, Bange G, Becker A. 2017. AraC-like transcriptional regulator CuxR binds c-di-GMP by a PilZ-like mechanism to regulate extracellular polysaccharide production. Proc Natl Acad Sci U S A 114:E4822-31.

Schäper S, Yau H, Krol E, Skotnicka D, Kaever V, Søgaard-Andersen L, Vollmer W, Becker A. A dynamic c-di-GMP phosphodiesterase is linked to alpha-rhizobial cell growth and division. In prep.

Schirmer T, Jenal U. 2009. Structural and mechanistic determinants of c-di-GMP signalling. Nat Rev Microbiol 7:724-35.

Schmidt AJ, Ryjenkov DA, Gomelsky M. 2005. The ubiquitous protein domain EAL is a cyclic diguanylate-specific phosphodiesterase: enzymatically active and inactive EAL domains. J Bacteriol 187:4774-81.

Schmitt R. 2002. Sinorhizobial chemotaxis: a departure from the enterobacterial paradigm. Microbiology 148:627-31.

Schumacher MA, Zeng W. 2016. Structures of the activator of *K. pneumonia* biofilm formation, MrkH, indicates PilZ domains involved in c-di-GMP and DNA binding. Proc Natl Acad Sci U S A 113:10067-72.

Schumacher MA, Zeng W, Findlay KC, Buttner MJ, Brennan RG, Tschowri N. 2017. The *Streptomyces* master regulator BldD binds c-di-GMP sequentially to create a functional $BldD_2$-$(c\text{-}di\text{-}GMP)_4$ complex. Nucleic Acids Res doi:10.1093/nar/gkx287.

Selbitschka W, Dresing U, Hagen M, Niemann S, Pühler A. 1995. A biological containment system for *Rhizobium meliloti* based on the use of recombination-deficient (*recA*$^-$) strains. FEMS Microbiology Ecology 16:223-232.

Serra DO, Richter AM, Hengge R. 2013. Cellulose as an architectural element in spatially structured *Escherichia coli* biofilms. J Bacteriol 195:5540-54.

Seshasayee AS, Fraser GM, Luscombe NM. 2010. Comparative genomics of cyclic-di-GMP signalling in bacteria: post-translational regulation and catalytic activity. Nucleic Acids Res 38:5970-81.

Sharypova LA, Niehaus K, Scheidle H, Holst O, Becker A. 2003. *Sinorhizobium meliloti acpXL* mutant lacks the C28 hydroxylated fatty acid moiety of lipid A and does not express a slow migrating form of lipopolysaccharide. J Biol Chem 278:12946-54.

Skorupska A, Janczarek M, Marczak M, Mazur A, Król J. 2006. Rhizobial exopolysaccharides: genetic control and symbiotic functions. Microb Cell Fact 5:7.

Skotnicka D, Smaldone GT, Petters T, Trampari E, Liang J, Kaever V, Malone JG, Singer M, Søgaard-Andersen L. 2016a. A minimal threshold of c-di-GMP is essential for fruiting body formation and sporulation in *Myxococcus xanthus*. PLoS Genet 12:e1006080.

Skotnicka D, Petters T, Heering J, Hoppert M, Kaever V, Søgaard-Andersen L. 2016b. Cyclic di-GMP regulates type IV pilus-dependent motility in *Myxococcus xanthus*. J Bacteriol 198:77-90.

Soisson SM, MacDougall-Shackleton B, Schleif R, Wolberger C. 1997. Structural basis for ligand-regulated oligomerization of AraC. Science 276:421-5.

Solano C, García B, Latasa C, Toledo-Arana A, Zorraquino V, Valle J, Casals J, Pedroso E, Lasa I. 2009. Genetic reductionist approach for dissecting individual roles of GGDEF proteins within the c-di-GMP signaling network in *Salmonella*. Proc Natl Acad Sci U S A 106:7997-8002.

Sourjik V, Muschler P, Scharf B, Schmitt R. 2000. VisN and VisR are global regulators of chemotaxis, flagellar, and motility genes in *Sinorhizobium (Rhizobium) meliloti*. J Bacteriol 182:782-8.

Spangler C, Böhm A, Jenal U, Seifert R, Kaever V. 2010. A liquid chromatography-coupled tandem mass spectrometry method for quantitation of cyclic di-guanosine monophosphate. J Microbiol Methods 81:226-31.

Sprecher KS, Hug I, Nesper J, Potthoff E, Mahi MA, Sangermani M, Kaever V,

Schwede T, Vorholt J, Jenal U. 2017. Cohesive Properties of the *Caulobacter crescentus* Holdfast Adhesin Are Regulated by a Novel c-di-GMP Effector Protein. MBio 8.

Srivastava D, Waters CM. 2012. A tangled web: regulatory connections between quorum sensing and cyclic Di-GMP. J Bacteriol 194:4485-93.

Steinchen W, Schuhmacher JS, Altegoer F, Fage CD, Srinivasan V, Linne U, Marahiel MA, Bange G. 2015. Catalytic mechanism and allosteric regulation of an oligomeric (p)ppGpp synthetase by an alarmone. Proc Natl Acad Sci U S A 112:13348-53.

Steiner S, Lori C, Boehm A, Jenal U. 2013. Allosteric activation of exopolysaccharide synthesis through cyclic di-GMP-stimulated protein-protein interaction. EMBO J 32:354-68.

Stock AM, Robinson VL, Goudreau PN. 2000. Two-component signal transduction. Annu Rev Biochem 69:183-215.

Sudarsan N, Lee ER, Weinberg Z, Moy RH, Kim JN, Link KH, Breaker RR. 2008. Riboswitches in eubacteria sense the second messenger cyclic di-GMP. Science 321:411-3.

Sundriyal A, Massa C, Samoray D, Zehender F, Sharpe T, Jenal U, Schirmer T. 2014. Inherent regulation of EAL domain-catalyzed hydrolysis of second messenger cyclic di-GMP. J Biol Chem 289:6978-90.

Tan H, West JA, Ramsay JP, Monson RE, Griffin JL, Toth IK, Salmond GP. 2014. Comprehensive overexpression analysis of cyclic-di-GMP signalling proteins in the phytopathogen *Pectobacterium atrosepticum* reveals diverse effects on motility and virulence phenotypes. Microbiology 160:1427-39.

Tanaka A, Takahashi H, Shimizu T. 2007. Critical role of the heme axial ligand, Met95, in locking catalysis of the phosphodiesterase from *Escherichia coli* (Ec DOS) toward cyclic diGMP. J Biol Chem 282:21301-7.

Tarutina M, Ryjenkov DA, Gomelsky M. 2006. An unorthodox bacteriophytochrome from *Rhodobacter sphaeroides* involved in turnover of the second messenger c-di-GMP. J Biol Chem 281:34751-8.

Tchigvintsev A, Xu X, Singer A, Chang C, Brown G, Proudfoot M, Cui H, Flick R, Anderson WF, Joachimiak A, Galperin MY, Savchenko A, Yakunin AF. 2010. Structural insight into the mechanism of c-di-GMP hydrolysis by EAL domain phosphodiesterases. J Mol Biol 402:524-38.

Torres-Quesada O, Millán V, Nisa-Martínez R, Bardou F, Crespi M, Toro N, Jiménez-Zurdo JI. 2013. Independent activity of the homologous small regulatory RNAs AbcR1 and AbcR2 in the legume symbiont *Sinorhizobium meliloti*. PLoS One 8:e68147.

Trampari E, Stevenson CE, Little RH, Wilhelm T, Lawson DM, Malone JG. 2015. Bacterial rotary export ATPases are allosterically regulated by the nucleotide second messenger cyclic-di-GMP. J Biol Chem 290:24470-83.

Trimble MJ, McCarter LL. 2011. Bis-(3'-5')-cyclic dimeric GMP-linked quorum sensing controls swarming in *Vibrio parahaemolyticus*. Proc Natl Acad Sci U S A 108:18079-84.

Tschowri N, Schumacher MA, Schlimpert S, Chinnam NB, Findlay KC, Brennan RG, Buttner MJ. 2014. Tetrameric c-di-GMP mediates effective transcription factor dimerization to control *Streptomyces* development. Cell 158:1136-47.

Typas A, Banzhaf M, Gross CA, Vollmer W. 2012. From the regulation of peptidoglycan synthesis to bacterial growth and morphology. Nat Rev Microbiol 10:123-36.

Urzainqui A, Walker GC. 1992. Exogenous suppression of the symbiotic deficiencies of *Rhizobium meliloti exo* mutants. J Bacteriol 174:3403-6.

Vasse J, de Billy F, Camut S, Truchet G. 1990. Correlation between ultrastructural differentiation of bacteroids and nitrogen fixation in alfalfa nodules. J Bacteriol 172:4295-306.

Vollmer W, Joris B, Charlier P, Foster S. 2008. Bacterial peptidoglycan (murein) hydrolases. FEMS Microbiol Rev 32:259-86.

Wang YC, Chin KH, Tu ZL, He J, Jones CJ, Sanchez DZ, Yildiz FH, Galperin MY, Chou SH. 2016. Nucleotide binding by the widespread high-affinity cyclic di-GMP receptor MshEN domain. Nat Commun 7:12481.

Wang Y, Xu J, Chen A, Zhu J, Yu G, Xu L, Luo L. 2010. GGDEF and EAL proteins play different roles in the control of *Sinorhizobium meliloti* growth, motility, exopolysaccharide production, and competitive nodulation on host alfalfa. Acta Biochim Biophys Sin (Shanghai) 42:410-7.

Wassmann P, Chan C, Paul R, Beck A, Heerklotz H, Jenal U, Schirmer T. 2007. Structure of BeF_3^--modified response regulator PleD: implications for diguanylate cyclase activation, catalysis, and feedback inhibition. Structure 15:915-27.

Whitchurch CB, Tolker-Nielsen T, Ragas PC, Mattick JS. 2002. Extracellular DNA required for bacterial biofilm formation. Science 295:1487.

Whitney JC, Colvin KM, Marmont LS, Robinson H, Parsek MR, Howell PL. 2012. Structure of the cytoplasmic region of PelD, a degenerate diguanylate cyclase receptor that regulates exopolysaccharide production in *Pseudomonas aeruginosa*. J Biol Chem 287:23582-93.

Whitney JC, Whitfield GB, Marmont LS, Yip P, Neculai AM, Lobsanov YD, Robinson H, Ohman DE, Howell PL. 2015. Dimeric c-di-GMP is required for post-translational regulation of alginate production in *Pseudomonas aeruginosa*. J Biol Chem 290:12451-62.

Wilksch JJ, Yang J, Clements A, Gabbe JL, Short KR, Cao H, Cavaliere R, James CE, Whitchurch CB, Schembri MA, Chuah ML, Liang ZX, Wijburg OL, Jenney AW, Lithgow T, Strugnell RA. 2011. MrkH, a novel c-di-GMP-dependent transcriptional activator, controls *Klebsiella pneumoniae* biofilm formation by regulating type 3 fimbriae expression. PLoS Pathog 7:e1002204.

Williams MN, Hollingsworth RI, Brzoska PM, Signer ER. 1990. *Rhizobium meliloti* chromosomal loci required for suppression of exopolysaccharide mutations by lipopolysaccharide. J Bacteriol 172:6596-8.

Xu J, Kim J, Koestler BJ, Choi JH, Waters CM, Fuqua C. 2013. Genetic analysis of *Agrobacterium tumefaciens* unipolar polysaccharide production reveals complex integrated control of the motile-to-sessile switch. Mol Microbiol 89:929-48.

Xu L, Xin L, Zeng Y, Yam JK, Ding Y, Venkataramani P, Cheang QW, Yang X, Tang X, Zhang LH, Chiam KH, Yang L, Liang ZX. 2016. A cyclic di-GMP-binding adaptor protein interacts with a chemotaxis methyltransferase to control flagellar motor switching. Sci Signal 9:ra102.

Xu M, Wang YZ, Yang XA, Jiang T, Xie W. 2017. Structural studies of the periplasmic portion of the diguanylate cyclase CdgH from *Vibrio cholerae*. Sci Rep 7:1861.

Zhan HJ, Lee CC, Leigh JA. 1991. Induction of the second exopolysaccharide (EPSb) in *Rhizobium meliloti* SU47 by low phosphate concentrations. J Bacteriol 173:7391-4.

Zogaj X, Nimtz M, Rohde M, Bokranz W, Römling U. 2001. The multicellular morphotypes of *Salmonella typhimurium* and *Escherichia coli* produce cellulose as the second component of the extracellular matrix. Mol Microbiol 39:1452-63.

Chapter 6: Cyclic di-GMP regulates multiple cellular functions in the symbiotic alphaproteobacterium *Sinorhizobium meliloti*

Simon Schäper, Elizaveta Krol, Dorota Skotnicka, Volkhard Kaever, Rolf Hilker, Lotte Søgaard-Andersen, Anke Becker

Accepted for publication in *Journal of Bacteriology*, November 2015.

Individual contribution:

- Construction of strains and plasmids (except pSRKGm-*parB-mcherry*)
- c-di-GMP extractions
- Phenotypic screening of *S. meliloti* mutant and overexpression strains
- Analysis of promoter activities and FRET measurements using fluorescence assay
- AHL sensitivity test
- Protein purifications
- Contributed to fluorescence and light microscopy
- Contributed to writing of the manuscript

AMERICAN SOCIETY FOR MICROBIOLOGY | Journal of Bacteriology

Cyclic Di-GMP Regulates Multiple Cellular Functions in the Symbiotic Alphaproteobacterium *Sinorhizobium meliloti*

Simon Schäper,[a] Elizaveta Krol,[a] Dorota Skotnicka,[b] Volkhard Kaever,[c] Rolf Hilker,[d] Lotte Søgaard-Andersen,[b] Anke Becker[a]

LOEWE Center for Synthetic Microbiology (SYNMIKRO), Philipps Universität Marburg, Marburg, Germany[a]; Department of Ecophysiology, Max Planck Institute for Terrestrial Microbiology, Marburg, Germany[b]; Research Core Unit Metabolomics, Hannover Medical School, Hannover, Germany[c]; Institute of Medical Microbiology, Justus Liebig University, Giessen, Germany[d]

ABSTRACT

***Sinorhizobium meliloti* undergoes major lifestyle changes between planktonic states, biofilm formation, and symbiosis with leguminous plant hosts. In many bacteria, the second messenger 3′,5′-cyclic di-GMP (c-di-GMP, or cdG) promotes a sessile lifestyle by regulating a plethora of processes involved in biofilm formation, including motility and biosynthesis of exopolysaccharides (EPS). Here, we systematically investigated the role of cdG in *S. meliloti* Rm2011 encoding 22 proteins putatively associated with cdG synthesis, degradation, or binding. Single mutations in 21 of these genes did not cause evident changes in biofilm formation, motility, or EPS biosynthesis. In contrast, manipulation of cdG levels by overproducing endogenous or heterologous diguanylate cyclases (DGCs) or phosphodiesterases (PDEs) affected these processes and accumulation of *N*-Acyl-homoserine lactones in the culture supernatant. Specifically, individual overexpression of the *S. meliloti* genes *pleD*, *SMb20523*, *SMb20447*, *SMc01464*, and *SMc03178* encoding putative DGCs and of *SMb21517* encoding a single-domain PDE protein had an impact and resulted in increased levels of cdG. Compared to the wild type, an *S. meliloti* strain that did not produce detectable levels of cdG (cdG^0) was more sensitive to acid stress. However, it was symbiotically potent, unaffected in motility, and only slightly reduced in biofilm formation. The *SMc01790-SMc01796* locus, homologous to the *Agrobacterium tumefaciens uppABCDEF* cluster governing biosynthesis of a unipolarly localized polysaccharide, was found to be required for cdG-stimulated biofilm formation, while the single-domain PilZ protein McrA was identified as a cdG receptor protein involved in regulation of motility.**

IMPORTANCE

We present the first systematic genome-wide investigation of the role of 3′,5′-cyclic di-GMP (c-di-GMP, or cdG) in regulation of motility, biosynthesis of exopolysaccharides, biofilm formation, quorum sensing, and symbiosis in a symbiotic alpha-rhizobial species. Phenotypes of an *S. meliloti* strain unable to produce cdG (cdG^0) demonstrated that this second messenger is not essential for root nodule symbiosis but may contribute to acid tolerance. Our data further suggest that enhanced levels of cdG promote sessility of *S. meliloti* and uncovered a single-domain PilZ protein as regulator of motility.

Alpha-rhizobia are soil-dwelling alphaproteobacteria existing either in free-living states or in symbiosis with a leguminous plant host. Motile rhizobia undergo a major switch in lifestyle when establishing a biofilm or symbiosis with the host. In the symbiotic state, the bacteria inhabit root nodules and differentiate into polyploid bacteroids that fix nitrogen to the benefit of the host (1).

3′,5′-Cyclic di-GMP (c-di-GMP, or cdG) is a common second messenger in the bacterial kingdom that is known to promote the transition from a planktonic, motile to a sessile, frequently biofilm-associated, lifestyle (2, 3). cdG levels are controlled by diguanylate cyclases (DGCs) that synthesize cdG from two GTP molecules and by phosphodiesterases (PDEs) that degrade it (4). For the synthetic reaction, DGCs require an active site with a conserved GG(D/E)EF motif embedded in a GGDEF domain that can be inhibited by binding of cdG to a primary inhibition site (I-site) containing an RXXD motif. PDEs contain either an EAL or HD-GYP domain, which cleaves cdG to pGpG or two molecules of GMP, respectively. DGC and PDE domains are often coupled to diverse sensory input domains which regulate the enzymatic activities upon perception of environmental stimuli (3). cdG levels are sensed by effectors, such as PilZ- or GIL-domain-containing proteins, degenerate GGDEF domains, or riboswitches (5–9). Binding of cdG to PilZ domains involves RXXXR and DXSXXG motifs, whereas the I-site-like motif RXGD is required for its binding to GIL domains.

High intracellular cdG concentrations favor production of exopolysaccharides (EPS), fimbriae, pili, and adhesins that contribute to biofilm formation (3). Transition to a sessile lifestyle also includes inhibition of flagellar motility by cdG (10). In *Escherichia coli*, *Salmonella enterica* serovar Typhimurium, and *Caulobacter crescentus*, this regulation involves PilZ domain proteins (11, 12). A variety of other cellular functions, not directly involved in the switch between motile and sessile states, are also subject to regulation by cdG. Examples are virulence-associated processes in

Received 26 September 2015 **Accepted** 9 November 2015

Accepted manuscript posted online 16 November 2015

Citation Schäper S, Krol E, Skotnicka D, Kaever V, Hilker R, Søgaard-Andersen L, Becker A. 2016. Cyclic di-GMP regulates multiple cellular functions in the symbiotic alphaproteobacterium *Sinorhizobium meliloti*. J Bacteriol 198:521–535. doi:10.1128/JB.00795-15.

Editor: A. M. Stock

Address correspondence to Anke Becker, anke.becker@synmikro.uni-marburg.de.

Supplemental material for this article may be found at http://dx.doi.org/10.1128/JB.00795-15.

Vibrio, *Yersinia*, *Xanthomonas*, *Salmonella*, and *Pseudomonas* (13–17), quorum sensing (QS) in *Vibrio* and *Xanthomonas* (18, 19), and cell cycle control and cell differentiation in *C. crescentus* (20, 21).

While experimental manipulation of cdG levels indicated a role of cdG in regulation of the sessile-motile switch in alpharhizobia as well, to date only a few cdG-related genes have been studied in these symbiotic bacteria. In *Rhizobium etli* and *Rhizobium leguminosarum*, overproduction of a heterologous DGC enhanced EPS production, biofilm formation, and adhesion to plant roots and decreased symbiotic efficiency and swimming motility (22). In *Sinorhizobium meliloti* 102F34, overproduction of the *E. coli* cdG-binding protein BdcA resulted in biofilm dispersal and enhanced motility, presumably by lowering intracellular cdG levels (23). An initial incomplete screen of *S. meliloti* Rm1021 single-gene mutants in cdG-related genes identified 11 out of 14 tested genes as weakly affecting growth rate, motility, EPS production, and nodule occupancy (24). Recently, enhanced levels of cdG were shown to induce production of a novel *S. meliloti* Rm8530 mixed-linkage β-glucan, supposedly by binding of cdG to the C-terminal portion of the membrane-bound glycosyltransferase BgsA (25). So far, experimental hints for enzymatic activities of suggested DGCs and PDEs were reported only for two hybrid GGDEF-EAL proteins from *R. etli* (26).

Computational screening of alpha-rhizobial genomes identified a high number of cdG-related genes, with the highest number of 55 genes in *Bradyrhizobium japonicum* (27). The *S. meliloti* Rm1021 type strain (28) encodes 20 proteins containing either a GGDEF or EAL domain or both and two PilZ domain proteins (26, 27). In contrast to the presence of HD-GYP-domain-encoding genes in *Rhizobium*, *Mesorhizobium*, and *Bradyrhizobium* species, such genes were not found in sequenced *Sinorhizobium* genomes (27). In this study, we systematically explored the role of 22 cdG-related genes in swimming motility, EPS production, biofilm formation, and symbiotic efficiency of *S. meliloti* Rm2011. A mutant with deletions of 16 genes encoding GGDEF-domain-containing proteins did not produce detectable levels of cdG and was symbiotically potent. We report on genetic factors responsible for a cdG-mediated increase in biofilm formation and inhibition of motility in *S. meliloti*.

MATERIALS AND METHODS

Bacterial strains and growth conditions. Bacterial strains and plasmids used in this study are listed in Table S1 in the supplemental material. This study was performed with *S. meliloti* Rm2011 (https://iant.toulouse.inra.fr/bacteria/annotation/cgi/rhime2011/rhime2011.cgi) which is very closely related to the Rm1021 type strain since both strains are streptomycin-resistant spontaneous derivatives of *S. meliloti* SU47 (29, 30). *S. meliloti* was grown at 30°C in tryptone-yeast extract (TY) medium (31), LB medium (32), modified yeast extract-mannitol (YM) medium (33), modified morpholinepropanesulfonic acid (MOPS)-buffered minimal medium (MM) (34), and nutrient-depleted 30% MM (nitrogen, carbon, and phosphate sources reduced to 30%). Phosphate-limiting MM contained 0.1 mM K_2HPO_4. *Agrobacterium tumefaciens* was grown in minimal glutamate mannitol (MGM) medium. Medium composition and antibiotic concentrations are provided in the supplemental material. Unless otherwise specified, isopropyl β-D-1-thiogalactopyranoside (IPTG) was added at 500 μM. Growth curves shown in Fig. S4 in the supplemental material were recorded using an Infinite F200 PRO fluorescence reader (Tecan) in 100-μl cultures in a flat-bottom 96-well plate incubated at 30°C with shaking.

Construction of strains and plasmids. Constructs used in this work were generated using standard cloning techniques. The primers used are listed in Table S2 in the supplemental material. All constructs were verified by sequencing. Plasmids were transferred to *S. meliloti* by *E. coli* S17-1-mediated conjugation (35) as previously described (36).

For generation of single knockouts by plasmid integration, 280- to 385-bp internal gene fragments were cloned into suicide vector pK19mob2ΩHMB. Integration of the resulting constructs into the *S. meliloti* genome resulted in truncation of the target gene and inactivation of the downstream part of the transcription unit. Correct plasmid integrations were verified by PCR.

For construction of deletion mutants, gene-flanking regions of 650 to 770 bp were cloned into suicide plasmid pK18mobsacB. Resulting constructs were integrated into the *S. meliloti* genome, and transconjugants were subjected to sucrose selection as previously described (37). Gene deletions were verified by PCR. Multiple mutants were generated by sequential gene deletions. The genomes of Rm2011 ΔXVI and Rm2011 *expR*$^+$ ΔXVI (strains with deletions of 16 of the 17 GGDEF-domain-encoding genes in Rm2011) as well as their parental strains Rm2011 and Rm2011 *expR*$^+$ were resequenced. Total DNA for resequencing was purified using a DNeasy blood and tissue kit (Qiagen). DNA libraries for sequencing were generated by applying a Nextera XT DNA Library Preparation kit (Illumina), and sequencing was performed on a MiSeq Desktop Sequencer (Illumina) using a MiSeq reagent kit, version 2, for 2 × 250-bp paired-end reads (Illumina). The following numbers of reads were obtained: Rm2011, 4.5×10^6; Rm2011 ΔXVI, 4.8×10^6; Rm2011 *expR*$^+$, 3.2×10^6; and Rm2011 *expR*$^+$ ΔXVI, 4.4×10^6. After quality trimming, the reads were mapped with Bowtie2 (38) using the "very sensitive" preset and returning up to five matches per read (-k 5). Single-nucleotide polymorphism (SNP) detection was performed by applying the ReadXplorer software, version 2.1 (39), requiring 90% of variation, a minimum mismatch coverage of 15, and including only the single perfect match and single best match mapping classes.

To generate C-terminal translation fusions to enhanced green fluorescent protein (EGFP) at the native genomic location, about 700 bp of the 3′ portion of the coding region excluding the stop codon was cloned into suicide plasmid pK18mob2-EGFP, and resulting constructs were integrated into the *S. meliloti* genome.

The promoter-EGFP fusions were generated by insertion of approximately 300-bp fragments including the region upstream of the start codon and up to 10 first codons of the gene into the replicative low-copy-number plasmid pPHU231-EGFP or replicative medium-copy-number plasmid pSRKKm-EGFP. This generated an in-frame fusion of these first codons of the gene of interest to *egfp*.

Gene overexpression constructs were generated by insertion of the full-length coding sequence downstream of the IPTG-inducible T5 promoter and a Shine-Dalgarno sequence into the replicative medium-copy-number vector pWBT. For combined overexpression of two genes, the coding regions were inserted in tandem downstream of the T5 promoter in pWBT, with each coding region preceded by an identical Shine-Dalgarno sequence.

Constructs for production of His_6-tagged McrA, McrA with R9A and R13A substitutions in the RXXXR motif ($McrA_{AXXXA}$), and SMc00074 consisting of residues 390 to 970 ($SMc00074_{390–970}$) were generated by insertion of the coding sequence into expression vector pWH844. For generation of the AXXXA substitutions encoded by *mcrA* (*mcrA*$_{AXXXA}$) splicing by overlap extension PCR was applied.

Phenotype assays. In phenotype assays of strains carrying pWBT-based constructs, gentamicin and IPTG (500 μM) were added to the medium to maintain the plasmid and to induce gene expression. Mucoidity was estimated on phosphate-limiting MM agar. Congo red staining was assayed on TY agar with 70 mg/liter Congo red. Calcofluor brightness was analyzed on LB agar with 200 mg/liter calcofluor. Fresh precultures grown on TY agar were resuspended in 0.9% NaCl to an optical density at 600 nm (OD_{600}) of 1 (strains carrying pWBT-based overexpression constructs) or

OD_{600} of 0.1 (all the other strains), and 50 μl was dropped onto the agar medium. Plates were incubated at 30°C and documented after 2 to 3 days.

Swimming motility was analyzed as follows: for each strain, 2 μl of stationary TY culture (similar growth confirmed by determination of OD_{600}) was spotted onto three separate petri dishes containing 20% TY agar, with a final agar concentration of 0.3%, and dried for 5 min. Plates were incubated at 30°C and documented after 3 days. To quantify swimming motility, sizes of swimming halos of three replicates were measured using image software GIMP, version 2.

Biofilm formation was determined in flat-bottom polystyrene 96-well plates (Greiner) in 30% MM, in triplicates, as previously described (40). A preculture in the same medium was diluted to an OD_{600} of 0.2, with a final volume 100 μl, and grown without shaking for 48 h at 30°C. Growth was recorded by determining the OD_{600}. The culture medium and nonattached cells were removed. Plate wells were washed with water, stained with 200 μl of 0.1% crystal violet solution for 30 min with gentle agitation, and washed twice with water. Stained attached cell material was dissolved in 200 μl of detaching solution (80% acetone–20% ethanol) for 20 min upon shaking. Biofilm formation was determined by quantification of crystal violet-bound attached cell material at the A_{570} and normalized to the OD_{600} of the culture.

Fluorescence measurements. For promoter-EGFP assays, TY precultures were diluted 1:500 in 100 μl of TY medium or 30% MM supplemented with 100 μM IPTG and grown in 96-well plates at 30°C with shaking. EGFP fluorescence (excitation wavelength [λ_{ex}] of 488 ± 9 nm; emission wavelength [λ_{em}] of 522 ± 20 nm; gain, 82) and growth (OD_{600}) were recorded using an Infinite 200 Pro multimode reader (Tecan). Strains carrying the empty vector pPHU-EGFP were used for measuring background fluorescence. Relative fluorescence units (RFU), calculated as EGFP signals, were normalized to the OD_{600} ($n = 2$ to 3).

For determination of the emission ratio of yellow fluorescent protein for energy transfer/cyan fluorescent protein for energy transfer (YPet/CyPet), Rm2011 carrying the fluorescent resonance energy transfer (FRET) CyPet/YPet expression constructs and either the empty vector pSRKKm or *pleD* expression plasmid pSRKKm-PT5-*pleD* was used. Cells were grown in triplicates in 100 μl of MM with 500 μM IPTG in 96-well plates at 30°C with shaking. Fluorescence was determined using a Tecan Infinite 200 Pro multimode reader (λ_{ex} of 425 ± 9 nm, λ_{em1} of 476 ± 20 nm, λ_{em2} of 526 ± 20 nm; gain, 82) and normalized to OD_{600}.

Microscopy. Microscopy of bacteria on 1% agarose pads was performed using a Nikon microscope Eclipse Ti-E with a differential interference contrast (DIC) CFI Apochromat TIRF oil objective (100×; numerical aperture of 1.49) and phase-contrast Plan Apo l oil objective (100×; numerical aperture, 1.45) with AHF HC filter sets F36-504 Texas Red (TxRed) (excitation band pass [ex bp] 562/40-nm, beam splitter [bs] 593-nm, and emission [em] bp 624/40-nm filters) and F36-525 EGFP (ex bp 472/30-nm, bs 495-nm, and em bp 520/35-nm filters). Images were acquired with an Andor iXon3 885 electron-multiplying charge-coupled-device (EMCCD) camera. For time-lapse analysis, MM agarose pads supplemented with 200 μM IPTG were used, and images were acquired every 20 min at 30°C.

Staining with Alexa Fluor 594-conjugated wheat germ agglutinin (WGA) (Life Technologies) was performed as described by Xu et al. (41) with modifications. One microliter of fluorescein (fl)-WGA stock solution (1 mg/ml) was added to 100-μl of stationary MM culture (500 μM IPTG), and the mixture was incubated for 20 min at room temperature (RT) and centrifuged at 6,000 × *g*. The pellets were washed twice with 1× phosphate-buffered saline (PBS) buffer. Bacteria were analyzed by microscopy using phase-contrast and TxRed settings.

Quantification of intracellular cdG. Quantification of intracellular cdG of bacterial cells was performed as previously described (42). Briefly, nucleotides were extracted from cell pellets with 40% acetonitrile, 40% methanol, and 20% water; samples were dried and subjected to liquid chromatography-tandem mass spectrometry (LC-MS/MS). cdG was normalized to total protein, determined using Bradford reagent. Strains overproducing selected DGC/PDEs were grown in TY medium and induced with IPTG (500 μM) at an OD_{600} of 0.2 and harvested after 8 h of induction. Growth rates of the wild type were determined by measuring the OD_{600} in 20-min intervals for 80 min around the OD_{600} of harvest.

AHL detection assay. Two replicate *S. meliloti* TY cultures were induced with 100 μM IPTG at an OD_{600} of 0.05 and grown for 24 h. Cultures were centrifuged for 10 min at 15,000 × *g*. Twenty microliters of supernatant was applied to an *N*-acyl-homoserine lactone (AHL) detection assay using *A. tumefaciens* NTL4(pZLR4) that was performed as previously described (36).

Protein purification. Overnight cultures of *E. coli* M15/pREP4 strains carrying pWH844-*SMc00507*, pWH844-*SMc00507*-R9A/R13A, or pWH844-$SMc00074_{390–970}$ were used to inoculate LB medium at an OD_{600} of 0.1 in flasks. At the OD_{600} of 0.6, 400 μM IPTG was added, and the cultures were further incubated with shaking at 140 rpm overnight at RT. Cultures were harvested by centrifugation (4,000 × *g*), resuspended in binding buffer (1.76 g/liter $Na_2HPO_4 \cdot 2H_2O$, 1.4 g/liter $NaH_2PO_4 \cdot H_2O$, 29.2 g/liter NaCl, 20 mM imidazole, 2 mM phenylmethylsulfonyl fluoride [PMSF], pH 7.4), and lysed using a French press (applied pressure, 1,000 lb/in^2). After centrifugation for 50 min at 15,000 rpm at 4°C, supernatants were applied to His SpinTrap columns (GE Healthcare) and washed with binding buffer containing 100 mM imidazole. Proteins were eluted with 500 mM imidazole. Purity of isolated proteins was assessed by SDS-PAGE and Coomassie brilliant blue staining. Protein concentration was determined using Bradford reagent.

***In vitro* cdG binding assay.** cdG binding was assayed using a differential radial capillary action of ligand assay (DRaCALA) with purified protein and ^{32}P-labeled c-di-GMP (6, 43). ^{32}P-labeled c-di-GMP was prepared by incubating 10 μM His_6-DgcA (*C. crescentus*) with 1 mM GTP/[α-^{32}P]GTP (0.1 μCi/μl) in reaction buffer (50 mM Tris-HCl, pH 8.0, 300 mM NaCl, 10 mM $MgCl_2$) overnight at 30°C. The reaction mixture was then incubated with 5 units of calf intestine alkaline phosphatase (Fermentas) for 1 h at 22°C to hydrolyze unreacted GTP. The reaction was stopped by incubation for 10 min at 95°C followed by centrifugation (10 min, 20,000 × *g*, 20°C). The supernatant was used for the cdG binding assay. ^{32}P-labeled cdG was mixed with a 20 μM concentration of His_6-McrA or His_6-$McrA_{AXXXA}$ and incubated for 10 min at RT in binding buffer (10 mM Tris, pH 8.0, 100 mM NaCl, 5 mM $MgCl_2$). Ten microliters of this reaction mixture was transferred to a nitrocellulose membrane and allowed to dry prior to being exposed to a phosphorimaging screen (Molecular Dynamics). Data were collected and analyzed using a Storm 840 scanner (Amersham Biosciences) and Image Quant, version 5.2, software. For competition experiments, 0.4 mM unlabeled cdG (Biolog) or GTP (Sigma) was added.

***In vitro* DGC activity assay.** DGC activity was determined essentially as described previously (44). Briefly, assays were performed with 10 μM purified proteins (final concentration) in a final volume of 40 μl. Reaction mixtures were preincubated for 5 min at 30°C in reaction buffer (50 mM Tris-HCl, pH 8.0, 300 mM NaCl, 10 mM $MgCl_2$). DGC reactions were initiated by the addition of 1 mM GTP/[α-^{32}P]GTP (0.1 μCi/μl) (Hartman Analytic) and incubated at 30°C for 0, 10, 20, 45, or 60 min. Reactions were then stopped by the addition of 1 volume of 0.5 M EDTA. Reaction products were analyzed by polyethyleneimine-cellulose thin-layer chromatography (TLC). Two-microliter aliquots were spotted onto TLC plates (Millipore), dried, and developed in 2:3 (vol/vol) 4 M $(NH_4)_2SO_4$–1.5 M KH_2PO_4 (pH 3.65). Plates were dried prior to exposure to a phosphorimaging screen (Molecular Dynamics). Data were collected and analyzed using a Storm 840 scanner (Amersham Biosciences) and Image Quant, version 5.2, software.

Plant assays. *Medicago sativa* cv. Eugenia seeds were surface sterilized by 95% sulfuric acid for 10 min, washed eight times with sterile water, and transferred to plant agar (45). The seeds were germinated in the dark overnight at 4°C and for 24 h at 30°C. Bacterial overnight TY cultures were diluted 1:10 with sterile 0.9% NaCl, and 100 μl of the suspensions was plated onto the lower half of plant agar plates (triplicates). For competi-

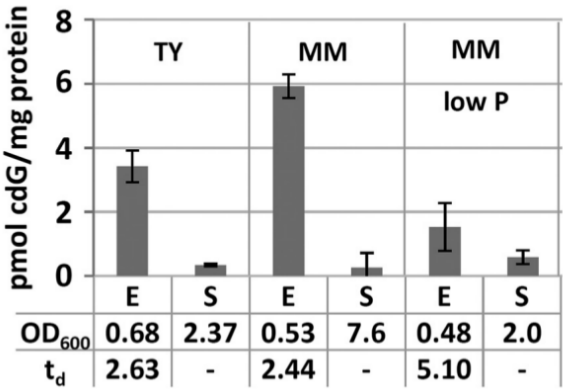

FIG 1 Quantification of cdG in Rm2011 grown in liquid TY and MM cultures. E, exponential growth phase; S, stationary growth phase; t_d, doubling time in hours. Error bars represent standard deviations of three biological replicates.

tion assays, test and control strains, of which only one carried a chromosomally integrated gentamicin resistance gene, were mixed 1:1. Four seedlings were placed onto each plate, and plants were incubated at 22°C and 90% humidity in an 18-h/6-h day/night rhythm for 4 weeks. To estimate nodulation kinetics, emerging nodules were counted every day. To analyze competitive nodulation, nodules were surface sterilized with 70% ethanol, washed three times with sterile water, and crushed. Different dilutions of these extracts were spread on TY agar containing either streptomycin or streptomycin and gentamicin. Nodule occupancy was determined by counting CFU of gentamicin-sensitive and -resistant strains. Nodules producing no gentamicin-resistant CFU were considered occupied by the gentamicin-sensitive strain, those with up to 60% gentamicin-resistant CFU were considered to have mixed occupancy, and those with more than 60% gentamicin-resistant CFU were considered to have predominant occupancy by the gentamicin-resistant strain.

RESULTS

Cellular cdG levels are higher in exponentially growing than in stationary-phase *S. meliloti* cells. To determine conditions of cdG accumulation in *S. meliloti* Rm2011, intracellular cdG concentrations were determined in complex TY medium and MOPS-buffered phosphate-sufficient or phosphate-limiting minimal medium (MM) (Fig. 1). In all media, the cdG content of exponentially growing cells was 10- to 30-fold higher than that of cells in stationary phase. Moreover, intracellular cdG levels of exponential-phase cells approximately inversely correlated with growth rate. Cells growing in phosphate-sufficient MM or TY medium had about 2-fold shorter doubling times and 2- to 4-fold higher cdG levels than phosphate-limited cells.

Individual or multiple knockout mutations in DCG- and PDE-encoding genes have no or only weak effects on motility and biofilm formation. Fig. 2 shows an overview of the domain architecture of cdG-related proteins in *S. meliloti* Rm1021. Six proteins contain a GGDEF domain, 1 contains an EAL domain, and 11 contain both domains. *SMa0369* codes for an internal fragment of an EAL domain, while the neighboring *SMc03142* and *SMc03141* encode the N-terminal and C-terminal parts of a putative bifunctional protein due to truncation of *SMc03142* by a nonsense mutation at codon 196. Sequencing of the corresponding

Name	Domain architecture	GGDEF domain motifs	EAL domain motifs	Length	Further domains
PleD		RxxD GGEEF	-	455	2x REC
SMa2301		RxxD GGEEF	-	448	-
SMb20389		RxxD GGDEF	-	341	GAF
SMb20523		PxxA GGEEF	-	402	-
SMc01464		AxxG GGEEF	-	426	-
SMc04015		RxxD GGEEF	-	307	-
SMa0137		AxxA GGDEF	EALxR N ExxE DD KxD ExxE	733	CHASE4
SMa1548		RxxE GGDEF	EALxR N ExxE DD KxD ExxE	1071	5x PAS
SMb20447		RxxE AGDEF	EALxR N ExxE DD KxD ExxE	564	-
SMb20900		GxxD GGDEF	EALxR - - DD KxD ExxE	644	MHYT. PAS
SMc00033		GxxK GGDDF	ESLxR N ExxE DD KxD ExxE	599	CBS
SMc00038		RxxD GGDEF	EALxR N ExxE DD KxD ExxE	772	PAS, GAF
SMc00074		RxxD GGDQF	EALxR N ExxE DD KxD ExxE	970	7TM-DISM, PAS
SMc00887		PxxA ADDEF	EALxR N ExxE DD KxD ExxE	448	-
SMc00992		QxxA SGDEF	EALxR N ExxE DD KxD ExxD	790	HAMP
SMc03141		- -	EALxR N ExxE DD KxD ExxE	349	-
SMc03178		RxxD GGDEF	EALxR N ExxE DD KxD ExxE	882	CHASE, PAS
SMc03942		GxxA MGDEF	EALxR N ExxE DD KxD ExxE	773	PAS
SMa0369		-	- - ExxE - - -	88	-
SMb21517		-	ECLxR N ExxE - KxD ExxE	271	-
SMc00507		-	-	101*	-
SMc00999		-	-	202	-

FIG 2 Overview of *S. meliloti* Rm2011 cdG-related genes. Green, GGDEF domain; red, EAL domain; blue, PilZ domain. Differences from consensus sequence motifs are labeled in red. Domain architectures are drawn to scale. Black bars, predicted transmembrane helices; white boxes, other domains; length, protein length in amino acids; *, corrected based on experimental validation.

genome region confirmed this mutation in the Rm2011 genome. Eleven of the 17 GGDEF domain proteins contain a canonical GGDEF motif, whereas an RXXD I-site motif was found in seven proteins.

For phenotypic characterization, knockout mutants in 19 of the 20 putative DGC and/or PDE-encoding genes (see Fig. S1 in the supplemental material) were generated in *S. meliloti* Rm2011, either by plasmid integration (18 genes) or by deletion (*SMa0369*). We failed to knock out *SMc00074*, in accordance with Cowie et al. (46), who identified this gene as potentially essential. The mutants were characterized for production of EPS, swimming motility, and the ability to form a biofilm on an abiotic surface (see Fig. S1) and to establish symbiosis with the host plant *Medicago sativa*. *S. meliloti* produces two main EPS, succinoglycan (EPS I) and galactoglucan (EPS II) (47, 48). On rich medium, Rm2011 predominantly produces EPS I, while EPS II production is promoted by phosphate limitation (34, 49). To evaluate production of EPS by cells grown on rich medium, we applied staining with calcofluor, a fluorescent dye binding to EPS I and, to a lesser extent, to other EPS, and staining with Congo red binding to cellulose and amyloid compounds. Furthermore, mucoidy on phosphate-limiting MM was assessed.

Compared to the wild type, the mutants did not show apparent differences in EPS production or in their ability to swim on semisolid agar (see Fig. S1 in the supplemental material). Under the conditions tested, most of the mutants also appeared to be unaffected in biofilm formation. Only *SMb20447*, *SMc00887*, and *SMc03942* mutants showed a 1.5- to 1.8-fold increase, while *pleD*, *SMb20523*, *SMc01464*, and *SMc03178* mutants exhibited a 1.4- to 1.5-fold decrease in cell material attached to polystyrene. None of the single-gene mutants was impaired in symbiosis. Plants inoculated with the single mutants formed pink, nitrogen-fixing root nodules and appeared healthy, indistinguishable from plants inoculated with the wild type (data not shown).

Functional redundancy or compensatory effects may be responsible for the absence of strong phenotypes of the single-gene mutants. We therefore constructed mutants with multiple mutations in *S. meliloti* Rm2011 and its *expR*-sufficient derivative Sm2B3001, here referred to as Rm2011 *expR*$^+$ (50). The latter was included in this study because Rm2011 carries a naturally occurring mutation in *expR* encoding the LuxR-type master transcription factor of QS regulation (51). Intracellular cdG levels of exponentially growing Rm2011 (4.25 ± 0.36 pmol/mg protein) and Rm2011 *expR*$^+$ (4.50 ± 0.11 pmol/mg protein) in TY medium were similar, implying that under these conditions cdG content was not influenced by *expR*.

Starting with deletion of *pleD*, we sequentially deleted 16 of the 17 GGDEF-domain-encoding genes in Rm2011 and Rm2011 *expR*$^+$, resulting in Rm2011 ΔXVI and Rm2011 *expR*$^+$ ΔXVI, respectively (see Table S1 in the supplemental material). Since *SMc00074* could not be deleted, the GGDEF-EAL-domain-containing portion of the encoded protein heterologously produced in *E. coli* was assayed for DGC activity (see Fig. S2). In agreement with the noncanonical GGDQF motif in the predicted GGDEF domain of SMc00074 (Fig. 2), DGC activity was not detected, whereas the positive-control protein DgcA from *C. crescentus* showed DGC activity. Exponentially growing Rm2011 ΔXVI and Rm2011 *expR*$^+$ ΔXVI cells did not detectably produce cdG as assessed by our mass spectrometry-based assay; thus, these strains were considered cdG^0. Genome resequencing of the *S. meliloti* cdG^0 strains confirmed deletion of the 16 targeted genes and did not identify potential suppressor mutations that may circumvent a need for cdG. In the genome sequences we did not detect differences other than the targeted deletions when comparing Rm2011 to Rm2011 ΔXVI, and we identified only one SNP when comparing Rm2011 *expR*$^+$ ΔXVI to Rm2011 *expR*$^+$. This SNP causes a nonsense mutation in *SMc02987* encoding the toxin of the putative SMc02987/SMc02988 toxin/antitoxin pair (52).

Assays for EPS production of the two cdG^0 strains and the intermediates generated by the serial deletions did not reveal significant alterations in mucoidity or calcofluor brightness (see Fig. S3 in the supplemental material). In the Rm2011 background, serial deletions of GGDEF-domain-encoding genes did not alter motility on semisolid agar (see Fig. S3). Swimming motility of mutants in the background of the QS-sufficient strain was not tested because ExpR strongly induces production of EPS II, which hampers this assay. Biofilm formation was diminished about 2-fold in the Rm2011 ΔIV, ΔXII, and ΔXIII mutants (see Table S1 in the supplemental material) compared to the level in the wild type, whereas it was only slightly reduced in both cdG^0 strains (see Fig. S3). Thus, contrary to expectations, the absence of cdG in these strains did not strongly affect any of the tested phenotypes that are typically associated with this second messenger. *M. sativa* plants inoculated with the cdG^0 strains were indistinguishable from plants inoculated with the wild type with respect to the color of nodules and appearance of shoots (see Fig. S4A in the supplemental material). No significant differences in nodulation efficiency, nodule occupancy, or competitiveness between wild-type and cdG^0 strains were observed (Fig. S4B and C). Thus, we conclude that preventing cdG synthesis does not significantly affect the symbiotic ability of *S. meliloti*.

Since we did not detect any strong phenotype of the cdG^0 strains under standard growth conditions, their resistance to osmotic and acid stress was tested since EPS is an important factor for resistance to these stress factors (53, 54). Whereas growth of the mutants was not affected in the presence of 0.4 M NaCl, growth of Rm2011 cdG^0 was significantly reduced at pH 5.7 (see Fig. S5A in the supplemental material). Complementation of Rm2011 cdG^0 with pWBT-*pleD* restored growth at pH 5.7 (see Fig. S5B), implying that cdG or PleD may have a role in acid resistance of this QS-impaired strain.

Overexpression of cdG-related genes affects intracellular cdG levels, motility, biofilm formation, and production of EPS. To functionally characterize *S. meliloti* cdG-related genes (Fig. 2) independent of their native expression conditions, IPTG-inducible overexpression constructs were generated in the medium-copy-number vector pWBT. Following the same strategy, we constructed overexpression plasmids of *C. crescentus dgcA* (55) and *E. coli yhjH* (56) encoding a well-characterized DGC and PDE, respectively. EPS production, motility, and biofilm formation of *S. meliloti* Rm2011 carrying these plasmids were characterized under conditions permitting overexpression of the plasmid-located cdG-related genes (Fig. 3).

Overproduction of the heterologous DGC DgcA inhibited motility on semisolid agar, increased Congo red staining, and promoted biofilm formation. In contrast, overproduction of the heterologous PDE YhjH reduced biofilm formation 2-fold but did not affect motility. Inhibition of motility as well as increased biofilm formation and Congo red staining was observed upon overexpression of *pleD*, *SMb20523*, *SMb20447*, *SMc01464*, and

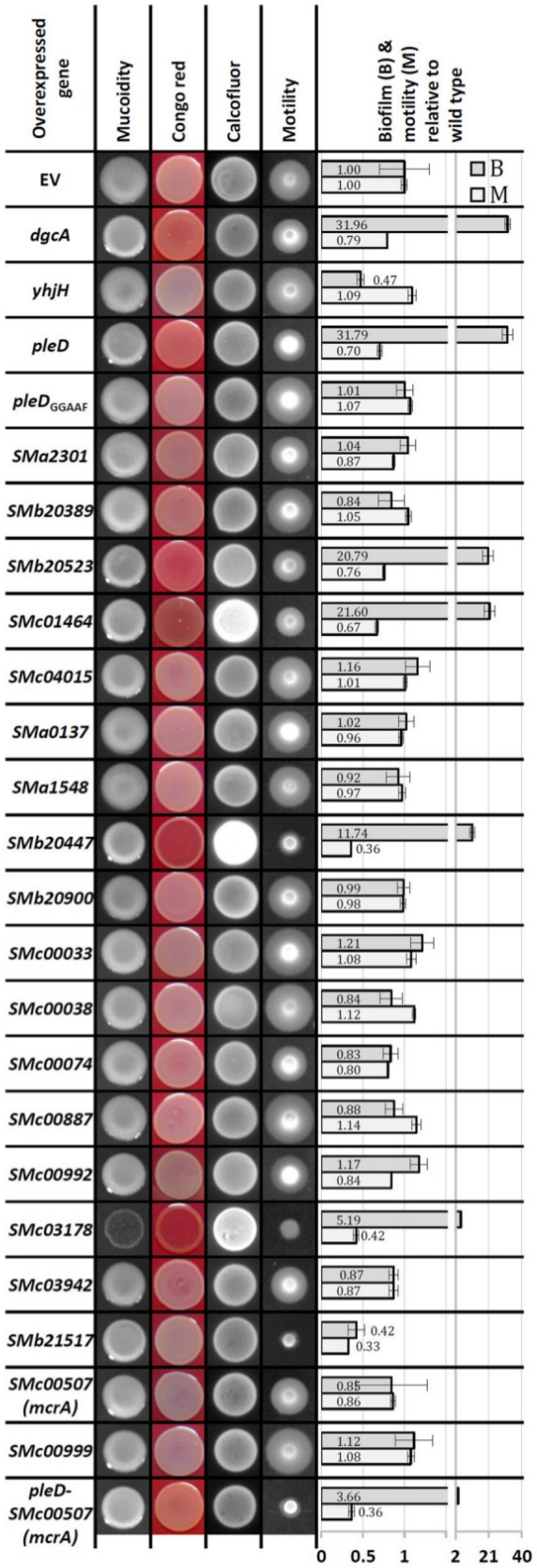

FIG 3 Phenotypic analysis of Rm2011 overexpressing the indicated cdG-related genes. EV, empty pWBT vector. The A_{570}/OD_{600} mean value for Rm2011 pWBT was 0.259 ± 0.079 (set to 1). Error bars represent standard deviations of three biological replicates.

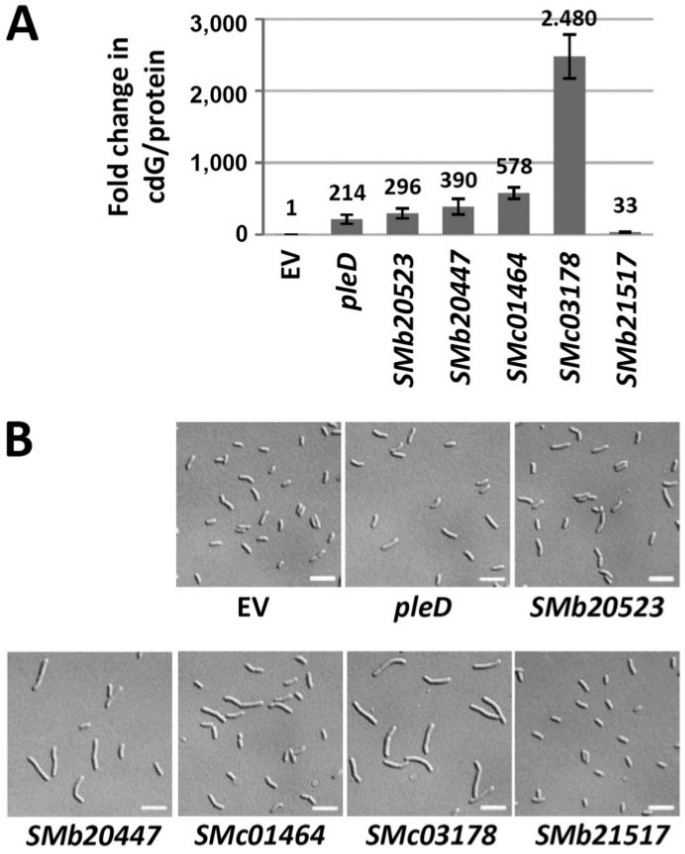

FIG 4 Effects of overexpression of DGC/PDE genes on cdG content and cell morphology. (A) Increase in cdG content of Rm2011 cells overexpressing the indicated genes relative to cells carrying the empty pWBT vector. Error bars represent standard deviations of three biological replicates. (B) Microscopy analysis of cells from the culture samples used for cdG quantification in panel A. Scale bar, 5 μm.

SMc03178, all encoding putatively functional GGDEF domains (Fig. 3). This implies that these five *S. meliloti* genes may indeed encode functional DGCs. Mutation of the PleD GGDEF motif to GGAAF ($pleD_{GGAAF}$) abolished the effects of *pleD* overexpression (Fig. 3), further supporting DGC activity of PleD and a cdG-dependent nature of the observed phenotypic changes. DGC activity of these five *S. meliloti* proteins is furthermore supported by a 214- to 2,480-fold increase in cdG content of cells overproducing these proteins compared to levels in the wild type (Fig. 4A). Interestingly, overexpression of the putative PDE gene *SMb21517* inhibited both motility and biofilm formation, whereas the intracellular cdG concentration increased 33-fold (Fig. 3 and 4). This unexpected increase in cdG content is inconsistent with the observed reduction in biofilm formation. Taken together, these data strongly suggest that motility, production of Congo red-binding compounds, and biofilm formation are influenced by cdG in *S. meliloti*. Although we cannot exclude the possibility that these phenotypes were caused by effects of overexpression other than increased levels of cdG, the observation that overproduction of the heterologous DGC DgcA caused similar defects strongly supports this notion.

Effects of elevated cdG content on cell morphology were analyzed by microscopy (Fig. 4B). In these assays, we investigated cells harvested from exponentially growing cultures used for cdG

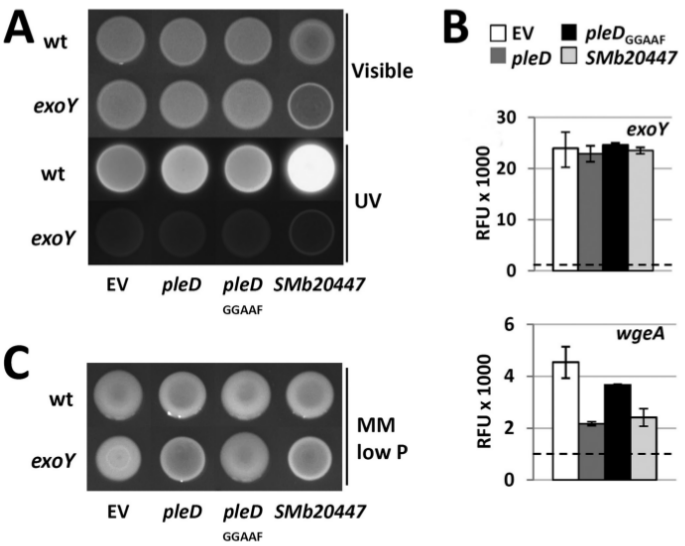

FIG 5 Effects of overexpression of *pleD*, $pleD_{GGAAF}$, or *SMb20447* on EPS production. (A) Rm2011 wild-type (wt) and *exoY* mutant strains, both carrying the indicated overexpression constructs, grown on LB agar (Visible) and the associated calcofluor brightness (UV). (B) Activities of *exoY* and *wgeA* promoters upon overexpression of *pleD*, $pleD_{GGAAF}$, or *SMb20447* in Rm2011 measured using promoter-*egfp* fusions in stationary growth phase (45 h after inoculation). Dashed lines represent fluorescence of the cells carrying the empty vector with promoterless *egfp*. RFU, relative EGFP fluorescence units. Error bars indicate standard deviations of two to three biological replicates. (C) Rm2011 wild-type and *exoY* mutant strains, both carrying the indicated overexpression constructs, grown on phosphate-limiting MM agar. EV, empty pWBT vector.

quantification (Fig. 4A). Overexpression of *pleD*, *SMb20523*, and *SMb21517* did not significantly affect cell morphology, whereas cells overexpressing *SMb20447*, *SMc01464*, and *SMc03178* were elongated. The impact on cell morphology correlated well with the magnitude of increase in cdG concentration, with the highest cdG content resulting in the strongest cell elongation. On minimal and rich media, growth of cells overexpressing *pleD*, *SMb20523*, *SMb20447*, or *SMc01464* was not significantly affected, whereas overexpression of *SMc03178* notably inhibited growth (Fig. 3). This suggests that very high levels of cdG may interfere with cell proliferation.

The degree of motility impairment and biofilm formation upon overproduction of the putative DGCs did not correlate with cdG content (Fig. 3 and 4A). Strongest biofilm formation was observed upon *pleD* overexpression, which caused the smallest increase in cdG content. Thus, the regulatory pathways governing cdG-mediated control of motility and biofilm formation may respond to different concentration ranges of cdG. Additionally, cell elongation and impaired growth caused by very high cdG concentrations may also contribute to the observed phenotypes.

High cdG levels correlated with enhanced calcofluor brightness and Congo red staining of the agar cultures of *SMb20447*-, *SMc01464*-, and *SMc03178*-overexpressing strains (Fig. 3), implying that EPS production is positively regulated by cdG. Since calcofluor fluorescence is typically associated with enhanced EPS I production, we overexpressed *SMb20447* in an *exoY* mutant, which is deficient in the galactosyltransferase initiating EPS I biosynthesis (57). The *exoY* background mutation abolished the calcofluor bright phenotype (Fig. 5A), confirming that it was caused by enhanced production of EPS I. Promoter activity of *exoY* was not affected by overexpression of *SMb20447* (Fig. 5B). Thus, enhanced production of EPS I may be mediated by transcriptional regulation of other genes of this biosynthetic pathway or posttranscriptionally.

We noted that mucoidity of agar cultures on phosphate-limiting MM was slightly reduced upon overexpression of *dgcA*, *pleD*, *SMb20523*, *SMc01464*, *SMb20447*, and *SMc03178*. This implies that the increase in cdG content may be inhibitory for EPS II biosynthesis. The mucoidity of an *exoY* mutant growing on phosphate-limiting MM is predominantly conferred by EPS II. In this mutant, the decrease in mucoidity upon overexpression of *pleD* or *SMb20447* was even more apparent than in the wild-type background, whereas overexpression of $pleD_{GGAAF}$ had no effect (Fig. 5C). This further supports the assumption that EPS II production was negatively affected by overexpression of these DGC candidate genes. Promoter activity of *wgeA*, a gene involved in EPS II biosynthesis, was reduced to about one-third in *pleD*- and *SMb20447*-overexpressing stationary-phase cells (Fig. 5B). This suggests that either a direct or indirect effect of enhanced levels of cdG on transcription of EPS II biosynthesis genes contributes to reduced mucoidy.

PleD localizes to the old pole of the smaller daughter cell of asymmetrically dividing *S. meliloti*. To learn about subcellular localization of the six DGC and PDE candidates that stood out in the overproduction assay (Fig. 3 and 4), we constructed C-terminal fusions of these proteins to EGFP. For this approach the encoding genes were replaced by the fusion constructs at their native genomic loci in Rm2011. Exponential- and stationary-phase cells of the resulting strains cultured in TY medium as well as in phosphate-sufficient and phosphate-limiting MM were analyzed by fluorescence microscopy (see Fig. S6 in the supplemental material). Out of these six fusion proteins only PleD-EGFP and SMc01464-EGFP produced a detectable fluorescence signal in cells cultured in the three media. SMb20447-EGFP fluorescence was detected only in cells growing in phosphate-limiting MM, and none of the strains with the remaining constructs produced a detectable fluorescence signal in any of the media tested.

Accumulation of PleD-EGFP in one or two predominantly polarly localized foci was observed in a considerable proportion of cells harvested from liquid cultures (Fig. 6A). We monitored the spatiotemporal localization of PleD-EGFP by time-lapse fluorescence microscopy (Fig. 6B). To unambiguously assign polar localization of PleD-EGFP to the mother or slightly smaller daughter cell of the asymmetrically dividing *S. meliloti* cells (58), the endogenous ParB was C-terminally tagged with mCherry in the *pleD-egfp*-expressing strain. ParB is known to bind close to the chromosomal origin of replication, and during chromosome segregation one copy moves from the old pole of the mother cell to the opposite pole (future old pole) of the emerging daughter cell (59, 60). Time-lapse microscopy revealed that during the *S. meliloti* cell cycle, a PleD-EGFP focus appeared in the daughter cell shortly before cells separated (Fig. 6B, arrow) and then disappeared and was no longer detectable at the time point when a second ParB-mCherry focus was visible at the new pole of the daughter cell.

Elevated levels of cdG diminish biosynthesis of QS signal molecules. Links between cdG-dependent regulation and QS have previously been reported in several bacterial species (reviewed in references 61 and 62). We therefore asked if elevated concentrations of cdG affect *N*-acyl-homoserine lactone (AHL)-mediated QS signaling. The expression level of the AHL synthase gene *sinI*

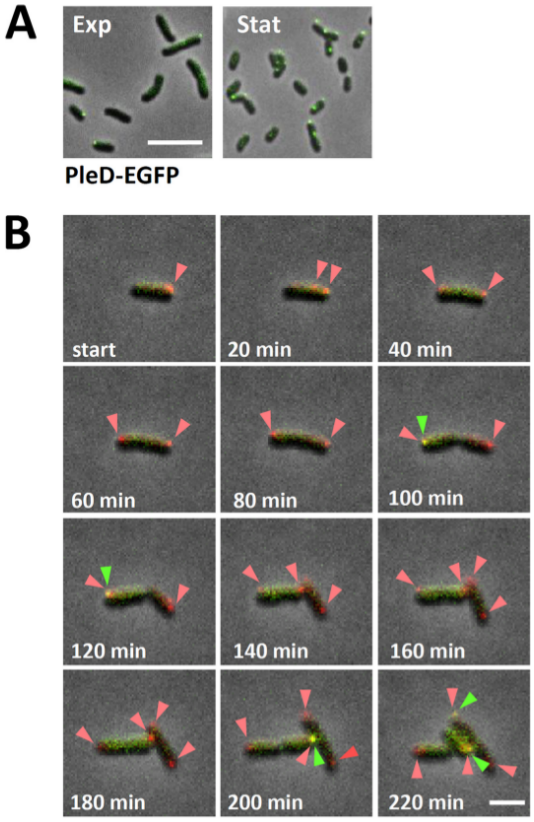

FIG 6 Spatiotemporal localization of PleD-EGFP during cell cycle. (A) Microscopy analysis of Rm2011 cells producing PleD-EGFP harvested from cultures in liquid TY medium in exponential (Exp) and stationary (Stat) growth phases. All images were taken using identical settings. Scale bar, 5 μm. (B) Time-lapse microscopy of Rm2011 carrying chromosomally integrated *pleD-egfp* and a *parB-mCherry* expression plasmid. Arrows point to PleD-EGFP foci overlapping ParB-mCherry foci. Green and red arrowheads point to PleD-EGFP and ParB-mCherry foci, respectively. Scale bar, 2 μm.

and overall AHL production were estimated in Rm2011 *expR*$^+$ upon overexpression of *pleD*, *pleD*$_{GGAAF}$, or *SMb20447*. Expression of *sinI* was assessed using a P$_{sinI}$-*egfp* fusion, and AHL production was detected by the *A. tumefaciens* indicator strain NTL4 (pZLR4) (Fig. 7). P$_{sinI}$ activity and AHL levels decreased when *pleD* or *SMb20447* was overexpressed, whereas overexpression of *pleD*$_{GGAAF}$ had no effect. These data suggest that cdG negatively regulates biosynthesis of QS signals. Repression of P$_{sinI}$ and reduction of AHL production were also observed in Rm2011 (Fig. 7). In this strain *expR* is disrupted by an insertion element (51). Therefore, this cdG-mediated regulation of *sinI* can be considered to be independent of *expR*. Moreover, in stationary-phase cultures of the Rm2011 cdG^0 strain, *sinI* promoter activity and AHL abundance increased (see Fig. S7 in the supplemental material), further supporting a cdG-mediated negative regulation of AHL synthesis.

cdG-stimulated biofilm formation is modulated by EPS. The *A. tumefaciens uppABCDEF* cluster (see Fig. S8A in the supplemental material) controls biosynthesis of a unipolarly localized polysaccharide (UPP) adhesin strictly required for surface attachment (63). Surface contact-independent production of this polysaccharide is induced by elevated levels of cdG (41). This gene cluster is highly conserved among rhizobia, including *S. meliloti* and *R. leguminosarum*. In *R. leguminosarum*, it drives biosynthesis of a polar glucomannan which is not required for biofilm formation but which significantly promotes attachment to roots and root hair infection (64, 65).

Looking for target processes that may contribute to cdG-mediated regulation of biofilm formation in *S. meliloti*, we studied the role of the *SMc01790-SMc01796* gene region showing homology to these gene clusters (see Fig. S8A in the supplemental material). A polar plasmid integration mutation in the *S. meliloti uppE* homolog *SMc01792*, also inactivating the downstream genes *SMc01791* and *SMc01790*, failed to respond to *pleD* overexpression with strong biofilm formation (Fig. 8A). *M. sativa* plants inoculated with this mutant were indistinguishable from plants inoculated with the wild type with respect to the number and color of nodules and the appearance of shoots. Since *SMc01794* promoter activity did not strongly alter upon *pleD* overexpression (see Fig. S8B), cdG-mediated regulation most likely occurs at the posttranscriptional level.

We further aimed at dissecting the contributions of EPS I, EPS II, and the biosynthetic product of the *SMc01790-SMc01796* gene cluster to cdG-enhanced biofilm formation. Biofilm formation induced by *pleD* overexpression was enhanced in an *exoY wgeB* double mutant, deficient in production of EPS I and EPS II (57, 66) compared to that in the *pleD*-overexpressing Rm2011 wild type (Fig. 8A). The presence of an intact *expR* gene increases both EPS I and EPS II production (67, 68). Biofilm formation caused by *pleD* overexpression in Rm2011 *expR*$^+$ was strongly reduced in comparison to the level in Rm2011 (Fig. 8A). Inactivation or

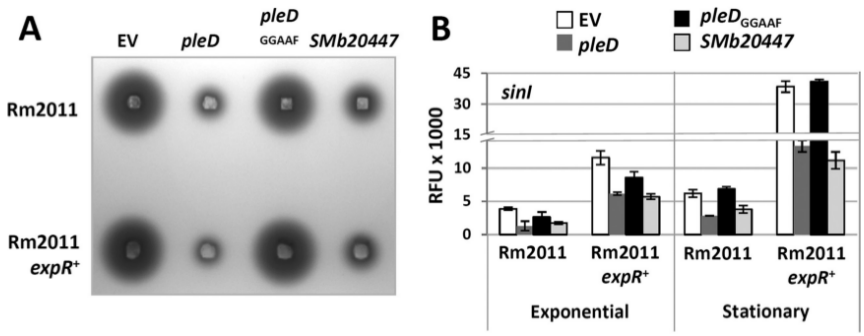

FIG 7 Elevated cdG content negatively affects AHL production at the level of *sinI* transcription. (A) Semiquantitative detection of AHLs in *S. meliloti* stationary-phase culture supernatants by *A. tumefaciens* NTL4(pZLR4). (B) *sinI* promoter activity determined using a P$_{sinI}$-*egfp* fusion. Exponential, 27 h after inoculation; stationary, 45 h after inoculation; EV, empty pWBT vector; RFU, relative EGFP fluorescence units. Error bars indicate standard deviations of three biological replicates.

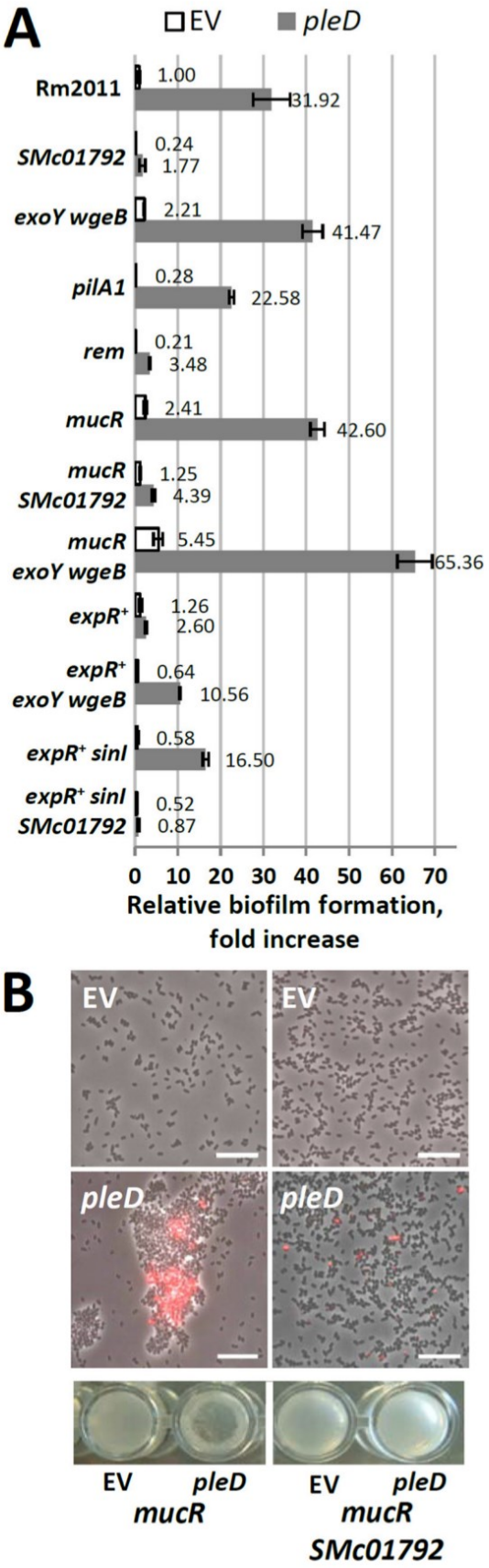

FIG 8 Biofilm formation and cell aggregation upon overexpression of *pleD*. (A) Biofilm formation in different genetic backgrounds relative to that of Rm2011 carrying the empty vector. EV, empty pWBT vector. The A_{570}/OD_{600} mean value for Rm2011 pWBT was 0.162 ± 0.046 (set to 1). Error bars indicate standard deviations of three biological replicates. (B) Cell clumping and fl-WGA staining in stationary 30% MM cultures grown in shaken liquid culture. Microscopy images (top) and wells of a 96-well plate (bottom) are shown. Scale bar, 10 μm.

strong reduction of EPS I and EPS II biosynthesis in Rm2011 *expR*$^+$ by *exoY wgeB* double mutation or by knockout of the AHL synthase gene *sinI* (69), respectively, partially restored cdG-stimulated biofilm formation upon *pleD* overexpression (Fig. 8A). Biofilm formation of the *pleD*-overexpressing Rm2011 *expR*$^+$ *sinI* strain was abolished by mutation of *SMc01792*, in the same way as in Rm2011 (Fig. 8A).

Mutation of *mucR* encoding a global transcriptional regulator leads to reduced production of EPS I and enhanced biosynthesis of EPS II (70). While EPS II produced by an *expR*$^+$ strain is composed of low-molecular-weight and high-molecular-weight fractions, a *mucR* mutant primarily produces high-molecular-weight EPS II (71). In contrast to Rm2011 *expR*$^+$, a *mucR* mutant responded to overexpression of *pleD* with strong biofilm formation, which was further enhanced upon mutation of *exoY* and *wgeB* (Fig. 8A). Mutation of *SMc01792* strongly reduced biofilm formation by the *pleD*-overexpressing *mucR* mutant, further supporting an important role of the *SMc01794-SMc01790* operon in cdG-enhanced surface attachment. Interestingly, *pleD*-overexpressing *mucR* cells clearly aggregated in agitated liquid cultures (Fig. 8B). Microscopy analysis confirmed the presence of large cell aggregates which were stainable with Alexa Fluor 594-conjugated wheat germ agglutinin (fl-WGA) binding to *N*-acetylglucosamine (GlcNAc), which is present in *A. tumefaciens* UPP (41) (Fig. 8B). Mutation of *SMc01792* abolished cell clumping and strongly reduced fl-WGA staining (Fig. 8B).

We further asked if *S. meliloti* flagella and pili contribute to biofilm formation. Mutations in *rem* and *flgH* strongly reduced biofilm formation, compared to the wild-type level, of both the *pleD*-overexpressing strain and the strain carrying the empty vector (Fig. 8A; see also Fig. S9 in the supplemental material). The *rem* mutant is nonmotile due to deficiency in flagellar gene expression (72), while the polar miniTn*5* insertion in *flgH* probably also disrupts transcription of the downstream genes *fliL* and *fliP*. The latter three genes encode membrane-associated components of the flagellar basal body. This implies that flagella or flagellar motility contributes to cdG-stimulated biofilm formation. In addition, a *pilA1* mutant strain also showed reduced biofilm formation (Fig. 8A), suggesting a role of type IVb pili in this process.

PilZ domain protein SMc00507 negatively regulates motility. The *S. meliloti* genome encodes two PilZ domain proteins (Fig. 2). The PilZ domains of both proteins contain conserved RXXXR and DXSXXG motifs separated by 21 amino acids in SMc00507 and by 19 amino acids in SMc00999. Whereas SMc00999 consists of an N-terminal domain of unknown function and a C-terminal PilZ domain, SMc00507 comprises only a single PilZ domain. *SMc00507* was annotated to encode a protein of 112 amino acids (GenBank accession number CAC46339.2). However, we found the predicted start codon to be incorrect. The *egfp* reporter gene fused to this TTG codon was not expressed, whereas it was expressed when fused to the downstream ATG at position 34. This strongly suggests that this ATG is the genuine start codon of *SMc00507* encoding a protein of 101 amino acids (see Fig. S10 in the supplemental material).

To learn about the role of *S. meliloti* PilZ domain proteins in cdG-dependent regulation, Rm2011 *SMc00507* and *SMc00999* single and double mutants were assayed for EPS production, motility, and biofilm formation (see Fig. S1 in the supplemental material). Under the conditions tested, no phenotypes could be assigned to these mutations. However, under conditions of elevated cdG levels caused by *pleD* overexpression, the *SMc00507 SMc00999* double mutant was slightly hypermotile, in contrast to the Rm2011 wild type that showed reduced motility (see Fig. S11A). In contrast, this double mutant was not affected in *pleD* overexpression-enhanced Congo red staining and biofilm formation (Fig. S11A). Characterization of the *SMc00507* and *SMc00999* single mutants identified the mutation in *SMc00507* to be responsible for enhanced motility upon *pleD* overexpression (Fig. 9A; see also Fig. S11B). Thus, *SMc00507* encodes a putative cdG receptor protein involved in regulation of motility in *S. meliloti*, and this protein was therefore was named *mcrA*, for motility-associated cdG receptor A.

Binding of cdG by His_6-McrA was tested by a differential radial capillary action of ligand assay (DRaCALA) (43) (Fig. 9B). Spotting of purified His_6-McrA preincubated with radiolabeled cdG on the membrane produced an intense signal in the middle of the spotting area originating from protein-bound cdG, whereas a surrounding weak signal was produced by nonbound cdG. This characteristic pattern indicates binding of radiolabeled cdG by His_6-McrA. Binding was outcompeted by nonlabeled cdG but not by nonlabeled GTP, supporting the idea that His_6-McrA specifically binds cdG. Moreover, mutating the conserved N-terminal RXXXR motif by the amino acid exchanges R9A and R13A in His_6-McrA (designated His_6-$McrA_{AXXXA}$) abolished cdG binding (Fig. 9B), supporting the idea that this motif is involved in cdG binding. We also attempted to mutate the conserved DXSXXG motif; however, the simultaneous amino acid exchanges D35A, S37A, and G40A rendered the protein insoluble (data not shown).

PilZ proteins were previously reported to undergo conformational changes upon cdG binding (4, 73). We tested for *in vivo* binding of cdG to McrA and a conformational change upon binding by employing a modified version of the fluorescence resonance energy transfer (FRET)-based cdG biosensor designed by Christen et al. (20). The original biosensor is composed of the cdG receptor protein YcgR flanked by CyPet and YPet fluorophores. A conformational change of YcgR upon cdG binding results in an altered YPet/CyPet emission ratio (526 nm/476 nm). In this biosensor, we replaced YcgR by McrA and produced this fusion protein in Rm2011 with and without *pleD* overexpression. The CyPet-YcgR-YPet and CyPet-12aa-YPet (CyPet and YPet with a 12-amino-acid linker) constructs were used as positive and negative controls, respectively. Compared to the Rm2011 wild-type background, in the *pleD*-overexpressing strain, the 526 nm/476 nm ratio of CyPet-12aa-YPet-mediated fluorescence did not change. In contrast, the 526 nm/476 nm ratio of CyPet-YcgR-YPet- and CyPet-McrA-YPet-mediated fluorescence decreased and increased, respectively (Fig. 9C). The former indicates that upon cdG binding to YcgR the expected conformational change moves the fluorophores farther apart (20), while the latter implies that cdG binding to McrA induces a conformational change moving the fluorophores closer together.

Overexpression of *mcrA* in the Rm2011 wild type resulted in slightly reduced motility, whereas EPS and biofilm phenotypes were unaffected (Fig. 3). Furthermore, combined overexpression

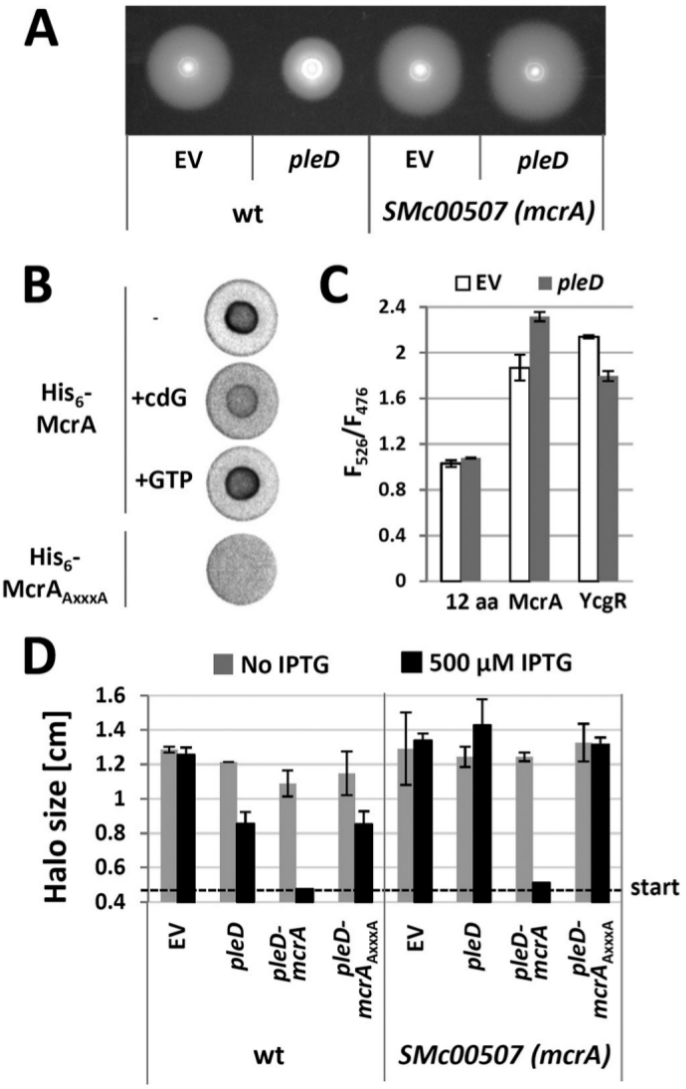

FIG 9 Identification of McrA (SMc00507) as a cdG receptor mediating repression of swimming motility upon *pleD* overexpression. (A) Swimming motility of the Rm2011 wild type (wt) and *mcrA* mutant upon *pleD* overexpression. EV, empty pWBT vector. (B) DRaCALA with radiolabeled cdG and His_6-McrA or His_6-$McrA_{AXXXA}$. (C) Detection of conformational change in McrA upon *pleD* overexpression in Rm2011 using the CyPet/YPet FRET biosensor. The negative control CyPet-12aa-YPet (12aa) and positive control (YcgR) were analyzed in parallel. EV, empty pSRKKm vector; F_{526}, emission at 526 nm normalized to OD_{600} (excitation at 425 nm); F_{476}, emission at 476 nm normalized to OD_{600} (excitation at 425 nm). Error bars indicate standard deviations of three biological replicates. (D) Swimming motility of wild-type Rm2011 and the *mcrA* mutant upon overexpression of *pleD* alone, in combination with *mcrA*, or in combination with $mcrA_{AXXXA}$. EV, empty pWBT vector. Error bars indicate standard deviations of three biological replicates.

of *pleD* and *mcrA* but not $mcrA_{AXXXA}$ led to a nonmotile phenotype (Fig. 3 and 9D), strongly suggesting that cdG-bound McrA negatively controls motility. Combined *pleD* and *mcrA* overexpression in Rm2011 did not affect EPS production, whereas biofilm formation decreased about 10-fold compared to the level of Rm2011 overexpressing *pleD* alone (Fig. 3). This outcome is consistent with our observation that the nonmotile *rem* mutant is defective in *pleD* overexpression-mediated biofilm formation (Fig. 8A).

DISCUSSION

The role of cdG in *S. meliloti*. Our systematic analysis of GGDEF-, EAL-, and PilZ-domain-encoding genes signified similarities but also differences of the role of cdG in *S. meliloti* compared to that in other bacteria. Single gene mutations in predicted cdG-related genes did not show striking changes in phenotypes typically associated with cdG, like EPS production, swimming motility, biofilm formation, and host infection. The only exception is the putatively essential gene *SMc00074*, predicted to encode an integral membrane protein with cytoplasmic EAL and inactive GGDEF domains. Single mutations in *dgcA* and *dgcB* encoding hybrid GGDEF-EAL domain proteins did not cause phenotypic changes in *R. etli* (26), a finding which is similar to our mutant screening data. However, our findings are in disagreement with those of Wang et al. (24), who reported weak changes in motility, symbiosis, and EPS production in 11 out of 14 single-gene mutants in GGDEF- and/or EAL-domain-encoding genes in *S. meliloti* Rm1021, which is closely related to the wild-type strain in our study. Slight differences between strains and assay conditions may account for this discrepancy.

While functional redundancies and compensatory effects may explain missing or weak effects of the single mutants in cdG-related genes, most unexpectedly the *S. meliloti* cdG^0 strains also did not show salient phenotypes in the physiological processes tested, except for increased sensitivity to acid stress. The acid stress response of Rm2011 involves repression of motility and activation of EPS biosynthesis (74), processes that were affected by elevated levels of cdG. To our knowledge, *S. meliloti* is the only bacterium described so far which does not require cdG or GGDEF/EAL domain proteins for swimming motility. A *C. crescentus* cdG^0 strain was nonmotile due to lack of flagella and impaired in surface attachment and cell differentiation, the latter impairment resulting in aberrant cell morphology (75). Deletion of all GGDEF-domain-encoding genes in *Salmonella* Typhimurium abolished virulence, resistance to desiccation, motility, biofilm formation, and synthesis of cellulose and fimbriae, while growth and resistance to acid, salt, or starvation stress were unaffected (16).

Since the cdG content was in the range of a few picomoles per milligram of total protein, similar to other bacteria studied (76–78), the phenotypic neutrality of the cdG^0 strains is unlikely to be due to low abundance or absence of cdG in the wild type under the growth conditions applied in this study. However, we cannot exclude the possibility that the Rm2011 laboratory strain has lost sensory and regulatory pathways that stimulate enhanced cdG production. In *S. meliloti*, cdG content strongly dropped in the stationary phase. Growth-dependent alterations in cdG concentrations were also reported for *E. coli* showing higher levels of cdG at the transition to stationary phase than in the exponential and stationary phases (78). In contrast, levels of cdG in *Myxococcus xanthus* cells seem not to be growth phase regulated (76).

Nevertheless, in agreement with a classical cdG-mediated motile-sessile switch, elevated levels of cdG caused by overexpression of heterologous or native DGC-encoding genes resulted in enhanced biofilm formation coinciding with changes in EPS biosynthesis and reduced motility (summarized in Fig. 10). Our study strongly suggests that PleD, SMb20523, SMb20447, SMc01464, and SMc03178 have DGC activity in *S. meliloti* although we cannot exclude the possibility that overexpression of GGDEF- and/or EAL-encoding genes indirectly influence other DGCs or PDEs.

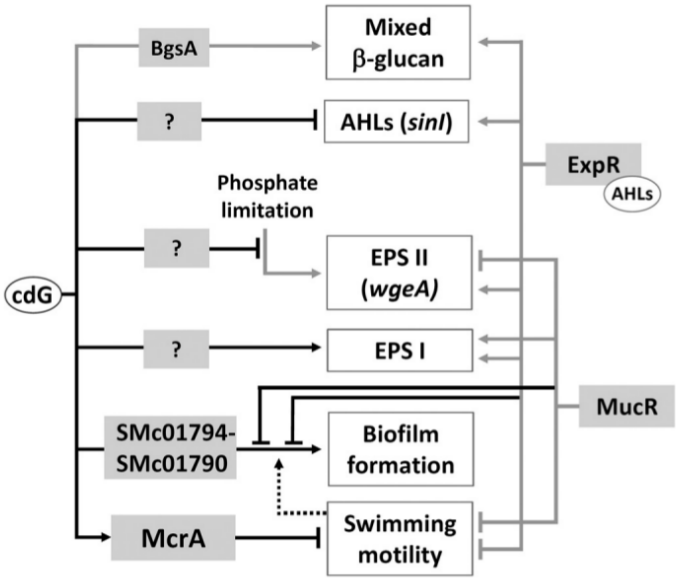

FIG 10 Summary of cdG-mediated regulation in *S. meliloti*. Black lines show regulatory interactions described in this study, and gray lines denote previously identified regulatory links (25, 34, 49, 50, 68, 69). Biosynthesis of QS signals is negatively regulated at the level of *sinI* transcription. EPS I and EPS II biosynthesis is affected by cdG via unknown pathways. Phosphate limitation-induced activation of EPS II biosynthesis is reduced at elevated cdG levels. This includes a change in *wgeA* promoter activity. Biofilm formation is enhanced involving gene products of the *SMc01794-SMc01790* operon and is negatively affected by the global regulators MucR and ExpR, which also regulate motility and EPS biosynthesis. Flagella contribute to biofilm formation. Repression of swimming motility involves binding of cdG to the PilZ-domain protein McrA.

Four of these proteins possess a canonical GG(D/E)EF motif, whereas SMb20447 has an AGDEF motif, as has been reported for the active DGC VCA0965 from *Vibrio cholerae* (79). Among the 20 proteins putatively associated with cdG synthesis, degradation, or binding, 11 have both complete GGDEF and EAL domains, including SMb20447 and SMc03178. Despite the presence of a well-conserved EAL domain, overproduction of either of these two proteins results in a strong increase in cdG levels. This suggests that under the conditions of overproduction, DGC activity of SMb20447 and SMc03178 is dominant. Control of the catalytic activities of such dual-function enzymes can be a key point of regulation. A regulatory control of both enzymatic functions has previously been reported for *Rhodobacter sphaeroides* BphG1, *Vibrio parahaemolyticus* ScrC, *Legionella pneumophila* Lpl0329, and *A. tumefaciens* DcpA (80–83). Unexpectedly, overproduction of the predicted PDE SMb21517, encoding a single EAL domain, resulted in a moderate increase in cdG content and inhibited motility. The same effects were observed upon overproduction of EAL-domain-containing or HD-GYP-domain-containing proteins in *Legionella pneumophila* or *Pectobacterium atrosepticum* (84, 85), indicating indirect effects on other DGCs or PDEs.

Effect of cdG on the cell cycle. Very high levels of cdG provoked *S. meliloti* cell elongation, which might have been directly caused by this second messenger or indirectly by exhausting the GTP pool. In *C. crescentus*, cdG and the single-domain response regulator DivK convergently regulate cell cycle progression (21). In this regulation, cdG-induced phosphatase activity of the cell cycle kinase CckA promotes replication initiation and cell cycle progression. The C-terminal part of the *S. meliloti* CckA, which

contains the catalytic and REC domains, shares 47% identity with its *C. crescentus* ortholog, including residue Y514, shown to be important for binding of cdG (21). Thus, it is tempting to speculate that, at least at very high cdG concentrations, binding of cdG to CckA possibly also impacts the *S. meliloti* cell cycle.

In *C. crescentus*, PleD is involved in regulation of cell cycle progression and was shown to be responsible for uneven distribution of cdG in mother and daughter cells, with the mother cell containing more cdG (20). Localization of PleD to the stalked cell pole (the old pole of the mother cell) is believed to be associated with its DGC activity (86). Although the *C. crescentus* and *S. meliloti* PleD proteins share 51% identity, their modes of regulation and roles in the cell cycle may be different. This is substantiated by different localization patterns and mutant phenotypes. Localization of PleD in *C. crescentus* and *S. meliloti* differs in that it localizes to the old poles of the mother and daughter cells, respectively. Furthermore, the *S. meliloti pleD* mutant did not differ from the wild type in motility, while the *C. crescentus pleD* mutant was hypermotile due to defects in flagellum ejection and stalk morphogenesis (87). Similarly to the *S. meliloti pleD* mutant, an *A. tumefaciens pleD* deletion mutant was unaffected in motility and showed no obvious developmental defects (88). However, the pattern of flagellation differs between these organisms. Swimming motility of *C. crescentus* is mediated by a single polar flagellum localized at the new pole (89), while *A. tumefaciens* exhibits two flagella in a polar or subpolar tuft at one pole, plus one or two lateral flagella on each side (90), and peritrichous flagella drive motility of *S. meliloti* (91).

Modulation of QS by cdG. Quorum sensing and cdG-dependent regulation are interconnected in several bacterial species. The most common mechanism is regulation of cdG biosynthesis or degradation by QS lowering cdG levels in the QS state (reviewed in references 61 and 62). Under the conditions tested, QS did not influence the total cdG content in *S. meliloti*, but both native and elevated levels of cdG negatively affected expression of the AHL synthase gene *sinI* and accumulation of AHLs in the growth medium. Similarly, the PDE activity of RpfR was required for normal levels of transcription of the AHL synthase gene *cepI* and AHL production in *Burkholderia cenocepacia*, whereas the factor mediating cdG-dependent negative regulation of the synthase gene remained unknown (92). Since the cdG content was higher in exponential- than in stationary-phase *S. meliloti* cells, negative regulation of AHL biosynthesis by cdG may serve as a fine-tuning mechanism attenuating AHL accumulation in rapidly growing cells.

The role of EPS in cdG-enhanced biofilm formation. Our data strongly suggest that *S. meliloti*, just like *A. tumefaciens* (41, 63), employs a GlcNAc-containing UPP required for cdG-mediated cell aggregation and attachment to abiotic surfaces. The architectures of the *S. meliloti SMc01796-SMc01790* and *A. tumefaciens uppABCDEF* biosynthetic gene clusters are similar, both encoding two polysaccharide export proteins, two proteins with unknown function, and two (*A. tumefaciens*) or three (*S. meliloti*) glycosyltransferases. GlcNAc polymers were also found to be important for surface attachment of *C. crescentus* as a component of the holdfast adhesin at the tip of the stalk (93, 94).

While this putative GlcNAc-containing UPP was essential for cdG-enhanced biofilm formation of *S. meliloti*, EPS I and/or EPS II seems to hamper this process, and the amount and composition of EPS may be relevant to this interference. This negative effect of EPS production on biofilm formation was clearly seen only under conditions of elevated levels of cdG. This is in agreement with EPS-deficient Rm1021 mutants which are unaffected in biofilm formation (95). In line with a negative role of EPS at least in initial steps of surface attachment and cell aggregation, overproduction of EPS I by an *S. meliloti* Rm1021 *emrR* mutant correlated with decreased biofilm formation (96). In contrast, extensive overproduction of EPS I may have a positive effect on biofilm formation, possibly by mechanisms not including the GlcNAc-containing UPP. An *S. meliloti* Rm1021 strain encoding a constitutively active variant of the receptor histidine kinase ExoS is nonmotile, extensively overproduces EPS I, and was reported to show stronger biofilm formation than the wild type (97).

Flagellar motility accelerates surface adhesion of various bacteria (reviewed in reference 98). Pili and flagella were suggested to mediate a first, reversible phase of surface attachment of *C. crescentus* (93). In *S. meliloti*, absence of flagella was reported to have a negative effect on biofilm formation (97). Our data suggest that cdG-enhanced biofilm formation of *S. meliloti* involves repression of swimming motility but also requires presence of pili and flagella.

A PilZ domain protein negatively regulates motility. PilZ domain proteins were reported to negatively regulate motility in diverse bacteria like *E. coli*, *C. crescentus*, *Azospirillum brasilense*, and *Pseudomonas fluorescens* (11, 99, 100) or to stimulate it in *Treponema denticola* and *Borrelia burgdorferi* (101, 102). In this study, we identified McrA as a cdG receptor protein, able to repress swimming motility at elevated cdG levels. McrA is a small protein of 101 amino acids solely comprising a PilZ domain. Such architecture is not uncommon; however, not much is known about the functions of these proteins. DgrA and DgrB are single-domain PilZ proteins involved in cdG-dependent repression of motility in *C. crescentus* (11). DgrA binds cdG *in vitro*, and its overexpression results in decreased abundance of the flagellar rotation protein FliL via an unknown mechanism (11). Although no significant homology exists between McrA and DgrA, the congruent architecture comprising just a PilZ domain implies that their function likely relies on interactions with other proteins.

Eliminating cdG-dependent McrA-mediated negative regulation of motility led to slight hypermotility at elevated cdG levels, which reveals an additional positive effect of cdG on motility. This observation is in line with a bipartite role of cdG in flagellar-based motility regulation proposed for *S.* Typhimurium and *C. crescentus* in that cdG may coordinate flagellar assembly and rotation (16, 73, 75). In a strikingly similar manner, overproduction of a heterologous DGC rendered an *S.* Typhimurium mutant in the PilZ domain-encoding *ycgR* gene hypermotile, and combined overproduction of this DGC and YcgR provoked a nonmotile phenotype in the same way as combined overexpression of *pleD* and *mcrA* in *S. meliloti* (73). An additional similarity is probably a conformational change triggered upon binding of cdG to YcgR (73) and McrA.

Consistent with the assumption of a common role of cdG in regulating the motile-sessile switch in bacteria, our findings indicate that high cdG levels favor a sessile lifestyle of *S. meliloti*. Yet no phenotypic differences were evident between mutants in 21 out of 22 cdG-related genes and the wild type, and only overexpression of seven of these genes resulted in phenotypic changes. Most unexpectedly, the *S. meliloti* mutants unable to produce cdG were not affected in processes typically controlled by this second messenger, including motility. Moreover, cdG was also not an impor-

tant bacterial factor in root nodule symbiosis. This suggests that these proteins are not active under the conditions tested or that they have a role in processes not assayed in this study. It may also be indicative of overlapping regulatory controls, as has been reported for the regulatory pathway driving cell cycle progression in *C. crescentus* (21).

ACKNOWLEDGMENTS

We thank Vincent Franz for assistance with protein purification and plant assays, Pornsri Charoenpanich and Matthew McIntosh for sharing plasmids, Hemantha Kulasekara for providing the FRET-based cdG biosensor construct, and Annette Garbe for technical help with LC-MS/MS measurements.

Financial support from the German Research Foundation (Collaborative Research Centre 987 Microbial Diversity in Environmental Signal Response), the LOEWE program of the State of Hesse (Germany), and the Max Planck Society is acknowledged. We acknowledge technical assistance and access to resources supported by BMBF grant FKZ 031A533 within the de.NBI network.

FUNDING INFORMATION

State of Hesse (Germany) provided funding to Elizaveta Krol and Anke Becker under grant number SYNMIKRO. Max Planck Society provided funding to Dorota Skotnicka and Lotte Søgaard-Andersen. Deutsche Forschungsgemeinschaft (DFG) provided funding to Simon Schäper, Elizaveta Krol, Lotte Søgaard-Andersen, and Anke Becker under grant number SFB 987.

REFERENCES

1. **Jones KM, Kobayashi H, Davies BW, Taga ME, Walker GC.** 2007. How rhizobial symbionts invade plants: the *Sinorhizobium-Medicago* model. Nat Rev Microbiol **5:**619–633. http://dx.doi.org/10.1038/nrmicro1705.
2. **Hengge R.** 2009. Principles of c-di-GMP signalling in bacteria. Nat Rev Microbiol **7:**263–273. http://dx.doi.org/10.1038/nrmicro2109.
3. **Römling U, Galperin MY, Gomelsky M.** 2013. Cyclic di-GMP: the first 25 years of a universal bacterial second messenger. Microbiol Mol Biol Rev **77:**1–52. http://dx.doi.org/10.1128/MMBR.00043-12.
4. **Schirmer T, Jenal U.** 2009. Structural and mechanistic determinants of c-di-GMP signalling. Nat Rev Microbiol **7:**724–735. http://dx.doi.org/10.1038/nrmicro2203.
5. **Sudarsan N, Lee ER, Weinberg Z, Moy RH, Kim JN, Link KH, Breaker RR.** 2008. Riboswitches in eubacteria sense the second messenger cyclic di-GMP. Science **321:**411–413. http://dx.doi.org/10.1126/science.1159519.
6. **Fang X, Ahmad I, Blanka A, Schottkowski M, Cimdins A, Galperin MY, Römling U, Gomelsky M.** 2014. GIL, a new c-di-GMP-binding protein domain involved in regulation of cellulose synthesis in enterobacteria. Mol Microbiol **93:**439–452. http://dx.doi.org/10.1111/mmi.12672.
7. **Duerig A, Abel S, Folcher M, Nicollier M, Schwede T, Amiot N, Giese B, Jenal U.** 2009. Second messenger-mediated spatiotemporal control of protein degradation regulates bacterial cell cycle progression. Genes Dev **23:**93–104. http://dx.doi.org/10.1101/gad.502409.
8. **Newell PD, Monds RD, O'Toole GA.** 2009. LapD is a bis-(3′,5′)-cyclic dimeric GMP-binding protein that regulates surface attachment by *Pseudomonas fluorescens* Pf0-1. Proc Natl Acad Sci U S A **106:**3461–3466. http://dx.doi.org/10.1073/pnas.0808933106.
9. **Amikam D, Galperin MY.** 2006. PilZ domain is part of the bacterial c-di-GMP binding protein. Bioinformatics **22:**3–6. http://dx.doi.org/10.1093/bioinformatics/bti739.
10. **Wolfe AJ, Visick KL.** 2008. Get the message out: cyclic-Di-GMP regulates multiple levels of flagellum-based motility. J Bacteriol **190:**463–475. http://dx.doi.org/10.1128/JB.01418-07.
11. **Christen M, Christen B, Allan MG, Folcher M, Jenö P, Grzesiek S, Jenal U.** 2007. DgrA is a member of a new family of cyclic diguanosine monophosphate receptors and controls flagellar motor function in *Caulobacter crescentus*. Proc Natl Acad Sci U S A **104:**4112–4117. http://dx.doi.org/10.1073/pnas.0607738104.
12. **Ryjenkov DA, Simm R, Römling U, Gomelsky M.** 2006. The PilZ domain is a receptor for the second messenger c-di-GMP: the PilZ domain protein YcgR controls motility in enterobacteria. J Biol Chem **281:**30310–30314. http://dx.doi.org/10.1074/jbc.C600179200.
13. **Tischler AD, Camilli A.** 2005. Cyclic diguanylate regulates *Vibrio cholerae* virulence gene expression. Infect Immun **73:**5873–5882. http://dx.doi.org/10.1128/IAI.73.9.5873-5882.2005.
14. **Kulasakara H, Lee V, Brencic A, Liberati N, Urbach J, Miyata S, Lee DG, Neely AN, Hyodo M, Hayakawa Y, Ausubel FM, Lory S.** 2006. Analysis of *Pseudomonas aeruginosa* diguanylate cyclases and phosphodiesterases reveals a role for bis-(3′-5′)-cyclic-GMP in virulence. Proc Natl Acad Sci U S A **103:**2839–2844. http://dx.doi.org/10.1073/pnas.0511090103.
15. **Ryan RP, Fouhy Y, Lucey JF, Jiang BL, He YQ, Feng JX, Tang JL, Dow JM.** 2007. Cyclic di-GMP signalling in the virulence and environmental adaptation of *Xanthomonas campestris*. Mol Microbiol **63:**429–442. http://dx.doi.org/10.1111/j.1365-2958.2006.05531.x.
16. **Solano C, García B, Latasa C, Toledo-Arana A, Zorraquino V, Valle J, Casals J, Pedroso E, Lasa I.** 2009. Genetic reductionist approach for dissecting individual roles of GGDEF proteins within the c-di-GMP signaling network in *Salmonella*. Proc Natl Acad Sci U S A **106:**7997–8002. http://dx.doi.org/10.1073/pnas.0812573106.
17. **Bobrov AG, Kirillina O, Ryjenkov DA, Waters CM, Price PA, Fetherston JD, Mack D, Goldman WE, Gomelsky M, Perry RD.** 2011. Systematic analysis of cyclic di-GMP signalling enzymes and their role in biofilm formation and virulence in *Yersinia pestis*. Mol Microbiol **79:**533–551. http://dx.doi.org/10.1111/j.1365-2958.2010.07470.x.
18. **Waters CM, Lu W, Rabinowitz JD, Bassler BL.** 2008. Quorum sensing controls biofilm formation in *Vibrio cholerae* through modulation of cyclic di-GMP levels and repression of *vpsT*. J Bacteriol **190:**2527–2536. http://dx.doi.org/10.1128/JB.01756-07.
19. **Andrade MO, Alegria MC, Guzzo CR, Docena C, Rosa MC, Ramos CH, Farah CS.** 2006. The HD-GYP domain of RpfG mediates a direct linkage between the Rpf quorum-sensing pathway and a subset of diguanylate cyclase proteins in the phytopathogen *Xanthomonas axonopodis* pv citri. Mol Microbiol **62:**537–551. http://dx.doi.org/10.1111/j.1365-2958.2006.05386.x.
20. **Christen M, Kulasekara HD, Christen B, Kulasekara BR, Hoffman LR, Miller SI.** 2010. Asymmetrical distribution of the second messenger c-di-GMP upon bacterial cell division. Science **328:**1295–1297. http://dx.doi.org/10.1126/science.1188658.
21. **Lori C, Ozaki S, Steiner S, Böhm R, Abel S, Dubey BN, Schirmer T, Hiller S, Jenal U.** 2015. Cyclic di-GMP acts as a cell cycle oscillator to drive chromosome replication. Nature **523:**236–239. http://dx.doi.org/10.1038/nature14473.
22. **Pérez-Mendoza D, Aragón IM, Prada-Ramírez HA, Romero-Jiménez L, Ramos C, Gallegos MT, Sanjuán J.** 2014. Responses to elevated c-di-GMP levels in mutualistic and pathogenic plant-interacting bacteria. PLoS One **9:**e91645. http://dx.doi.org/10.1371/journal.pone.0091645.
23. **Ma Q, Zhang G, Wood TK.** 2011. *Escherichia coli* BdcA controls biofilm dispersal in *Pseudomonas aeruginosa* and *Rhizobium meliloti*. BMC Res Notes **4:**447. http://dx.doi.org/10.1186/1756-0500-4-447.
24. **Wang Y, Xu J, Chen A, Zhu J, Yu G, Xu L, Luo L.** 2010. GGDEF and EAL proteins play different roles in the control of *Sinorhizobium meliloti* growth, motility, exopolysaccharide production, and competitive nodulation on host alfalfa. Acta Biochim Biophys Sin (Shanghai) **42:**410–417. http://dx.doi.org/10.1093/abbs/gmq034.
25. **Pérez-Mendoza D, Rodríguez-Carvajal M, Romero-Jiménez L, Farias GeA, Lloret J, Gallegos MT, Sanjuán J.** 2015. Novel mixed-linkage β-glucan activated by c-di-GMP in *Sinorhizobium meliloti*. Proc Natl Acad Sci U S A **112:**E757–E765. http://dx.doi.org/10.1073/pnas.1421748112.
26. **Gao S, Romdhane SB, Beullens S, Kaever V, Lambrichts I, Fauvart M, Michiels J.** 2014. Genomic analysis of cyclic-di-GMP-related genes in rhizobial type strains and functional analysis in *Rhizobium etli*. Appl Microbiol Biotechnol **98:**4589–4602. http://dx.doi.org/10.1007/s00253-014-5722-7.
27. **Chou SH, Galperin MY.** 8 June 2015. Diversity of c-di-GMP-binding proteins and mechanisms. J Bacteriol http://dx.doi.org/10.1128/JB.00333-15.
28. **Galibert F, Finan TM, Long SR, Puhler A, Abola P, Ampe F, Barloy-Hubler F, Barnett MJ, Becker A, Boistard P, Bothe G, Boutry M, Bowser L, Buhrmester J, Cadieu E, Capela D, Chain P, Cowie A, Davis RW, Dreano S, Federspiel NA, Fisher RF, Gloux S, Godrie T, Goffeau A, Golding B, Gouzy J, Gurjal M, Hernandez-Lucas I, Hong A, Huizar L, Hyman RW, Jones T, Kahn D, Kahn ML, Kalman S, Keating DH, Kiss E, Komp C, Lelaure V, Masuy D, Palm C, Peck MC, Pohl TM, Portetelle D, Purnelle B, Ramsperger U, Surzycki R, Thebault P,**

Vandenbol M, et al. 2001. The composite genome of the legume symbiont *Sinorhizobium meliloti*. Science **293:**668–672. http://dx.doi.org/10.1126/science.1060966.

29. **Casse F, Boucher C, Julliot J, Michel M, Dénarié J.** 1979. Identification and characterization of large plasmids in *Rhizobium meliloti* using agarose gel electrophoresis. Microbiology **113:**229–242.
30. **Meade HM, Long SR, Ruvkun GB, Brown SE, Ausubel FM.** 1982. Physical and genetic characterization of symbiotic and auxotrophic mutants of *Rhizobium meliloti* induced by transposon Tn*5* mutagenesis. J Bacteriol **149:**114–122.
31. **Beringer JE.** 1974. R factor transfer in *Rhizobium leguminosarum*. J Gen Microbiol **84:**188–198. http://dx.doi.org/10.1099/00221287-84-1-188.
32. **Green MR, Sambrook J.** 2012. Molecular cloning: a laboratory manual, 4th ed. Cold Spring Harbor Laboratory Press, Cold Spring Harbor, NY.
33. **Tombolini R, Nuti MP.** 1990. Poly(β-hydroxyalkanoate) biosynthesis and accumulation by different *Rhizobium* species. FEMS Microbiol Lett **60:**299–304.
34. **Zhan HJ, Lee CC, Leigh JA.** 1991. Induction of the second exopolysaccharide (EPSb) in *Rhizobium meliloti* SU47 by low phosphate concentrations. J Bacteriol **173:**7391–7394.
35. **Simon R, Priefer U, Pühler A.** 1983. A broad host range mobilization system for *in vivo* genetic engineering: transposon mutagenesis in gram-negative bacteria. Nat Biotechnol **1:**784–791. http://dx.doi.org/10.1038/nbt1183-784.
36. **Krol E, Becker A.** 2014. Rhizobial homologs of the fatty acid transporter FadL facilitate perception of long-chain acyl-homoserine lactone signals. Proc Natl Acad Sci U S A **111:**10702–10707. http://dx.doi.org/10.1073/pnas.1404929111.
37. **Schäfer A, Tauch A, Jäger W, Kalinowski J, Thierbach G, Pühler A.** 1994. Small mobilizable multi-purpose cloning vectors derived from the *Escherichia coli* plasmids pK18 and pK19: selection of defined deletions in the chromosome of *Corynebacterium glutamicum*. Gene **145:**69–73. http://dx.doi.org/10.1016/0378-1119(94)90324-7.
38. **Langmead B, Salzberg S.** 2012. Fast gapped-read alignment with Bowtie 2. Nat Methods **9:**357–359. http://dx.doi.org/10.1038/nmeth.1923.
39. **Hilker R, Stadermann KB, Doppmeier D, Kalinowski J, Stoye J, Straube J, Winnebald J, Goesmann A.** 2014. ReadXplorer—visualization and analysis of mapped sequences. Bioinformatics **30:**2247–2254. http://dx.doi.org/10.1093/bioinformatics/btu205.
40. **Robledo M, Rivera L, Jiménez-Zurdo JI, Rivas R, Dazzo F, Velázquez E, Martínez-Molina E, Hirsch AM, Mateos PF.** 2012. Role of *Rhizobium* endoglucanase CelC2 in cellulose biosynthesis and biofilm formation on plant roots and abiotic surfaces. Microb Cell Fact **11:**125. http://dx.doi.org/10.1186/1475-2859-11-125.
41. **Xu J, Kim J, Koestler BJ, Choi JH, Waters CM, Fuqua C.** 2013. Genetic analysis of *Agrobacterium tumefaciens* unipolar polysaccharide production reveals complex integrated control of the motile-to-sessile switch. Mol Microbiol **89:**929–948. http://dx.doi.org/10.1111/mmi.12321.
42. **Burhenne H, Kaever V.** 2013. Quantification of cyclic dinucleotides by reversed-phase LC-MS/MS. Methods Mol Biol **1016:**27–37. http://dx.doi.org/10.1007/978-1-62703-441-8_3.
43. **Roelofs KG, Wang J, Sintim HO, Lee VT.** 2011. Differential radial capillary action of ligand assay for high-throughput detection of protein-metabolite interactions. Proc Natl Acad Sci U S A **108:**15528–15533. http://dx.doi.org/10.1073/pnas.1018949108.
44. **Bordeleau E, Brouillette E, Robichaud N, Burrus V.** 2010. Beyond antibiotic resistance: integrating conjugative elements of the SXT/R391 family that encode novel diguanylate cyclases participate to c-di-GMP signalling in *Vibrio cholerae*. Environ Microbiol **12:**510–523. http://dx.doi.org/10.1111/j.1462-2920.2009.02094.x.
45. **Broughton WJ, Dilworth MJ.** 1971. Control of leghaemoglobin synthesis in snake beans. Biochem J **125:**1075–1080. http://dx.doi.org/10.1042/bj1251075.
46. **Cowie A, Cheng J, Sibley CD, Fong Y, Zaheer R, Patten CL, Morton RM, Golding GB, Finan TM.** 2006. An integrated approach to functional genomics: construction of a novel reporter gene fusion library for *Sinorhizobium meliloti*. Appl Environ Microbiol **72:**7156–7167. http://dx.doi.org/10.1128/AEM.01397-06.
47. **Reinhold BB, Chan SY, Reuber TL, Marra A, Walker GC, Reinhold VN.** 1994. Detailed structural characterization of succinoglycan, the major exopolysaccharide of *Rhizobium meliloti* Rm1021. J Bacteriol **176:**1997–2002.
48. **Her GR, Glazebrook J, Walker GC, Reinhold VN.** 1990. Structural studies of a novel exopolysaccharide produced by a mutant of *Rhizobium meliloti* strain Rm1021. Carbohydr Res **198:**305–312. http://dx.doi.org/10.1016/0008-6215(90)84300-J.
49. **Bahlawane C, Baumgarth B, Serrania J, Rüberg S, Becker A.** 2008. Fine-tuning of galactoglucan biosynthesis in *Sinorhizobium meliloti* by differential ExpG- (WggR-), PhoB-, and MucR-dependent regulation of two promoters. J Bacteriol **190:**3456–3466. http://dx.doi.org/10.1128/JB.00062-08.
50. **Bahlawane C, McIntosh M, Krol E, Becker A.** 2008. *Sinorhizobium meliloti* regulator MucR couples exopolysaccharide synthesis and motility. Mol Plant Microbe Interact **21:**1498–1509. http://dx.doi.org/10.1094/MPMI-21-11-1498.
51. **Pellock BJ, Teplitski M, Boinay RP, Bauer WD, Walker GC.** 2002. A LuxR homolog controls production of symbiotically active extracellular polysaccharide II by *Sinorhizobium meliloti*. J Bacteriol **184:**5067–5076. http://dx.doi.org/10.1128/JB.184.18.5067-5076.2002.
52. **Sevin EW, Barloy-Hubler F.** 2007. RASTA-Bacteria: a web-based tool for identifying toxin-antitoxin loci in prokaryotes. Genome Biol **8:**R155. http://dx.doi.org/10.1186/gb-2007-8-8-r155.
53. **Morris J, González JE.** 2009. The novel genes *emmABC* are associated with exopolysaccharide production, motility, stress adaptation, and symbiosis in *Sinorhizobium meliloti*. J Bacteriol **191:**5890–5900. http://dx.doi.org/10.1128/JB.00760-09.
54. **Geddes BA, González JE, Oresnik IJ.** 2014. Exopolysaccharide production in response to medium acidification is correlated with an increase in competition for nodule occupancy. Mol Plant Microbe Interact **27:**1307–1317. http://dx.doi.org/10.1094/MPMI-06-14-0168-R.
55. **Christen B, Christen M, Paul R, Schmid F, Folcher M, Jenoe P, Meuwly M, Jenal U.** 2006. Allosteric control of cyclic di-GMP signaling. J Biol Chem **281:**32015–32024. http://dx.doi.org/10.1074/jbc.M603589200.
56. **Pesavento C, Becker G, Sommerfeldt N, Possling A, Tschowri N, Mehlis A, Hengge R.** 2008. Inverse regulatory coordination of motility and curli-mediated adhesion in *Escherichia coli*. Genes Dev **22:**2434–2446. http://dx.doi.org/10.1101/gad.475808.
57. **Reuber TL, Walker GC.** 1993. Biosynthesis of succinoglycan, a symbiotically important exopolysaccharide of *Rhizobium meliloti*. Cell **74:**269–280. http://dx.doi.org/10.1016/0092-8674(93)90418-P.
58. **Hallez R, Bellefontaine AF, Letesson JJ, De Bolle X.** 2004. Morphological and functional asymmetry in α-proteobacteria. Trends Microbiol **12:**361–365. http://dx.doi.org/10.1016/j.tim.2004.06.002.
59. **Mohl DA, Easter J, Gober JW.** 2001. The chromosome partitioning protein, ParB, is required for cytokinesis in *Caulobacter crescentus*. Mol Microbiol **42:**741–755.
60. **Fogel MA, Waldor MK.** 2006. A dynamic, mitotic-like mechanism for bacterial chromosome segregation. Genes Dev **20:**3269–3282. http://dx.doi.org/10.1101/gad.1496506.
61. **Srivastava D, Waters CM.** 2012. A tangled web: regulatory connections between quorum sensing and cyclic di-GMP. J Bacteriol **194:**4485–4493. http://dx.doi.org/10.1128/JB.00379-12.
62. **Kozlova EV, Khajanchi BK, Sha J, Chopra AK.** 2011. Quorum sensing and c-di-GMP-dependent alterations in gene transcripts and virulence-associated phenotypes in a clinical isolate of *Aeromonas hydrophila*. Microb Pathog **50:**213–223. http://dx.doi.org/10.1016/j.micpath.2011.01.007.
63. **Xu J, Kim J, Danhorn T, Merritt PM, Fuqua C.** 2012. Phosphorus limitation increases attachment in *Agrobacterium tumefaciens* and reveals a conditional functional redundancy in adhesin biosynthesis. Res Microbiol **163:**674–684. http://dx.doi.org/10.1016/j.resmic.2012.10.013.
64. **Laus MC, Logman TJ, Lamers GE, Van Brussel AA, Carlson RW, Kijne JW.** 2006. A novel polar surface polysaccharide from *Rhizobium leguminosarum* binds host plant lectin. Mol Microbiol **59:**1704–1713. http://dx.doi.org/10.1111/j.1365-2958.2006.05057.x.
65. **Williams A, Wilkinson A, Krehenbrink M, Russo DM, Zorreguieta A, Downie JA.** 2008. Glucomannan-mediated attachment of *Rhizobium leguminosarum* to pea root hairs is required for competitive nodule infection. J Bacteriol **190:**4706–4715. http://dx.doi.org/10.1128/JB.01694-07.
66. **Becker A, Rüberg S, Küster H, Roxlau AA, Keller M, Ivashina T, Cheng HP, Walker GC, Pühler A.** 1997. The 32-kilobase *exp* gene cluster of *Rhizobium meliloti* directing the biosynthesis of galactoglucan: genetic organization and properties of the encoded gene products. J Bacteriol **179:**1375–1384.

67. **Glazebrook J, Walker GC.** 1989. A novel exopolysaccharide can function in place of the calcofluor-binding exopolysaccharide in nodulation of alfalfa by *Rhizobium meliloti*. Cell **56:**661–672. http://dx.doi.org/10.1016/0092-8674(89)90588-6.
68. **Glenn SA, Gurich N, Feeney MA, González JE.** 2007. The ExpR/Sin quorum-sensing system controls succinoglycan production in *Sinorhizobium meliloti*. J Bacteriol **189:**7077–7088. http://dx.doi.org/10.1128/JB.00906-07.
69. **Charoenpanich P, Meyer S, Becker A, McIntosh M.** 2013. Temporal expression program of quorum sensing-based transcription regulation in *Sinorhizobium meliloti*. J Bacteriol **195:**3224–3236. http://dx.doi.org/10.1128/JB.00234-13.
70. **Keller M, Roxlau A, Weng WM, Schmidt M, Quandt J, Niehaus K, Jording D, Arnold W, Pühler A.** 1995. Molecular analysis of the *Rhizobium meliloti mucR* gene regulating the biosynthesis of the exopolysaccharides succinoglycan and galactoglucan. Mol Plant Microbe Interact **8:**267–277. http://dx.doi.org/10.1094/MPMI-8-0267.
71. **González JE, Reuhs BL, Walker GC.** 1996. Low molecular weight EPS II of *Rhizobium meliloti* allows nodule invasion in *Medicago sativa*. Proc Natl Acad Sci U S A **93:**8636–8641. http://dx.doi.org/10.1073/pnas.93.16.8636.
72. **Rotter C, Mühlbacher S, Salamon D, Schmitt R, Scharf B.** 2006. Rem, a new transcriptional activator of motility and chemotaxis in *Sinorhizobium meliloti*. J Bacteriol **188:**6932–6942. http://dx.doi.org/10.1128/JB.01902-05.
73. **Pultz IS, Christen M, Kulasekara HD, Kennard A, Kulasekara B, Miller SI.** 2012. The response threshold of *Salmonella* PilZ domain proteins is determined by their binding affinities for c-di-GMP. Mol Microbiol **86:**1424–1440. http://dx.doi.org/10.1111/mmi.12066.
74. **Hellweg C, Pühler A, Weidner S.** 2009. The time course of the transcriptomic response of *Sinorhizobium meliloti* 1021 following a shift to acidic pH. BMC Microbiol **9:**37. http://dx.doi.org/10.1186/1471-2180-9-37.
75. **Abel S, Bucher T, Nicollier M, Hug I, Kaever V, Abel Zur Wiesch P, Jenal U.** 2013. Bi-modal distribution of the second messenger c-di-GMP controls cell fate and asymmetry during the caulobacter cell cycle. PLoS Genet **9:**e1003744. http://dx.doi.org/10.1371/journal.pgen.1003744.
76. **Skotnicka D, Petters T, Heering J, Hoppert M, Kaever V, Søgaard-Andersen L.** 29 June 2015. c-di-GMP regulates type IV pili-dependent motility in *Myxococcus xanthus*. J Bacteriol http://dx.doi.org/10.1128/JB.00281-15.
77. **Blanka A, Düvel J, Dötsch A, Klinkert B, Abraham WR, Kaever V, Ritter C, Narberhaus F, Häussler S.** 2015. Constitutive production of c-di-GMP is associated with mutations in a variant of *Pseudomonas aeruginosa* with altered membrane composition. Sci Signal **8:**ra36. http://dx.doi.org/10.1126/scisignal.2005943.
78. **Spangler C, Böhm A, Jenal U, Seifert R, Kaever V.** 2010. A liquid chromatography-coupled tandem mass spectrometry method for quantitation of cyclic di-guanosine monophosphate. J Microbiol Methods **81:**226–231. http://dx.doi.org/10.1016/j.mimet.2010.03.020.
79. **Hunter JL, Severin GB, Koestler BJ, Waters CM.** 2014. The *Vibrio cholerae* diguanylate cyclase VCA0965 has an AGDEF active site and synthesizes cyclic di-GMP. BMC Microbiol **14:**22. http://dx.doi.org/10.1186/1471-2180-14-22.
80. **Tarutina M, Ryjenkov DA, Gomelsky M.** 2006. An unorthodox bacteriophytochrome from *Rhodobacter sphaeroides* involved in turnover of the second messenger c-di-GMP. J Biol Chem **281:**34751–34758. http://dx.doi.org/10.1074/jbc.M604819200.
81. **Ferreira RB, Antunes LC, Greenberg EP, McCarter LL.** 2008. *Vibrio parahaemolyticus* ScrC modulates cyclic dimeric GMP regulation of gene expression relevant to growth on surfaces. J Bacteriol **190:**851–860. http://dx.doi.org/10.1128/JB.01462-07.
82. **Levet-Paulo M, Lazzaroni JC, Gilbert C, Atlan D, Doublet P, Vianney A.** 2011. The atypical two-component sensor kinase Lpl0330 from *Legionella pneumophila* controls the bifunctional diguanylate cyclase-phosphodiesterase Lpl0329 to modulate bis-(3′-5′)-cyclic dimeric GMP synthesis. J Biol Chem **286:**31136–31144. http://dx.doi.org/10.1074/jbc.M111.231340.
83. **Feirer N, Xu J, Allen KD, Koestler BJ, Bruger EL, Waters CM, White RH, Fuqua C.** 2015. A pterin-dependent signaling pathway regulates a dual-function diguanylate cyclase-phosphodiesterase controlling surface attachment in *Agrobacterium tumefaciens*. mBio **6:**e00156. http://dx.doi.org/10.1128/mBio.00156-15.
84. **Levi A, Folcher M, Jenal U, Shuman HA.** 2011. Cyclic diguanylate signaling proteins control intracellular growth of *Legionella pneumophila*. mBio **2:**e00316–10. http://dx.doi.org/10.1128/mBio.00316-10.
85. **Tan H, West JA, Ramsay JP, Monson RE, Griffin JL, Toth IK, Salmond GP.** 2014. Comprehensive overexpression analysis of cyclic-di-GMP signalling proteins in the phytopathogen *Pectobacterium atrosepticum* reveals diverse effects on motility and virulence phenotypes. Microbiology **160:**1427–1439. http://dx.doi.org/10.1099/mic.0.076828-0.
86. **Paul R, Weiser S, Amiot NC, Chan C, Schirmer T, Giese B, Jenal U.** 2004. Cell cycle-dependent dynamic localization of a bacterial response regulator with a novel di-guanylate cyclase output domain. Genes Dev **18:**715–727. http://dx.doi.org/10.1101/gad.289504.
87. **Hecht GB, Newton A.** 1995. Identification of a novel response regulator required for the swarmer-to-stalked-cell transition in *Caulobacter crescentus*. J Bacteriol **177:**6223–6229.
88. **Kim J, Heindl JE, Fuqua C.** 2013. Coordination of division and development influences complex multicellular behavior in *Agrobacterium tumefaciens*. PLoS One **8:**e56682. http://dx.doi.org/10.1371/journal.pone.0056682.
89. **Shapiro L, Agabian-Keshishian N, Bendis I.** 1971. Bacterial differentiation. Science **173:**884–892. http://dx.doi.org/10.1126/science.173.4000.884.
90. **Shaw CH, Loake GJ, Brown AP, Garrett CS, Deakin W, Alton G, Hall M, Jones SA, O'Leary M, Primavesi L.** 1991. Isolation and characterization of behavioural mutants and genes of *Agrobacterium tumefaciens*. Microbiology **137:**1939–1953.
91. **Platzer J, Sterr W, Hausmann M, Schmitt R.** 1997. Three genes of a motility operon and their role in flagellar rotary speed variation in *Rhizobium meliloti*. J Bacteriol **179:**6391–6399.
92. **Deng Y, Lim A, Wang J, Zhou T, Chen S, Lee J, Dong YH, Zhang LH.** 2013. *cis*-2-Dodecenoic acid quorum sensing system modulates N-acyl homoserine lactone production through RpfR and cyclic di-GMP turnover in *Burkholderia cenocepacia*. BMC Microbiol **13:**148. http://dx.doi.org/10.1186/1471-2180-13-148.
93. **Li G, Brown PJ, Tang JX, Xu J, Quardokus EM, Fuqua C, Brun YV.** 2012. Surface contact stimulates the just-in-time deployment of bacterial adhesins. Mol Microbiol **83:**41–51. http://dx.doi.org/10.1111/j.1365-2958.2011.07909.x.
94. **Li G, Smith CS, Brun YV, Tang JX.** 2005. The elastic properties of the *Caulobacter crescentus* adhesive holdfast are dependent on oligomers of *N*-acetylglucosamine. J Bacteriol **187:**257–265. http://dx.doi.org/10.1128/JB.187.1.257-265.2005.
95. **Rinaudi LV, Sorroche F, Zorreguieta A, Giordano W.** 2010. Analysis of the *mucR* gene regulating biosynthesis of exopolysaccharides: implications for biofilm formation in *Sinorhizobium meliloti* Rm1021. FEMS Microbiol Lett **302:**15–21. http://dx.doi.org/10.1111/j.1574-6968.2009.01826.x.
96. **Santos MR, Marques AT, Becker JD, Moreira LM.** 2014. The *Sinorhizobium meliloti* EmrR regulator is required for efficient colonization of *Medicago* sativa root nodules. Mol Plant Microbe Interact **27:**388–399. http://dx.doi.org/10.1094/MPMI-09-13-0284-R.
97. **Fujishige NA, Kapadia NN, De Hoff PL, Hirsch AM.** 2006. Investigations of *Rhizobium biofilm* formation. FEMS Microbiol Ecol **56:**195–206. http://dx.doi.org/10.1111/j.1574-6941.2005.00044.x.
98. **Karatan E, Watnick P.** 2009. Signals, regulatory networks, and materials that build and break bacterial biofilms. Microbiol Mol Biol Rev **73:**310–347. http://dx.doi.org/10.1128/MMBR.00041-08.
99. **Russell MH, Bible AN, Fang X, Gooding JR, Campagna SR, Gomelsky M, Alexandre G.** 2013. Integration of the second messenger c-di-GMP into the chemotactic signaling pathway. mBio **4:**e00001–13. http://dx.doi.org/10.1128/mBio.00001-13.
100. **Martínez-Granero F, Navazo A, Barahona E, Redondo-Nieto M, González de Heredia E, Baena I, Martín-Martín I, Rivilla R, Martín M.** 2014. Identification of *flgZ* as a flagellar gene encoding a PilZ domain protein that regulates swimming motility and biofilm formation in *Pseudomonas*. PLoS One **9:**e87608. http://dx.doi.org/10.1371/journal.pone.0087608.
101. **Bian J, Liu X, Cheng YQ, Li C.** 2013. Inactivation of cyclic di-GMP binding protein TDE0214 affects the motility, biofilm formation, and virulence of *Treponema denticola*. J Bacteriol **195:**3897–3905. http://dx.doi.org/10.1128/JB.00610-13.
102. **Pitzer JE, Sultan SZ, Hayakawa Y, Hobbs G, Miller MR, Motaleb MA.** 2011. Analysis of the *Borrelia burgdorferi* cyclic-di-GMP-binding protein PlzA reveals a role in motility and virulence. Infect Immun **79:**1815–1825. http://dx.doi.org/10.1128/IAI.00075-11.

SUPPLEMENT

Cyclic di-GMP regulates multiple cellular functions in the symbiotic α-proteobacterium *Sinorhizobium meliloti*

Simon Schäper[a], Elizaveta Krol[a], Dorota Skotnicka[b], Volkhard Kaever[c], Rolf Hilker[d], Lotte Søgaard-Andersen[b], Anke Becker[a]

LOEWE Center for Synthetic Microbiology (SYNMIKRO), Philipps-Universität Marburg, Marburg, Germany[a]; Department of Ecophysiology, Max Planck Institute for Terrestrial Microbiology, Marburg, Germany[b]; Research Core Unit Metabolomics, Hannover Medical School, Hannover, Germany[c]; Institute of Medical Microbiology, Justus-Liebig University, Giessen, Germany[d]

Media and antibiotic concentrations

TY medium (5 g/L tryptone, 3 g/L yeast extract, 0.4 g $CaCl_2$*$2H_2O$). LB medium (10 g/L tryptone, 5 g/L yeast extract, 5 g/L NaCl). YM medium (0.5 g/L K_2HPO_4, 0.5 g/L KH_2PO_4, 0.2 g/L $MgSO_4$*$7H_2O$, 0.1 g/L NaCl, 1 g/L yeast extract, 10 g/L mannitol, pH 7.2). MOPS-buffered minimal medium (MM) (10 g/L MOPS, 10 g/L mannitol, 3.55 g/L sodium glutamate, 0.246 g/L $MgSO_4$*$7H_2O$, 0.25 mM $CaCl_2$, 2 mM K_2HPO_4, 10 mg/L $FeCl_3$*$6H_2O$, 1 mg/L biotin, 3 mg/L H_3BO_3, 2.23 mg/L $MnSO_4$*H_2O, 0.287 mg/L $ZnSO_4$*$7H_2O$, 0.125 mg/L $CuSO_4$*$5H_2O$, 0.065 mg/L $CoCl_2$*$6H_2O$, 0.12 mg/L $NaMoO_4$*$2H_2O$, pH 7.2). MGM medium (11 g/L Na_2HPO_4*$2H_2O$, 3 g/L KH_2PO_4, 0.5 g/L NaCl, 1 g/L sodium glutamate, 10 g/L mannitol, 0.2 mM $CaCl_2$, 1 mM $MgSO_4$, 1 mg/L biotin).

Plant medium (147 mg/L $CaCl_2$*$2H_2O$, 68 mg/L KH_2PO_4, 3.35 mg/L Fe citrate, 61.7 mg/L $MgSO_4$*$7H_2O$, 43.5 mg/L K_2SO_4, 0.169 mg/L $MnSO_4$*H_2O, 123.5 mg/L H_3BO_4, 0.144 mg/L $ZnSO_4$*$7H_2O$, 0.05 mg/L $CuSO_4$*$5H_2O$, 0.028 mg/L $CoSO_4$*$7H_2O$, 0.024 mg/L Na_2MoO_2*$2H_2O$)

Antibiotics were added to *S. meliloti* or *A. tumefaciens* cultures at the following concentrations: streptomycin, 600 mg/L, gentamicin, 40 mg/L, kanamycin, 200 mg/L tetracyclin, 10 mg/L. For liquid cultures of *S. meliloti* antibiotic concentrations were reduced to the half. For *E. coli,* 100 mg/L ampicillin, 10 mg/L gentamicin, 50 mg/L kanamycin and 5 mg/L tetracyclin were used.

TABLE S1 Strains and plasmids used in this study.

Strain or plasmid	Properties	Reference
S. meliloti		
Rm2011	Wild type, Str^r	Casse *et al.* (1979)
Rm101	Rm2011 *mucR*::Spec^r	Becker *et al.* (1997)
Sm2B5001	Rm2011 Δ*rem*	Bahlawane *et al.* (2008)
Rm2011mTn5STM.1.08.H02	Rm2011 mTn5 insertion into *rem*	Pobigaylo *et al.* (2006)
Rm2011mTn5STM.1.08.B07	Rm2011 mTn5 insertion into *flgH*	Pobigaylo *et al.* (2006)
Rm2011mTn5STM.2.11.F09	Rm2011 mTn5 insertion into *SMa0453-SMa0461* intergenic locus	Pobigaylo *et al.* (2006)
Sm2B3001	Rm2011 restored *expR*	Bahlawane *et al.* (2008)
Rm2011 *expR*$^+$ *exoY wgeB*	Sm2B3001 Δ*exoY wgeB*::pK18mob2-mCh	Charoenpanich *et al.* (2015)
Rm2011 *expR*$^+$ *sinI*	Sm2B3001 Δ*sinI*	McIntosh *et al.* (2009)
Rm2011 *exoY*	Rm2011 Δ*exoY*	This work
Rm2011 *exoY wgeB*	Rm2011 Δ*exoY wgeB*::pK18mob2-mCh	This work
mucR exoY wgeB	Rm101 Δ*exoY wgeB*::pK18mob2-mCh	This work
mucR SMc01792	Rm101 *SMc01792*::pK19mob2ΩHMB	This work
Rm2011 *expR*$^+$ *SMc01792*	Sm2B3001 *SMc01792*::pK19mob2ΩHMB	This work
Rm2011 *expR*$^+$ *sinI SMc01792*	Sm2B3001 Δ*sinI SMc01792*::pK19mob2ΩHMB	This work
Rm2011 *pilA1*	Rm2011 Δ*pilA1*	This work
Rm2011 *pleD*	Rm2011 *pleD*::pK19mob2ΩHMB	This work
Rm2011 *SMa0137*	Rm2011 *SMa0137*::pK19mob2ΩHMB	This work
Rm2011 *SMa0369*	Rm2011 Δ*SMa0369*	This work
Rm2011 *SMa1548*	Rm2011 *SMa1548*::pK19mob2ΩHMB	This work
Rm2011 *SMa2301*	Rm2011 *SMa2301*::pK19mob2ΩHMB	This work
Rm2011 *SMb20389*	Rm2011 *SMb20389*::pK19mob2ΩHMB	This work
Rm2011 *SMb20447*	Rm2011 *SMb20447*::pK19mob2ΩHMB	This work
Rm2011 *SMb20523*	Rm2011 *SMb20523*::pK19mob2ΩHMB	This work
Rm2011 *SMb20900*	Rm2011 *SMb20900*::pK19mob2ΩHMB	This work
Rm2011 *SMb21517*	Rm2011 *SMb21517*::pK19mob2ΩHMB	This work
Rm2011 *SMc00033*	Rm2011 *SMc00033*::pK19mob2ΩHMB	This work
Rm2011 *SMc00038*	Rm2011 *SMc00038*::pK19mob2ΩHMB	This work
Rm2011 *SMc00507*	Rm2011 Δ*SMc00507* (Δ*mcrA*)	This work
Rm2011 *SMc00507 SMc00999*	*SMc00507 SMc00999*::pK19mob2ΩHMB	This work
Rm2011 *SMc00887*	Rm2011 *SMc00887*::pK19mob2ΩHMB	This work
Rm2011 *SMc00992*	Rm2011 *SMc00992*::pK19mob2ΩHMB	This work
Rm2011 *SMc00999*	Rm2011 *SMc00999*::pK19mob2ΩHMB	This work
Rm2011 *SMc01464*	Rm2011 *SMc01464*::pK19mob2ΩHMB	This work
Rm2011 *SMc01792*	Rm2011 *SMc01792*::pK19mob2ΩHMB	This work
Rm2011 *SMc03141*	Rm2011 *SMc03141*::pK19mob2ΩHMB	This work
Rm2011 *SMc03178*	Rm2011 *SMc03178*::pK19mob2ΩHMB	This work
Rm2011 *SMc03942*	Rm2011 *SMc03942*::pK19mob2ΩHMB	This work
Rm2011 *SMc04015*	Rm2011 *SMc04015*::pK19mob2ΩHMB	This work
Rm2011 ΔI	Rm2011 Δ*pleD*	This work
Rm2011 ΔII	Rm2011 ΔI Δ*SMc04015*	This work
Rm2011 ΔIII	Rm2011 ΔII Δ*SMb20523*	This work
Rm2011 ΔIV	Rm2011 ΔIII Δ*SMc01464*	This work
Rm2011 ΔV	Rm2011 ΔIV Δ*SMa2301*	This work
Rm2011 ΔVI	Rm2011 ΔV Δ*SMb20389*	This work
Rm2011 ΔVII	Rm2011 ΔVI Δ*SMb20447*	This work
Rm2011 ΔVIII	Rm2011 ΔVII Δ*SMb20900*	This work
Rm2011 ΔIX	Rm2011 ΔVIII Δ*SMc00038*	This work
Rm2011 ΔX	Rm2011 ΔIX Δ*SMa1548*	This work
Rm2011 ΔXI	Rm2011 ΔX Δ*SMc03178*	This work
Rm2011 ΔXII	Rm2011 ΔXI Δ*SMa0137*	This work
Rm2011 ΔXIII	Rm2011 ΔXII Δ*SMc00992*	This work
Rm2011 ΔXIV	Rm2011 ΔXIII Δ*SMc03942*	This work
Rm2011 ΔXV	Rm2011 ΔXIV Δ*SMc00887*	This work
Rm2011 ΔXVI	Rm2011 ΔXV Δ*SMc00033*	This work
Rm2011 *expR*$^+$ ΔI	Sm2B3001 Δ*pleD*	This work
Rm2011 *expR*$^+$ ΔII	Rm2011 *expR*$^+$ ΔI Δ*SMc04015*	This work
Rm2011 *expR*$^+$ ΔIII	Rm2011 *expR*$^+$ ΔII Δ*SMb20523*	This work
Rm2011 *expR*$^+$ ΔIV	Rm2011 *expR*$^+$ ΔIII Δ*SMc01464*	This work
Rm2011 *expR*$^+$ ΔV	Rm2011 *expR*$^+$ ΔIV Δ*SMa2301*	This work
Rm2011 *expR*$^+$ ΔVI	Rm2011 *expR*$^+$ ΔV Δ*SMb20389*	This work
Rm2011 *expR*$^+$ ΔVII	Rm2011 *expR*$^+$ ΔVI Δ*SMb20447*	This work
Rm2011 *expR*$^+$ ΔVIII	Rm2011 *expR*$^+$ ΔVII Δ*SMb20900*	This work
Rm2011 *expR*$^+$ ΔIX	Rm2011 *expR*$^+$ ΔVIII Δ*SMc00038*	This work
Rm2011 *expR*$^+$ ΔX	Rm2011 *expR*$^+$ ΔIX Δ*SMa1548*	This work
Rm2011 *expR*$^+$ ΔXI	Rm2011 *expR*$^+$ ΔX Δ*SMc03178*	This work
Rm2011 *expR*$^+$ ΔXII	Rm2011 *expR*$^+$ ΔXI Δ*SMa0137*	This work
Rm2011 *expR*$^+$ ΔXIII	Rm2011 *expR*$^+$ ΔXII Δ*SMc00992*	This work

Rm2011 *expR*$^+$ ΔXIV	Rm2011 *expR*$^+$ ΔXIII *SMc03942*	This work
Rm2011 *expR*$^+$ ΔXV	Rm2011 *expR*$^+$ ΔXIV *SMc00887*	This work
Rm2011 *expR*$^+$ ΔXVI	Rm2011 *expR*$^+$ ΔXV *SMc00033*	This work
Rm2011 Gm^R	Rm2011 pSM10 integrated into the chromosome	This work
Rm2011 ΔXVI Gm^R	Rm2011 ΔXVI pSM10 integrated into the chromosome	This work
Rm2011 *expR*$^+$ Gm^R	Sm2B3001 pSM10 integrated into the chromosome	This work
Rm2011 *expR*$^+$ ΔXVI Gm^R	Rm2011 *expR*$^+$ ΔXVI pSM10 integrated into the chromosome	This work
PleD-EGFP	Rm2011 *pleD*::pK18mob2-*pleD-egfp*	This work
SMb20447-EGFP	Rm2011 *SMb20447*::pK18mob2-*SMb20447*-EGFP	This work
SMb20523-EGFP	Rm2011 *SMb20523*::pK18mob2-*SMb20523*-EGFP	This work
SMb21517-EGFP	Rm2011 *SMb21517*::pK18mob2-*SMb21517*-EGFP	This work
SMc01464-EGFP	Rm2011 *SMc01464*::pK18mob2-*SMc01464*-EGFP	This work
SMc03178-EGFP	Rm2011 *SMc03178*::pK18mob2-*SMc03178*-EGFP	This work
A. tumefaciens		
NTL4 (pZLR4)	Derivative of NT1 with an internal deletion of the *tetC58* locus, *traG-lacZ,* Gm^r	Shaw *et al.* (1997)
E. coli		
S17-1	*E. coli* 294 Thi RP4-2-Tc::Mu-Km::Tn7 integrated into the chromosome	Simon *et al.* (1983)
DH5α	F$^-$ *endA1 supE44 thi-1l-recA1 gyrA96 relA1 deoRD*(*lacZYA-argF*)U169	Grant *et al*. (1990)
M15pREP4	Nx^s Str^s Rif^s Thi$^-$ Lac$^-$ Ara$^+$ Gal$^+$ Mtl$^-$ F$^-$ RecA$^+$ Uvr$^+$ Lon$^+$	Qiagen, Hilden, Germany
Plasmid		
pDJS31	pET24b(+); *dgcA*WT, Km^r	Skotnicka *et al.* (2015)
pK18mob2-EGFP	pK18mob2::EGFP, *lacZ*, *mob,* Km^r	N. Meier
pK18mobsacB	*lacZ*, *mob*, *sacB,* Km^r	Schäfer *et al.* (1994)
pK19mob2ΩHMB	integrative plasmid containing a transcription-termination sequence, Km^r	Luo *et al.* (2005)
pPHU231-EGFP	broad-host-range low copy expression vector containing *egfp*, used for generating promoter-EGFP fusions, Tc^r	M. McIntosh
pMMB67EH	broad-host-range expression vector containing *tac* promoter, Gm^r	Fürste *et al.* (1986)
pSM10	*S. meliloti* integrative vector containing partial *recA* and *alaS* sequences, Gm^r	Selbitschka *et al.* (1995)
pSRKKm	pBBR1MCS-2-derived broad-host-range expression vector containing *lac* promoter and *lacI*^{q}, lacZα$^+$, Km^r	Khan *et al.* (2008)
pWBT	pSRKGm containing T5 promoter, Gm^r	M. McIntosh
pWH844	expression vector containing His_6-tag sequence and T5 promoter, Amp^r	Schirmer *et al.* (1997)
pSRKKm-EGFP	pSRKKm containing EGFP, Km^r	This work
pSRKGm-*parB-mcherry*	pSRKGm carrying *S. meliloti parB* translationally fused to mCherry, Gm^r	This work
Integrative plasmids for gene mutation		
pK19mob2ΩHMB-*SMb20389*	pK19mob2ΩHMB carrying internal fragment of *SMb20389*	Becker *et al.* (2009)
pK18mob2-*wgeB*-mCh	pK18mob2-mCh carrying internal fragment of *wgeB*	P. Charoenpanich
pK19mob2ΩHMB-*pleD*	pK19mob2ΩHMB carrying internal fragment of *pleD*	This work
pK19mob2ΩHMB-*SMa2301*	pK19mob2ΩHMB carrying internal fragment of *SMa2301*	This work
pK19mob2ΩHMB-*SMb20523*	pK19mob2ΩHMB carrying internal fragment of *SMb20523*	This work
pK19mob2ΩHMB-*SMc01464*	pK19mob2ΩHMB carrying internal fragment of *SMc01464*	This work
pK19mob2ΩHMB-*SMc04015*	pK19mob2ΩHMB carrying internal fragment of *SMc04015*	This work
pK19mob2ΩHMB-*SMa0137*	pK19mob2ΩHMB carrying internal fragment of *SMa0137*	This work
pK19mob2ΩHMB-*SMa1548*	pK19mob2ΩHMB carrying internal fragment of *SMa1548*	This work
pK19mob2ΩHMB-*SMb20447*	pK19mob2ΩHMB carrying internal fragment of *SMb20447*	This work
pK19mob2ΩHMB-*SMb20900*	pK19mob2ΩHMB carrying internal fragment of *SMb20900*	This work
pK19mob2ΩHMB-*SMc00033*	pK19mob2ΩHMB carrying internal fragment of *SMc00033*	This work
pK19mob2ΩHMB-*SMc00038*	pK19mob2ΩHMB carrying internal fragment of *SMc00038*	This work
pK19mob2ΩHMB-*SMc00074*	pK19mob2ΩHMB carrying internal fragment of *SMc00074*	This work
pK19mob2ΩHMB-*SMc00887*	pK19mob2ΩHMB carrying internal fragment of *SMc00887*	This work
pK19mob2ΩHMB-*SMc00992*	pK19mob2ΩHMB carrying internal fragment of *SMc00992*	This work
pK19mob2ΩHMB-*SMc03141*	pK19mob2ΩHMB carrying internal fragment of *SMc03141*	This work
pK19mob2ΩHMB-*SMc03178*	pK19mob2ΩHMB carrying internal fragment of *SMc03178*	This work
pK19mob2ΩHMB-*SMc03942*	pK19mob2ΩHMB carrying internal fragment of *SMc03942*	This work
pK19mob2ΩHMB-*SMb21517*	pK19mob2ΩHMB carrying internal fragment of *SMb21517*	This work
pK19mob2ΩHMB-*SMc00999*	pK19mob2ΩHMB carrying internal fragment of *SMc00999*	This work
pK19mob2ΩHMB-*SMc01792*	pK19mob2ΩHMB carrying internal fragment of *SMc01792*	This work
Integrative plasmids for C-terminal EGFP tagging		
pK18mob2-*pleD*-EGFP	pK18mob2-EGFP carrying C-terminal portion of *pleD*	This work
pK18mob2-*SMb20523*-EGFP	pK18mob2-EGFP carrying C-terminal portion of *SMb20523*	This work
pK18mob2-*SMc01464*-EGFP	pK18mob2-EGFP carrying C-terminal portion of *SMc01464*	This work
pK18mob2-*SMb20447*-EGFP	pK18mob2-EGFP carrying C-terminal portion of *SMb20447*	This work
pK18mob2-*SMc03178*-EGFP	pK18mob2-EGFP carrying C-terminal portion of *SMc03178*	This work

pK18mob2-*SMb21517*-EGFP	pK18mob2-EGFP carrying C-terminal portion of *SMb21517*	This work
Deletion constructs		
pK18mobsacB-*exoY*	pK18mobsacB carrying flanking regions of *exoY*	P. Charoenpanich
pK18mobsacB-*pleD*	pK18mobsacB carrying flanking regions of *pleD*	This work
pK18mobsacB-*SMa2301*	pK18mobsacB carrying flanking regions of *SMa2301*	This work
pK18mobsacB-*SMb20389*	pK18mobsacB carrying flanking regions of *SMb20389*	This work
pK18mobsacB-*SMb20523*	pK18mobsacB carrying flanking regions of *SMb20523*	This work
pK18mobsacB-*SMc01464*	pK18mobsacB carrying flanking regions of *SMc01464*	This work
pK18mobsacB-*SMc04015*	pK18mobsacB carrying flanking regions of *SMc04015*	This work
pK18mobsacB-*SMa0137*	pK18mobsacB carrying flanking regions of *SMa0137*	This work
pK18mobsacB-*SMa1548*	pK18mobsacB carrying flanking regions of *SMa1548*	This work
pK18mobsacB-*SMb20447*	pK18mobsacB carrying flanking regions of *SMb20447*	This work
pK18mobsacB-*SMb20900*	pK18mobsacB carrying flanking regions of *SMb20900*	This work
pK18mobsacB-*SMc00033*	pK18mobsacB carrying flanking regions of *SMc00033*	This work
pK18mobsacB-*SMc00038*	pK18mobsacB carrying flanking regions of *SMc00038*	This work
pK18mobsacB-*SMc00887*	pK18mobsacB carrying flanking regions of *SMc00887*	This work
pK18mobsacB-*SMc00992*	pK18mobsacB carrying flanking regions of *SMc00992*	This work
pK18mobsacB-*SMc03178*	pK18mobsacB carrying flanking regions of *SMc03178*	This work
pK18mobsacB-*SMc03942*	pK18mobsacB carrying flanking regions of *SMc03942*	This work
pK18mobsacB-*SMa0369*	pK18mobsacB carrying flanking regions of *SMa0369*	This work
pK18mobsacB-*SMc00507*	pK18mobsacB carrying flanking regions of *SMc00507* (*mcrA*)	This work
pK18mobsacB-*pilA1*	pK18mobsacB carrying flanking regions of *pilA1*	This work
Overexpression constructs		
pWBT-*SMb20447*	pWBT carrying *SMb20447* coding sequence	P. Charoenpanich
pWBT-*pleD*	pWBT carrying *pleD* coding sequence	This work
pWBT-*pleD*$_{GGAAF}$	pWBT carrying *pleD*$_{GGAAF}$ coding sequence	This work
pWBT-*SMa2301*	pWBT carrying *SMa2301* coding sequence	This work
pWBT-*SMb20389*	pWBT carrying *SMb20389* coding sequence	This work
pWBT-*SMb20523*	pWBT carrying *SMb20523* coding sequence	This work
pWBT-*SMc01464*	pWBT carrying *SMc01464* coding sequence	This work
pWBT-*SMc04015*	pWBT carrying *SMc04015* coding sequence	This work
pWBT-*SMa0137*	pWBT carrying *SMa0137* coding sequence	This work
pWBT-*SMa1548*	pWBT carrying *SMa1548* coding sequence	This work
pWBT-*SMb20900*	pWBT carrying *SMb20900* coding sequence	This work
pWBT-*SMc00033*	pWBT carrying *SMc00033* coding sequence	This work
pWBT-*SMc00038*	pWBT carrying *SMc00038* coding sequence	This work
pWBT-*SMc00074*	pWBT carrying *SMc00074* coding sequence	This work
pWBT-*SMc00887*	pWBT carrying *SMc00887* coding sequence	This work
pWBT-*SMc00992*	pWBT carrying *SMc00992* coding sequence	This work
pWBT-*SMc03178*	pWBT carrying *SMc03178* coding sequence	This work
pWBT-*SMc03942*	pWBT carrying *SMc03942* coding sequence	This work
pWBT-*SMb21517*	pWBT carrying *SMb21517* coding sequence	This work
pWBT-*SMc00507*	pWBT carrying *SMc00507* (*mcrA*) coding sequence	This work
pWBT-*SMc00999*	pWBT carrying *SMc00999* coding sequence	This work
pWBT-*pleD-SMc00507*	pWBT carrying *pleD and SMc00507* (*mcrA*) coding sequences	This work
pWBT-*pleD SMc00507*$_{AxxxA}$	pWBT carrying *pleD and SMc00507*$_{AxxxA}$ (*mcrA*$_{AxxxA}$) coding sequences	This work
pWBT-*dgcA*	pWBT carrying *C. crescentus dgcA* coding sequence	This work
pWBT-*yhjH*	pWBT carrying *E. coli yhjH* coding sequence	This work
pSRKKm-PT5-*pleD*	NdeI/HindIII fragment from pWBT-*pleD* cloned into pSRKKm	This work
pMMB67EH-*pleD*	EcoRI/HindIII fragment from pWBT-*pleD* cloned into pMMB67EH	This work
pWH844-McrA	pWH844 carrying *SMc00507* (*mcrA*) coding sequence	This work
pWH844-McrA$_{AxxxA}$	pWH844 carrying *SMc00507*$_{AxxxA}$ (*mcrA*$_{AxxxA}$) coding sequence	This work
pWH844-McrA$_{D35A/S37A/G40A}$	pWH844 carrying *SMc00507*$_{D35A/S37A/G40A}$ (*mcrA*$_{D35A/S37A/G40A}$) coding sequence	This work
pWH844-*SMc00074*$_{390-970}$	pWH844 carrying *SMc00074* (aa 390-970) coding sequence	This work
FRET-based biosensor constructs		
pMMB67EH-Spy	pMMB67EH containing synthetic *ycgR* fused to CYPet and YPet	Christen *et al.* (2010)
pMMB67EH-CYPet-*12aa*-YPet	pMMB67EH containing a 12 aa linker fused to CYPet and YPet	This work
pMMB67EH-CYPet-*mcrA*-YPet	pMMB67EH containing *SMc00507* (*mcrA*) fused to CYPet and YPet	This work
Promoter-EGFP fusion plasmids		
pLK115	pPHU231-EGFP containing *wgeA* promoter	Charoenpanich *et al.* (2013)
pLK64	pPHU231-EGFP containing *sinI* promoter	McIntosh *et al.* (2008)
pPHU231-P*exoY*-EGFP	pPHU231-EGFP containing *exoY* promoter	This work
pPHU231-P*SMc00507*$_{ATG}$-EGFP	pPHU231-EGFP containing *SMc00507*$_{ATG}$ promoter	This work
pPHU231-P*SMc00507*$_{TTG}$-EGFP	pPHU231-EGFP containing *SMc00507*$_{TTG}$ promoter	This work
pSRKKm-P*SMc01794*-EGFP	pSRKKm-EGFP containing *SMc01794* promoter	This work

TABLE S2 Primers used in this study.

Primer	Sequence	Purpose
SMc03142-stop-f	GTTTCGGCTGGATGCCGAGA	*SMc03142* stop codon verification
SMc03142-stop-r	ATCGACTCCTTCAGTGCATTG	
pleD-int-f	ATATAAGCTTACCAGCCAATGTGAAGCTCCT	*pleD* internal fragment
pleD-int-r	ATATCTGCAGTGCAGATCGTTCACGGGC	
SMa2301-int-f	ATATAAGCTTCCCTAGATGGGCAAGGATG	*SMa2301* internal fragment
SMa2301-int-r	ATATCTGCAGTGAAGGCGGTGGCCAGAG	
SMb20523-int-f	ATATAAGCTTCTTCGTGGTTGCGTTTCTGA	*SMb20523* internal fragment
SMb20523-int-r	ATATCTGCAGTGGATCAGGAAGAACGGCAT	
SMc01464-int-f	ATATAAGCTTAATGAGCTTTCTCTCCGCCATA	*SMc01464* internal fragment
SMc01464-int-r	ATATCTGCAGAAGGACGAGAAGTAGAGCTGCG	
SMc04015-int-f	ATATAAGCTTTATGATCCGCATGATCGACTG	*SMc04015* internal fragment
SMc04015-int-r	ATATCTGCAGTACGTCCGTAATGTCAACGGC	
SMa0137-int-f	ATATAAGCTTATCGCAATGGCCTTGATG	*SMa0137* internal fragment
SMa0137-int-r	ATATCTGCAGAGCTTCCTGCTCGTTGGTCT	
SMa1548-int-f	ATATAAGCTTTCTCTTCCAGCGGCTTATGG	*SMa1548* internal fragment
SMa1548-int-r	ATATCTGCAGTGATATCCACGATCGTTACGAC	
SMb20447-int-f	ATATAAGCTTCGCCCATTCCGACGAACTT	*SMb20447* internal fragment
SMb20447-int-r	ATATCTGCAGGGGTCGCCTGATGTAGGAGAA	
SMb20900-int-f	ATATAAGCTTGAGCTTTTCCATCGCGGT	*SMb20900* internal fragment
SMb20900-int-r	ATATCTGCAGGGTCGGGGATCAGGACGA	
SMc00033-int-f	ATATAAGCTTCCAAATCGTGACGCTTGC	*SMc00033* internal fragment
SMc00033-int-r	ATATCTGCAGAGCAAAGCGAGGAAGGAGC	
SMc00038-int-f	ATATAAGCTTTGAACGCGGACGACAATG	*SMc00038* internal fragment
SMc00038-int-r	ATATCTGCAGAAGATCGGTTCGCCGGTTT	
SMc00074-int-f	ATATAAGCTTGTTTCTGGTCGCACTCGTCGT	*SMc00074* internal fragment
SMc00074-int-r	ATATCTGCAGAGAGTATGCGCTGCGAGC	
SMc00887-int-f	ATATAAGCTTCGTTCGTCGATCCATTGACC	*SMc00887* internal fragment
SMc00887-int-r	ATATCTGCAGGCACTTCCTTGAGCATCTGG	
SMc00992-int-f	ATATAAGCTTTGCAGGAGAGCCTGACGT	*SMc00992* internal fragment
SMc00992-int-r	ATATCTGCAGTGCAGCCTGAGAAAGCGGT	
SMc03141-int-f	ATATAAGCTTCGGCACAGTGTCGAGACG	*SMc03141* internal fragment
SMc03141-int-r	ATATCTGCAGACGTGCCATCCAGCATCTT	
SMc03178-int-f	ATATAAGCTTCTACCTTCCGGCCGTCAT	*SMc03178* internal fragment
SMc03178-int-r	ATATCTGCAGGGTAATCGAGGCCGATCGC	
SMc03942-int-f	ATATAAGCTTCGTAAGCTCGCTCTACCAGAAT	*SMc03942* internal fragment
SMc03942-int-r	ATATCTGCAGGTGAGATCATCGAGGCAAGC	
SMb21517-int-f	ATATAAGCTTTGCAGCAGGTCAATGCGGT	*SMb21517* internal fragment
SMb21517-int-r	ATATCTGCAGCAAGGCGCGAGGCCATTT	
SMc00999-int-f	ATATAAGCTTAGAACAGCGCCCCGAAAC	*SMc00999* internal fragment
SMc00999-int-r	ATATCTGCAGAGCTTCTCGCGCTTGCGT	
SMc01792-int-f	ATATAAGCTTAAGGACGGGACAAGGGGCAAT	*SMc01792* internal fragment
SMc01792-int-r	ATATCTGCAGCGATTTGAGAAAGAAGAGGCCGA	
pleD-C-f	ATATGTCGACCCCGCTTCATTCCGATCCT	*pleD* 3'-end for protein localization
pleD-C-r	ATATTCTAGAGGCAGCGGCAGCGACGAC	
SMb20523-C-f	ATATGTCGACATCTATGCCGCAGTTGCG	*SMb20523* 3' end for protein localization
SMb20523-C-r	ATATTCTAGACGTCGGTCGATACTTTCCAGA	

SMc01464-C-f	ATATGTCGACTTCGAGCCTGTTCGATTTCCT	*SMc01464* 3'-end for protein localization
SMc01464-C-r	ATATTCTAGACGCCGAGTGGCGCAGTTC	
SMb20447-C-f	ATATGTCGACCGGTCGTCGGTTTCGAAG	*SMb20447* 3'-end for protein localization
SMb20447-C-r	ATATTCTAGATGTTCGCTGAAGACCTGCC	
SMc03178-C-f	ATATGTCGACAGTTCTGTCCGAGCTCGCT	*SMc03178* 3'-end for protein localization
SMc03178-C-r	ATATTCTAGAGGCGGCGCGCCACCGCCGCTCGAAGA	
SMb21517-C-f	ATATAAGCTTTCGATACATGGTCGGTCTCG	*SMb21517* 3'-end for protein localization
SMb21517-C-r	ATATTCTAGAGGAATGCAGCTGCCGCGAT	
pleD-l-f	ATATGAATTCAACGCAACGAGTCCGCCCAT	*pleD* left flanking region
pleD-l-r	ATATTCTAGAATCGATCTTTCCGGCAGTCA	
pleD-r-f	ATATTCTAGATCCGCCGCACATGCTGAG	*pleD* right flanking region
pleD-r-r	ATATAAGCTTCAATCGGTTGTCCACGGCTTT	
SMa2301-l-f	ATATGAATTCTTTGGCTGGAAGACGACAC	*SMa2301* left flanking region
SMa2301-l-r	ATATGGTACCTTCATATGGCAAATCGTGGC	
SMa2301-r-f	ATATGGTACCCGGCGCGACGAGAGCGGGATTA	*SMa2301* right flanking region
SMa2301-r-r	ATATGGATCCTTGGCGAGCAAGGTTTCG	
SMb20389-l-f	ATATGAATTCTTCGATGATCGGTGCGCA	*SMb20389* left flanking region
SMb20389-l-r	ATATGGTACCTTCTATCTCCCTCGTTCGTGA	
SMb20389-r-f	ATATGGTACCGTCATCCTCGACGCCTGA	*SMb20389* right flanking region
SMb20389-r-r	ATATAAGCTTAGCATCGCGACATTCGTG	
SMb20523-l-f	ATATGAATTCCATTCGGCGGGCAATCAC	*SMb20523* left flanking region
SMb20523-l-r	ATATTCTAGATGGCAGAATCCAATATACGCA	
SMb20523-r-f	ATATTCTAGAGGCCAAGCGGGCAATTGAT	*SMb20523* right flanking region
SMb20523-r-r	ATATAAGCTTTATGCTGTGATGAGTTTCGGC	
SMc01464-l-f	ATATGGATCCACGAGCCGGTCCACGTCGT	*SMc01464* left flanking region
SMc01464-l-r	ATATTCTAGATATGCGAGGCCATTGGTAA	
SMc01464-r-f	ATATTCTAGACTTCTCGCACGATGGATCCT	*SMc01464* right flanking region
SMc01464-r-r	ATATAAGCTTATGCGGCAGACCTTAGTCTC	
SMc04015-l-f	ATATGGATCCAGGTGTCGACCGAGAGATTGA	*SMc04015* left flanking region
SMc04015-l-r	ATATTCTAGACAGGGCCTTGAGGTGATCA	
SMc04015-r-f	ATATTCTAGACGCGTCAAGCGTCATACG	*SMc04015* right flanking region
SMc04015-r-r	ATATAAGCTTAATGCCTGTTGAAGGCCC	
SMa0137-l-f	ATATGGATCCGCGCCCTGACGAATACCCA	*SMa0137* left flanking region
SMa0137-l-r	ATATTCTAGACCGCACTCCTCCTGATAGG	
SMa0137-r-f	ATATTCTAGATTTTGGCCCGAGCGTCCCTAA	*SMa0137* right flanking region
SMa0137-r-r	ATATAAGCTTGCTGCTTGACGATACTGGCA	
SMa1548-l-f	ATATGGATCCACGGGTAATGGCAGCGAT	*SMa1548* left flanking region
SMa1548-l-r	ATATTCTAGAGACACGACACTTAGACCGGTGA	
SMa1548-r-f	ATATTCTAGACTCGATTGGCGCAGTTGC	*SMa1548* right flanking region
SMa1548-r-r	ATATAAGCTTCGAGAAGCCCTGTACAAGGA	
SMb20447-l-f	ATATGAATTCGCGCATTCTGTCGAACGC	*SMb20447* left flanking region
SMb20447-l-r	ATATTCTAGATCTCGCCTTTCCCTTCCGTT	
SMb20447-r-f	ATATTCTAGAAGTGGGTCAATGCCGGGAAATTA	*SMb20447* right flanking region
SMb20447-r-r	ATATAAGCTTCACCTCTTCGATGGCGCCTTTA	
SMb20900-l-f	ATATGAATTCAGGTGCCCTCCGACACGATA	*SMb20900* left flanking region
SMb20900-l-r	ATATGGTACCCGCGATGAAATGCGTCGA	
SMb20900-r-f	ATATGGTACCCTCGTCATGAGACAAAAAGGC	*SMb20900* right flanking region
SMb20900-r-r	ATATGGATCCGATGGTTGGCTTCAACCG	
SMc00033-l-f	ATATGAATTCAATCAGCGGGAGGCGTCCAT	*SMc00033* left flanking region

SMc00033-l-r	ATATTCTAGAGCCGGGCTCCAGGGATAGGACA	
SMc00033-r-f	ATATTCTAGAGCAGCGATGCAAGGCGACCTTT	*SMc00033* right flanking region
SMc00033-r-r	ATATGGTACCGCAGCACGACAGCCTTGAAAT	
SMc00038-l-f	ATATGGATCCTTCGAGTACGGCAAAGGCTTT	*SMc00038* left flanking region
SMc00038-l-r	ATATTCTAGAGCGAAACCTCCGAAGGAGC	
SMc00038-r-f	ATATTCTAGATGTTCGCGAGCGGCGGTAA	*SMc00038* right flanking region
SMc00038-r-r	ATATAAGCTTATCATTTCGTTCGGCGGC	
SMc00887-l-f	ATATGGATCCAATGGCGAGGAGCTCGAC	*SMc00887* left flanking region
SMc00887-l-r	ATATTCTAGATGTCATTGCGATCCGCTCCG	
SMc00887-r-f	ATATTCTAGAGAGCATTATCGGGATACGGC	*SMc00887* right flanking region
SMc00887-r-r	ATATAAGCTTTTCGCCTCCATGTGGATG	
SMc00992-l-f	ATATGGTACCACTATGCGCCGGAATGGC	*SMc00992* left flanking region
SMc00992-l-r	ATATTCTAGAGGTCACTGGAAGTTCGCC	
SMc00992-r-f	ATATTCTAGACGTCACTTGCGAGAGAAGGA	*SMc00992* right flanking region
SMc00992-r-r	ATATGAATTCTGCCGTCGCAAAGGCAGAA	
SMc03178-l-f	ATATGGATCCTCGCCGCTCGTCGGCTTTT	*SMc03178* left flanking region
SMc03178-l-r	ATATTCTAGAGGTGCGGCTTCAAAAGAGCAAT	
SMc03178-r-f	ATATTCTAGACCGGTATCCGGCCCTCGCCTTCA	*SMc03178* right flanking region
SMc03178-r-r	ATATAAGCTTGTCGCGGGCGTGTGCGTTATGG	
SMc03942-l-f	ATATGGATCCTTCACGACCACATCCTGGC	*SMc03942* left flanking region
SMc03942-l-r	ATATTCTAGAGAACCTAAGCTCCGGTTTGC	
SMc03942-r-f	ATATTCTAGACGCCTTTCGGCGCAATGT	*SMc03942* right flanking region
SMc03942-r-r	ATATAAGCTTTTGTCCTCCAGGCGACAGCATT	
SMa0369-l-f	ATATGAATTCCTGGAGCCTCGGTCGGGA	*SMa0369* left flanking region
SMa0369-l-r	ATATTCTAGATCTGAGCCTCAACGGCCGC	
SMa0369-r-f	ATATGAATTCCTGGAGCCTCGGTCGGGA	*SMa0369* right flanking region
SMa0369-r-r	ATATTCTAGATCTGAGCCTCAACGGCCGC	
SMc00507-l-f	ATATGAATTCAATATTTCTCTCCGGGCCAGAA	*SMc00507* left flanking region
SMc00507-l-r	ATATTCTAGATCTTCACATGGAGCACCTAAAG	
SMc00507-r-f	ATATTCTAGACCTTGAGTGAAGGACCGGAT	*SMc00507* right flanking region
SMc00507-r-r	ATATAAGCTTTGTGCCTCATATATCCAATCGC	
pilA1-l-f	ATATGAATTCTTAGGGTGAGGGGCAGGG	*pilA1* left flanking region
pilA1-l-r	ATATTCTAGAGACTATTCTCCTCAAACTTCACTTGT	
pilA1-r-f	ATATTCTAGACGGCCGACTGATTACCTAACA	*pilA1* right flanking region
pilA1-r-r	ATATAAGCTTAGGTTGATCAGGAATTGGTGTAA	
pleD-f	ATATTCTAGAATGACTGCGCGCATCCTC	*pleD* ORF cloning
pleD-r	ATATAAGCTTTCAGGCAGCGGCAGCGAC	
pleD-GGAAF-f	gccgccTTCGTGGTCGTCATGCCGGATA	*pleD* GGEEF mutation to GGAAF
pleD-GGAAF-r	TGACGACCACGAAggcggcCCCGCCGAAACGGCAGGCA	
SMa2301-f	ATATTCTAGAATGCAACTCGCGAGTTCAT	*SMa2301* ORF cloning
SMa2301-r	ATATGTCGACCTATACGGTCGGCAGATCG	
SMb20389-f	ATATAAGCTTATTAAAGAGGAGAAATCTAGAATGGGAC AAGCCGTACGAATC	*SMb20389* ORF cloning, usage of XbaI recognition site
SMb20389-r	ATATGGTACCTCAGGCGTCGAGGATGACGAA	
SMb20523-f	ATATGTCGACATTAAAGAGGAGAAATCTAGAATGGGC GGTGCGATCTCACTT	*SMb20523* ORF cloning, usage of XbaI recognition site
SMb20523-r	ATATGGTACCTTACGTCGGTCGATACTTTCCA	
SMc01464-f	ATATTCTAGAATGGCTGAAACGCAAGCCG	*SMc01464* ORF cloning
SMc01464-r	ATATAAGCTTTCACGCCGAGTGGCGCAGTT	
SMc04015-f	ATATTCTAGAATGGGCCTGCAAGCCGCA	*SMc04015* ORF cloning
SMc04015-r	ATATGTCGACCTAAGGGGTCTGATCCGGG	

SMa0137-f	ATATTCTAGAATGAGGTTTGTGGCTGGCAAA	*SMa0137* ORF cloning
SMa0137-r	ATATGGTACCTCATGAGCGTGAGCTAGAAGAG	
SMa1548-f	ATATTCTAGAATGAACGCACCGACGCCC	*SMa1548* ORF cloning
SMa1548-r	ATATGGTACCTTAGAGGGAACCGGCCGC	
SMb20900-f	ATATTCTAGAATGCTCGCCTATGACGGGGGA	*SMb20900* ORF cloning
SMb20900-r	ATATAAGCTTTTAAGCCCCTACCCGATGC	
SMc00033-f	ATATAAGCTTATTAAAGAGGAGAAATCTAGAATGTCGG CCGCCCCCGCAGAAAT	*SMc00033* ORF cloning, usage of XbaI recognition site
SMc00033-r	ATATGGTACCTCAGGCGCGGTCGAGGGGCT	
SMc00038-f	ATATTCTAGAATGGCAAGAAAAACGTCCC	*SMc00038* ORF cloning
SMc00038-r	ATATAAGCTTTCACCGCCGCTCAGAGGAAA	
SMc00074-f	ATATTCTAGAATGCCCCTGACCCGTAAG	*SMc00074* ORF cloning
SMc00074-r	ATATGGATCCTCAAGCCCGCTTCATCAG	
SMc00887-f	ATATTCTAGAATGACATTGCAGGAACTCGGTA	*SMc00887* ORF cloning
SMc00887-r	ATATAAGCTTTCAGCGCACCGCCGTATC	
SMc00992-f	ATATTCTAGAATGACCCTCGGCAAGCGT	*SMc00992* ORF cloning
SMc00992-r	ATATAAGCTTTCAGCGCCGGCTTGCAGC	
SMc03178-f	ATATTCTAGAATGTCCCCTCTGTCGCGCTTTCTC	*SMc03178* ORF cloning
SMc03178-r	ATATAAGCTTTCAGGCGGCGCGCCACCG	
SMc03942-f	ATATTCTAGAATGACCCGCAATGAACGGG	*SMc03942* ORF cloning
SMc03942-r	ATATGGTACCTCAGGCGGTCCGCTCCGC	
SMb21517-f	ATATAAGCTTATTAAAGAGGAGAAATCTAGAATGGAAC ATCTGAGAAGATTCGA	*SMb21517* ORF cloning, usage of XbaI recognition site
SMb21517-r	ATATGGTACCCTAGGAATGCAGCTGCCG	
SMc00507-f	ATATAAGCTTATTAAAGAGGAGAAATCTAGAATGGTTT ACAAGGACAGTGTTCAG	*SMc00507* ORF cloning, usage of XbaI recognition site; usage of HindIII recognition site for combined overexpression with *pleD*
SMc00507-r	ATATGGTACCTCAGCGAAAGAACTTGTAATAGGA	
SMc00999-f	ATATTCTAGAATGTTCTCCTTCCAGCATGCG	*SMc00999* ORF cloning
SMc00999-r	ATATGGTACCTTACAGAAACTCGGTCAGTGCCT	
SMc00507-RxxxR-f	gccgcctcttcggccGAAGAGACCAAGATAACCGGAA	*SMc00507* mutation to R9A/R13A
SMc00507-RxxxR-r	TCTTGGTCTCTTCggccgaagaggcggcctgaacactgtccttgtaaa ccat	
SMc00507-DxSxxG-f	gcccttgccgacgaagccATCTGCTTCAGGCTGCTCTTC	*SMc00507* mutation to D35A/S37A/G40A
SMc00507-DxSxxG-r	GCCTGAAGCAGATggcttcgtcggcaagggcCACCACAATCC CGTTGGTC	
dgcA-f	ATATTCTAGAATGAAAATCTCAGGCGCCC	*dgcA* ORF cloning
dgcA-r	atatAAGCTTtcaAGCGCTCCTGCGCTTG	
yjhH-f	ATATTCTAGAATGATAAGGCAGGTTATCCAGC	*yjhH* ORF cloning
yjhH-r	ATATAAGCTTTTATAGCGCCAGAACCGCCGTATT	
12aa-oligo1	ATATACTAGTGGCTCGCCGGGCCTCCAGGAGTTCGGT ACCTATA	12 aa linker for CYPet and YPet
12aa-oligo2	TATAGGTACCGAACTCCTGGAGGCCCGGCGAGCCACT AGTATAT	
SMc00507-FRET-f	ATATACTAGTCAGCTGTCTCAATCAGGTTTCGA	*SMc00507* as a linker for CYPet and YPet
SMc00507-FRET-r	ATATGGTACCGCGAAAGAACTTGTAATAGGACG	
His6-*SMc00507*-f	ATATGGATCCGTTTACAAGGACAGTGTTCAGCGT	*SMc00507* ORF cloning for N-terminal His6-tagging
His6-*SMc00507*-r	ATATAAGCTTTCAGCGAAAGAACTTGTAATAGGA	
His6-*SMc00074*-f	ATATGGATCCACCGTCATGCAGCACGCCTTTT	*SMc00074*$^{390\text{-}970}$ ORF cloning for N-terminal His6-tagging
His6-*SMc00074*-r	ATATGTCGACTCAAGCCCGCTTCATCAG	
P*exoY*-f	gttcaagcttTGCCTTGGGTGCTACCTCTTG	*exoY* upstream intergenic region
P*exoY*-r	tgctctagaCTTCATAGAGGTGACTCCAT	
P*SMc00507*-f	ATATAAGCTTCTACTGCATGTTTCCTTTAATCG	*SMc00507* upstream intergenic regions
P*SMc00507*-TTG-r	ATATTCTAGACAGCTGCAATCTTCACATGGA	
P*SMc00507*-ATG-r	ATATTCTAGAGTAAACCATGGTTTCCTCGAA	

P*SMc01794*-f	ATATCTGCAGCGAACATCCGGTCGGAGC	*SMc01794* upstream intergenic region
P*SMc01794*-r	ATATTCTAGAGGTCGACATGCGGTTAGG	
egfp-f	ggaggagctcttaagcttgtatctagactgcagATGGTGAGCAAGGGCGAGG	*egfp* ORF cloning
egfp-r	gtacggtaccTTACTTGTACAGCTCGTCCATG	
pleD-valid	AAACTGCTTTCGGCGGCCT	validation of integration site for *pleD* mutation, combined with PCR1
SMa2301-valid	AGATCAGGTAAAGGCCGAGC	validation of integration site for *SMa2301* mutation, combined with PCR1
SMb20389-valid	CGCATTCTGTAGTTGGTTATGG	validation of integration site for *SMb20389* mutation, combined with PCR1
SMb20523-valid	AGATAATCCGCCGCCGTG	validation of integration site for *SMb20523* mutation, combined with PCR1
SMc01464-valid	AAATCGAACAGGCTCGAAGC	validation of integration site for *SMc01464* mutation, combined with PCR1
SMc04015-valid	TAGTCGATGTCGATGATCGC	validation of integration site for *SMc04015* mutation, combined with PCR1
SMa0137-valid	ACCAGATCGCTCTCGCCG	validation of integration site for *SMa0137* mutation, combined with PCR1
SMa1548-valid	AACTTGCGGGTGAAGGTCGA	validation of integration site for *SMa1548* mutation, combined with PCR1
SMb20447-valid	CCCAATGTGTCGTTGATCG	validation of integration site for *SMb20447* mutation, combined with PCR1
SMb20900-valid	GGCGAAGGATCACCATGC	validation of integration site for *SMb20900* mutation, combined with PCR1
SMc00033-valid	CGCAGAGCAGTTTCAAGCC	validation of integration site for *SMc00033* mutation, combined with PCR1
SMc00038-valid	GCTTCGATCAGCAGCACCA	validation of integration site for *SMc00038* mutation, combined with PCR1
SMc00074-valid	AAGGCGTTGACGGTATCCTT	validation of integration site for *SMc00074* mutation, combined with PCR1
SMc00887-valid	CTCAAGCTGCGTCGCGTG	validation of integration site for *SMc00887* mutation, combined with PCR1
SMc00992-valid	TTTCTGACGCAGCATCTGG	validation of integration site for *SMc00992* mutation, combined with PCR1
SMc03141-valid	GAAGCCTGGCGATCTGAGCT	validation of integration site for *SMc03141* mutation, combined with PCR1
SMc03178-valid	TTCCGGACCGGTGGTTAC	validation of integration site for *SMc03178* mutation, combined with PCR1
SMc03942-valid	ATCATCATCGGCAGGCAG	validation of integration site for *SMc03942* mutation, combined with PCR1
SMb21517-valid	GAAACTGTCCAAGGCGATTCT	validation of integration site for *SMb21517* mutation, combined with PCR1
SMc00999-valid	CCCTTCATGTTACCCAGCCT	validation of integration site for *SMc00999* mutation, combined with PCR1
SMc01792-valid	ATCGAATAGGCGATGAATGC	validation of integration site for *SMc01792* mutation, combined with PCR1
PCR1	CGGGCCTCTTCGCTATT	Standard sequencing primer 1
PCR2	TTAGCTCACTCATTAGG	Standard sequencing primer 2
SMc03942-seq	TGGCGCTCGACCCGGAAAGAA	*SMc03942* sequencing primer
SMa0137-seq	GAAACGATAGGATATTTCTCC	*SMa0137* sequencing primer
SMa1548-seq1	CGCAAAGCGTGACGCGGATGG	*SMa1548* sequencing primer 1
SMa1548-seq2	ACCATCACGGAAAGCCGTTCCGAAT	*SMa1548* sequencing primer 2
SMa1548-seq3	TACAACCTCTGACGGAGTCAC	*SMa1548* sequencing primer 3
SMb20900-seq	AAGCGAGGGAGAGCTCCTTC	*SMb20900* sequencing primer
SMc00033-seq	TGCGATCTGATGCAGGGCTA	*SMc00033* sequencing primer
SMc00038-seq	TGCGCTGCCATCCATGGCCTCG	*SMc00038* sequencing primer
SMc00992-seq	CAGATGCTGCGTCAGAAAGTACT	*SMc00992* sequencing primer
SMc03178-seq1	TCTTCGGCGACCCGGCAATCT	*SMc03178* sequencing primer 1
SMc03178-seq2	CGCTTCCTGGACCAGATTCT	*SMc03178* sequencing primer 2
SMc00074-seq1	ACGCCTACAAGGATACCGTCA	*SMc00074* sequencing primer 1
SMc00074-seq2	ATCGTGCTCCTGATCGGC	*SMc00074* sequencing primer 2
SMc00074-seq3	ACAATGTCCTCATCGCGCT	*SMc00074* sequencing primer 3

REFERENCES

1. **Bahlawane C, McIntosh M, Krol E, Becker A.** 2008. *Sinorhizobium meliloti* regulator MucR couples exopolysaccharide synthesis and motility. Mol Plant Microbe Interact **21:**1498-1509.
2. **Becker A, Barnett MJ, Capela D, Dondrup M, Kamp PB, Krol E, Linke B, Rüberg S, Runte K, Schroeder BK, Weidner S, Yurgel SN, Batut J, Long SR, Pühler A, Goesmann A.** 2009. A portal for rhizobial genomes: RhizoGATE integrates a *Sinorhizobium meliloti* genome annotation update with postgenome data. J Biotechnol **140:**45-50.
3. **Becker A, Rüberg S, Küster H, Roxlau AA, Keller M, Ivashina T, Cheng HP, Walker GC, Pühler A.** 1997. The 32-kilobase exp gene cluster of *Rhizobium meliloti* directing the biosynthesis of galactoglucan: genetic organization and properties of the encoded gene products. J Bacteriol **179:**1375-1384.
4. **Boehm A, Steiner S, Zaehringer F, Casanova A, Hamburger F, Ritz D, Keck W, Ackermann M, Schirmer T, Jenal U.** 2009. Second messenger signalling governs *Escherichia coli* biofilm induction upon ribosomal stress. Mol Microbiol **72:**1500-1516.
5. **Casse F, Boucher C, Julliot J, Michel M, Dénarié J.** 1979. Identification and characterization of large plasmids in *Rhizobium meliloti* using agarose gel electrophoresis. Microbiology **113**:229-242.
6. **Charoenpanich P, Meyer S, Becker A, McIntosh M.** 2013. Temporal expression program of quorum sensing-based transcription regulation in *Sinorhizobium meliloti*. J Bacteriol **195:**3224-3236.
7. **Charoenpanich P, Soto MJ, Becker A, McIntosh M.** 2015. Quorum sensing restrains growth and is rapidly inactivated during domestication of *Sinorhizobium meliloti*. Environ Microbiol Rep **7:**373-382.
8. **Christen M, Kulasekara HD, Christen B, Kulasekara BR, Hoffman LR, Miller SI.** 2010. Asymmetrical distribution of the second messenger c-di-GMP upon bacterial cell division. Science **328:**1295-1297.
9. **Fürste JP, Pansegrau W, Frank R, Blöcker H, Scholz P, Bagdasarian M, Lanka E.** 1986. Molecular cloning of the plasmid RP4 primase region in a multi-host-range *tacP* expression vector. Gene **48:**119-131.
10. **Grant SG, Jessee J, Bloom FR, Hanahan D.** 1990. Differential plasmid rescue from transgenic mouse DNAs into *Escherichia coli* methylation-restriction mutants. Proc Natl Acad Sci U S A **87:**4645-4649.
11. **Khan SR, Gaines J, Roop RM, Farrand SK.** 2008. Broad-host-range expression vectors with tightly regulated promoters and their use to examine the influence of TraR and TraM expression on Ti plasmid quorum sensing. Appl Environ Microbiol **74:**5053-5062.
12. **Luo L, Yao SY, Becker A, Rüberg S, Yu GQ, Zhu JB, Cheng HP.** 2005. Two new *Sinorhizobium meliloti* LysR-type transcriptional regulators required for nodulation. J Bacteriol **187:**4562-4572.
13. **McIntosh M, Krol E, Becker A.** 2008. Competitive and cooperative effects in quorum-sensing-regulated galactoglucan biosynthesis in *Sinorhizobium meliloti*. J Bacteriol **190:**5308-5317.
14. **McIntosh M, Meyer S, Becker A.** 2009. Novel *Sinorhizobium meliloti* quorum sensing positive and negative regulatory feedback mechanisms respond to phosphate availability. Mol Microbiol **74:**1238-1256.

15. **Pobigaylo N, Wetter D, Szymczak S, Schiller U, Kurtz S, Meyer F, Nattkemper TW, Becker A.** 2006. Construction of a large sequence signature-tagged miniTn*5* transposon library and its application to mutagenesis of *Sinorhizobium meliloti*. Appl Environ Microbiol **72:**4329-4337.

16. **Schäfer A, Tauch A, Jäger W, Kalinowski J, Thierbach G, Pühler A.** 1994. Small mobilizable multi-purpose cloning vectors derived from the *Escherichia coli* plasmids pK18 and pK19: selection of defined deletions in the chromosome of *Corynebacterium glutamicum*. Gene **145:**69-73.

17. **Schirmer F, Ehrt S, Hillen W.** 1997. Expression, inducer spectrum, domain structure, and function of MopR, the regulator of phenol degradation in *Acinetobacter calcoaceticus* NCIB8250. J Bacteriol **179:**1329-1336.

18. **Selbitschka W, Dresing U, Hagen M, Niemann S, Pühler A.** 1995. A biological containment system for *Rhizobium meliloti* based on the use of recombination-deficient (*recA*$^-$) strains. FEMS Microbiology Ecology **16:**223-232.

19. **Shaw PD, Ping G, Daly SL, Cha C, Cronan JE, Rinehart KL, Farrand SK.** 1997. Detecting and characterizing N-acyl-homoserine lactone signal molecules by thin-layer chromatography. Proc Natl Acad Sci U S A **94:**6036-6041.

20. **Simon R, Priefer U, Pühler A.** 1983. A broad host range mobilization system for *in vivo* genetic engineering: transposon mutagenesis in gram-negative bacteria. Nature Biotechnology **1:**784-791.

21. **Skotnicka D, Petters T, Heering J, Hoppert M, Kaever V, Søgaard-Andersen L.** 2015. c-di-GMP regulates type IV pili-dependent-motility in *Myxococcus xanthus*. J Bacteriol doi: 10.1128/JB.00281-15.

Supplemental figures

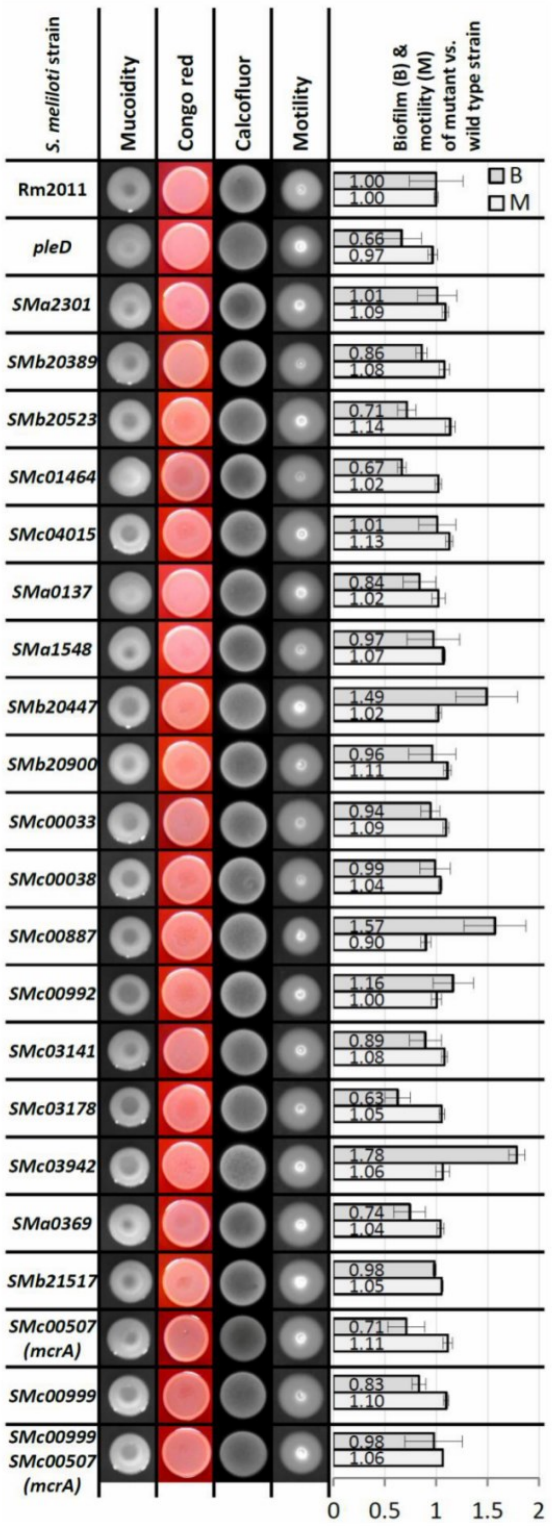

FIG S1 Phenotypic analysis of gene knock-outs in Rm2011. Error bars indicate standard deviations of three biological replicates. The A_{570}/OD_{600} mean value for Rm2011 was 0.131±0.034 (set to 1).

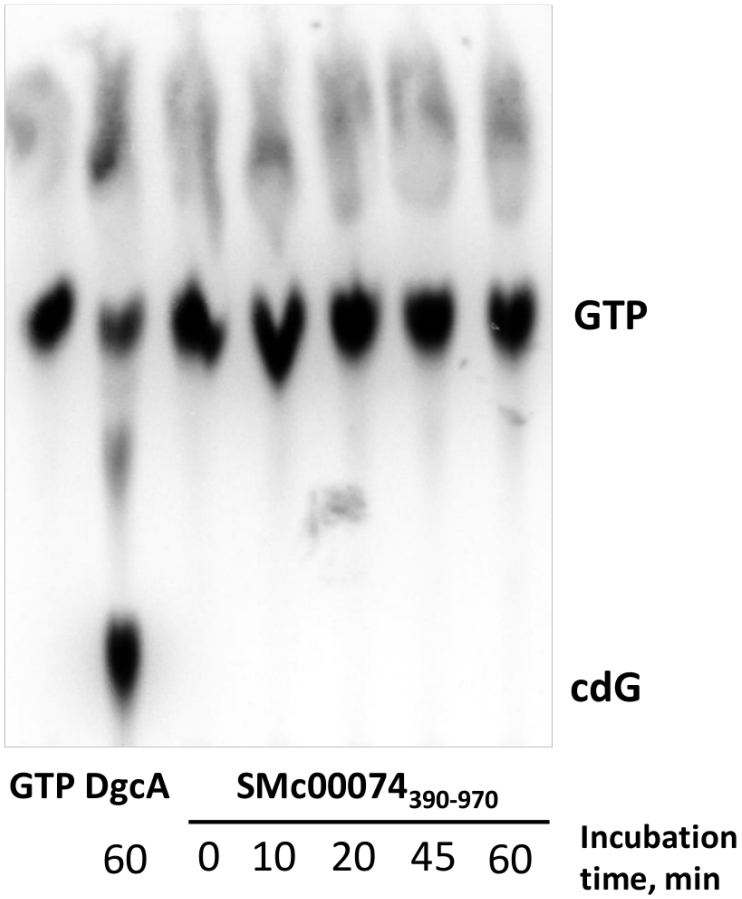

FIG S2 Assay for DGC activity of the C-terminal portion of SMc00074 containing the predicted DGC and PDE domains. Thin-layer chromatography of reaction mixtures containing radiolabelled GTP and purified protein. Absence of a cdG signal and unchanged intensity of the GTP band indicate that SMc00074$_{390\text{-}970}$ does not have DGC activity.

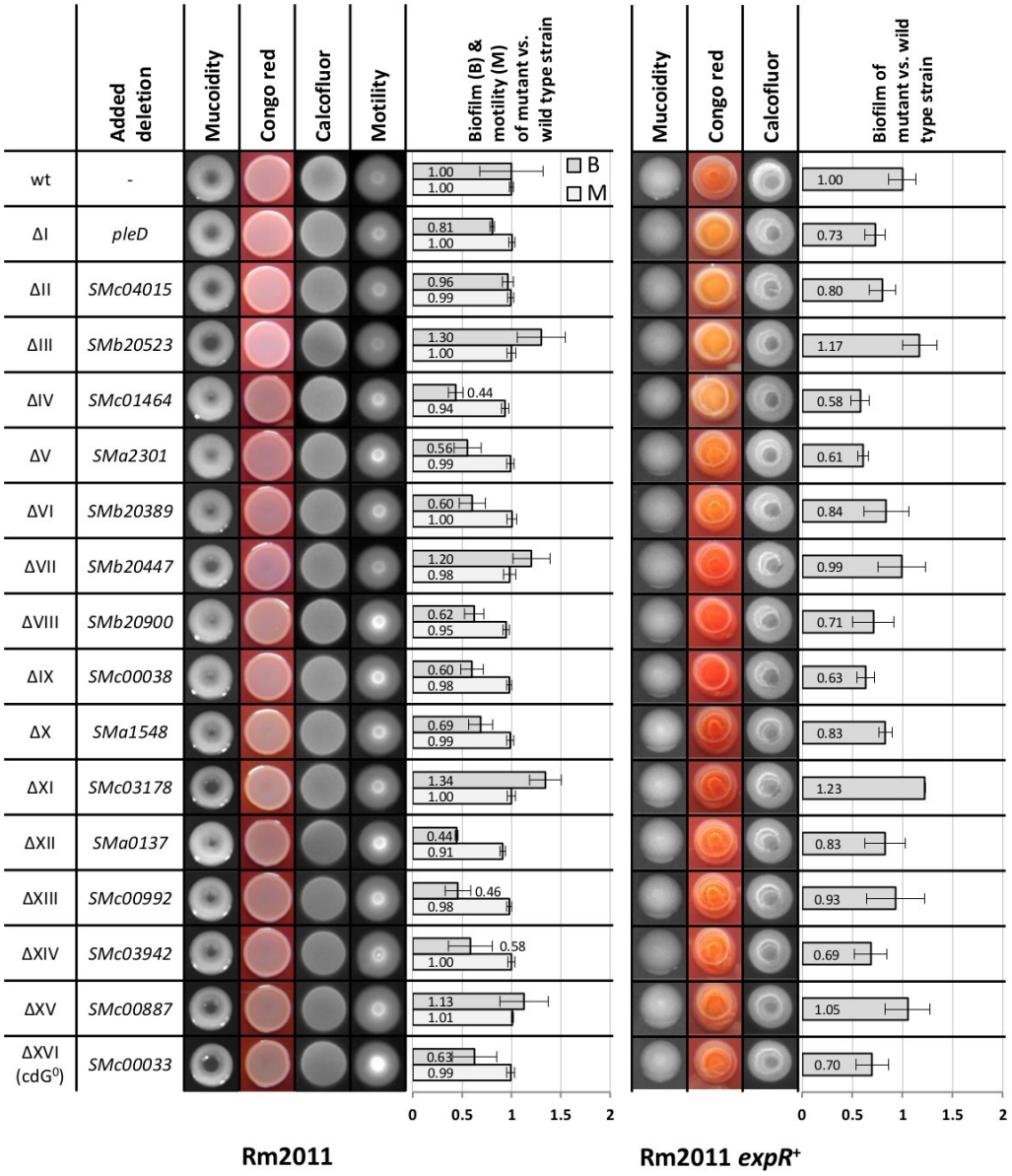

FIG S3 Phenotypic analysis of Rm2011 and Rm2011 *expR*$^+$ carrying multiple markerless deletions of DGC/PDE genes. Error bars indicate standard deviations of three biological replicates. The A_{570}/OD_{600} mean values for Rm2011 and Rm2011 *expR*$^+$ were 0.110±0.035 and 0.343±0.047, respectively (set to 1).

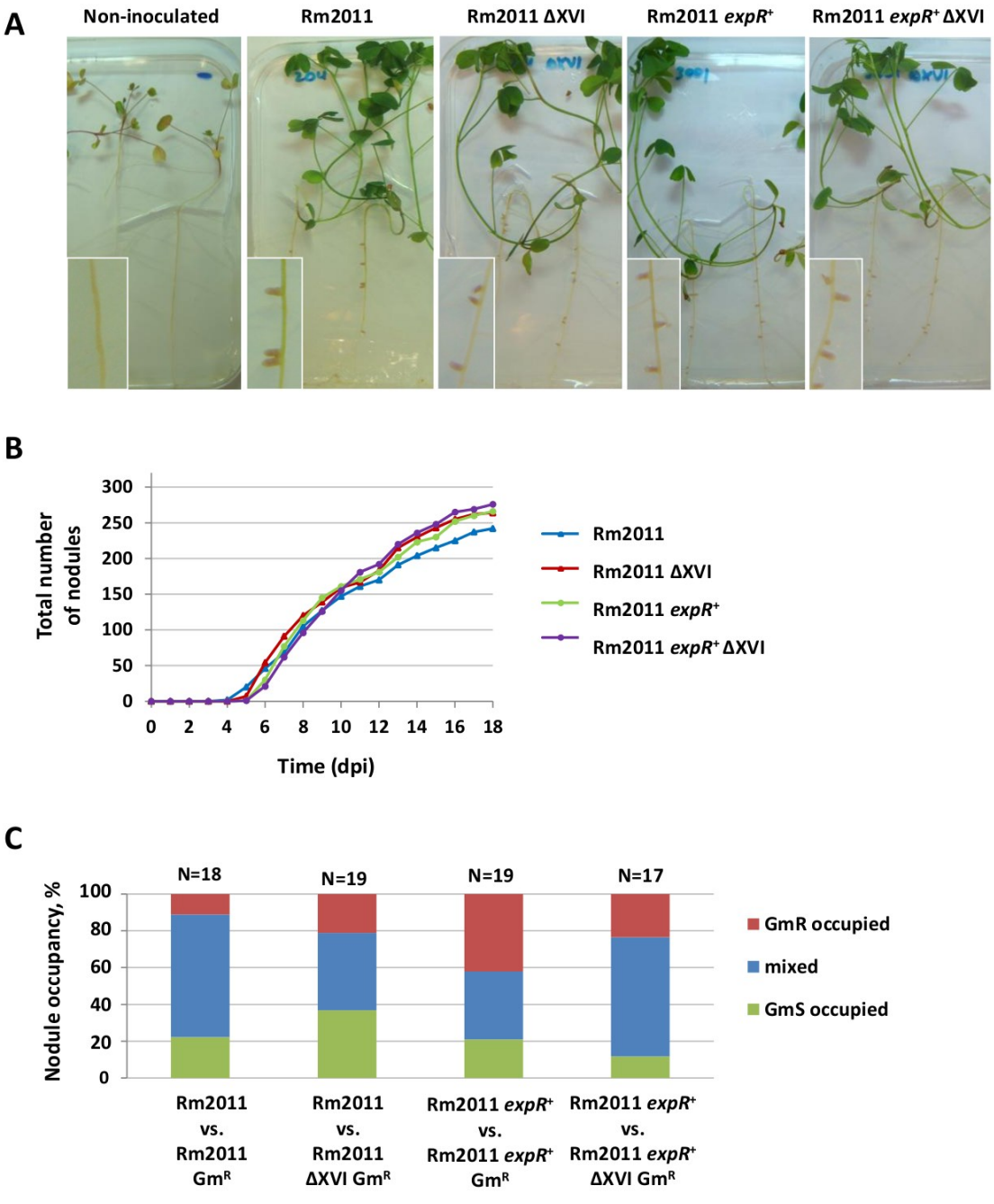

FIG S4 Symbiotic phenotype of cdG^0 strains. (A) Macroscopic appearance of *M. sativa* plants with root nodules formed by cdG^0 strains or corresponding parental strains 24 days post inoculation. Pink nitrogen-fixing nodules indicate efficient symbiosis. (B) Nodulation kinetics, determined for 32 plants per strain. (C) Competitive nodulation assay. Before inoculation, strains were mixed 1:1. N, number of analyzed nodules.

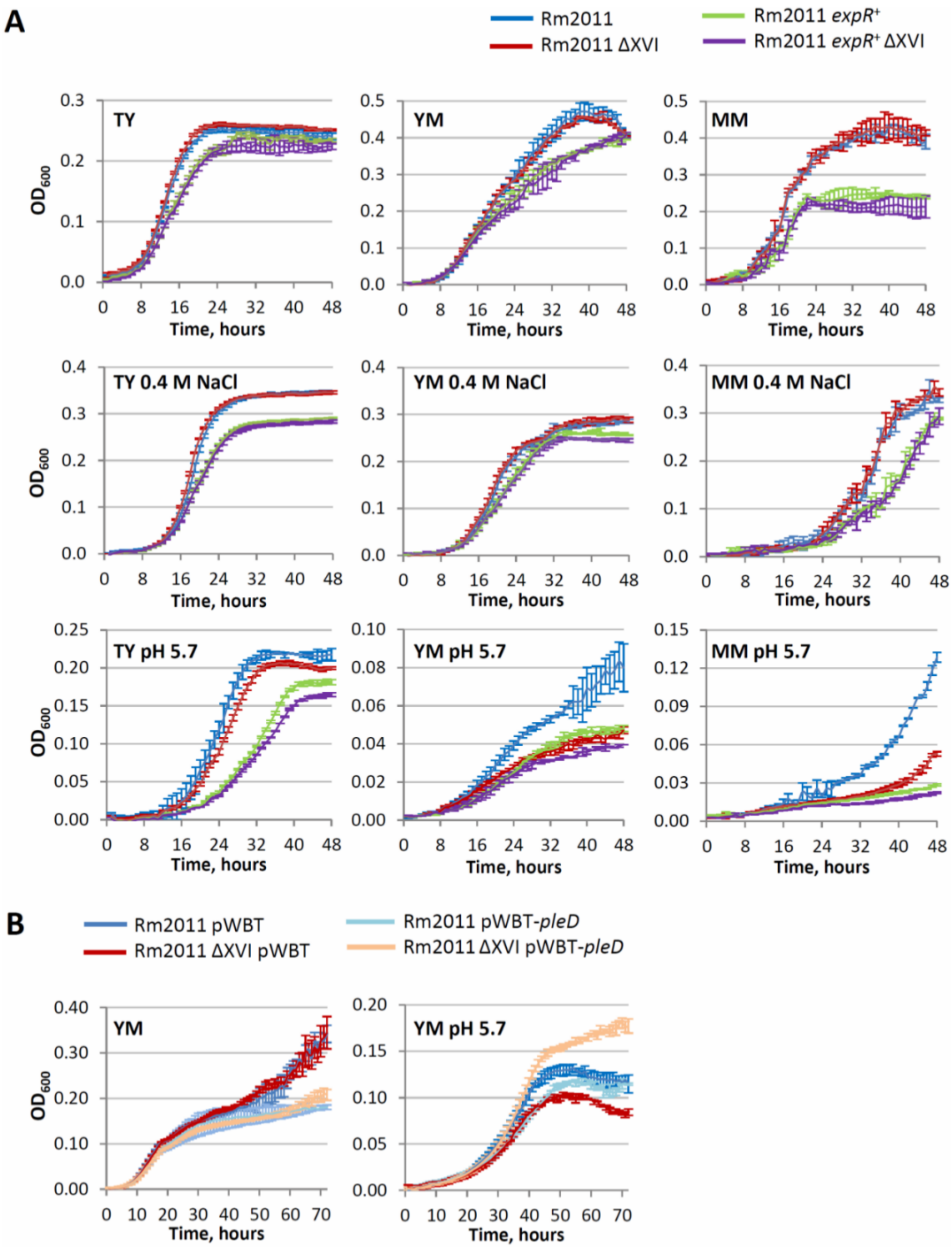

FIG S5 Growth of cdG^0 strains in different media. (A) Growth under normal, high-salt and acidic conditions. (B) Complementation of the growth defect of the Rm2011 cdG^0 strain at pH 5.7 by pWBT-*pleD* in presence of 100 µM IPTG. Error bars indicate standard deviations of three biological replicates.

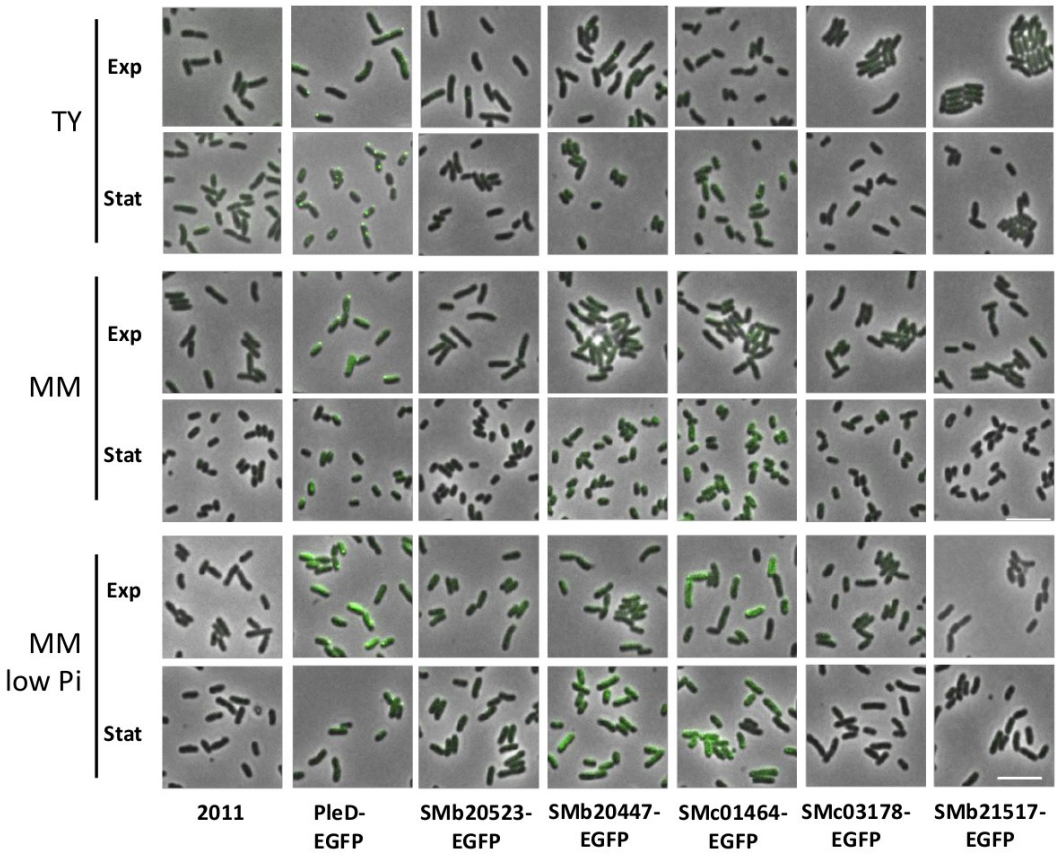

FIG S6 Detection of EGFP-tagged putative DGC/PDEs in Rm2011 cells grown on TY, MM or phosphate-limiting MM. Exp, exponential growth phase (OD_{600} of 0.6 to 0.8); Stat, stationary growth phase (after 40 h of growth). Scale bar, 5 µm. All images were taken using identical settings.

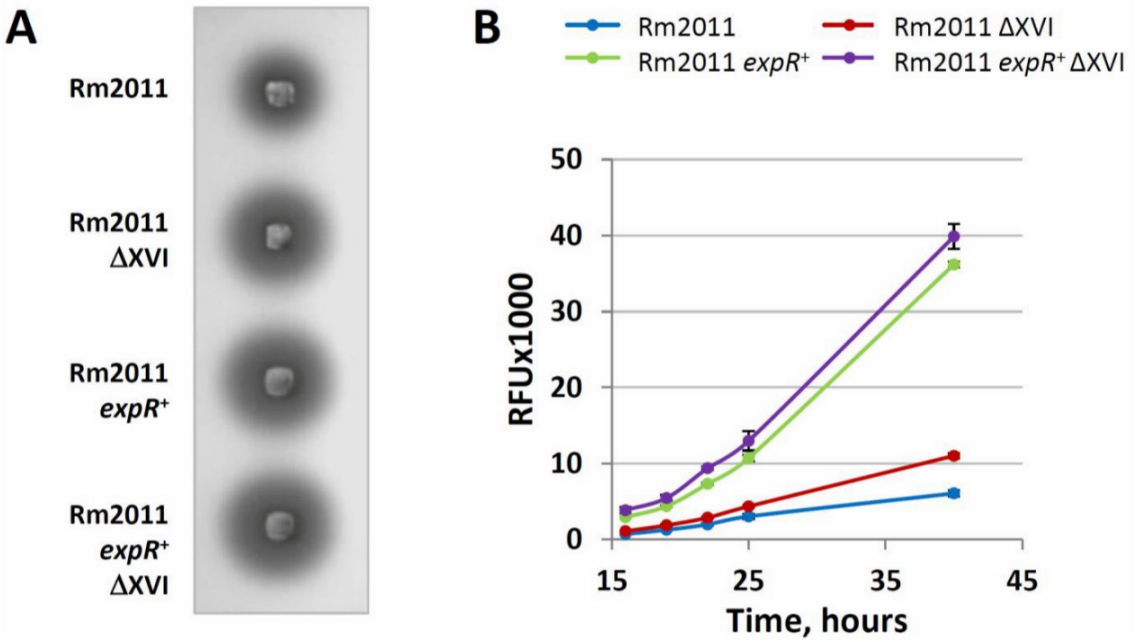

FIG S7 cdG negatively affects AHL production at the level of *sinI* transcription. (A) Semiquantitative detection of AHLs in supernatants of *S. meliloti* stationary phase cultures by *A. tumefaciens* NTL4 (pZLR4). (B) *sinI* promoter activity determined using a P_{sinI}-*egfp* fusion. RFU, relative EGFP fluorescence units. Error bars indicate standard deviations of three biological replicates.

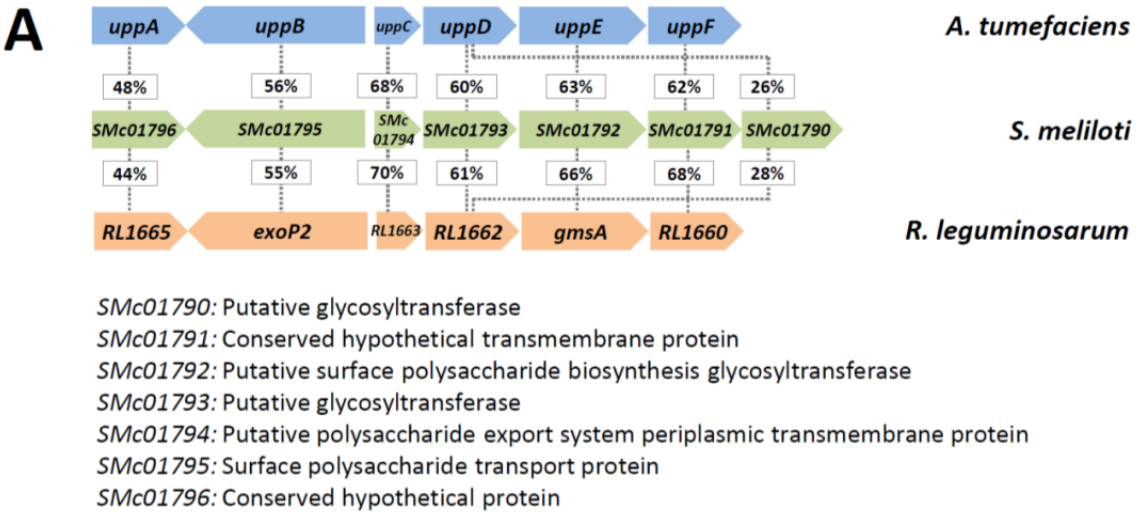

SMc01790: Putative glycosyltransferase
SMc01791: Conserved hypothetical transmembrane protein
SMc01792: Putative surface polysaccharide biosynthesis glycosyltransferase
SMc01793: Putative glycosyltransferase
SMc01794: Putative polysaccharide export system periplasmic transmembrane protein
SMc01795: Surface polysaccharide transport protein
SMc01796: Conserved hypothetical protein

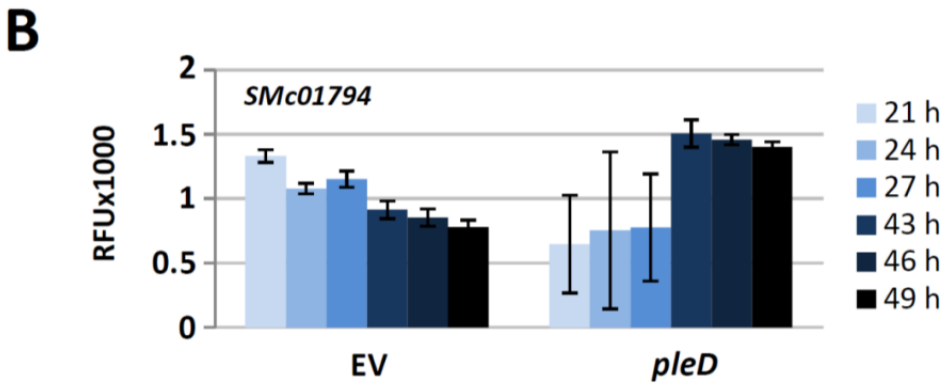

FIG S8 *S. meliloti SMc01790-SMc01796* gene cluster: architecture and expression upon overproduction of PleD. (A) Homology of the *SMc01790-SMc01796* gene cluster to the *A. tumefaciens upp* and *R. leguminosarum RL1660-RL1665* gene clusters. Percent numbers indicate amino acid sequence identities. (B) *SMc01794* promoter activity during growth in 30 % MM with or without *pleD* overexpression determined using a promoter-*egfp* fusion. EV, empty vector. RFU, relative EGFP fluorescence units. Error bars indicate standard deviations of three biological replicates.

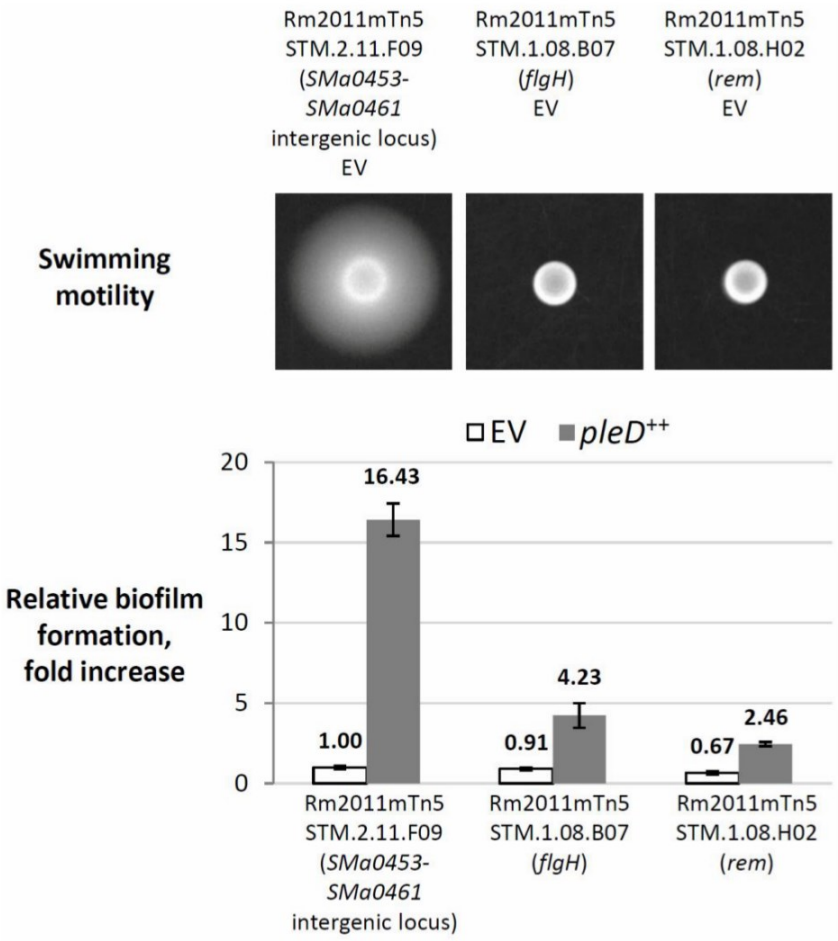

FIG S9 Biofilm formation of motility-deficient strains upon *pleD* overexpression. EV, empty pWBT vector. The A_{570}/OD_{600} mean value for Rm2011mTn5STM.2.11.F09 pWBT was 0.338±0.038 (set to 1). This control strain carrying an intergenic mTn5STM insertion is not affected in any phenotype analyzed in this study. Error bars represent standard deviations of three biological replicates.

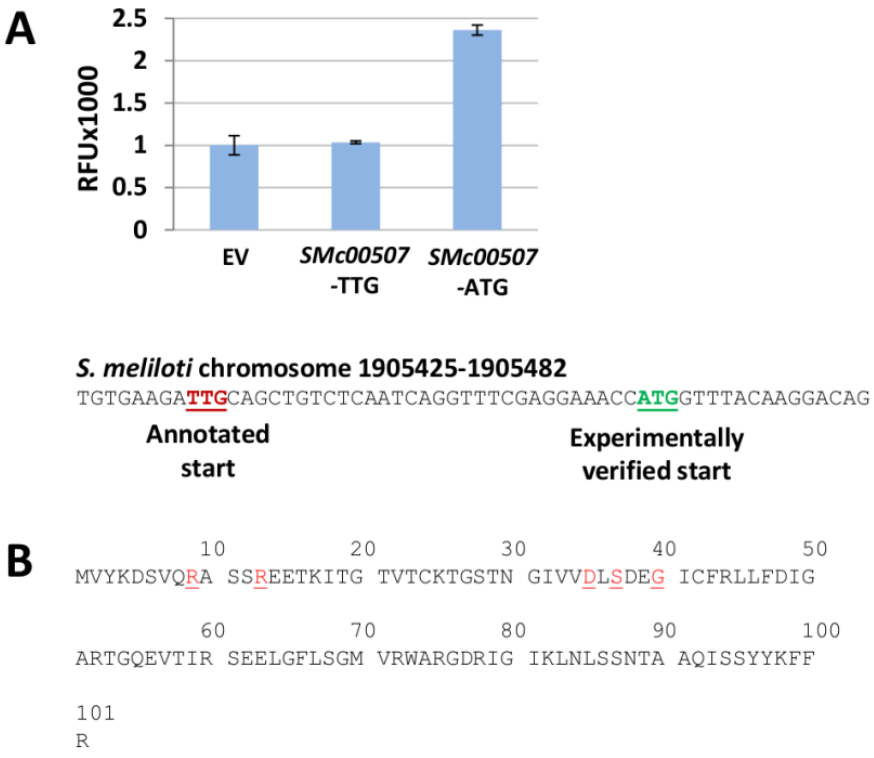

FIG S10 Experimental validation of the SM*c00507 (mcrA)* start codon. (A) *mcrA* promoter activity determined using promoter fusions to *egfp*, which were generated either using the annotated start codon TTG or the alternative start codon ATG. EV, empty vector. RFU, relative EGFP fluorescence units. Error bars indicate standard deviations of three biological replicates. (B) SMc00507 amino acid sequence with the ATG as translation start. RxxxR and DxSxxG motifs are indicated.

.

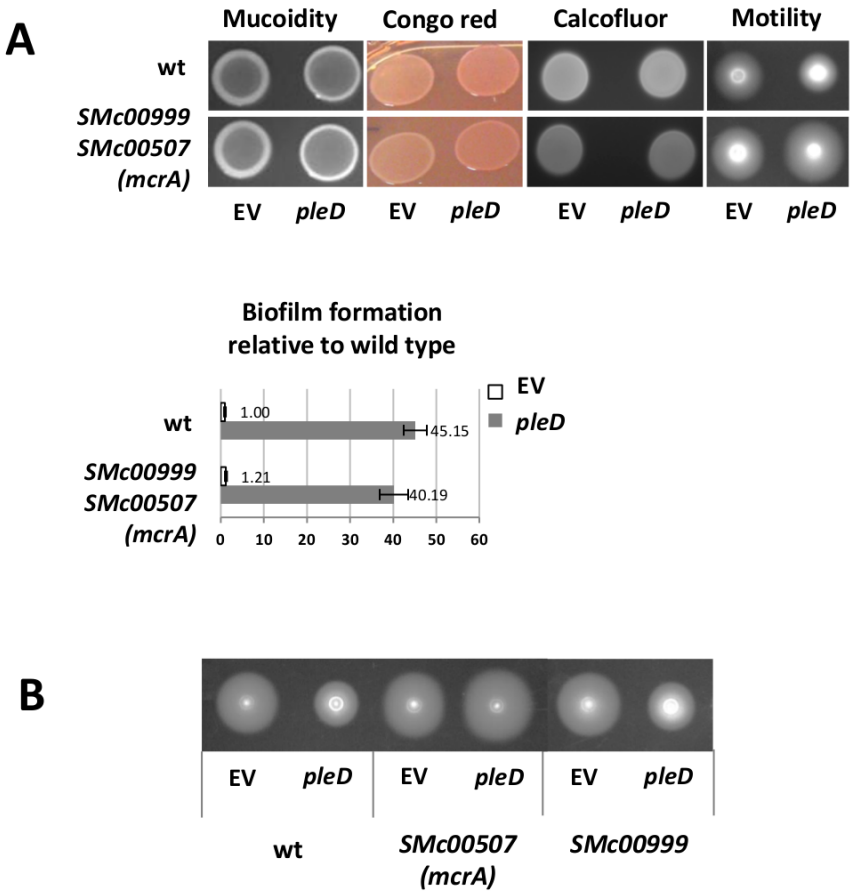

FIG S11 Identification of McrA (SMc00507) as a PilZ domain cdG receptor mediating repression of swimming motility upon *pleD* overexpression. (A) Phenotypic analysis of a double mutant in the PilZ domain protein-encoding genes *SMc00507* and *SMc00999* with or without *pleD* overexpression. Error bars indicate standard deviations of three biological replicates. The A_{570}/OD_{600} mean value for Rm2011 pWBT was 0.087±0.020 (set to 1). (B) Effect of *pleD* overexpression on motility of single mutants in *SMc00507* and *SMc00999*. EV, empty pWBT vector.

Chapter 7: AraC-like transcriptional activator CuxR binds c-di-GMP by a PilZ-like mechanism to regulate extracellular polysaccharide production

Simon Schäper*, Wieland Steinchen*, Elizaveta Krol, Florian Altegoer, Dorota Skotnicka, Lotte Søgaard-Andersen, Gert Bange, Anke Becker

*Co-first author

Accepted for publication in *Proceedings of the National Academy of Sciences of the United States of America*, May 2017.

Individual contribution:

- Construction of strains and plasmids
- Congo red binding assays
- Analysis of promoter activities using EGFP fluorescence assay
- EMSA experiments
- Contributed to protein purifications
- Contributed to protein cross-linking experiments
- Contributed to transcriptome profiling
- Contributed to writing of the manuscript

AraC-like transcriptional activator CuxR binds c-di-GMP by a PilZ-like mechanism to regulate extracellular polysaccharide production

Simon Schäper[a,b,1], Wieland Steinchen[a,c,1], Elizaveta Krol[a,b], Florian Altegoer[a,c], Dorota Skotnicka[d], Lotte Søgaard-Andersen[d], Gert Bange[a,c,2], and Anke Becker[a,b,2]

[a]LOEWE Center for Synthetic Microbiology, Philipps-Universität Marburg, 35043 Marburg, Germany; [b]Faculty of Biology, Philipps-Universität Marburg, 35043 Marburg, Germany; [c]Faculty of Chemistry, Philipps-Universität Marburg, 35043 Marburg, Germany; and [d]Department of Ecophysiology, Max Planck Institute for Terrestrial Microbiology, 35043 Marburg, Germany

Edited by Graham C. Walker, Massachusetts Institute of Technology, Cambridge, MA, and approved May 8, 2017 (received for review February 12, 2017)

Cyclic dimeric GMP (c-di-GMP) has emerged as a key regulatory player in the transition between planktonic and sedentary biofilm-associated bacterial lifestyles. It controls a multitude of processes including production of extracellular polysaccharides (EPSs). The PilZ domain, consisting of an N-terminal "RxxxR" motif and a β-barrel domain, represents a prototype c-di-GMP receptor. We identified a class of c-di-GMP–responsive proteins, represented by the AraC-like transcription factor CuxR in plant symbiotic α-proteobacteria. In *Sinorhizobium meliloti*, CuxR stimulates transcription of an EPS biosynthesis gene cluster at elevated c-di-GMP levels. CuxR consists of a Cupin domain, a helical hairpin, and bipartite helix-turn-helix motif. Although unrelated in sequence, the mode of c-di-GMP binding to CuxR is highly reminiscent to that of PilZ domains. c-di-GMP interacts with a conserved N-terminal RxxxR motif and the Cupin domain, thereby promoting CuxR dimerization and DNA binding. We unravel structure and mechanism of a previously unrecognized c-di-GMP–responsive transcription factor and provide insights into the molecular evolution of c-di-GMP binding to proteins.

c-di-GMP | transcription factor | PilZ | extracellular polysaccharide | *Sinorhizobium meliloti*

Many bacteria form aggregates of cells, which are embedded in a self-produced extracellular matrix, to protect themselves against environmental perturbations. These multicellular structures are often referred to as biofilms. Crucial to biofilm formation is the production of extracellular polysaccharides (EPSs), which constitute a major part of the extracellular matrix. The EPSs serve as a structural component of biofilms and promote multicellular morphotypes or cooperative bacterial cell movements (1–3). The composition of EPSs is species-specific and has most likely adapted to the individual lifestyles of bacteria during the course of evolution.

In recent years, the cyclic dinucleotide c-di-GMP has been recognized as an important bacterial second messenger playing key roles in lifestyle changes of many bacteria. c-di-GMP has been demonstrated to be important for the regulation of EPS production in a plethora of different bacterial species (4). Biosynthesis of c-di-GMP is catalyzed by diguanylate cyclases (DGCs) of the GGDEF domain family, whereas its degradation is performed by specific phosphodiesterases containing either an EAL or HD-GYP domain (5). Intracellular levels of c-di-GMP are recognized by specific receptors that show a high degree of structural diversity.

The PilZ domain serves as a common c-di-GMP receptor, which binds c-di-GMP through conserved "RxxxR" and "(D/N)x(S/A)xxG" motifs present within its disordered N terminus and the adjacent β-barrel domain, respectively (4, 6, 7). PilZ domains occur as stand-alone domains and as parts of multidomain proteins. For example, cellulose biosynthesis in *Gluconacetobacter xylinus* and *Escherichia coli* is allosterically controlled by c-di-GMP binding to the PilZ domain in the cellulose synthase (7, 8). Similarly, production of alginate in mucoid *Pseudomonas aeruginosa* requires c-di-GMP binding to the PilZ domain in Alg44, which is part of the alginate synthase complex (9). In addition to PilZ domains, c-di-GMP can be recognized by other receptors including GGDEF domains with an I-site, enzymatically inactive EAL domains, GIL domain, the MshEN domain, and c-di-GMP–specific riboswitches (10–18). Moreover, several c-di-GMP receptors function as transcriptional regulators, belong to diverse protein families, and regulate various cellular functions. In *Vibrio cholerae,* c-di-GMP stimulates polysaccharide biosynthesis by inducing dimerization of the transcriptional activator VpsT (19). In *Streptomyces*, c-di-GMP mediates the switch from vegetative growth to sporulation through its binding to the transcriptional repressor BldD (20). In *Pseudomonas*, c-di-GMP binding to the NtrC-like protein FleQ results in stimulation of *pel* transcription (21–23). In *Klebsiella pneumoniae*, the PilZ domain-containing transcriptional activator MrkH activates genes for fimbriae synthesis upon c-di-GMP binding (24). Finally, in *Burkholderia cenocepacia*, the CRP-like transcriptional regulator Bcam1349 binds c-di-GMP to stimulate expression of genes for cellulose synthesis (25). Taken together, these examples show that c-di-GMP can serve as positive or negative signal for the regulation of transcription.

Significance

Cyclic dimeric GMP (c-di-GMP) has emerged as ubiquitous bacterial second messenger, regulating multiple cellular functions, such as cell cycle, virulence, and biofilm formation. However, our knowledge on the molecular inventory, diversity, and function of c-di-GMP receptors, and the molecular evolution of c-di-GMP–responsive proteins is still incomplete. We have identified a class of c-di-GMP–responsive transcription factors, strikingly illustrating how a classical transcription factor has acquired the ability to sense this signaling molecule. The mode of c-di-GMP binding to the AraC-like transcription factor CuxR is highly reminiscent to that of the PilZ domain, the prototypic c-di-GMP receptor. PilZ and CuxR provide an example of convergent evolution in which c-di-GMP binding sites of similar topology have evolved independently in two distinct protein families.

Author contributions: E.K., G.B., and A.B. designed research; S.S., W.S., E.K., F.A., and D.S. performed research; S.S., W.S., E.K., L.S.-A., G.B., and A.B. analyzed data; and S.S., W.S., G.B., and A.B. wrote the paper.

The authors declare no conflict of interest.

This article is a PNAS Direct Submission.

Data deposition: The data reported in this paper have been deposited in ArrayExpress (accession code E-MTAB-5410). The atomic coordinates and structure factors have been deposited in the Protein Data Bank, www.pdb.org (PDB ID code 5NLA).

[1]S.S. and W.S. contributed equally to this work.

[2]To whom correspondence may be addressed. Email: anke.becker@synmikro.uni-marburg.de or gert@bangelab.org.

This article contains supporting information online at www.pnas.org/lookup/suppl/doi:10.1073/pnas.1702435114/-/DCSupplemental.

The plant symbiotic nitrogen-fixing α-proteobacterium *Sinorhizobium meliloti* produces two major exopolysaccharides, that is, succinoglycan and galactoglucan, and a capsular polysaccharide (26, 27). Moreover, several gene clusters potentially related to production of unknown EPSs have been identified on megaplasmid pSymB of the tripartite *S. meliloti* genome, which is composed of a main chromosome and two megaplasmids (28, 29). Succinoglycan and galactoglucan contribute to sliding on surfaces (30) and biofilm formation (31, 32), and promote establishment of a productive symbiosis of *S. meliloti* with its host plant (33, 34). In *S. meliloti*, production of succinoglycan and galactoglucan is controlled by multiple regulators at the transcriptional level (26). In planktonic cells, the zinc-finger–type transcriptional repressor MucR regulates a multitude of processes, including EPS biosynthesis and flagellar motility (35, 36). Recently, we showed that EPS production is also regulated by c-di-GMP (37).

Here, we set out to understand how c-di-GMP signaling and EPS production are interlinked to promote biofilm formation in *S. meliloti*. We report the structural and functional characterization of the AraC/XylS-like transcription factor CuxR, which induces expression of an EPS biosynthesis gene cluster. Comparative analyses suggest that CuxR represents a class of transcription factors that, during the course of molecular evolution, acquired the ability to bind c-di-GMP by a mechanism resembling that of PilZ domains.

Results

c-di-GMP Positively Affects EPS Production in *S. meliloti*. We have recently shown that elevated c-di-GMP levels caused by overproduction of the DGC PleD led to increased staining of *S. meliloti* macrocolonies with the hydrophobic dye Congo red (CR) (37) (Fig. 1*A*). This observation suggested to us that EPS production might be enhanced because CR is well known to bind to polysaccharides (38). This assumption is supported by the observation that a strain lacking the transcriptional repressor MucR showed even stronger CR staining upon *pleD* overexpression (Fig. 1*A*).

To identify the underlying mechanism, we performed transcriptomic profiling of *S. meliloti* in the absence and presence of plasmid-encoded PleD under the control of an isopropyl β-D-1-thiogalactopyranoside (IPTG)-inducible promoter. Upon overproduction of PleD, five genes were significantly up-regulated (i.e., M values greater than 1) (Fig. 1*B* and Table S1). Four of these genes cluster on megaplasmid pSymB. They are part of a putative six-gene operon predicted to encode an UDP-xylose synthase (*uxs1*), UDP-xylose 4-epimerase (*uxe*), family 2 glycosyltransferase (*SMb20460*), endoglucanase H (*SMb20462*), and two proteins of unknown function (*SMb20463* and *SMb20461*) (Fig. 1*B*). The predicted enzymatic activities of Uxs1 and Uxe have previously been experimentally confirmed (39). Predicted protein functions suggest that this cluster might be involved in the production of the putative CR-binding EPS.

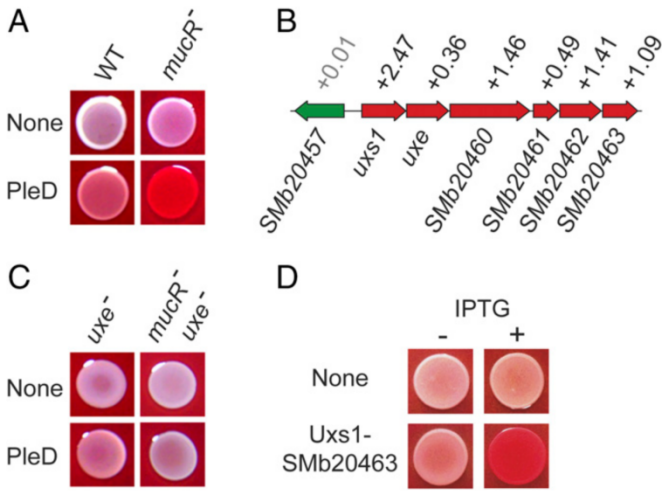

Fig. 1. Identification of a gene cluster involved in EPS production. (*A*) CR-binding assays of *S. meliloti* strains carrying empty vector ("None") or overproducing PleD. (*B*) Up-regulation of genes located in the *uxs1-SMb20463* cluster upon overproduction of PleD in transcriptome analysis. Numbers indicate M values (values of $P \leq 0.05$ labeled in black; values of $P > 0.05$ labeled in gray). (*C*) CR-binding assays of *S. meliloti uxe* mutant strains carrying empty vector (None) or overproducing PleD. (*D*) CR-binding assays of *S. meliloti* overexpressing the *uxs1-SMb20463* gene cluster upon induction by IPTG.

To determine whether increased transcription of this operon was responsible for enhanced CR staining, we interrupted the putative *uxs1-SMb20463* operon by integration of pK19mob2ΩHMB-*uxe* (40) into *uxe* in wild-type *S. meliloti* and in the *mucR* mutant. Integration of pK19mob2ΩHMB has been shown to disrupt transcription due to a strong transcription terminator encoded by this plasmid (40). Under PleD overproduction conditions, CR staining was decreased in both *uxe* mutant strains compared with the parental strains overexpressing *pleD* (Fig. 1 *A* and *C*). Furthermore, ectopic expression of the entire *uxs1-SMb20463* gene cluster under the control of an IPTG-inducible promoter in the wild type resulted in increased CR staining (Fig. 1*D*). Taken together, our results strongly suggest that the CR phenotype is dependent on genes of the *uxs1-SMb20463* operon and elevated intracellular c-di-GMP levels.

c-di-GMP Activates the *uxs1* Promoter Through CuxR. To better understand how c-di-GMP activates EPS production through the *uxs1-SMb20463* gene cluster, we generated *uxs1* promoter (P*uxs1*)-*egfp* fusions and tested their activities in absence and presence of plasmid-encoded PleD. When PleD production was induced by 0.5 mM IPTG in the wild type, P*uxs1* yielded a ~16-fold higher fluorescence signal compared with noninduced conditions (Fig. 2*A*). To support that P*uxs1* activation was solely dependent on c-di-GMP and not specifically caused by PleD, we also probed the effect of overproduction of the DGCs DgcA from *Caulobacter crescentus* and SMc01464 from *S. meliloti*, which have previously been applied to increase c-di-GMP levels in *S. meliloti* (37). Overproduction of either of these DGCs resulted in similar P*uxs1* activation as observed for PleD. Moreover, overproduction of a catalytically inactive PleD variant (i.e., $PleD_{GGAAF}$) did not result in activation of P*uxs1* (Fig. 2*A*). Altogether, our results demonstrate that c-di-GMP regulates the activity of the *uxs1* promoter.

In the next step, we asked how c-di-GMP affects P*uxs1* activity. Closer inspection of the genomic context revealed the presence of the *SMb20457* gene coding for a putative transcriptional regulator of the AraC family upstream of the *uxs1-SMb20463* gene cluster (Fig. 1*B*). To test whether this protein was involved in c-di-GMP–mediated activation of *uxs1-SMb20463* expression, P*uxs1* activity was measured in a strain lacking SMb20457. In this mutant, PleD-dependent activation of P*uxs1* was abolished (Fig. 2*B*). Vice versa, overproduction of SMb20457 in a strain lacking all DGC-encoding genes (cdG^0) did not result in P*uxs1* activation (Fig. 2*C*). Moreover, overproduction of both PleD and SMb20457 resulted in a 50-fold or 23-fold higher fluorescence signal compared with single PleD and SMb20457 overproduction, respectively (Fig. 2*C*). These results show that SMb20457 is important for the c-di-GMP–dependent activation of EPS production via the *uxs1* promoter. From hereon, we refer to *SMb20457* as *cuxR* (for c-di-GMP–responsive UDP-xylose regulator).

CuxR Specifically Interacts with c-di-GMP. Our in vivo studies suggested that CuxR might interact with c-di-GMP. To test this

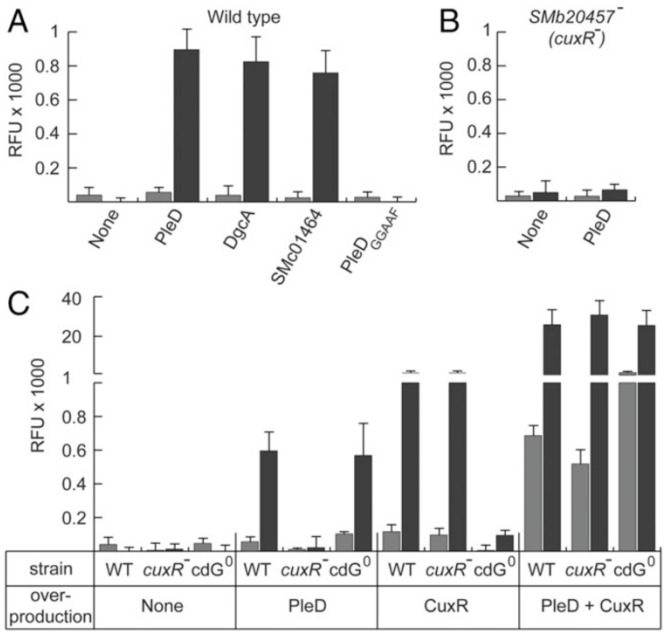

Fig. 2. c-di-GMP–dependent activation of the *uxs1* promoter by CuxR. (*A*–*C*) P*uxs1* activity without (gray bars) or upon overproduction (black bars) of the indicated proteins in *S. meliloti*. "None" denotes the empty vector control. (*A*) P*uxs1* activity upon overexpression of DGC-encoding genes in *S. meliloti*. (*B*) P*uxs1* activity upon PleD overproduction is disrupted in a *S. meliloti SMb20457 (cuxR)* mutant strain. (*C*) P*uxs1* activity in different *S. meliloti* genetic backgrounds upon overproduction of either PleD, CuxR, or both. Error bars indicate SDs of three biological replicates. RFU, relative EGFP fluorescence units.

notion, we probed the interaction between purified CuxR protein and ^{32}P-labeled c-di-GMP by a differential radial capillary action of ligand assay (DRaCALA) (41). Increased signal density in the center of the spotting area was detected using purified CuxR protein preincubated with ^{32}P-labeled c-di-GMP (Fig. 3*A*). Addition of unlabeled GTP did not alter the migration behavior of ^{32}P-labeled c-di-GMP. By contrast, unlabeled c-di-GMP resulted in a diffuse distribution of the radioactive signal, providing evidence for specific competition with its labeled counterpart (Fig. 3*A*). To determine the affinity between CuxR and c-di-GMP, we performed biolayer interferometry (BLI) using biotinylated c-di-GMP and streptavidin-coated biosensors (42), revealing a dissociation constant (K_d) of 6.7 μM (Fig. S1).

CuxR Activates the *uxs1* Promoter in a c-di-GMP–Dependent Manner. Knowing that the in vivo activation of P*uxs1* was dependent on the presence of the c-di-GMP binding protein CuxR and elevated c-di-GMP levels, we probed binding of CuxR to a DNA fragment containing the intergenic region (IR) located between *cuxR* and *uxs1* by electrophoretic mobility shift assay (EMSA) (43). In the absence of c-di-GMP, no binding of CuxR to the IR was observed (Fig. 3*B*). However, in the presence of c-di-GMP, but not GTP, we observed a clear band shift demonstrating c-di-GMP–dependent binding of CuxR to the IR (Fig. 3*B*).

To define the CuxR binding site, the IR was systematically shortened and tested by EMSA. A fragment containing 186 bp upstream of the *uxs1* start codon did not bind CuxR in the presence of c-di-GMP, whereas a fragment containing 196 bp did (Fig. 3*C*). This result shows that sequences crucial for binding of CuxR localize between positions 186 and 196 upstream of the *uxs1* start codon. Closer inspection of this region revealed the presence of a direct-repeat motif CGGGAT-N_6-CGGGAT that partially overlapped with a palindromic sequence CAATC-N_2-GATTG (Fig. 3*D*). To investigate whether this region was sufficient for CuxR binding, we inserted a 30-bp fragment (P*uxs1*$_{166–195}$) containing both motifs into a plasmid and generated a 240-bp PCR product composed of this region and flanking sequences derived from the plasmid. An EMSA revealed CuxR binding to this PCR product containing P*uxs1*$_{166–195}$, and this binding was dependent on the presence of c-di-GMP in the reaction mixture (Fig. 3*E*). To further dissect the c-di-GMP–dependent binding of CuxR to P*uxs1*$_{166–195}$, we systematically mutated nucleotides within the direct repeat and the palindromic region. Exchanging the direct-repeat left half-site without affecting the palindrome sequence (m1), resulted in a complete loss of CuxR binding. In contrast, mutation of the palindrome left half-site, which also contains one nucleotide of the direct-repeat right half-site (m6), did not notably affect DNA binding by CuxR upon c-di-GMP addition (Fig. 3 *D*

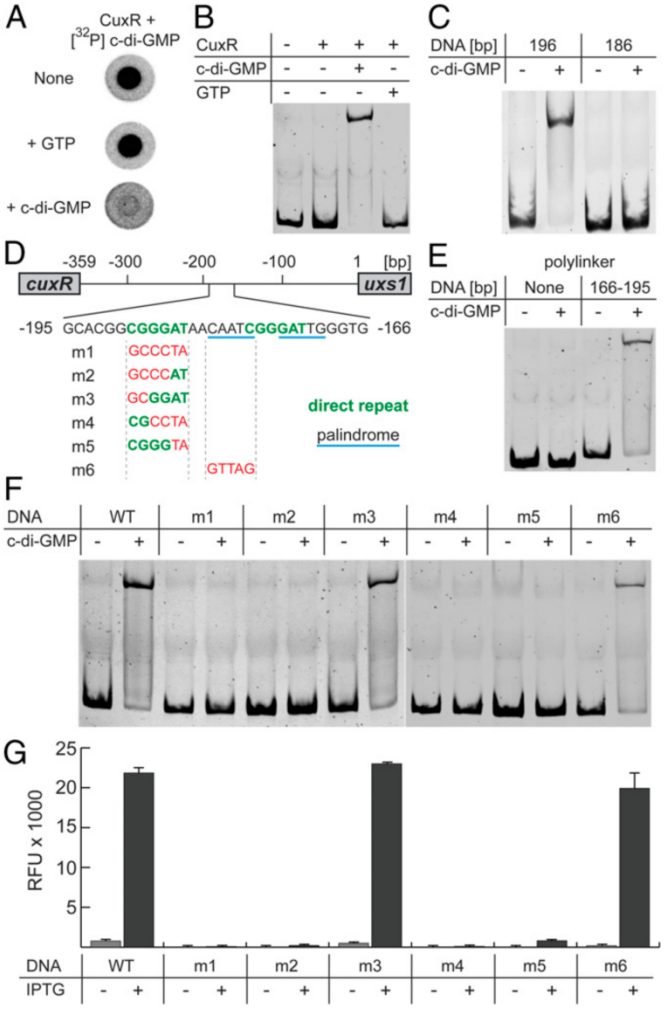

Fig. 3. c-di-GMP–dependent binding of CuxR to a direct-repeat element located within the *uxs1* promoter region. (*A*) CuxR specifically binds to c-di-GMP in DRaCALA. (*B*) CuxR requires c-di-GMP for binding to the intergenic region (IR) between *cuxR* and *uxs1* in EMSA. (*C*) CuxR binds to a DNA fragment containing 196 bp upstream of the *uxs1* start codon, but not to a fragment containing 186 bp, in the presence of c-di-GMP. (*D*) The IR between *cuxR* and *uxs1* contains a direct repeat and a palindromic sequence motif. Mutations within both motifs are denoted as m1 to m6. (*E*) The IR from positions 166–195 upstream of the *uxs1* start codon is sufficient for c-di-GMP–dependent CuxR interaction with the DNA in EMSA. (*F*) Mutations in the direct-repeat element but not within the palindrome of the IR abolish DNA binding by CuxR. (*G*) Overproduction of both CuxR and PleD in *S. meliloti* does not stimulate P*uxs1* containing mutations in the direct-repeat element of the IR. Error bars indicate SDs of three biological replicates. RFU, relative EGFP fluorescence units.

and *F*). Gradual mutagenesis of the direct-repeat left half-site CGGGAT suggests that the nucleotides GGAT in positions 3–6 are essential for DNA binding by CuxR, whereas C and G in positions 1 and 2 are apparently not (m2–m5 and m6 in Fig. 3 *D* and *F*).

Next, the same set of promoter fragments and mutations was probed for c-di-GMP–dependent stimulation of P*uxs1* activity by CuxR using the P*uxs1-egfp* reporter assay (see above). Strikingly, only those promoter mutants that showed a c-di-GMP–dependent binding of CuxR in the EMSAs stimulated c-di-GMP–dependent fluorescence (Fig. 3*G*). This identifies the direct-repeat CGGGAT-N_6-CGGGAT as the primary DNA binding site of CuxR within the P*uxs1* region.

Crystal Structure of CuxR. To better understand the molecular details of CuxR, we determined its crystal structure. Orthorhombic crystals of the native protein were obtained after 1 d and diffracted to 2.7-Å resolution. Although CuxR is predicted to belong to the AraC-like family of transcription factors, molecular replacement with a variety of different AraC-like protein structures failed. Therefore, we prepared selenomethionine-labeled crystals of CuxR that diffracted to 3.0-Å resolution. These crystals were used for structure determination by single-wavelength anomalous dispersion (SAD) (Table S2). The so-obtained structural coordinates served as a search model for structure determination by molecular replacement using the native crystals diffracting to 2.7-Å resolution (Table S2). The asymmetric unit contained one monomer and the structure was refined to R_{work}/R_{free} values of 23.6/28.1%, respectively. The structure could be built to completeness apart from the following highly disordered regions that could not be unambiguously built (i.e., amino acids 1–46, 310–370).

The architecture of CuxR can be divided into a Cupin-like domain, a helical hairpin (HP), a bipartite helix-turn-helix (bi-HTH) domain, and a C-terminal helix (CTH) connected to the bi-HTH through a disordered linker of ∼15 aa (Fig. 4*A*). The Cupin-like domain comprises the β-strands β1 to β12 that arrange in a "barrel"-like structure. The Cupin-like domain is reminiscent of the arabinose-binding domain of AraC from *E. coli* (44); however, the two domains significantly differ in size and topology (Fig. S2). The Cupin-like domain is followed by helices α4 and α5 that form a HP and localize to the outer surface of the Cupin-like domain barrel. Thereafter, helices α6 to α12 provide the basis for a bi-HTH of the AraC/XylS-type (Fig. 4*A*). Helices α6 to α8 and α10 to α12 constitute the two trihelical parts of this bipartite HTH and are connected with each other through helix α9 (Fig. 4*A*). Noteworthy, the second half of the bi-HTH is much less ordered in our crystal structure than the first one. Nevertheless, its location can be inferred by superimposing helices α6 to α9 of CuxR with the crystal structure of an AraC/XylS-type bi-HTH–containing protein from *Chromobacterium violaceum* (PDB ID code 3OIO; Fig. S3). A highly disordered region to which the CTH is connected follows the bi-HTH. The CTH could be unambiguously built because it interacts with the Cupin-like domain in a groove formed by β1, β3, β4, and α1 (Fig. 4*A*). Our structural analysis of CuxR shows that it displays an overall topology reminiscent of AraC-like transcriptional regulators such as AraC, but greatly differs in the Cupin-like domain and the C-terminal architecture.

A c-di-GMP–Dependent Homodimer of CuxR Activates the *uxs1* Promoter. Investigation of crystallographic contacts showed that the HP of one CuxR interacts with that of a symmetry-related HP through an interface of ∼800 Å^2 of buried surface area (Fig. 4*B*). In this regard, CuxR equals the transcriptional regulator AraC in which homodimerization is mediated via α2 of the HP, albeit differences between both proteins are apparent (Fig. 4*C*). To investigate whether homodimerization of CuxR via its HPs would be a prerequisite for its DNA binding in c-di-GMP–dependent manner, we exchanged amino acids located in this putative dimerization interface (i.e., L200E, N203E, R222E; Fig. 4 *D* and *E*) and tested the corresponding protein variants by EMSA. Although variant R222E was still able to bind to P*uxs1* in the presence of c-di-GMP, the L200E and N203E variants were not (Fig. 5*A*). To consolidate that the inability to bind to DNA was indeed caused by a defect in homodimerization of CuxR, we additionally performed cross-linking experiments with purified CuxR and its variants in the absence and presence of c-di-GMP using ethylene glycol bis(succinimidyl succinate) (EGS). Although wild-type CuxR and the R222E variants showed a protein band corresponding to a homodimer in the presence of c-di-GMP, the L200E and N203E variants did not (Fig. 5*B*). To exclude that the inability of the L200E and N203E variants to homodimerize was caused by impaired c-di-GMP binding, DRaCALA binding assays with CuxR and the three variants were performed revealing that c-di-GMP binding was not abolished (Fig. 5*C*).

Our in vitro data are in good agreement with CR-binding and P*uxs1* activation assays using the overproduced CuxR variants in a *cuxR* mutant strain also overproducing PleD. In these assays,

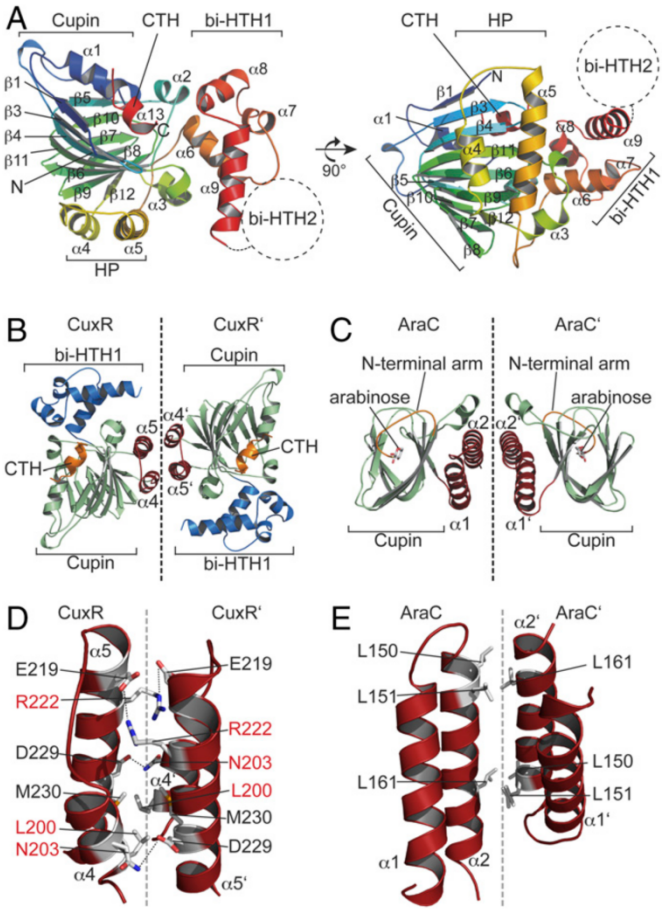

Fig. 4. Crystal structure of CuxR. (*A*) The crystal structure of CuxR is shown as cartoon in rainbow colors from N to C terminus, indicated by "N" and "C," respectively. Structural elements and domains are indicated. (*B* and *C*) Cartoon representations of the crystal structures of CuxR (*B*) and AraC bound to arabinose [*C*; PDB ID code 2ARC (44)]. The Cupin domain, helical hairpin, bi-HTH, and structural elements at the top of the Cupin domain (CTH in CuxR, N-terminal arm in AraC) are shown in green, red, blue, and orange, respectively. Arabinose is shown as sticks and colored by element. (*D* and *E*) Cartoon representation of the helical hairpins of CuxR (*D*) and AraC (*E*). Amino acids involved in dimer formation are shown as sticks. Amino acids varied in CuxR are labeled red.

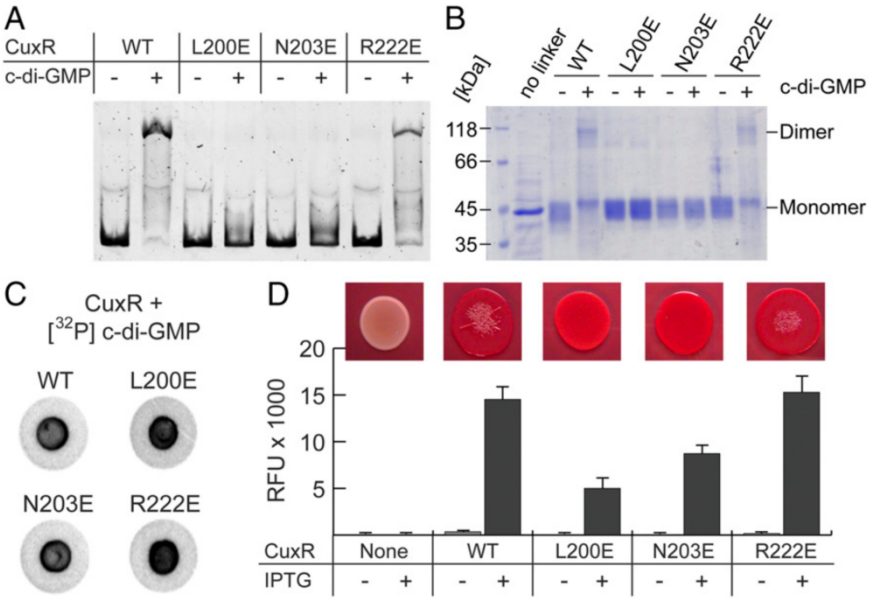

Fig. 5. CuxR forms c-di-GMP–dependent homodimers, which are essential for its functionality. (*A*) Variations within the homodimerization interface of CuxR affect binding of CuxR to the *uxs1* promoter region in EMSA. (*B*) In vitro cross-linking of CuxR variants in absence or presence of c-di-GMP. Protein bands corresponding to monomeric and dimeric CuxR are indicated. (*C*) CuxR variants still bind to c-di-GMP in DRaCALA assays. (*D*) P*uxs1* activity and CR binding of an *S. meliloti cuxR* mutant strain overexpressing *pleD* together with *cuxR* variants. Error bars indicate SDs of three biological replicates. RFU, relative EGFP fluorescence units.

the R222E variant behaved like wild-type CuxR, whereas the L200E and N203E variants showed decreased CR staining and P*uxs1* activation (Fig. 5*D*). Although significantly reduced, the remaining activation of P*uxs1* by the L200E and N203E CuxR variants implies that these variants may have a residual ability to dimerize or to bind DNA in the monomeric form, which might be aided by other factor(s) in vivo. Taken together, our results suggest that the HP of CuxR is important for the c-di-GMP–dependent homodimerization, which in turn is relevant for DNA binding and activation of P*uxs1*.

A Conserved RxxxR Motif and the Cupin Domain Mediate c-di-GMP Binding. To identify the c-di-GMP binding site of CuxR, we used hydrogen–deuterium exchange mass spectrometry (HDX-MS), also because we were unsuccessful to obtain crystals of CuxR bound to c-di-GMP. This method allows determining conformational changes within proteins upon their interaction with ligands (45, 46). Specifically, CuxR and c-di-GMP–bound CuxR were incubated in deuterated buffer for 0.5, 2, or 10 min. After quenching of the HDX reactions, the protein was digested using protease type XIII, and the resulting peptides were analyzed by electrospray ionization mass spectrometry. A total of 107 unique and deuterated peptides of CuxR could be assigned to their nondeuterated counterparts, resulting in 93% coverage of the CuxR amino acid sequence with a 3.5-fold redundancy (Table S3). Four regions of CuxR (named as R1 to R4) displayed significant differences in deuterium incorporation upon addition of c-di-GMP (Fig. 6 *A* and *B*). The R1 region (amino acids 25–53) contains the disordered N terminus of CuxR and β1 of the Cupin-like domain; regions R2 and R3 contain β-strands β6–β8 constituting the lower tip of the Cupin β-barrel and a flexible linker region followed by the HP helix α4, respectively; and region R4 solely contains the CTH of CuxR. Our HDX-MS results substantiate that c-di-GMP mediates homodimerization of CuxR as shown by the strong stabilization of the R3 region. However, they do not discriminate whether R1, R2, or R4 contain the c-di-GMP binding site. To elucidate which of these regions contributes to c-di-GMP binding, we first probed c-di-GMP binding of a CuxR variant lacking the CTH (CuxR ΔCTH) by DRaCALA. This variant did not show any alteration in c-di-GMP binding, suggesting that R4 is not involved in c-di-GMP binding (Fig. 6*C*). Multisequence alignments of the N termini of CuxR proteins from various rhizobial species revealed a conserved RxxxR motif (where "x" is any amino acid) in the N-terminal region of the protein. The presence of this motif seems to be restricted to rhizobial species and resembles the RxxxR motif found in PilZ proteins involved in c-di-GMP binding (Fig. S4 *A* and *B*). Substitution of both arginines with alanine (i.e., R24A and R28A) eliminated c-di-GMP binding to CuxR in the DRaCALA assays (Fig. 6*C*). Additionally, a screen for residues located in region R2 and its close proximity revealed that R162 is critical for c-di-GMP–dependent binding of CuxR to DNA (Fig. S5 *A* and *B*). This R162A variant showed impaired c-di-GMP binding in the DRaCALA assay (Fig. 6*C*). Similar to R162A variant, CuxR R24–R28 was unable to form homodimers and did not bind to DNA in the presence of c-di-GMP (Fig. 6 *D* and *E*, respectively). In vivo, these CuxR variants failed to stimulate P*uxs1* activity, and the mutants showed reduced CR staining (Fig. 6*F*). Taken together, these results show that c-di-GMP binding to CuxR requires a conserved RxxxR motif provided by the disordered N terminus and the arginine residue R162 located in the β-barrel domain of CuxR.

Discussion

CuxR Employs a PilZ-Like Mechanism to Interact with c-di-GMP. We have shown that CuxR requires the c-di-GMP–dependent homodimerization to interact with the *uxs1* promoter via its bi-HTH. Our HDX-MS measurements and the crystal structure together with our functional data suggest a model in which coordination of c-di-GMP to CuxR is mediated by two distinct binding sites: (*i*) an RxxxR motif located in the disordered N terminus and (*ii*) arginine residue R162 provided by the Cupin domain of CuxR. We postulate that c-di-GMP binding to CuxR enforces a conformation enabling homodimerization via helices α4 and α5 of the HP. Because of the rotational symmetry of this homodimer, no contact between c-di-GMPs bound to each of the subunits of the homodimer is possible. This is in contrast to the master regulatory protein BldD from *Streptomyces venezuelae*, where

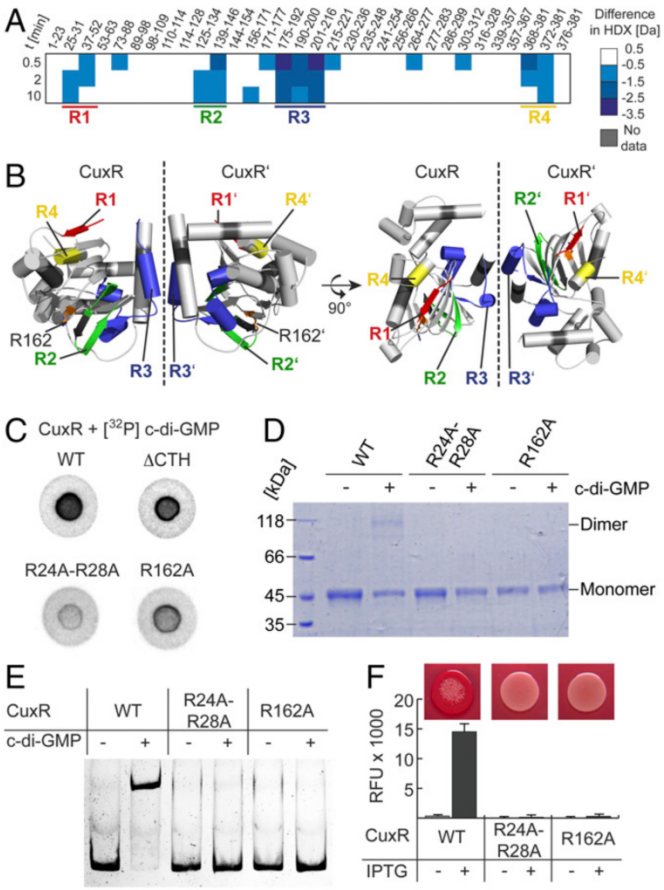

Fig. 6. A conserved RxxxR motif and the Cupin domain of CuxR mediate c-di-GMP binding. (*A*) Representative peptides of CuxR are colored according to their difference in HDX between c-di-GMP–bound CuxR and apo-CuxR. (*B*) Differences in HDX mapped onto the structure of the CuxR dimer. (*C*) Variations of the RxxxR motif (R24A–R28A) and R162 of CuxR abolish binding to c-di-GMP in the DRaCALA assay. (*D*) CuxR variants R24A–R28A and R162A are impaired in homodimerization in an in vitro cross-linking assay in the presence of c-di-GMP. Protein bands corresponding to monomeric and dimeric CuxR are indicated. (*E*) CuxR variants R24A–R28A and R162A are unable to interact with the *uxs1* promoter region in presence of c-di-GMP in an EMSA. (*F*) P*uxs1* activity and CR binding of an *S. meliloti cuxR* mutant strain overexpressing *pleD* together with *cuxR* variants. Error bars indicate SDs of three biological replicates. RFU, relative EGFP fluorescence units.

homodimerization is enabled via two dimers of intercalated c-di-GMP (20).

Surprisingly and unpredicted, the mode of c-di-GMP binding to CuxR is highly reminiscent to that of PilZ domains (Fig. 7). In the PilZ domain, two intercalated c-di-GMP molecules primarily interact with the two arginines present within the conserved RxxxR motif of the disordered N terminus. Moreover, one of the two intercalated c-di-GMP molecules interacts with amino acid side chains at the outer surface of the β-barrel of PilZ through a (D/N)x(S/A)xxG motif (motif 2) (4, 6, 7). A conserved arginine residue [i.e., R95 in *P. aeruginosa* Alg44 (47)] provided by the β-barrel establishes further contact to one c-di-GMP molecule and influences the number of c-di-GMP bound to the protein (47). In this regard, CuxR shows surprising similarities to PilZ, although its structure and sequence do not suggest so at first glance. CuxR—like PilZ—primarily interacts with c-di-GMP via a conserved RxxxR motif present within its disordered N terminus. Moreover, our HDX-MS experiments suggested that the outer surface of the β-barrel of its Cupin-like domain is involved in c-di-GMP binding (Fig. 6 *A* and *B*). Consequently, substitution of the conserved R162 in CuxR (resembling R95 in *P. aeruginosa* Alg44) disrupted c-di-GMP–dependent binding of CuxR to the *uxs1* promotor region and failed to promote EPS production (Fig. 6 *E* and *F*). We suspect that dimeric c-di-GMP is needed for DNA recognition by CuxR as a similar variation in the PilZ protein Alg44 led to binding of only one c-di-GMP molecule (47).

We therefore speculate that PilZ and CuxR provide an example of convergent evolution in which c-di-GMP binding sites of similar topology have evolved independently in two distinct protein families. In this sense, PilZ and CuxR share two structurally conserved features for their interaction with c-di-GMP: a disordered N terminus containing a RxxxR motif and a β-barrel structure providing additional amino acids contacting c-di-GMP (Fig. 7).

Comparing CuxR with its close structural homolog AraC suggests how proteins of this type might have acquired the ability to bind c-di-GMP during the course of evolution. Seemingly, such a new feature can be achieved simply by the addition of a disordered N terminus containing the c-di-GMP binding motif RxxxR and the parallel coevolution of amino acid residues at the outer surface of the β-barrel domain. Interestingly, β-barrel domains, such as Cupin, show high structural identities despite a huge diversity in their amino acid sequences (48, 49), making an evolutionary adaptation to c-di-GMP binding possible. In this light, we expect that other proteins with a β-barrel domain may also have acquired sensitivity to c-di-GMP in a similar manner.

c-di-GMP–Dependent Regulation of CuxR in the Framework of EPS Production. In this work, we identified CuxR as a c-di-GMP–dependent transcriptional activator of genes involved in polysaccharide production in the α-proteobacterium *S. meliloti*. Our analysis shows that CuxR belongs to the AraC/XylS family of transcription factors that contain a duplication of the trihelical version of the HTH domain and typically occur fused to a sugar-binding domain (50). Members of this transcription factor family are widely distributed in diverse prokaryote genera and are functionally related to carbon and nitrogen source metabolism, virulence, and stress responses (51). The most prominent member of the AraC/XylS family is AraC from *E. coli* that regulates the expression of genes involved in arabinose transport and catabolism (52, 53). In the absence of arabinose, the N-terminal arm of the dimerization domain binds to the DNA-binding domain of AraC and helps to hold the two DNA-binding domains in dimeric AraC apart from one another, favoring DNA looping (54). In this state, one monomer of the AraC dimer occupies the half-site $araI_1$, whereas the other one occupies the half-site $araO_2$, 210 bp apart from each other, leading to repression of the *araBAD* operon (55). In the presence of arabinose, however, the N termini of the AraC dimer bind to their dimerization domains facilitated by interaction with the ligand, thus freeing the DNA-binding domains and allowing their binding to the adjacent half-sites $araI_1$ and $araI_2$ with direct-repeat symmetry (54). This initiates transcription of the *ara* genes, which additionally requires cAMP receptor protein, CAP.

In CuxR, the Cupin-like domain followed by the HP and the bi-HTH essentially features the same topology as AraC from *E. coli*. Similarly to AraC, CuxR serves as transcription factor binding to the direct-repeat sequence CGGGAT-N_6-CGGGAT in the *uxs1* promoter region, which is 78 bp upstream from the putative transcriptional start site of *uxs1* (56). AraC from *E. coli* specifically binds to at least one half-site of the direct-repeat sequence TAGCattTttatCCatA-N_4-TAGCggaTcctaCCtgA, whereas the second half-site forms a partial overlap with the −35 region in P_{BAD} (55). A comparison between the two binding sites allows conclusions on the binding mode of CuxR to DNA. The AraC dimerization domain is loosely connected to its DNA-binding domain, and the connection between the two domains permits both extension and rotation. Arabinose binding to AraC tightens the connection between both domains and stabilizes binding to half-sites separated by zero or one turn of DNA, because the AraC protein

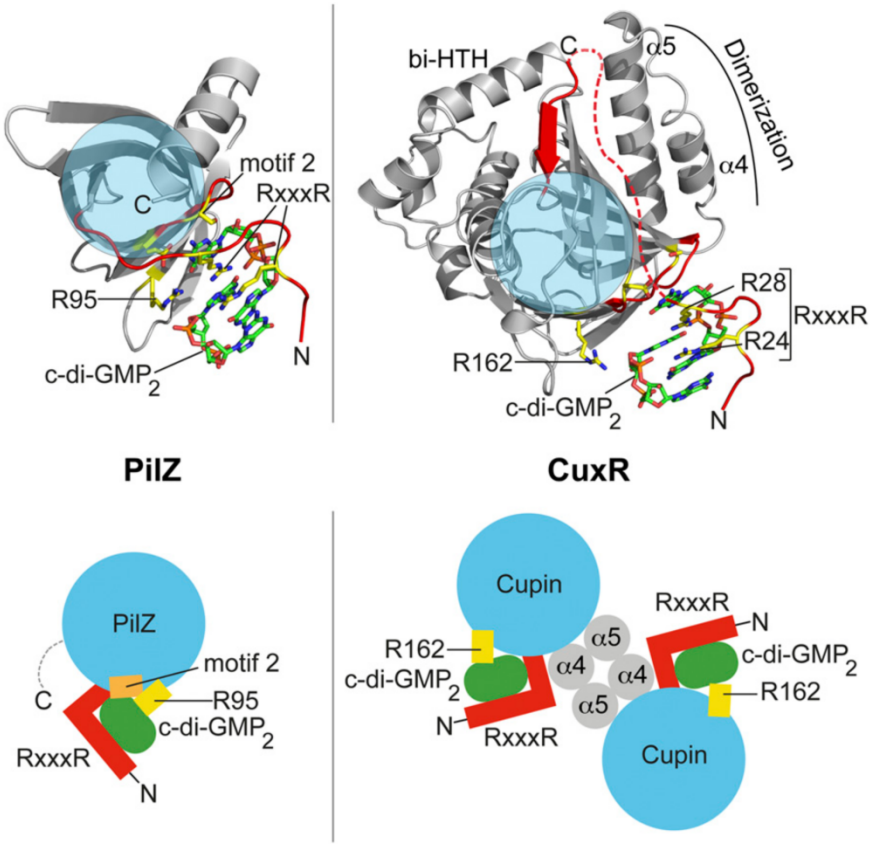

Fig. 7. c-di-GMP–mediated homodimerization and mechanism of CuxR. CuxR employs a c-di-GMP binding mechanism reminiscent to PilZ. (*Left*) Structure and scheme of a PilZ domain [*P. aeruginosa* Alg44; PDB ID code 4RT0 (47)] in complex with $(c\text{-di-GMP})_2$ are shown in the upper and lower panels, respectively. (*Right*) Structural model of CuxR monomer with a modeled N-terminal domain and $(c\text{-di-GMP})_2$ are shown in the upper panel. The scheme in the lower panel depicts the c-di-GMP–dependent homodimerization of CuxR. The color codes are as follows: blue, the β-barrel domains of PilZ and CuxR; red, the disordered N termini containing the RxxxR motif essential for c-di-GMP binding; orange, motif 2 required for c-di-GMP binding in PilZ; yellow, arginines 95 (Alg44) and 162 (CuxR) involved in c-di-GMP coordination; gray, helices α4 and α5 of the helical hairpin mediating homodimerization of CuxR; green, an intercalated dimer of c-di-GMP. "N" indicates the N terminus.

dimer cannot simultaneously contact two half-sites on opposites faces of the DNA (55). In case of CuxR, the two half-sites of the DNA binding site almost lie on the same face of the DNA helix.

AraC and CuxR also differ in that the latter contains a significantly longer and disordered N terminus carrying the RxxxR motif. As described above, this disordered region together with the Cupin-like domain renders CuxR sensitive to c-di-GMP and controls the c-di-GMP–dependent homodimerization of CuxR via its HP. Unlike AraC, which primarily exists as homodimer even in the absence of its ligand arabinose, CuxR is a monomer in the absence of c-di-GMP. Another notable difference between CuxR and AraC is located within the region responsible for arabinose binding in AraC. Residues required for arabinose binding in AraC are not conserved in CuxR. Instead, the Cupin-like domain of CuxR is extended by three additional β-strands resulting in a pocket, which is roughly double the size of that found in AraC. Moreover, helix α1 blocks the entrance to this putative binding site (Fig. 4*A*). This raises the question whether CuxR has kept its ability to interact with sugars in a way similar to AraC. The fact that CuxR is a transcriptional regulator controlling the c-di-GMP–dependent expression of genes involved in the production of a so-far structurally uncharacterized EPS via the *uxs1* promoter, renders an interaction of CuxR with monoaccharides or disaccharides a plausible hypothesis. In one scenario, an accumulating cytoplasmic intermediate of EPS production could tune the activity of CuxR as feedback inhibitor to prevent futile rounds of synthesis. Alternatively, monosaccharides serving as substrates for EPS production could act in concert with c-di-GMP to further stimulate CuxR in activating the *uxs1* promoter. However, it remains to be shown whether CuxR is able to interact with any sugar and if so, what the regulatory consequences might be.

Finally, our data show that CuxR is not a stand-alone regulator, but acts in the context of other regulatory mechanisms of EPS biosynthesis. This is exemplified by the observation that knockout of *mucR* leads to increased CuxR-dependent production of CR-binding EPS. In addition to activation of succinoglycan and repression of galactoglucan biosynthesis genes, MucR also represses transcription of *rem* encoding an activator of motility gene expression (35). Additional regulation of *cuxR* by MucR could provide the basis for the hierarchical integration of diverse environmental conditions into the molecular framework of EPS production.

Methods

Bacterial Strains and Growth Conditions. Bacterial strains and plasmids used in this study are shown in Table S4. *S. meliloti* was grown at 30 °C in tryptone–yeast extract (TY) medium (57), Luria–Bertani (LB) medium (58), and modified MOPS-buffered minimal medium (MM) (10 g/L MOPS, pH 7.2, 3 g/L mannitol, 1.07 g/L sodium glutamate, 0.246 g/L $MgSO_4{\cdot}7H_2O$, 36.75 mg/L $CaCl_2{\cdot}2H_2O$, 81.6 mg/L K_2HPO_4, 10 mg/L $FeCl_3{\cdot}6H_2O$, 1 mg/L biotin, 3 mg/L H_3BO_3, 2.23 mg/L $MnSO_4{\cdot}H_2O$, 0.287 mg/L $ZnSO_4{\cdot}7H_2O$, 0.125 mg/L $CuSO_4{\cdot}5H_2O$, 0.065 mg/L $CoCl_2{\cdot}6H_2O$, 0.12 mg/L $NaMoO_4{\cdot}2H_2O$) (59). *E. coli* was grown in LB medium at 37 °C. For *S. meliloti*, antibiotics were used at the following concentrations (mg/L; liquid/solid medium): kanamycin, 100/200; gentamicin, 20/40; tetracycline, 5/10; and streptomycin, 600/600. For *E. coli*, the

following concentrations were used: kanamycin, 50/50; gentamicin, 5/8; tetracycline, 5/10; and ampicillin, 100/100. Unless stated otherwise, IPTG was added at 100 μM final concentration.

Construction of Strains and Plasmids. Constructs used in this work were generated using standard cloning techniques. The oligonucleotide primers used are listed in Table S5. All constructs were verified by sequencing. Plasmids were transferred to *S. meliloti* by *E. coli* S17-1–mediated conjugation as previously described (60, 61). Correct plasmid integrations were verified by PCR. The *uxs1* promoter-*egfp* fusion was generated by insertion of a 368-bp fragment including the *cuxR-uxs1* IR and the three first codons of the *uxs1* gene into the replicative low-copy number plasmid pPHU231-EGFP. This generated an in-frame fusion of these first codons of the *uxs1* gene to *egfp*. Gene overexpression constructs were generated by insertion of the full-length coding sequence into the replicative medium-copy number vectors pWBT and pSRKGm. For combined overexpression of two genes in pWBT, the coding regions were inserted in tandem downstream of the T5 promoter. Constructs for production of N-terminally His_6-tagged CuxR and corresponding mutant variants were generated by insertion of the coding sequence excluding the start codon into expression vector pWH844. For generation of amino acid substitutions, splicing by overlap extension PCR was applied.

CR Assay. CR staining was assayed on TY agar containing 120 mg/L CR and 500 μM IPTG. In case of *pleD-cuxR* overexpression, IPTG was added at 100 μM. Fresh precultures grown on TY agar were resuspended in 0.9% (wt/vol) NaCl to an optical density at 600 nm (OD_{600}) of 0.1, and 50 μL were dropped onto the agar medium. Plates were incubated at 30 °C and documented after 3 d.

Transcriptome Analysis. Four independent bacterial cultures of Rm2011 carrying either pWBT or pWBT-*pleD* were grown in 100 mL of MM overnight to an OD_{600} of 0.5. IPTG was added at 500 μM, and cells were harvested after 4 additional hours of growth. RNA was isolated from bacterial cultures with the RNeasy Mini Kit (Qiagen). cDNA synthesis, Cy3 and Cy5 labeling, hybridization, image acquisition, and data analysis were performed as previously described (62). Normalization and *t* statistics were carried out using the EMMA 2.8.2 microarray data analysis software (63). Genes with value of $P \leq 0.05$ were included in the analysis. The M value represents the $\log_2$ ratio of both channels.

Fluorescence Measurements. For promoter-EGFP assays, TY precultures were diluted 1:500 in 100 μL of MM without or with addition of 100 μM IPTG and grown in 96-well plates at 30 °C with shaking. EGFP fluorescence [excitation wavelength (λ_{ex}) of 488 ± 9 nm; emission wavelength (λ_{em}) of 522 ± 20 nm; gain, 82] and growth (OD_{600}) were recorded using an Infinite 200 Pro multimode reader (Tecan). Strains carrying the empty vector pPHU231-EGFP were used for measuring background fluorescence. Relative fluorescence units (RFUs), calculated as EGFP signals, were normalized to OD_{600} ($n = 3$).

Protein Production and Purification. For production of native CuxR and its variants, *E. coli* BL21 (DE3) (Novagen) carrying the expression plasmids were grown in LB medium supplemented with 12.5 g/L D(+)-lactose-monohydrate and ampicillin (100 μg/mL) or kanamycin (50 μg/mL) for 16 h at 30 °C. The cells were harvested (3,500 × *g*, 20 min, 4 °C), resuspended in lysis buffer (20 mM Hepes-Na, pH 8.0, 250 mM NaCl, 40 mM imidazole, 20 mM $MgCl_2$, 20 mM KCl) and lysed with a M-110L Microfluidizer (Microfluidics). After centrifugation of cell debris (47,850 × *g*, 20 min, 4 °C), the clear supernatant was loaded on a 1-mL HisTrap HP column (GE Healthcare) equilibrated with 10 column volumes (CV) of lysis buffer. After washing with 10 CV of lysis buffer, CuxR was eluted with 5 CV of elution buffer (lysis buffer containing 500 mM imidazole). CuxR was concentrated using an Amicon Ultracel-10 concentration unit (Merck Millipore) and subjected to size-exclusion chromatography (SEC) using a HiLoad 26/600 Superdex 200 pg column (GE Healthcare) equilibrated in SEC buffer (20 mM Hepes-Na, pH 7.5, 200 mM NaCl, 20 mM $MgCl_2$, 20 mM KCl). CuxR-containing fractions were pooled and concentrated using an Amicon Ultracel-10 concentration unit (Merck Millipore) according to the experimental requirements. Protein concentration was determined with a spectrophotometer (NanoDrop Lite; Thermo Scientific). Selenomethionine (Se-Met)-labeled CuxR was produced using M9 medium (50 mM Na_2HPO_4, 25 mM KH_2PO_4, 10 mM NaCl, 20 mM NH_4Cl, pH 7.4) supplemented with 100 mg of lysine, 100 mg of threonine, 100 mg of phenylalanine, 50 mg of leucine, 50 mg of isoleucine, 50 mg of valine, 4 g of glucose, 50 mg of seleno-L-methionine, 2 mM $MgCl_2$, and 100 μM $CaCl_2$ per liter. Protein production was induced at an OD_{600} of 0.6 by addition of 1 mM IPTG and the culture incubated at 37 °C under vigorous shaking for 16 h. Protein purification was carried out as described for native CuxR (see above). For crystallization of native and Se-Met labeled CuxR, 10 mM DTT was included in the SEC buffer.

Preparation of α-^{32}P–Labeled c-di-GMP. Radiolabeled c-di-GMP was produced as described (64). Briefly, ^{32}P-labeled c-di-GMP was synthesized using 10 μM purified *C. crescentus* His_6-DgcA and 1 mM GTP/[α-^{32}P]GTP (0.1 μCi/μL) overnight at 30 °C in a buffer containing 50 mM Tris·HCl, pH 8.0, 300 mM NaCl, and 10 mM $MgCl_2$. The reaction was then treated with 5 units of calf intestine alkaline phosphatase (Fermentas) for 1 h at 22 °C to hydrolyze unreacted GTP and stopped by incubation for 10 min at 95 °C. The precipitated proteins were removed by centrifugation (10 min, 20,000 × *g*, 22 °C) and the supernatant used in c-di-GMP binding assays.

In Vitro c-di-GMP Binding Assay. c-di-GMP binding was determined using a DRaCALA with ^{32}P-labeled c-di-GMP, as described (41). Reaction mixtures (50 μL) containing ^{32}P-labeled c-di-GMP and 20 μM protein in the binding buffer (10 mM Tris·HCl, pH 8.0, 100 mM NaCl, 5 mM $MgCl_2$) were incubated for 10 min at room temperature. Ten microliters of this reaction mixture was spotted onto nitrocellulose membrane and allowed to dry before exposing a phosphor-imaging screen (Molecular Dynamics). Data were collected using a STORM 840 scanner (Amersham Biosciences).

BLI Binding Measurements. The dissociation constant of c-di-GMP binding to CuxR was determined by BLI using the BLItz system (forteBio, Inc.) equipped with Streptavidin SA biosensor (forteBio, Inc.) (42). The 500 nM biotinylated c-di-GMP in SEC buffer supplemented with 0.01% (wt/vol) Tween 20 was immobilized onto the biosensors for 120 s, and unbound molecules were washed off for 30 s. Different concentrations of CuxR were applied to the biosensor tip for 120 s, and dissociation was carried out by washing for 120 s. Nonspecific binding of CuxR to the biosensor was determined by addition of CuxR to the biosensor without prior immobilization of biotinylated c-di-GMP.

EMSA. EMSA was performed as previously described including small modifications (65). An EMSA reaction mixture contained 50 mM KCl, 0.85 μg of sonicated salmon sperm DNA (Invitrogen), 100 μg of BSA (Sigma), 0.5 μg of CuxR, and 15 ng of Cy3-labeled DNA in a final volume of 10 μL. Where indicated, c-di-GMP was added in a final concentration of 200 μM. Cy3-labeled DNA fragments were obtained by PCR with primer Cy3-egfp-28-rev and a primer binding inside the *cuxR-uxs1* IR using pPHU-P*uxs1*-EGFP as template. Synthetic pSRKKm-*cuxR*$_{bs}$-EGFP construct carrying a 30-bp fragment of the *cuxR-uxs1* IR including the CuxR-binding site was obtained using oligonucleotides extended by six nucleotides and sticky end overhangs for XbaI/HindIII cloning into pSRKKm-EGFP. The resulting plasmid was used as template for amplification of the DNA fragments for EMSA using the primers PCR2 and Cy3-egfp-28-rev. The reaction mixtures were incubated at room temperature for 30 min. Subsequently, 1.5 μL of 90% glycerol and 1.25 μL of 10× TBE buffer were added, and the reaction was loaded onto a 10% polyacrylamide gel in TBE. After electrophoresis at 90 V for 2.5 h, gel images were scanned using a Typhoon 8600 variable-mode imager (Amersham Bioscience).

Preparation of c-di-GMP. c-di-GMP was produced and purified as described previously (66). For production of c-di-GMP, a variant of the DGC TM1788 from *Thermotoga maritima* (tDGC harboring amino acids 88–241 of TM1788 with variation R158A) was used (66). c-di-GMP was produced by incubating 5 μM tDGC R158A together with 1 mM GTP at 45 °C in a buffer containing 50 mM Tris·HCl, pH 8.0, 250 mM $NaCl_2$, 20 mM $MgCl_2$, and 1 mM DTT. A total of 10 mM GTP was added during 10 h of incubation after which ∼95% of GTP were converted to c-di-GMP as estimated by HPLC (45). The reaction was stopped by addition of 2 volume parts chloroform and the aqueous phase injected into an Agilent 1100 Series HPLC (Agilent Technologies) equipped with a VP 250/21 Nucleodur C18 HTec, 5-μm column (Macherey-Nagel). c-di-GMP was eluted with a buffer containing 20 mM trimethylammonium bicarbonate, pH 7.0, and 9% (vol/vol) methanol at 18 mL/min flow rate. c-di-GMP–containing fractions were pooled and concentrated by evaporation at 20 mbar and 45 °C water bath temperature finally yielding a white powder. Identity and purity of c-di-GMP were estimated by HPLC in agreement with standards.

Crystallization of CuxR. Crystallization experiments were carried out by the sitting-drop method using SWISSCI MRC two-well crystallization plates with a reservoir volume of 50 μL. All crystallization experiments were carried out at room temperature. Initial crystallization hits were obtained after 1 d in 2 M

NaCl and 0.1 M Na-acetate, pH 4.6, with a protein concentration of ~300 μM and a drop size of 1 μL obtained by a 1:1 mixture of protein and precipitant solution. Diffraction-quality crystals were obtained after 3 d in 1.2 M NaCl and 0.1 M Na-acetate, pH 4.8, with a protein concentration of ~300 μM and a drop size of a 2 μL obtained by a 3:1 mixture of protein and precipitant solution.

Data Collection, Structure Determination, and Analysis. Crystals were flash-frozen in liquid nitrogen after transfer into a cryoprotection solution consisting of mother liquor supplemented with 30% (vol/vol) glycerol. Data collection was performed at the European Synchrotron Radiation Facility in Grenoble, France, at ID23-1. Data were collected under laminar nitrogen flow at 100 K (Oxford Cryosystems 700 Series) with a DECTRIS PILATUS 6M detector and processed with XDS (67) and CCP4-implemented SCALA (68). The structure of Se-Met–labeled CuxR was determined by SAD and subsequently served as search model for determination of the crystal structure of native CuxR by molecular replacement (MR). MR was performed using the CCP4-implemented program PHASER (69). Structures were built in COOT (70) and refined with PHENIX refine (71). Figures were prepared with PyMOL (www.pymol.org).

Constitution of CuxR–c-di-GMP Complex. For HDX and cross-linking experiments, CuxR–c-di-GMP complex was constituted by adding 1 mM c-di-GMP to ~10 μM CuxR in SEC buffer and concentrated using an Amicon Ultracel-10 concentration unit (Merck Millipore) according to the experimental requirements.

Protein Cross-Linking. The 10 μM CuxR or CuxR–c-di-GMP was incubated with 1 mM EGS for 30 min at 25 °C. The reaction was stopped by addition of Tris·HCl, pH 7.5, to a final concentration of 100 mM. Analysis of dimer formation was implemented by SDS/PAGE (72).

HDX-MS. The 50 μM CuxR or CuxR–c-di-GMP was diluted 10-fold in D_2O-containing SEC buffer to start the H/D exchange. After incubation at 25 °C for 30/120/600 s, the reaction was quenched by addition of an equal volume of ice-cold quench buffer (400 mM KH_2PO_4/H_3PO_4, pH 2.2) and directly injected into an ACQUITY UPLC M-class system with HDX technology (Waters) (73). CuxR was digested on-line using a self-packed column of protease type XIII from *Aspergillus saitoi* (74) at 0.5 °C running with water plus 0.1% formic acid at a flow rate of 100 μL/min and the resulting peptides trapped for 3 min using a C18 column. Subsequently, the trap column was placed in line with an ACQUITY UPLC BEH C18 1.7-μm 1.0 × 100-mm column (Waters) and the peptides eluted at 0.5 °C using a gradient of water plus 0.1% formic acid (A) and acetonitrile plus 0.1% formic acid (B) at 30 μL/min flow rate: linear increase from 5% to 35% B within 7 min followed by a ramp to 85% B within 1 min and hold at 85% B for 2 min. Thereafter, the column was washed for 1 min at 95% B and reequilibrated at 5% B for 5 min. Mass spectra were measured in positive ion mode using a G2-Si HDMS mass spectrometer equipped with an electrospray ionization source (Waters). Lock mass spectra were obtained every 30–45 s using [Glu1]-Fibrinopeptide B standard (Waters). Undeuterated peptides were generated as described above by 10-fold dilution of CuxR in H_2O-containing SEC buffer and detected in enhanced high-definition MS ($HDMS^E$) mode including ion mobility separation (IMS) of precursor ions within the gas phase and alternating high and low energies applied to the transfer cell (Waters). Deuterated peptides were detected in high-definition MS (HDMS) including IMS (75, 76). All measurements were performed in triplicates. Blank runs were performed between each sample to avoid peptide carryover. Peptide identification and data analysis were basically carried out as described previously (45, 77) using the software PLGS (Waters) with a custom-created database and the setting "no enzyme." Peptides identified in at least two replicates were included in further analysis with DynamX 3.0 (Waters). Tolerance thresholds of 0.5 min and 25 ppm for retention time and *m/z* values, respectively, were applied for correlation of undeuterated and deuterated peptides. Deuterium incorporation was calculated by subtraction of the centroid of the isotope distribution of the undeuterated from the deuterated peptides. Relative deuterium incorporation was calculated as the quotient of absolute deuteration and the number of backbone amide hydrogens of the respective peptides.

ACKNOWLEDGMENTS. We thank the European Synchrotron Radiation Facility in Grenoble, France, for excellent support during the X-ray crystallographic measurements; Dr. Uwe Linne (Philipps University Marburg) for support during HDX-MS measurements; Dr. Magdalena Polatynska for performing the BLI experiment; Barbara Herte for technical assistance in transcriptome profile analysis; and Dr. Matthew McIntosh for sharing plasmids. This work was funded by Deutsche Forschungsgemeinschaft through Collaborative Research Centre SFB 987 (to A.B., G.B., and L.S.-A.) and the Large Research Instrumentation Grants [INST 160/621-1 FUGG (to G.B.) and INST 160/536-1 FUGG (to A.B.)]. We acknowledge financial support by the LOEWE Excellence Initiative of the State of Hesse, Germany (A.B. and G.B.), and the Max Planck Society (L.S.-A.).

1. Zogaj X, Nimtz M, Rohde M, Bokranz W, Römling U (2001) The multicellular morphotypes of *Salmonella typhimurium* and *Escherichia coli* produce cellulose as the second component of the extracellular matrix. *Mol Microbiol* 39:1452–1463.
2. Gao M, Coggin A, Yagnik K, Teplitski M (2012) Role of specific quorum-sensing signals in the regulation of exopolysaccharide II production within *Sinorhizobium meliloti* spreading colonies. *PLoS One* 7:e42611.
3. Serra DO, Richter AM, Hengge R (2013) Cellulose as an architectural element in spatially structured *Escherichia coli* biofilms. *J Bacteriol* 195:5540–5554.
4. Römling U, Galperin MY, Gomelsky M (2013) Cyclic di-GMP: The first 25 years of a universal bacterial second messenger. *Microbiol Mol Biol Rev* 77:1–52.
5. Schirmer T, Jenal U (2009) Structural and mechanistic determinants of c-di-GMP signalling. *Nat Rev Microbiol* 7:724–735.
6. Amikam D, Galperin MY (2006) PilZ domain is part of the bacterial c-di-GMP binding protein. *Bioinformatics* 22:3–6.
7. Ryjenkov DA, Simm R, Römling U, Gomelsky M (2006) The PilZ domain is a receptor for the second messenger c-di-GMP: The PilZ domain protein YcgR controls motility in enterobacteria. *J Biol Chem* 281:30310–30314.
8. Ross P, et al. (1987) Regulation of cellulose synthesis in *Acetobacter xylinum* by cyclic diguanylic acid. *Nature* 325:279–281.
9. Merighi M, Lee VT, Hyodo M, Hayakawa Y, Lory S (2007) The second messenger bis-(3′-5′)-cyclic-GMP and its PilZ domain-containing receptor Alg44 are required for alginate biosynthesis in *Pseudomonas aeruginosa*. *Mol Microbiol* 65:876–895.
10. Fang X, et al. (2014) GIL, a new c-di-GMP-binding protein domain involved in regulation of cellulose synthesis in enterobacteria. *Mol Microbiol* 93:439–452.
11. Sudarsan N, et al. (2008) Riboswitches in eubacteria sense the second messenger cyclic di-GMP. *Science* 321:411–413.
12. Duerig A, et al. (2009) Second messenger-mediated spatiotemporal control of protein degradation regulates bacterial cell cycle progression. *Genes Dev* 23:93–104.
13. Lee VT, et al. (2007) A cyclic-di-GMP receptor required for bacterial exopolysaccharide production. *Mol Microbiol* 65:1474–1484.
14. De N, et al. (2008) Phosphorylation-independent regulation of the diguanylate cyclase WspR. *PLoS Biol* 6:e67.
15. Qi Y, et al. (2011) Binding of cyclic diguanylate in the non-catalytic EAL domain of FimX induces a long-range conformational change. *J Biol Chem* 286:2910–2917.
16. Newell PD, Monds RD, O'Toole GA (2009) LapD is a bis-(3′,5′)-cyclic dimeric GMP-binding protein that regulates surface attachment by *Pseudomonas fluorescens* Pf0-1. *Proc Natl Acad Sci USA* 106:3461–3466.
17. Wang YC, et al. (2016) Nucleotide binding by the widespread high-affinity cyclic di-GMP receptor MshEN domain. *Nat Commun* 7:12481.
18. Whitney JC, et al. (2012) Structure of the cytoplasmic region of PelD, a degenerate diguanylate cyclase receptor that regulates exopolysaccharide production in *Pseudomonas aeruginosa*. *J Biol Chem* 287:23582–23593.
19. Krasteva PV, et al. (2010) *Vibrio cholerae* VpsT regulates matrix production and motility by directly sensing cyclic di-GMP. *Science* 327:866–868.
20. Tschowri N, et al. (2014) Tetrameric c-di-GMP mediates effective transcription factor dimerization to control *Streptomyces* development. *Cell* 158:1136–1147.
21. Baraquet C, Murakami K, Parsek MR, Harwood CS (2012) The FleQ protein from *Pseudomonas aeruginosa* functions as both a repressor and an activator to control gene expression from the *pel* operon promoter in response to c-di-GMP. *Nucleic Acids Res* 40:7207–7218.
22. Matsuyama BY, et al. (2016) Mechanistic insights into c-di-GMP-dependent control of the biofilm regulator FleQ from *Pseudomonas aeruginosa*. *Proc Natl Acad Sci USA* 113:E209–E218.
23. Hickman JW, Harwood CS (2008) Identification of FleQ from *Pseudomonas aeruginosa* as a c-di-GMP-responsive transcription factor. *Mol Microbiol* 69:376–389.
24. Wilksch JJ, et al. (2011) MrkH, a novel c-di-GMP-dependent transcriptional activator, controls *Klebsiella pneumoniae* biofilm formation by regulating type 3 fimbriae expression. *PLoS Pathog* 7:e1002204.
25. Fazli M, et al. (2011) The CRP/FNR family protein Bcam1349 is a c-di-GMP effector that regulates biofilm formation in the respiratory pathogen *Burkholderia cenocepacia*. *Mol Microbiol* 82:327–341.
26. Becker A, et al. (2002) Regulation of succinoglycan and galactoglucan biosynthesis in *Sinorhizobium meliloti*. *J Mol Microbiol Biotechnol* 4:187–190.
27. Skorupska A, Janczarek M, Marczak M, Mazur A, Król J (2006) Rhizobial exopolysaccharides: Genetic control and symbiotic functions. *Microb Cell Fact* 5:7.
28. Finan TM, et al. (2001) The complete sequence of the 1,683-kb pSymB megaplasmid from the N_2-fixing endosymbiont *Sinorhizobium meliloti*. *Proc Natl Acad Sci USA* 98:9889–9894.
29. Galibert F, et al. (2001) The composite genome of the legume symbiont *Sinorhizobium meliloti*. *Science* 293:668–672.
30. Nogales J, Bernabéu-Roda L, Cuéllar V, Soto MJ (2012) ExpR is not required for swarming but promotes sliding in *Sinorhizobium meliloti*. *J Bacteriol* 194:2027–2035.
31. Rinaudi LV, González JE (2009) The low-molecular-weight fraction of exopolysaccharide II from *Sinorhizobium meliloti* is a crucial determinant of biofilm formation. *J Bacteriol* 191:7216–7224.

32. Fujishige NA, Kapadia NN, De Hoff PL, Hirsch AM (2006) Investigations of *Rhizobium* biofilm formation. *FEMS Microbiol Ecol* 56:195–206.
33. Leigh JA, Signer ER, Walker GC (1985) Exopolysaccharide-deficient mutants of *Rhizobium meliloti* that form ineffective nodules. *Proc Natl Acad Sci USA* 82:6231–6235.
34. Zhan HJ, Levery SB, Lee CC, Leigh JA (1989) A second exopolysaccharide of *Rhizobium meliloti* strain SU47 that can function in root nodule invasion. *Proc Natl Acad Sci USA* 86:3055–3059.
35. Bahlawane C, McIntosh M, Krol E, Becker A (2008) *Sinorhizobium meliloti* regulator MucR couples exopolysaccharide synthesis and motility. *Mol Plant Microbe Interact* 21:1498–1509.
36. Mueller K, González JE (2011) Complex regulation of symbiotic functions is coordinated by MucR and quorum sensing in *Sinorhizobium meliloti*. *J Bacteriol* 193: 485–496.
37. Schäper S, et al. (2015) Cyclic di-GMP regulates multiple cellular functions in the symbiotic alphaproteobacterium *Sinorhizobium meliloti*. *J Bacteriol* 198:521–535.
38. Wood PJ (1980) Specificity in the interaction of direct dyes with polysaccharides. *Carbohydr Res* 85:271–287.
39. Gu X, Lee SG, Bar-Peled M (2011) Biosynthesis of UDP-xylose and UDP-arabinose in *Sinorhizobium meliloti* 1021: First characterization of a bacterial UDP-xylose synthase, and UDP-xylose 4-epimerase. *Microbiology* 157:260–269.
40. Becker A, et al. (2009) A portal for rhizobial genomes: RhizoGATE integrates a *Sinorhizobium meliloti* genome annotation update with postgenome data. *J Biotechnol* 140:45–50.
41. Roelofs KG, Wang J, Sintim HO, Lee VT (2011) Differential radial capillary action of ligand assay for high-throughput detection of protein-metabolite interactions. *Proc Natl Acad Sci USA* 108:15528–15533.
42. Sultana A, Lee JE (2015) Measuring protein-protein and protein-nucleic acid interactions by biolayer interferometry. *Curr Protoc Protein Sci* 79:19.25.1–19.25.26.
43. Garner MM, Revzin A (1981) A gel electrophoresis method for quantifying the binding of proteins to specific DNA regions: Application to components of the *Escherichia coli* lactose operon regulatory system. *Nucleic Acids Res* 9:3047–3060.
44. Soisson SM, MacDougall-Shackleton B, Schleif R, Wolberger C (1997) Structural basis for ligand-regulated oligomerization of AraC. *Science* 276:421–425.
45. Steinchen W, et al. (2015) Catalytic mechanism and allosteric regulation of an oligomeric (p)ppGpp synthetase by an alarmone. *Proc Natl Acad Sci USA* 112: 13348–13353.
46. Marciano DP, Dharmarajan V, Griffin PR (2014) HDX-MS guided drug discovery: Small molecules and biopharmaceuticals. *Curr Opin Struct Biol* 28:105–111.
47. Whitney JC, et al. (2015) Dimeric c-di-GMP is required for post-translational regulation of alginate production in *Pseudomonas aeruginosa*. *J Biol Chem* 290: 12451–12462.
48. Smith TF, Gaitatzes C, Saxena K, Neer EJ (1999) The WD repeat: A common architecture for diverse functions. *Trends Biochem Sci* 24:181–185.
49. Stirnimann CU, Petsalaki E, Russell RB, Müller CW (2010) WD40 proteins propel cellular networks. *Trends Biochem Sci* 35:565–574.
50. Aravind L, Anantharaman V, Balaji S, Babu MM, Iyer LM (2005) The many faces of the helix-turn-helix domain: Transcription regulation and beyond. *FEMS Microbiol Rev* 29: 231–262.
51. Ibarra JA, Pérez-Rueda E, Segovia L, Puente JL (2008) The DNA-binding domain as a functional indicator: The case of the AraC/XylS family of transcription factors. *Genetica* 133:65–76.
52. Johnson CM, Schleif RF (1995) *In vivo* induction kinetics of the arabinose promoters in *Escherichia coli*. *J Bacteriol* 177:3438–3442.
53. Schleif R (2010) AraC protein, regulation of the l-arabinose operon in *Escherichia coli*, and the light switch mechanism of AraC action. *FEMS Microbiol Rev* 34:779–796.
54. Saviola B, Seabold R, Schleif RF (1998) Arm-domain interactions in AraC. *J Mol Biol* 278:539–548.
55. Carra JH, Schleif RF (1993) Variation of half-site organization and DNA looping by AraC protein. *EMBO J* 12:35–44.
56. Sallet E, et al. (2013) Next-generation annotation of prokaryotic genomes with EuGene-P: Application to *Sinorhizobium meliloti* 2011. *DNA Res* 20:339–354.
57. Beringer JE (1974) R factor transfer in *Rhizobium leguminosarum*. *J Gen Microbiol* 84: 188–198.
58. Green MR, Sambrook J (2012) *Molecular Cloning: A Laboratory Manual* (Cold Spring Harbor Lab Press, Cold Spring Harbor, NY), 4th Ed.
59. Zhan HJ, Lee CC, Leigh JA (1991) Induction of the second exopolysaccharide (EPSb) in *Rhizobium meliloti* SU47 by low phosphate concentrations. *J Bacteriol* 173: 7391–7394.
60. Simon R, Priefer U, Pühler A (1983) A broad host range mobilization system for *in vivo* genetic engineering: Transposon mutagenesis in gram-negative bacteria. *Nat Biotechnol* 1:784–791.
61. Krol E, Becker A (2014) Rhizobial homologs of the fatty acid transporter FadL facilitate perception of long-chain acyl-homoserine lactone signals. *Proc Natl Acad Sci USA* 111:10702–10707.
62. Serrania J, Vorhölter FJ, Niehaus K, Pühler A, Becker A (2008) Identification of *Xanthomonas campestris* pv. campestris galactose utilization genes from transcriptome data. *J Biotechnol* 135:309–317.
63. Dondrup M, et al. (2009) EMMA 2—a MAGE-compliant system for the collaborative analysis and integration of microarray data. *BMC Bioinformatics* 10:50.
64. Skotnicka D, et al. (2016) A minimal threshold of c-di-GMP is essential for fruiting body formation and sporulation in *Myxococcus xanthus*. *PLoS Genet* 12:e1006080.
65. Krol E, et al. (2016) Cyclic mononucleotide- and Clr-dependent gene regulation in *Sinorhizobium meliloti*. *Microbiology* 162:1840–1856.
66. Rao F, et al. (2009) Enzymatic synthesis of c-di-GMP using a thermophilic diguanylate cyclase. *Anal Biochem* 389:138–142.
67. Kabsch W (2010) XDS. *Acta Crystallogr D Biol Crystallogr* 66:125–132.
68. Winn MD, et al. (2011) Overview of the CCP4 suite and current developments. *Acta Crystallogr D Biol Crystallogr* 67:235–242.
69. McCoy AJ (2007) Solving structures of protein complexes by molecular replacement with Phaser. *Acta Crystallogr D Biol Crystallogr* 63:32–41.
70. Emsley P, Cowtan K (2004) Coot: Model-building tools for molecular graphics. *Acta Crystallogr D Biol Crystallogr* 60:2126–2132.
71. Adams PD, et al. (2010) PHENIX: A comprehensive Python-based system for macromolecular structure solution. *Acta Crystallogr D Biol Crystallogr* 66:213–221.
72. Laemmli UK (1970) Cleavage of structural proteins during the assembly of the head of bacteriophage T4. *Nature* 227:680–685.
73. Wales TE, Fadgen KE, Gerhardt GC, Engen JR (2008) High-speed and high-resolution UPLC separation at zero degrees Celsius. *Anal Chem* 80:6815–6820.
74. Cravello L, Lascoux D, Forest E (2003) Use of different proteases working in acidic conditions to improve sequence coverage and resolution in hydrogen/deuterium exchange of large proteins. *Rapid Commun Mass Spectrom* 17:2387–2393.
75. Geromanos SJ, et al. (2009) The detection, correlation, and comparison of peptide precursor and product ions from data independent LC-MS with data dependant LC-MS/MS. *Proteomics* 9:1683–1695.
76. Li GZ, et al. (2009) Database searching and accounting of multiplexed precursor and product ion spectra from the data independent analysis of simple and complex peptide mixtures. *Proteomics* 9:1696–1719.
77. Nevin P, Engen JR, Beuning PJ (2015) Steric gate residues of Y-family DNA polymerases DinB and pol kappa are crucial for dNTP-induced conformational change. *DNA Repair (Amst)* 29:65–73.
78. Casse F, Boucher C, Julliot J, Michel M, Dénarié J (1979) Identification and characterization of large plasmids in *Rhizobium meliloti* using agarose gel electrophoresis. *Microbiology* 113:229–242.
79. Becker A, et al. (1997) The 32-kilobase exp gene cluster of *Rhizobium meliloti* directing the biosynthesis of galactoglucan: Genetic organization and properties of the encoded gene products. *J Bacteriol* 179:1375–1384.
80. Khan SR, Gaines J, Roop RM, 2nd, Farrand SK (2008) Broad-host-range expression vectors with tightly regulated promoters and their use to examine the influence of TraR and TraM expression on Ti plasmid quorum sensing. *Appl Environ Microbiol* 74: 5053–5062.
81. Schirmer F, Ehrt S, Hillen W (1997) Expression, inducer spectrum, domain structure, and function of MopR, the regulator of phenol degradation in *Acinetobacter calcoaceticus* NCIB8250. *J Bacteriol* 179:1329–1336.
82. Skotnicka D, et al. (2015) c-di-GMP regulates type IV pili-dependent-motility in *Myxococcus xanthus*. *J Bacteriol* 198:77–90.

Supporting Information

Schäper et al. 10.1073/pnas.1702435114

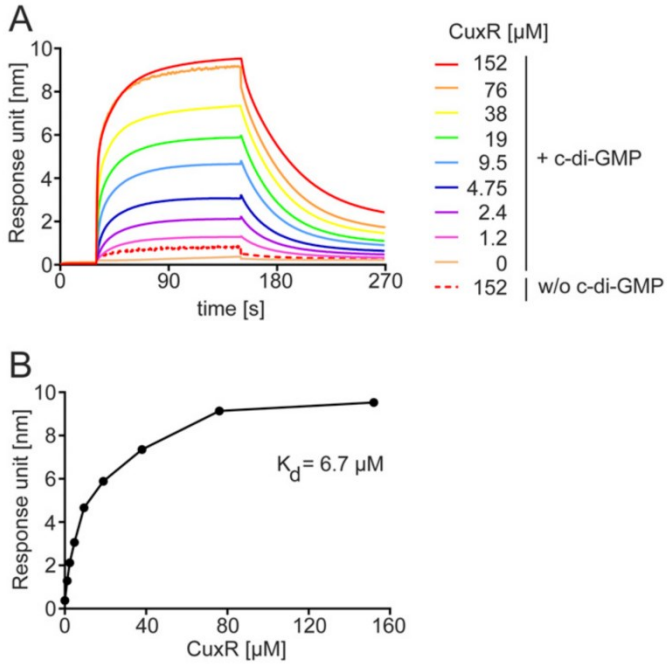

Fig. S1. Affinity of c-di-GMP binding to CuxR. (*A*) BLI sensograms of CuxR binding to biotinylated c-di-GMP immobilized on streptavidin-coated biosensors. CuxR was used at 0, 1.2, 2.4, 4.75, 9.5, 19, 38, 76, and 152 µM (solid lines). Unspecific binding of CuxR to the biosensor tip in absence of c-di-GMP was estimated using 152 µM CuxR (dotted line). (*B*) Saturation curve and dissociation constant of CuxR binding to biotinylated c-di-GMP.

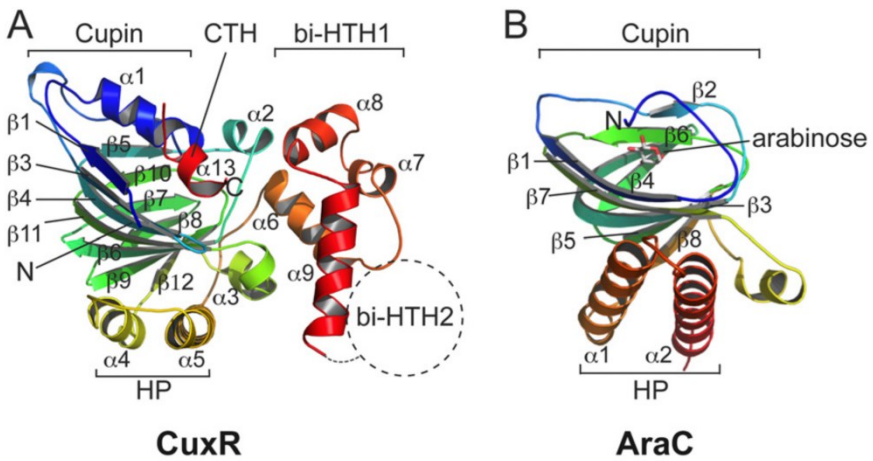

Fig. S2. Topology of CuxR and AraC. (*A* and *B*) Cartoon representation of the crystal structures of CuxR (*A*) and AraC from *E. coli* [*B*; PDB ID code 2ARC (44)] colored in rainbow from N to C termini, indicated by N and C, respectively. Arabinose bound to AraC is shown as sticks.

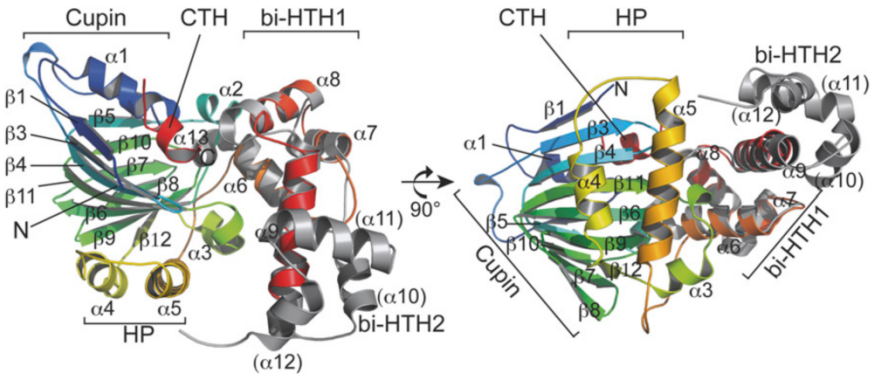

Fig. S3. Location of the second part of the HTH (bi-HTH2) of CuxR. Superimposition of the crystal structures of CuxR and an AraC/XylS-type bi-HTH–containing protein from *Chromobacterium violaceum* (PDB ID code 3OIO) allows for location of the bi-HTH2 of CuxR. The crystal structure of CuxR is shown as cartoon in rainbow colors from N to C terminus, indicated by N and C, respectively. Structural elements and domains of CuxR are indicated. The crystal structure of the AraC/XylS-type bi-HTH is shown in cartoon representation and colored in gray.

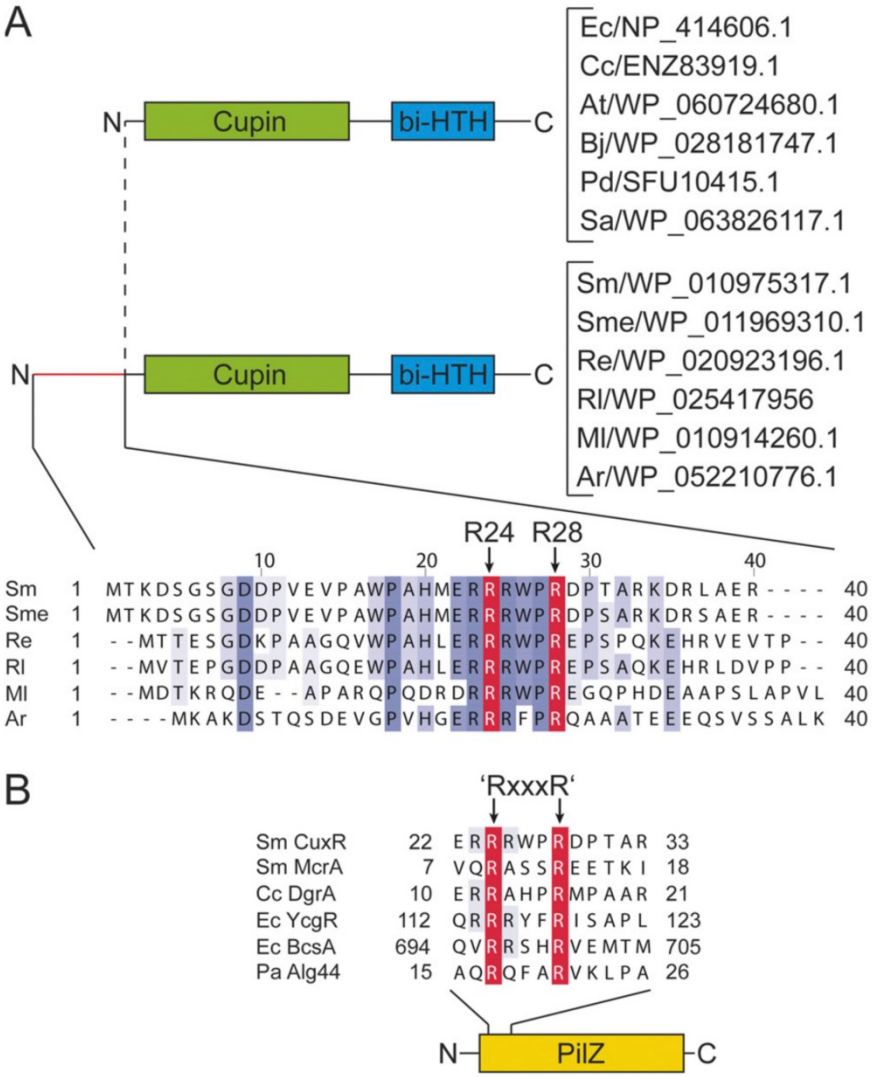

Fig. S4. The conserved RxxxR motif mediating c-di-GMP binding to CuxR and PilZ proteins. (*A*) Schematic domain architecture of proteins containing a Cupin and AraC/XylS-type helix-turn-helix (bi-HTH) domain from different bacterial species based on BLAST search using *S. meliloti* CuxR. Amino acid sequence alignment of the N terminus (red) of various rhizobial CuxR orthologs reveals the presence of two conserved arginine residues R24 and R28 in *S. meliloti* CuxR. The abbreviations are as follows: Ar, *Agrobacterium rhizogenes*; At, *Agrobacterium tumefaciens*; Bj, *Bradyrhizobium japonicum*; Cc, *Caulobacter crescentus*; Ec, *Escherichia coli*; Ml, *Mesorhizobium loti*; Pa, *Pseudomonas aeruginosa*; Pd, *Pseudovibrio denitrificans*; Re, *Rhizobium etli*; Rl, *Rhizobium leguminosarum*; Sa, *Streptomyces antibioticus*; Sm, *Sinorhizobium meliloti*; and Sme, *Sinorhizobium medicae*. National Center for Biotechnology Information sequence IDs of the proteins are indicated. (*B*) Amino acid sequence alignment of *S. meliloti* CuxR and PilZ proteins from different bacterial species reveals conservation of the RxxxR motif between CuxR and PilZ proteins.

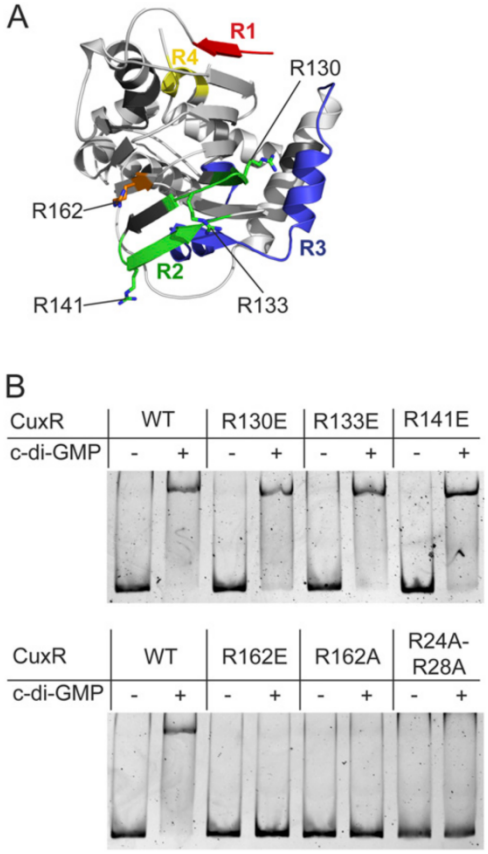

Fig. S5. Screen for arginine residues located in the Cupin domain of CuxR involved in c-di-GMP binding. (*A*) Location of arginine residues on the lower tip of the Cupin domain of CuxR. Regions R1–R4 displaying c-di-GMP–dependent differences in HDX of CuxR are colored as in Fig. 6*B*. Arginine 162 is shown in orange. (*B*) CuxR variants R162E and R162A are unable to interact with the *uxs1* promoter region in presence of c-di-GMP in an EMSA.

Table S1. Transcriptome profile analysis of Rm2011 overexpressing *pleD* (*SMc01370*) vs. Rm2011 harboring the empty vector pWBT

Reporter name	Reporter description	M value
SMc01370	*pleD*, putative transcription regulator protein	4.59
SMb20458	Putative dTDP-glucose 4,6-dehydratase protein	2.47
SMb20460	Putative cellulose synthase protein	1.46
SMb20462	Putative cellulase H precursor protein	1.41
SMc02435	*hemK1*, putative methyltransferase protein	1.36
SMb20463	Conserved hypothetical protein	1.09
SMc04114	*pilA1*, putative pilin subunit protein	0.85
SMc00159	Hypothetical signal peptide protein	0.71
SMc04153	Putative aminomethyltransferase protein	0.67
SMc00158	Hypothetical/unknown protein	0.50
SMb20461	Conserved hypothetical protein	0.49
SMb20194	Conserved hypothetical protein	0.45
SMc04152	Hypothetical protein	0.42
SMb20993	Putative FMNH2-dependent monooxygenase protein	0.42
SMb20453	Putative gluconolactonase precursor protein	0.41
SMa2237	Hypothetical protein	0.40
SMc03044	*motD*, chemotaxis protein (motility protein D)	0.39
SMc02940	Hypothetical protein	0.37
SMb20198	*cbbL*, putative ribulose-1,5-bisphosphate carboxylase large subunit protein	0.37
SMb20459	Putative UDP-glucose 4-epimerase protein	0.36
SMc02610	*glxB*, putative amidotransferase protein	0.34
SMc02612	*glxD*, putative oxidoreductase protein	0.34
SMc04113	*cpaA1*, putative pilus assembly transmembrane protein	0.34
SMc01488	Hypothetical transmembrane protein	0.33
SMb21644	Putative ABC transporter ATP-binding protein	−0.27
SMb20813	*msbA1*, putative lipid A + LPS core exporting ABC transporter protein, consisting of ATP-binding and permease domains	−0.29
SMb20605	Putative urea short-chain amide or branched-chain amino acid uptake ABC transporter periplasmic solute-binding protein precursor	−0.29
SMa1077	*nex18*, Nex18 symbiotically induced conserved protein	−0.30
SMb20318	Putative sugar ABC transporter permease protein	−0.30
SMb21082	*manC/manA*, probable mannose-6-phosphate isomerase, GDP-mannose pyrophosphorylase protein	−0.30
SMc02635	Hypothetical protein	−0.30
SMa0659	Cytochrome *c* binding protein, probable carboxyl terminus	−0.31
SMb21212	Putative protein	−0.31
SMb20668	Conserved hypothetical protein	−0.32
SMc04304	*cobW*, probable cobalamine biosynthesis protein	−0.32
SMb21036	Hypothetical protein	−0.32
SMc01531	*kdgK*, putative 2-dehydro-3-deoxygluconokinase protein	−0.32
SMa0185	Possible transmembrane-transport protein	−0.33
SMa0457	Hypothetical protein	−0.35
SMb20878	Conserved hypothetical protein	−0.35
SMa1538	Putative oxidoreductase	−0.37
SMb21314	*expE1*, putative secreted calcium-binding protein	−0.38
SMa2047	TRm24 putative transposase	−0.39
SMa2065	Hypothetical protein	−0.42
SMa1471	Hypothetical protein	−0.42
SMc04171	Putative hemolysin-type calcium-binding protein	−0.42
SMa2041	Probable oxidoreductase	−0.43
SMc01847	Putative methyltransferase protein	−0.45

Data were filtered for 48 genes with minimal and maximal M-values (value of $P \leq 0.05$).

Table S2. Data collection and refinement of CuxR

	SeMet-CuxR*	CuxR*
Data collection		
Space group	$P4_322$	$P4_322$
Cell dimensions		
a, *b*, *c*, Å	80.991	80.662
	80.991	80.662
	125.958	125.596
α, β, γ, °	90.00	90.00
	90.00	90.00
	90.00	90.00
Energy, Å	0.978	0.991
Resolution, Å	42.37–3.00	42.22–2.70
	(3.18–3.00)	(2.83–2.70)
R_{merge}	0.104 (1.065)	0.052 (0.901)
$I/\sigma I$	24.2 (3.7)	23.7 (2.2)
Completeness, %	100.0 (100.0)	99.7 (98.1)
Redundancy	24.5 (26.0)	8.3 (8.0)
Anomalous completeness, %	100.0 (100.0)	
Anomalous redundancy	13.6 (13.9)	
Refinement		
Resolution, Å		80.62–2.70
No. reflections		11,907
R_{work}/R_{free}		23.6/28.1
No. atoms		2,151
Protein		2,148
Ligand		0
Water		3
R.m.s. deviations		
Bond lengths, Å		0.009
Bond angles, °		1.37
Ramachandran, %		
Preferred		94.0
Allowed		4.9
Outliers		1.1

*Statistics for the highest-resolution shell are shown in parentheses.

Table S3. Hydrogen–deuterium exchange of CuxR peptides

Peptide			CuxR: uptake ± SEM, Da			c-di-GMP-CuxR: uptake ± SEM, Da		
Start	End	Maximum uptake	0.5 min	2 min	10 min	0.5 min	2 min	10 min
0	13	12	5.2 ± 0.1	5.2 ± 0.1	5.2 ± 0.1	5.0 ± 0.1	5.2 ± 0.1	5.1 ± 0.1
0	19	16	6.3 ± 0.1	6.4 ± 0.1	6.4 ± 0.1	6.6 ± 0.1	6.6 ± 0.1	6.6 ± 0.1
0	22	19	7.6 ± 0.1	7.7 ± 0.1	7.7 ± 0.1	7.7 ± 0.2	7.8 ± 0.1	7.8 ± 0.1
0	23	20	8.0 ± 0.1	8.0 ± 0.1	8.0 ± 0.1	7.7 ± 0.2	8.1 ± 0.1	8.2 ± 0.1
4	21	14	6.5 ± 0.1	6.6 ± 0.1	6.6 ± 0.1	6.5 ± 0.1	6.7 ± 0.1	6.6 ± 0.1
13	18	3	0.8 ± 0.1	0.9 ± 0.1	1.2 ± 0.1	0.7 ± 0.1	0.8 ± 0.1	1.0 ± 0.1
13	22	7	3.8 ± 0.1	4.4 ± 0.1	4.5 ± 0.1	3.2 ± 0.1	4.1 ± 0.1	4.4 ± 0.1
14	23	7	2.7 ± 0.1	3.5 ± 0.1	3.7 ± 0.1	2.2 ± 0.1	3.4 ± 0.1	3.8 ± 0.1
24	30	4	0.4 ± 0.1	0.4 ± 0.1	0.7 ± 0.1	0.4 ± 0.1	0.4 ± 0.1	0.5 ± 0.1
25	31	4	1.5 ± 0.1	1.9 ± 0.1	3.0 ± 0.1	1.1 ± 0.1	1.4 ± 0.1	2.0 ± 0.1
31	43	11	4.7 ± 0.1	6.4 ± 0.1	6.6 ± 0.1	3.9 ± 0.1	6.0 ± 0.1	6.7 ± 0.1
37	42	4	2.3 ± 0.1	2.3 ± 0.1	2.3 ± 0.1	2.1 ± 0.1	2.2 ± 0.1	2.2 ± 0.1
37	43	5	3.1 ± 0.1	3.1 ± 0.1	3.1 ± 0.1	2.7 ± 0.1	3.0 ± 0.1	3.0 ± 0.1
37	52	13	7.3 ± 0.1	7.7 ± 0.1	7.9 ± 0.1	6.6 ± 0.1	7.1 ± 0.1	7.4 ± 0.1
38	59	17	7.4 ± 0.1	8.0 ± 0.1	8.9 ± 0.1	6.7 ± 0.1	7.4 ± 0.1	8.1 ± 0.1
39	52	11	5.9 ± 0.1	6.3 ± 0.1	6.4 ± 0.1	5.4 ± 0.1	5.8 ± 0.1	6.1 ± 0.1
40	52	10	5.3 ± 0.1	5.6 ± 0.1	5.8 ± 0.1	4.7 ± 0.1	5.2 ± 0.1	5.4 ± 0.1
43	49	5	1.9 ± 0.1	2.4 ± 0.1	2.7 ± 0.1	1.5 ± 0.1	1.9 ± 0.1	2.1 ± 0.1
44	59	12	4.1 ± 0.1	4.7 ± 0.1	5.5 ± 0.1	3.8 ± 0.1	4.1 ± 0.1	4.8 ± 0.1
46	51	4	1.9 ± 0.1	3.1 ± 0.1	3.1 ± 0.1	0.9 ± 0.1	2.7 ± 0.1	3.1 ± 0.1
53	59	4	0.6 ± 0.1	0.8 ± 0.1	1.3 ± 0.1	0.6 ± 0.1	0.7 ± 0.1	1.0 ± 0.1
53	63	8	1.6 ± 0.1	2.6 ± 0.1	3.7 ± 0.1	1.1 ± 0.1	2.2 ± 0.1	3.4 ± 0.1
54	61	5	0.2 ± 0.1	0.3 ± 0.1	0.9 ± 0.1	0.1 ± 0.1	0.3 ± 0.1	0.7 ± 0.1
73	88	13	4.0 ± 0.1	5.0 ± 0.1	5.3 ± 0.1	3.5 ± 0.1	4.8 ± 0.1	5.4 ± 0.1
74	86	10	3.2 ± 0.1	3.3 ± 0.1	3.3 ± 0.1	3.0 ± 0.1	3.2 ± 0.1	3.3 ± 0.1
77	93	15	2.7 ± 0.1	3.5 ± 0.1	3.9 ± 0.1	2.4 ± 0.1	3.3 ± 0.1	3.8 ± 0.1
78	89	10	4.0 ± 0.1	4.1 ± 0.1	4.1 ± 0.1	3.9 ± 0.1	4.1 ± 0.1	4.1 ± 0.1
83	89	5	0.1 ± 0.1	0.1 ± 0.1	0.3 ± 0.1	0.1 ± 0.1	0.1 ± 0.1	0.2 ± 0.1
83	97	13	0.7 ± 0.1	0.9 ± 0.1	1.6 ± 0.1	0.8 ± 0.1	0.9 ± 0.1	1.3 ± 0.1
83	98	14	0.5 ± 0.1	0.7 ± 0.1	1.4 ± 0.1	0.7 ± 0.1	0.7 ± 0.1	1.2 ± 0.1
89	98	9	0.3 ± 0.1	0.4 ± 0.1	0.8 ± 0.1	0.3 ± 0.1	0.4 ± 0.1	0.6 ± 0.1
91	98	7	0.1 ± 0.1	0.1 ± 0.1	0.7 ± 0.1	0.2 ± 0.1	0.3 ± 0.1	0.5 ± 0.1
98	109	10	2.0 ± 0.1	2.0 ± 0.1	2.0 ± 0.1	1.9 ± 0.1	2.0 ± 0.1	2.1 ± 0.1
99	107	7	0.1 ± 0.1	0.2 ± 0.1	0.8 ± 0.1	0.1 ± 0.1	0.2 ± 0.1	0.6 ± 0.1
102	109	6	0.1 ± 0.1	0.2 ± 0.1	0.7 ± 0.1	0.1 ± 0.1	0.1 ± 0.1	0.5 ± 0.1
102	111	8	0.3 ± 0.1	0.4 ± 0.1	0.9 ± 0.1	0.2 ± 0.1	0.3 ± 0.1	0.7 ± 0.1
103	108	4	0.1 ± 0.1	0.4 ± 0.1	0.8 ± 0.1	0.1 ± 0.1	0.3 ± 0.1	0.7 ± 0.1
110	114	4	0.6 ± 0.1	0.7 ± 0.1	1.0 ± 0.1	0.5 ± 0.1	0.5 ± 0.1	0.8 ± 0.1
114	128	13	3.2 ± 0.1	3.4 ± 0.1	3.3 ± 0.1	3.1 ± 0.1	3.3 ± 0.1	3.4 ± 0.1
115	127	11	2.0 ± 0.1	2.1 ± 0.1	2.1 ± 0.1	2.0 ± 0.1	2.1 ± 0.1	2.2 ± 0.1
118	124	5	0.9 ± 0.1	1.0 ± 0.1	1.1 ± 0.1	0.8 ± 0.1	0.9 ± 0.1	1.0 ± 0.1
118	132	13	4.5 ± 0.1	4.6 ± 0.1	4.7 ± 0.1	4.4 ± 0.1	4.6 ± 0.1	4.7 ± 0.1
121	128	7	0 ± 0.1	0 ± 0.1	0 ± 0.1	0 ± 0.1	0 ± 0.1	0 ± 0.1
125	134	9	1.4 ± 0.1	1.9 ± 0.1	3.3 ± 0.1	1.0 ± 0.1	1.3 ± 0.1	2.0 ± 0.1
139	146	7	2.1 ± 0.1	2.1 ± 0.1	2.1 ± 0.1	0.4 ± 0.1	0.8 ± 0.1	1.4 ± 0.1
144	154	9	0.6 ± 0.1	0.7 ± 0.1	1.0 ± 0.1	0.5 ± 0.1	0.7 ± 0.1	1.0 ± 0.1
148	153	5	0.1 ± 0.1	0.1 ± 0.1	0.5 ± 0.1	0.1 ± 0.1	0.1 ± 0.1	0.3 ± 0.1
155	160	4	0.3 ± 0.1	0.3 ± 0.1	0.5 ± 0.1	0.2 ± 0.1	0.2 ± 0.1	0.3 ± 0.1
156	171	14	0.7 ± 0.1	1.0 ± 0.1	1.7 ± 0.1	0.6 ± 0.1	0.9 ± 0.1	1.1 ± 0.1
158	169	10	1.5 ± 0.1	1.6 ± 0.1	1.6 ± 0.1	1.6 ± 0.1	1.7 ± 0.1	1.7 ± 0.1
163	170	7	0.5 ± 0.1	0.7 ± 0.1	1.1 ± 0.1	0.4 ± 0.1	0.6 ± 0.1	1.1 ± 0.1
171	177	5	1.6 ± 0.1	2.0 ± 0.1	2.0 ± 0.1	1.1 ± 0.1	1.8 ± 0.1	2.0 ± 0.1
172	176	3	1.1 ± 0.2	1.5 ± 0.2	1.5 ± 0.2	0.6 ± 0.1	1.0 ± 0.1	1.3 ± 0.1
172	177	4	1.7 ± 0.1	2.2 ± 0.1	2.3 ± 0.1	1.3 ± 0.1	2.1 ± 0.1	2.3 ± 0.1
175	192	17	6.1 ± 0.2	7.6 ± 0.1	8.9 ± 0.1	2.9 ± 0.1	5.2 ± 0.1	7.2 ± 0.1
181	200	19	10.7 ± 0.1	11.8 ± 0.1	12.3 ± 0.1	9.7 ± 0.1	10.6 ± 0.1	11.6 ± 0.1
182	200	18	9.8 ± 0.1	10.9 ± 0.1	11.3 ± 0.1	8.8 ± 0.1	9.8 ± 0.1	10.6 ± 0.1
184	200	16	8.2 ± 0.1	9.3 ± 0.1	9.8 ± 0.1	7.2 ± 0.1	8.1 ± 0.1	9.0 ± 0.3
187	191	4	0.7 ± 0.1	1.0 ± 0.1	1.0 ± 0.1	0.4 ± 0.1	0.8 ± 0.1	1.0 ± 0.1
190	200	10	4.8 ± 0.1	5.7 ± 0.1	6.2 ± 0.1	3.5 ± 0.1	4.3 ± 0.1	5.2 ± 0.1
200	206	6	0.1 ± 0.1	0.3 ± 0.1	1.3 ± 0.1	0 ± 0.1	0 ± 0.1	0.2 ± 0.1

Table S3. Cont.

Peptide			CuxR: uptake ± SEM, Da			c-di-GMP-CuxR: uptake ± SEM, Da		
Start	End	Maximum uptake	0.5 min	2 min	10 min	0.5 min	2 min	10 min
201	206	5	0.1 ± 0.1	0.3 ± 0.1	1.2 ± 0.1	0 ± 0.1	0.1 ± 0.1	0.2 ± 0.1
201	216	15	6.0 ± 0.1	7.5 ± 0.1	8.5 ± 0.1	2.8 ± 0.1	5.1 ± 0.1	7.1 ± 0.1
203	218	15	6.1 ± 0.1	7.6 ± 0.1	8.6 ± 0.1	2.8 ± 0.1	5.2 ± 0.1	7.1 ± 0.1
210	216	6	3.2 ± 0.1	3.8 ± 0.1	3.9 ± 0.1	1.4 ± 0.1	2.4 ± 0.1	3.5 ± 0.1
215	221	5	3.4 ± 0.1	3.7 ± 0.1	3.6 ± 0.1	2.5 ± 0.1	3.6 ± 0.1	3.6 ± 0.1
226	250	23	7.4 ± 0.1	8.0 ± 0.1	8.9 ± 0.1	6.8 ± 0.2	7.4 ± 0.1	8.1 ± 0.1
230	236	6	0.7 ± 0.1	0.8 ± 0.1	1.1 ± 0.1	0.8 ± 0.1	0.9 ± 0.1	1.0 ± 0.1
235	248	12	7.8 ± 0.1	7.8 ± 0.1	7.8 ± 0.1	7.6 ± 0.1	7.8 ± 0.1	7.7 ± 0.1
241	254	13	8.0 ± 0.1	8.1 ± 0.1	8.1 ± 0.1	8.1 ± 0.1	8.1 ± 0.1	8.2 ± 0.1
256	266	10	5.7 ± 0.1	6.1 ± 0.1	6.0 ± 0.1	5.4 ± 0.1	6.2 ± 0.1	6.1 ± 0.1
259	275	15	7.9 ± 0.1	9.1 ± 0.1	9.3 ± 0.1	7.3 ± 0.1	8.9 ± 0.1	9.5 ± 0.1
261	277	15	7.4 ± 0.1	9.5 ± 0.1	10.0 ± 0.1	6.7 ± 0.1	8.9 ± 0.1	9.9 ± 0.1
262	277	14	6.7 ± 0.1	8.6 ± 0.1	9.1 ± 0.1	6.0 ± 0.1	8.2 ± 0.8	9.2 ± 0.1
264	277	12	5.1 ± 0.1	7.1 ± 0.1	7.6 ± 0.1	4.4 ± 0.1	6.6 ± 0.1	7.7 ± 0.1
276	287	11	4.7 ± 0.1	6.5 ± 0.1	6.7 ± 0.1	4.0 ± 0.1	6.1 ± 0.1	6.9 ± 0.1
277	281	4	0.9 ± 0.1	1.0 ± 0.1	0.9 ± 0.1	0.8 ± 0.1	0.9 ± 0.1	0.9 ± 0.1
277	283	6	2.5 ± 0.1	3.0 ± 0.1	3.1 ± 0.1	2.4 ± 0.1	2.9 ± 0.1	3.1 ± 0.1
286	299	12	6.2 ± 0.1	7.5 ± 0.1	8.0 ± 0.1	5.8 ± 0.1	7.3 ± 0.1	8.2 ± 0.1
287	299	11	5.7 ± 0.1	6.7 ± 0.1	7.3 ± 0.1	5.3 ± 0.1	6.6 ± 0.1	7.3 ± 0.1
288	295	6	3.4 ± 0.1	3.4 ± 0.1	3.4 ± 0.1	3.3 ± 0.1	3.4 ± 0.1	3.5 ± 0.1
288	296	7	4.1 ± 0.1	4.1 ± 0.1	4.2 ± 0.1	4.0 ± 0.1	4.1 ± 0.1	4.1 ± 0.1
303	309	6	2.4 ± 0.1	3.8 ± 0.1	3.9 ± 0.1	1.2 ± 0.1	3.4 ± 0.1	3.9 ± 0.1
303	312	9	3.7 ± 0.1	4.3 ± 0.1	4.3 ± 0.1	3.2 ± 0.1	3.9 ± 0.1	4.3 ± 0.1
306	321	13	7.7 ± 0.1	8.5 ± 0.1	8.5 ± 0.1	6.8 ± 0.1	8.3 ± 0.1	8.5 ± 0.1
309	321	10	6.2 ± 0.1	6.2 ± 0.1	6.2 ± 0.1	5.9 ± 0.1	6.1 ± 0.1	6.1 ± 0.1
310	324	12	7.6 ± 0.1	7.8 ± 0.1	7.8 ± 0.1	6.9 ± 0.1	7.8 ± 0.1	7.9 ± 0.1
311	330	17	10.7 ± 0.1	11.0 ± 0.1	11.0 ± 0.1	9.6 ± 0.1	11.2 ± 0.1	11.2 ± 0.1
316	328	11	7.4 ± 0.1	7.4 ± 0.1	7.4 ± 0.1	7.2 ± 0.2	7.3 ± 0.1	7.3 ± 0.1
317	329	11	6.0 ± 0.1	6.5 ± 0.1	6.5 ± 0.1	5.8 ± 0.7	6.6 ± 0.1	6.6 ± 0.1
320	325	5	1.1 ± 0.1	1.3 ± 0.1	1.3 ± 0.1	0.9 ± 0.1	1.2 ± 0.1	1.2 ± 0.1
322	330	8	4.6 ± 0.1	4.7 ± 0.1	4.8 ± 0.1	4.0 ± 0.1	4.8 ± 0.1	4.8 ± 0.1
325	333	8	4.9 ± 0.1	5.0 ± 0.1	5.0 ± 0.1	4.7 ± 0.2	5.0 ± 0.1	4.9 ± 0.1
339	357	17	10.7 ± 0.1	10.8 ± 0.1	10.8 ± 0.1	10.4 ± 0.1	11.0 ± 0.1	10.9 ± 0.1
343	357	13	9.0 ± 0.1	9.1 ± 0.1	9.0 ± 0.1	8.9 ± 0.1	9.1 ± 0.1	9.2 ± 0.1
357	367	8	5.6 ± 0.1	5.6 ± 0.1	5.6 ± 0.1	5.5 ± 0.1	5.6 ± 0.1	5.6 ± 0.1
358	375	15	9.0 ± 0.1	9.3 ± 0.2	9.2 ± 0.1	8.1 ± 0.1	9.3 ± 0.1	9.3 ± 0.1
360	364	2	0.5 ± 0.1	0.5 ± 0.1	0.5 ± 0.5	0.4 ± 0.1	0.5 ± 0.1	0.5 ± 0.1
367	370	3	2.0 ± 0.1	2.0 ± 0.1	2.0 ± 0.1	1.9 ± 0.1	1.9 ± 0.1	2.0 ± 0.1
368	373	5	2.7 ± 0.1	2.7 ± 0.1	2.7 ± 0.1	2.6 ± 0.1	2.7 ± 0.1	2.7 ± 0.1
368	374	6	3.4 ± 0.1	3.6 ± 0.1	3.7 ± 0.1	2.2 ± 0.1	3.4 ± 0.1	3.6 ± 0.1
368	381	13	7.7 ± 0.1	8.5 ± 0.1	8.7 ± 0.1	5.8 ± 0.1	7.7 ± 0.1	8.3 ± 0.1
372	378	6	2.4 ± 0.1	3.2 ± 0.1	3.3 ± 0.1	1.2 ± 0.1	2.4 ± 0.1	3.0 ± 0.1
372	381	9	4.8 ± 0.1	5.8 ± 0.1	6.2 ± 0.1	3.7 ± 0.1	4.7 ± 0.1	5.5 ± 0.1
376	381	5	2.7 ± 0.1	2.8 ± 0.1	2.9 ± 0.1	2.6 ± 0.1	2.9 ± 0.1	2.9 ± 0.1
376	383	7	3.9 ± 0.1	4.0 ± 0.1	4.1 ± 0.1	3.7 ± 0.1	4.0 ± 0.1	4.0 ± 0.1
376	386	10	6.3 ± 0.1	6.3 ± 0.1	6.5 ± 0.1	6.4 ± 0.1	6.6 ± 0.1	6.6 ± 0.1

Table S4. Strains and plasmids

Strain	Properties	Source
S. meliloti		
Rm2011	Wild type, Str^r	Ref. 78
Rm2011 ΔXVI	Rm2011 containing 16 deletions for GGDEF domain encoding genes	Ref. 37
Rm101	Rm2011 *mucR*::$Spec^r$	Ref. 79
Rm2011 *uxe*	Rm2011 *uxe*::pK19mob2ΩHMB, Km^r	This work
Rm2011 *cuxR*	Rm2011 *cuxR*::pK19mob2ΩHMB, Km^r	This work
Rm101 *uxe*	Rm101 *uxe*::pK19mob2ΩHMB, Km^r	This work
E. coli		
S17-1	*E. coli* 294 Thi RP4-2-Tc::Mu-K_m::Tn7 integrated into the chromosome	Ref. 60
BL21(DE3)	F^- *ompT gal dcm lon hsdS*$_B$($r_B^-m_B^-$) λ(DE3 [*lacI lacUV5-T7 gene 1 ind1 sam7 nin5*]) [*malB*$^+$]$_{K\text{-}12}$(λ^S)	New England Biolabs
Plasmids		
pPHU231-EGFP	Broad–host-range low copy expression vector containing *egfp*, used for generating promoter-EGFP fusions, Tc^r	M. McIntosh
pSRKKm-EGFP	pBBR1MCS-2-derived broad–host-range expression vector containing EGFP, lacZα^+, Km^r	Ref. 37
pSRKGm	pBBR1MCS-2-derived broad–host-range expression vector containing *lac* promoter and *lacI*^{q}, lacZα^+, Gm^r	Ref. 80
pWBT	pSRKGm containing T5 promoter, Gm^r	M. McIntosh
pWH844	Expression vector containing His6-tag sequence and T5 promoter, Amp^r	Ref. 81
pSRKKm-*cuxR*$_{bs}$-EGFP	pSRKKm-EGFP containing *uxs1*$_{166–195}$ promoter fragment	This work
Plasmids for gene mutation		
pK19mob2ΩHMB-*uxe*	pK19mob2ΩHMB carrying internal fragment of *uxe*	Ref. 40
pK19mob2ΩHMB-*SMb20457*	pK19mob2ΩHMB carrying internal fragment of *SMb20457 (cuxR)*	Ref. 40
Overexpression constructs		
pDJS31	pET24b(+) carrying *C. crescentus dgcA* coding sequence, Km^r	Ref. 82
pET28b(+)-TM1788	pET28b(+) carrying *T. maritima TM1788* coding sequence, Km^r	Ref. 66
pWBT-*pleD*	pWBT carrying *pleD* coding sequence	Ref. 37
pWBT-*pleD*$_{GGAAF}$	pWBT carrying *pleD*$_{GGAAF}$ coding sequence	Ref. 37
pWBT-*dgcA*	pWBT carrying *C. crescentus dgcA* coding sequence	Ref. 37
pWBT-*SMc01464*	pWBT carrying *SMc01464* coding sequence	Ref. 37
pSRKGm-*uxs1-SMb20463*	pSRKGm carrying *uxs1-SMb20463* cluster sequence	This work
pWBT-*SMb20457*	pWBT carrying *SMb20457* (*cuxR*) coding sequence	This work
pWBT-*pleD-SMb20457*	pWBT-*pleD* carrying *SMb20457* (*cuxR*) coding sequence	This work
pWBT-*pleD-SMb20457*$_{AxxxA}$	pWBT-*pleD-SMb20457* containing R24A and R28A mutations	This work
pWBT-*pleD-SMb20457*$_{L200E}$	pWBT-*pleD-SMb20457* containing L200E mutation	This work
pWBT-*pleD-SMb20457*$_{N203E}$	pWBT-*pleD-SMb20457* containing N203E mutation	This work
pWBT-*pleD-SMb20457*$_{R222E}$	pWBT-*pleD-SMb20457* containing R222E mutation	This work
pWBT-*pleD-SMb20457*$_{R162A}$	pWBT-*pleD-SMb20457* containing R162A mutation	This work
pWH844-*SMb20457*	pWH844 carrying *SMb20457*(AA$_{2–382}$)	This work
pWH844-*SMb20457*$_{AxxxA}$	pWH844-*SMb20457* containing R24A-R28A mutations	This work
pWH844-*SMb20457*$_{L200E}$	pWH844-*SMb20457* containing L200E mutation	This work
pWH844-*SMb20457*$_{N203E}$	pWH844-*SMb20457* containing N203E mutation	This work
pWH844-*SMb20457*$_{R222E}$	pWH844-*SMb20457* containing R222E mutation	This work
pWH844-*SMb20457*$_{R162A}$	pWH844-*SMb20457* containing R162A mutation	This work
pWH844-*SMb20457*$_{R162E}$	pWH844-*SMb20457* containing R162E mutation	This work
pWH844-*SMb20457*$_{R130E}$	pWH844-*SMb20457* containing R130E mutation	This work
pWH844-*SMb20457*$_{R133E}$	pWH844-*SMb20457* containing R133E mutation	This work
pWH844-*SMb20457*$_{R141E}$	pWH844-*SMb20457* containing R141E mutation	This work
pWH844-*SMb20457*$_{ΔCTH}$	pWH844 carrying *SMb20457*(AA$_{2–360}$)	This work
Promoter-EGFP fusion plasmids		
pPHU-P*uxs1*-EGFP	pPHU231-EGFP containing *uxs1* promoter	This work
pPHU-P*uxs1*$_{m1}$-EGFP	pPHU-P*uxs1*-EGFP with CGGGAT-to-GCCCTA exchange	This work
pPHU-P*uxs1*$_{m2}$-EGFP	pPHU-P*uxs1*-EGFP with CGGG-to-GCCC exchange	This work
pPHU-P*uxs1*$_{m3}$-EGFP	pPHU-P*uxs1*-EGFP with CG-to-GC exchange	This work
pPHU-P*uxs1*$_{m4}$-EGFP	pPHU-P*uxs1*-EGFP with GGAT-to-CCTA exchange	This work
pPHU-P*uxs1*$_{m5}$-EGFP	pPHU-P*uxs1*-EGFP with AT-to-TA exchange	This work
pPHU-P*uxs1*$_{m6}$-EGFP	pPHU-P*uxs1*-EGFP with CAATC-to-GTTAG exchange	This work

Table S5. Oligonucleotides

Primer	Sequence	Purpose
uxs1_Bam*-TIR-RBS-Nde_fwd	ATATGGATCCTGATTAACTTTATAAGGAGGAAAAACATATGAAT-TATTTTAGAAATGACTTCAGGGG	Amplification of *uxs1-SMb20463* for constructing pSRKGm-*uxs1-SMb20463*
smb20463_SpeI_rev	ATATACTAGTTTACTCGACCCGGCCGAG	
smb20457-Hind-Xba_f	ATATAAGCTTATTAAAGAGGAGAAATCTAGAATGACGAAGGACTCCGGATCA	Amplification of *SMb20457 (cuxR)* for constructing pWBT-*pleD-SMb20457*
smb20457-Kpn_r	ATATGGTACCTCATCCTTGAACCGATTTGAGC	
smb20457-24-RxxxR > AxxxA_f	GCCCGTTGGCCGGCCGATCCAACAGCTCGAAAGGAC	Generating $SMb20457_{AxxxA}$
smb20457-24-RxxxR > AxxxA_r	AGCTGTTGGATCGGCCGGCCAACGGGCCCGCTCCATATGAGCGGG	
smb20457_L200E_f	GAGCTCGCCAATTATATCAACGGCA	Generating $SMb20457_{L200E}$
smb20457_L200E_r	TGATATAATTGGCGAGCTCGTCGGCGAGGTTGCCGGAC	
smb20457_N203E_f	GAGTATATCAACGGCATGGAAGAAAAC	Generating $SMb20457_{N203E}$
smb20457_N203E_r	TCCATGCCGTTGATATACTCGGCGAGGAGGTCGGCGAGGTT	
smb20457_R222E_f	GAGATCGTTCGCACGATACGCGA	Generating $SMb20457_{R222E}$
smb20457_R222E_r	GTATCGTGCGAACGATCTCCGGCACTTCTTCCACGGTGAT	
smb20457_R162A_f	GCCATGACGGATGCCGCATCGA	Generating $SMb20457_{R162A}$
smb20457_R162A_r	GATGCGGCATCCGTCATGGCCCCACGATAGGGATAGCCGA	
smb20457_R162E_f	GAGATGACGGATGCCGCATCGA	Generating $SMb20457_{R162E}$
smb20457_R162E_r	GATGCGGCATCCGTCATCTCCCCACGATAGGGATAGCCGA	
smb20457_R130E_f	GAGAGCGGCCGGTCATGGACCGAA	Generating $SMb20457_{R130E}$
smb20457_R130E_r	GGTCCATGACCGGCCGCTCTCAAAGAGGCCGACGTTCCAAT	
smb20457_R133E_f	GAGTCATGGACCGAAGCCGAC	Generating $SMb20457_{R133E}$
smb20457_R133E_r	TCGGCTTCGGTCCATGACTCGCCGCTGCGAAAGAGGCC	
smb20457_R141E_f	GAGGTGACCGAGACGGGGCCG	Generating $SMb20457_{R141E}$
smb20457_R141E_r	GGCCCCGTCTCGGTCACCTCGCGGTCGGCTTCGGTCCAT	
smb20457_-atg_BamHI_fwd	ATATGGATCCACGAAGGACTCCGGATCAG	Amplification of *SMb20457 (cuxR)* for constructing pWH844-*SMb20457*
smb20457_HindIII_rev	ATATAAGCTTTCATCCTTGAACCGATTTGAGC	
smb20457-360-HindIII_rev	ATATAAGCTTTCACGTGGCGAGGCGTTCGGT	Generating $SMb20457_{\Delta CTH}$
Psmb20458_Hind_f	ATATAAGCTTGCAACCCTCCAGCGAAAT	Amplification of P*uxs1* for constructing pPHU-P*uxs1*-EGFP
Psmb20458_XbaI_r	ATATTCTAGAATAATTCACGGAATATTCCTCACAC	
Psmb20458_mut10_j_f	GCCCTAAACAATCGGGATTGGGTGAT	Generating P$uxs1_{m1}$
Psmb20458_mut10_j_r	ACCCAATCCCGATTGTTTAGGGCCCGTGCATTTCTACATATAAAGGGG	
Psmb20458_mut1_j_f	GCCCATAACAATCGGGATTGGGTGA	Generating P$uxs1_{m2}$
Psmb20458_mut1_j_r	CCAATCCCGATTGTTATGGGCCCGTGCATTTCTACATATAAAGGGG	
Psmb20458_mut7_j_f	GCGGATAACAATCGGGATTGGGT	Generating P$uxs1_{m3}$
Psmb20458_mut7_j_r	AATCCCGATTGTTATCCGCCCGTGCATTTCTACATATAAAGGGG	
Psmb20458_mut11_j_f	CCTAAACAATCGGGATTGGGTGAT	Generating P$uxs1_{m4}$
Psmb20458_mut11_j_r	ACCCAATCCCGATTGTTTAGGCGCCGTGCATTTCTACATATAAAG	
Psmb20458_mut12_j_f	TAAACAATCGGGATTGGGTGAT	Generating P$uxs1_{m5}$
Psmb20458_mut12_j_r	ACCCAATCCCGATTGTTTACCCGCCGTGCATTTCTACATATAA	
Psmb20458_mut15_j_f	GTTAGGGGATTGGGTGATAATGACAAT	Generating P$uxs1_{m6}$
Psmb20458_mut15_j_r	CATTATCACCCAATCCCCTAACTTATCCCGCCGTGCATTT	
Psmb20458_oligo1	CTAGCACCCAATCCCGATTGTTATCCCGCCGTGC	Constructing pSRKKm-$cuxR_{bs}$-EGFP
Psmb20458_oligo2	AGCTGCACGGCGGGATAACAATCGGGATTGGGTG	
Psmb20458_-205_Hind_f	ATATAAGCTTATGTAGAAATGCACGGCGGGATAA	Amplification of P*uxs1*-205 for EMSA
Psmb20458_-196_Hind_f	ATATAAGCTTTGCACGGCGGGATAACAAT	Amplification of P*uxs1*-196 for EMSA
Psmb20458_-186_Hind_f	ATATAAGCTTGATAACAATCGGGATTGGGTGA	Amplification of P*uxs1*-186 for EMSA
Psmb20458_mut10_f	ATATAAGCTTATGTAGAAATGCACGGGCCCTAAACAATCGGGATT-GGGTGATAATGACAATCCCCATCC	Amplification of P*uxs1*-205$_{m1}$ for EMSA
Psmb20458_mut1_f	ATATAAGCTTATGTAGAAATGCACGGGCCCATAACAATCGGGATTG-GGTGATAATGACAATCCCCATCC	Amplification of P*uxs1*-205$_{m2}$ for EMSA
Psmb20458_mut7_f	ATATAAGCTTATGTAGAAATGCACGGGCGGATAACAATCGGGATTG-GGTGATAATGACAATCCCCATCC	Amplification of P*uxs1*-205$_{m3}$ for EMSA
Psmb20458_mut11_f	ATATAAGCTTATGTAGAAATGCACGGCGCCTAAACAATCGGGATTG-GGTGATAATGACAATCCCCATCC	Amplification of P*uxs1*-205$_{m4}$ for EMSA
Psmb20458_mut12_f	ATATAAGCTTATGTAGAAATGCACGGCGGGTAAACAATCGGGATTGG-GTGATAATGACAATCCCCATCC	Amplification of P*uxs1*-205$_{m5}$ for EMSA
Psmb20458_mut15_f	ATATAAGCTTATGTAGAAATGCACGGCGGGATAAGTTAGGGGATTGGG-TGATAATGACAATCCCCATCC	Amplification of P*uxs1*-205$_{m6}$ for EMSA
Cy3-egfp-28-rev	TGAACAGCTCCTCGCCCTT	Cy3-labeled *egfp* reverse primer
smb20457_valid	TGTTCGTCGGATCGCTGAGCT	Verification of *SMb20457* mutation
smb20459_valid	CATAGGGGTTGATCGGTGCCT	Verification of *uxe* mutation
PCR1	CGGGCCTCTTCGCTATT	Standard sequencing primer 1
PCR2	TTAGCTCACTCATTAGG	Standard sequencing primer 2
pQE_fwd	CGGATAACAATTTCACACAG	Standard sequencing primer 3

Table S5. Cont.

Primer	Sequence	Purpose
pQE_rev2	CAAGCTAGCTTGGATTCTCACC	Standard sequencing primer 4
egfp_rev	ACTTCAGGGTCAGCTTGCCGTA	Standard sequencing primer 5
ux-cluster_seq1	TCAAGATCGTCCGTATCTTCAAC	Gene cluster sequencing primer 1
ux-cluster_seq2	GCCTATGTTGGCGAATCCGT	Gene cluster sequencing primer 2
ux-cluster_seq3	CGGCTTCTCAATAAAGGAAGTC	Gene cluster sequencing primer 3
ux-cluster_seq4	CGGAACCATTTTCGGTCGTG	Gene cluster sequencing primer 4
ux-cluster_seq5	GAGTTCCAATGGTCGCGTA	Gene cluster sequencing primer 5
ux-cluster_seq6	ACTGCCTGCTTCTGCTGGT	Gene cluster sequencing primer 6
ux-cluster_seq7	TTTCGGCGCTTACGATCCTC	Gene cluster sequencing primer 7
ux-cluster_seq8	CAGGGTTCGATGGTGATCAT	Gene cluster sequencing primer 8

Chapter 8: A dynamic c-di-GMP phosphodiesterase is linked to alpha-rhizobial cell growth and division

Simon Schäper[1,2], Hamish Yau[3], Elizaveta Krol[1,2], Dorota Skotnicka[4], Volkhard Kaever[5], Lotte Søgaard-Andersen[4], Waldemar Vollmer[3], Anke Becker[1,2]

[1]LOEWE Centre for Synthetic Microbiology (SYNMIKRO), Philipps-Universität Marburg, Marburg, Germany; [2]Faculty of Biology, Philipps-Universität Marburg, Marburg, Germany; [3]Centre for Bacterial Cell Biology, Institute for Cell and Molecular Biosciences, University of Newcastle, Newcastle upon Tyne, United Kingdom; [4]Department of Ecophysiology, Max Planck Institute for Terrestrial Microbiology, Marburg, Germany; [5]Research Core Unit Metabolomics, Hannover Medical School, Hannover, Germany

Manuscript in preparation.

Individual contribution:

- Construction of strains and plasmids (except pG18mob2-3xFLAG, pWBT-*gdpM*$_{\Delta LytM}$ and *phoA* fusions)
- Recording of growth curves
- Analysis of promoter-*egfp* activities
- Fluorescence and light microscopy (except GdcP-GdpM co-localization time-lapse)
- HADA staining
- c-di-GMP extractions
- GdcP and GdpM co-immunoprecipitation experiments
- Cell wall leakiness assay
- Generation of cell lysates for muropeptide profiling
- Contributed to protein purifications
- Contributed to transmission electron microscopy
- Contributed to writing of the manuscript

ABSTRACT

Members of the Rhizobiales display zonal growth in contrast to dispersed growth along the sidewalls of many other rod-shaped bacteria. In this work, we identified the thus far uncharacterized seven-transmembrane protein GdcP, which plays a crucial role in polar cell growth and division in *Sinorhizobium meliloti*. GdcP is an essential multidomain protein composed of an extracellular globular 7TMR-DISMED2 domain, a membrane-spanning region, and cytoplasmic PAS, GGDEF and EAL domains. Although being dispensable for the essential function of GdcP, the EAL domain of GdcP confers phosphodiesterase activity towards the second messenger cyclic di-GMP, a key regulatory player in the transition between bacterial lifestyles. The subcellular localization pattern of GdcP to sites of zonal cell wall synthesis and cross-complementation with *gdcP* homologs from related alpha-rhizobial species pointed to a conserved mechanism for cell wall remodeling within the Rhizobiales. This was further supported by GdcP acting in concert with membrane-anchored GdpM, a putative murein metallopeptidase, which was found to be essential for proliferation of *S. meliloti*. Overall, our findings suggest that GdcP and GdpM contribute to cell envelope biogenesis and are components of the machinery driving the cell elongation-division cycle in alpha-rhizobia.

INTRODUCTION

Seven-transmembrane receptors (7TMRs) form the largest, most ubiquitous and most versatile family of membrane receptors. In eukaryotes, they are involved in signaling via interaction with cytoplasmic G-proteins (Pierce *et al.*, 2002). Bacterial rhodopsins, representing light-activated 7TMRs with either signaling or ion-transporting functions (Ernst *et al.*, 2014), are among the best characterized bacterial 7TMR proteins. A distinct class of bacterial 7TMRs was classified as 7TMR-DISMs for 7TMR with diverse intracellular signaling modules (Anantharaman & Aravind, 2003). 7TMR-DISM proteins contain seven transmembrane α-helices (7TMR-DISM_7TM) fused to various cytoplasmic signaling domains as well as N-terminal extracellular globular 7TMR-DISMED1 or 7TMR-DISMED2 domains predicted to bind ligands such as carbohydrates (Anantharaman & Aravind, 2003).

With one to 14 copies per genome, 7TMR-DISMs are widely distributed in both Gram-negative and Gram-positive species (Anantharaman & Aravind, 2003). Currently, more than five thousands of bacterial proteins containing 7TMR-DISM domains are listed in

the InterPro database (www.ebi.ac.uk/interpro/). The most common cytoplasmic signaling domains are GGDEF and/or EAL domains as well as regulatory histidine kinase, REC and PAS domains. GGDEF and EAL domains are involved in synthesis and degradation of bis-(3′,5′)-cyclic dimeric guanosine monophosphate (c-di-GMP). This bacterial second messenger is well-known for its central role in regulation of swimming motility, adherence, biofilm formation and virulence, and in several bacterial species it also promotes cell cycle progression and development (Abel *et al.*, 2013; Römling *et al.*, 2013; Tschowri *et al.*, 2014; Lori *et al.*, 2015; Skotnicka *et al.*, 2016). Histidine kinase and REC domains are involved in phosphorelay, whereas PAS domains are present in many bacterial signal transduction proteins and can directly sense small molecules, ions, gases, light and redox state (Robinson *et al.*, 2000; Henry & Crosson, 2011).

Despite the outstanding number of representatives in different bacterial species, only few 7TMR-DISM proteins were functionally studied. The regulatory output can involve either modulation of enzymatic activity of the cytoplasmic portion or protein-protein interactions. For example, in *Pseudomonas aeruginosa*, 7TMR-DISMED2 domain-coupled histidine kinases RetS and LadS antagonistically regulate sensor histidine kinase GacS, which is central for the regulation of biofilm formation (Davies *et al.*, 2007). Whereas RetS inactivates GacS upon heterodimerization of the cytoplasmic domains, LadS activates GacS by phosphorylation (Chambonnier *et al*., 2016). Also in *P. aeruginosa,* the protein NicD contains a 7TMR-DISMED2 domain in tandem with a cytoplasmic GGDEF domain. Binding of glutamate to the 7TMR-DISMED2 domain of NicD promotes both c-di-GMP synthesis and interactions with other proteins, together triggering biofilm dispersal (Basu Roy & Sauer, 2014).

In the plant-symbiotic alphaproteobacterium *Sinorhizobium meliloti*, the *SMc00074* gene (further referred to as *gdcP* for growth zone dynamic c-di-GMP phosphodiesterase), encoding a protein containing 7TMR-DISMED2, 7TMR-DISM_7TM, PAS, GGDEF and EAL domains, was found to be essential (Cowie *et al.*, 2006; Schäper *et al.*, 2016). Similar to other alphaproteobacteria, *S. meliloti* grows by asymmetrical cell division and elongates the cell wall at the cell pole of the growing daughter cell (Brown *et al.*, 2012). This growth pattern contrasts with dispersed cell elongation, which is characteristic for other Gram-negatives such as the enteric bacterium *Escherichia coli* (Brown *et al.*, 2011). GdcP is the only 7TMR-DISM protein encoded in the *S. meliloti* genome and is most likely to be inactive as diguanylate

cyclase (DGC) since the corresponding active site (A site) is represented by a degenerate GGDQF motif and an enzymatic *in vitro* assay did not reveal DGC activity (Schäper *et al.*, 2016). In contrast, the inhibitory site (I site) motif RxxD and the c-di-GMP phosphodiestherase (PDE) active site EAL are intact. Thus, the protein might be able to bind and to degrade c-di-GMP. In our previous study, we showed that although c-di-GMP at native levels was not required for viability of *S. meliloti*, strong overproduction of c-di-GMP inhibited growth and promoted cell filamentation (Schäper *et al.*, 2016).

In this study, we present evidence for the previously unrecognized 7TMR-DISM protein GdcP and the putative membrane-anchored periplasmic murein metallopeptidase GdpM to play a crucial role in polar cell growth and cell division in *S. meliloti* and related Rhizobiales species. Furthermore, we prove GdcP to act as a c-di-GMP PDE, thus potentially interconnecting c-di-GMP signaling with spatiotemporal control of cell growth and division.

MATERIAL AND METHODS

Bacterial strains and growth conditions. Bacterial strains and plasmids used in this study are shown in Table S1. *S. meliloti* was grown at 30 °C in tryptone-yeast extract (TY) medium (Beringer, 1974), LB medium (Green & Sambrook, 2012), modified MOPS-buffered minimal medium (Zhan *et al.*, 1991), and nutrient-depleted 30 % MM (nitrogen, carbon, and phosphate sources reduced to 30 %). Medium composition is provided in the supplemental material. *Rhizobium etli* was grown in TY medium and *A. tumefaciens* was grown in LB medium at 30 °C. *E. coli* was grown in LB medium at 37 °C. For *S. meliloti*, antibiotics were used at the following concentrations (mg/L; liquid/solid medium): kanamycin, 100/200, gentamicin, 20/40, tetracycline, 5/10, spectinomycin, 200/200 and streptomycin, 600/600. For *E. coli* the following concentrations were used: kanamycin, 50/50, gentamicin, 5/8, tetracyclin, 5/10, spectinomycin 100/100, and ampicillin 100/100. For *A. tumefaciens* kanamycin was used at 100/200 and for *R. etli* at 30/30. Unless otherwise specified, isopropyl β-D-1-thiogalactopyranoside (IPTG) was added at 0.5 mM and taurine at 20 mM. Chlorophenol red-β-D-galactopyranoside (CPRG) was added at 20 µg/mL and 5-bromo-4-chloro-3-indolylphosphate (BCIP) at 50 µg/mL.

Growth assays were performed using 100 µL cultures in flat-bottom 96-well plates (Greiner), grown at 30 ^{o}C with shaking at 1,200 rpm. Three culture replicates were

analyzed per strain. Optical density (OD_{600}) was recorded using Infinite M200 PRO fluorescence reader (Tecan). For growth assays involving protein depletion, cultures with or without IPTG were inoculated with 0.15 µL of stationary TY preculture with IPTG and grown for 24 h. Relative growth was calculated as a ratio of OD_{600} of cultures grown without IPTG and OD_{600} of cultures supplemented with 0.5 mM IPTG. For growth assays, involving taurine- or IPTG-induced gene overexpression, the cultures containing or not containing taurine or IPTG were inoculated with 0.15 µL of stationary TY preculture and the growth was recorded at the indicated time points.

Construction of strains and plasmids. Constructs used in this work were generated using standard cloning techniques and are listed in Table S1. The primers used are listed in Table S2. All constructs were verified by sequencing. Plasmids were transferred to *S. meliloti* by *E. coli* S17-1-mediated conjugation as previously described (Krol & Becker, 2014). Electroporation was used to introduce plasmids to *R. etli* and *A. tumefaciens* following the protocol previously described (Ferri *et al.*, 2010).

To generate chromosomally integrated constructs encoding GdcP or GdpM with C-terminally fused enhanced green fluorescent protein (EGFP) or triple FLAG-tag (3xFLAG), the 700 to 800 bp 3' portion of the gene excluding the stop codon was cloned into suicide plasmids pK18mob2-EGFP or pG18mob2-3xFLAG. Plasmid pG18mob2-3xFLAG was obtained by inserting the 3xFLAG coding sequence including a stop codon into the XbaI and HindIII restriction sites of vector pG18mob2. Integration of these gene fusion constructs into the *S. meliloti* genome generated single-copy gene fusions at the corresponding native chromosomal location.

To construct markerless translational fusions of *gdcP* and *gdpM* to *egfp* or *mCherry* at the native chromosomal location, the 700-800 bp 3' portion of the gene fused to *egfp* or *mCherry* was cloned into suicide plasmid pK18mobsacB (Schäfer *et al.*, 1994) together with 700-800 bp of adjacent downstream genomic region. The resulting constructs were introduced into *S. meliloti* and transconjugants were subjected to sucrose selection to obtain double recombinants that have lost the integrated vector (Schäfer *et al.*, 1994). Correct positions of chromosomally encoded gene fusions were verified by PCR.

To obtain GdcP and GdpM depletion strains, plasmids designed to uncouple the native promoter from the coding sequence and to place the coding sequence under the control of IPTG-inducible promoters were constructed. To this end, a DNA fragment containing the IPTG-inducible T5 promoter and a Shine-Dalgarno sequence followed by the partial 5' *gdcP* coding sequence starting from the start codon (586 bp) was PCR-amplified from

gdcP expression plasmid pWBT-*SMc00074* (Schäper *et al.*, 2016). This fragment was inserted into pK18mob2 (Schäfer *et al.*, 1994) downstream of the IPTG-inducible *lac* promoter, thus generating a *lac*-T5 tandem promoter. In the case of GdpM depletion, the partial 5' *gdpM* coding sequence starting from the start codon (406 bp) was PCR-amplified from *S. meliloti* genomic DNA and inserted into pK18mob2 downstream of the IPTG-inducible *lac* promoter. Integration of these constructs into the genome placed the full-length protein coding sequence under the control of the corresponding IPTG-inducible promoter. Adjacent open reading frames were not affected by integration of these constructs.

Gene overexpression constructs were generated by insertion of the corresponding coding sequences downstream of either the IPTG-inducible *lac* promoter in medium-copy vectors pSRKKm and pSRKGm (Khan *et al.*, 2008), the IPTG-inducible T5 promoter in medium-copy vector pWBT, the taurine-inducible *tauA* promoter in low-copy vector pR-P_{tau}, or a constitutive synthetic promoter in low-copy vector pR_EGFP (Torres-Quesada *et al.*, 2013). In the case of pR_EGFP, a 114 bp region upstream of the *gdcP* coding region was included.

To generate single-copy ectopic *gdcP* or *gdcP-egfp* expression constructs, the 944 bp *gdcP* upstream region with an artificially introduced nonsense mutation at nucleotide position 64 downstream of the start codon of *rimJ* (designated P^*_{gdcP}, Fig. S1) and the *gdcP* or *gdcP-egfp* coding sequence were inserted into single-copy plasmid pABC2S-mob (Döhlemann *et al.*, 2017). For generation of amino acid substitutions or protein variants lacking specific domains splicing by overlap extension PCR was applied.

The *gdcP* promoter-*egfp* fusions were generated by insertion of the upstream non-coding region (either long [944 bp] or short [300 bp]) and the three first codons of *gdcP* into replicative medium-copy number plasmid pSRKKm-EGFP (Schäper *et al.*, 2016). Constructs for purification of His_6-tagged proteins were generated by insertion of the coding sequence excluding the start codon into expression vector pWH844 (Schirmer *et al.*, 1997). Fusions of *gdpM* to *phoA* were assembled from the full-length or partial *gdpM* coding sequence and the *E. coli phoA* coding sequence missing the first 26 codons.

Fluorescence measurements. For promoter-*egfp* activity assays, TY overnight cultures were diluted 1:500 in 100 µl of TY medium or 30 % MM and grown in 96-well plates at 30 °C with shaking at 1,200 rpm. To quantify GdpM-mCherry fluorescence, strains

were grown in 5 mL of TY medium without IPTG for 24 h at 30 °C with shaking at 200 rpm, centrifuged for 3 min at 6,000 rpm, washed with 0.9 % NaCl and adjusted to an OD_{600} of 1. EGFP fluorescence (excitation 488 ± 9 nm; emission 522 ± 20 nm, gain 82), mCherry fluorescence (excitation 552 ± 9 nm; emission 612 ± 20 nm, gain 97) and OD_{600} were determined using the Infinite 200 Pro multimode reader (Tecan) and calculated as relative fluorescence units (RFU), which represent fluorescence values divided by optical density. Background EGFP fluorescence was determined using a control strain harboring pSRKKm-EGFP. Fluorescence of three independent transconjugants was measured as biological replicates.

Fluorescence microscopy. Microscopy of bacteria on 1 % agarose pads was performed using the Nikon microscope Eclipse Ti-E equipped with a differential interference contrast (DIC) CFI Apochromat TIRF oil objective (100x; numerical aperture of 1.49) and a phase-contrast Plan Apo l oil objective (100x; numerical aperture, 1.45) with the AHF HC filter sets F36-513 DAPI (excitation band pass [ex bp] 387/11 nm, beam splitter [bs] 409 nm, and emission [em] bp 447/60 nm), F36-504 Texas Red (ex bp 562/40 nm, bs 593 nm, and em bp 624/40 nm filters) and F36-525 EGFP (ex bp 472/30 nm, bs 495 nm, and em bp 520/35 nm filters). Images were acquired with an Andor iXon3 885 electron-multiplying charge-coupled device (EMCCD) camera. For time-lapse analysis, MM 1 % agarose pads were used, and images were acquired every 2, 15 or 20 min at 30 °C. IPTG was added to the medium at 0.2 mM for microscopy of cells harboring pSRKGm-*parB*-mCherry.

Treatment of *S. meliloti, R. etli* and *A. tumefaciens* cells with fluorescently-labeled D-amino acid HADA was performed as previously described (Kuru *et al.,* 2015). Briefly, cells were grown for 24 h in liquid medium to an OD_{600} of 0.4-0.6. 80 µL of the cultures were then mixed with 0.25 µL 100 mM HADA solution and incubated for 2.5 min (*A. tumefaciens*), 3 min (*S. meliloti*) or 3.5 min (*R. etli*) at 30 ^{o}C with shaking at 800 rpm. After addition of 186 µL 100 % ethanol and incubation for 20 min at RT, cells were washed three times with 0.9 % NaCl and subsequently placed onto 1 % agarose pads.

Transmission electron microscopy. Concentrated cell suspensions were high pressure frozen (HPF Compact 02, Wohlwend, CH) and freeze-substituted (AFS2, Leica, Wetzlar, Germany) in a medium based on acetone, containing 0.25 % osmium tetroxide, 0.2 % uranyl acetate and 5 % ddH_2O according to the following protocol: -90 °C for 20 h, from -90 °C to -60 °C in 1 h, -60 °C for 8 h, -60 °C to -30 °C in 1 h, -30 °C for

8 h, -30 °C to 0 °C in 1 h, 0 °C for 3 h. Still at 0 °C, samples were washed three times with acetone before a 1:1 mixture of Epon 812 substitute resin (Fluka, Buchs, CH) and acetone was applied at room temperature for 2 h. The 1:1 mixture was substituted with pure resin to impregnate the samples overnight. After another substitution with fresh Epon, samples were polymerized at 60 °C for 2 days. The sample containing polymerized Epon blocks were then trimmed with razor blades and cut to 50 nm ultrathin sections using an ultramicrotome (UC7, Leica, Wetzlar, Germany) and a diamond knife (Diatome, Biel, Switzerland). Sections were applied onto 100 mesh copper grids coated with pioloform. For additional contrast, mounted sections were post-stained with 2 % uranyl acetate for 20-30 min and subsequently with lead citrate for another 1-2 min. The sections were finally analyzed and imaged using a JEM-2100 transmission electron microscope (JEOL, Tokyo, Japan) equipped with a 2k x 2k F214 fast-scan CCD camera (TVIPS, Gauting, Germany).

Quantification of intracellular c-di-GMP. Strain Rm2011 GdcP^{dep} ectopically expressing *gdcP* variants from P^*_{gdcP} was grown in triplicates in liquid TY medium without IPTG and harvested in the exponential growth phase 24 h after inoculation. Quantification of intracellular c-di-GMP was performed as previously described (Burhenne & Kaever, 2013). Briefly, cells were collected by centrifugation and nucleotides were extracted three times with acetonitrile/methanol/water (2:2:1), dried and subjected to liquid chromatography-tandem mass spectrometry. c-di-GMP was normalized to total protein, determined using Bradford reagent.

Protein purification. Heterologous protein expression and purification was performed as previously described (Schäper *et al.*, 2016). *E. coli* BL21(DE3) harboring expression plasmids were grown in LB medium to OD_{600} of 0.5-0.6 and protein expression was induced with 0.4 mM IPTG overnight at RT. Cells were lysed using French press (pressure 1,000 lb/in^2) and the lysates were centrifuged for 60 min at 16,000 rpm and 4 ^{o}C. Cleared lysates were applied to His SpinTrap columns (GE Healthcare) following the manufacturer's instructions and eluted with 0.5 M imidazole. Purity of isolated proteins was assessed by SDS-PAGE and Coomassie brilliant blue staining. Protein concentration was determined using Bradford reagent.

Preparation of [α-^{32}P]-labeled c-di-GMP. [α-^{32}P]-labeled c-di-GMP was synthesized using purified *Caulobacter crescentus* His_6-DgcA at 10 µM from GTP and [α-^{32}P]-GTP (0.1 µCi/µL) at 1 mM in the reaction buffer (50 mM Tris-HCl, 300 mM NaCl, 10 mM $MgCl_2$, pH 8.0), overnight at 30°C. The reaction was then treated with 5 units of calf

intestine alkaline phosphatase (Fermentas) for 1 h at 22 °C to hydrolyze unreacted GTP and stopped by incubation for 10 min at 95 °C. The precipitated proteins were removed by centrifugation (10 min, 20,000 x g, 22 °C) and the supernatant was used for the PDE activity and the c-di-GMP binding assays.

***In vitro* DGC and PDE activity assay.** DGC and PDE activities were determined as previously described (Bordeleau *et al.*, 2010; Sultan *et al.*, 2011). Reaction mixtures (40 µL) containing purified proteins at 10 µM, in reaction buffer (50 mM Tris-HCl, 300 mM NaCl, 10 mM $MgCl_2$, pH 8.0) were first pre-incubated for 5 min at 30 °C. DGC reactions were initiated by adding GTP/[α-^{32}P]-GTP (0.1 µCi/µL) to 1 mM, incubated at 30 °C for the indicated periods of time and stopped by adding an equal volume of 0.5 M EDTA. PDE reactions were initiated by adding [α-^{32}P]-labeled c-di-GMP and stopped by adding an equal volume of 0.5 M EDTA after indicated time periods. 2 µL of the PDE or DGC reaction mixtures were spotted on polyethyleneimine-cellulose TLC chromatography plates, developed in 2:3 (v/v) 4 M $(NH_4)_2SO_4$/1.5 M KH_2PO_4 (pH 3.65). Plates were dried prior to exposing a phosphor-imaging screen (Molecular Dynamics). Data were collected and analyzed using a STORM 840 scanner (Amersham Biosciences).

***In vitro* c-di-GMP binding assay.** c-di-GMP binding was determined using a differential radial capillary action of ligand assay (DRaCALA) with [α-^{32}P]-labeled c-di-GMP, as previously described (Roelofs *et al.*, 2011). Reaction mixtures (50 µL) containing [α-^{32}P]-labeled c-di-GMP and 20 µM of indicated protein in the binding buffer (10 mM Tris, 100 mM NaCl, 5 mM $MgCl_2$, pH 8.0) were incubated for 10 min at RT. 10 µL of this reaction mixture was spotted onto nitrocellulose membrane and allowed to dry prior to exposing a phosphor-imaging screen (Molecular Dynamics). Data were collected using a STORM 840 scanner.

Co-immunoprecipitation and protein identification by mass spectrometry. Cultures of Rm2011 GdcP-FLAG, Rm2011 GdpM-FLAG and control strain Rm2011 harboring the empty vector pWBT were grown to an OD_{600} of 0.6 and cross-linked with 0.1 % formaldehyde for 15 min at RT. Reaction was quenched by adding glycine at a final concentration of 0.35 M. Cells were washed, resuspended in lysis buffer (50 mM Tris-HCl, 150 mM NaCl, 1 mM EDTA, 1 % Triton X-100, 2 mM phenylmethylsulfonyl-fluorid, pH 7.4) and lysed using a French press (pressure 1,000 lb/in^2). Cleared lysates obtained after ultracentrifugation (100,000 x g, 1 h, 4 °C) were incubated with anti-FLAG M2 affinity gel (FLAG® Immunoprecipitation Kit, Sigma) overnight at 4 °C on

a rolling shaker. Bound proteins were eluted with 3xFLAG peptide solution.

For mass-spectrometry analysis, proteins were digested by Sequencing Grade Modified Trypsin (Promega) at 37 °C overnight. The mass spectrometric analysis was performed using an Orbitrap Velos Pro mass spectrometer (ThermoScientific). An Ultimate nanoRSLC-HPLC system (Dionex), equipped with a custom 20 cm x 75 µm C18 RP column filled with 1.7 µm beads was connected online to the mass spectrometer through a Proxeon nanospray source. 1-15 µL of the tryptic digest were injected onto a C18 pre-concentration column. Automated trapping and desalting of the sample was performed at a flow rate of 6 µL/min using water/0.05 % formic acid as solvent. Separation of the tryptic peptides was achieved with the following gradient of water/0.05 % formic acid (solvent A) and 80 % acetonitrile/0.045 % formic acid (solvent B) at a flow rate of 300 nL/min: holding 4 % B for 5 min, followed by a linear gradient to 45 % B within 30 min and linear increase to 95 % solvent B in additional 5 min. The column was connected to a stainless steel nanoemitter (Proxeon, Denmark)) and the eluent was sprayed directly towards the heated capillary of the mass spectrometer using a potential of 2,300 V. A survey scan with a resolution of 60,000 within the Orbitrap mass analyzer was combined with at least three data-dependent MS/MS scans with dynamic exclusion for 30 s either using CID with the linear ion-trap or using HCD combined with orbitrap detection at a resolution of 7,500. Data analysis was performed using Proteome Discoverer (ThermoScientific) with SEQUEST and MASCOT (version 2.2; Matrix science) search engines using either SwissProt or NCBI databases.

Muropeptide profiling. *S. meliloti* strains were grown in 400 mL medium for 24 h at 30 °C until OD_{600} reached 0.4-0.8. Cells were harvested by centrifugation, resuspended in PBS buffer, added drop by drop to boiling 8 % SDS solution and stirred for 30 min. *To be completed by HY & WV*

***In vitro* peptidoglycan binding assay.** *To be completed by HY & WV*

***In vitro* peptidoglycan hydrolase activity assay.** *To be completed by HY & WV*

RESULTS

GdcP is required for normal growth and cell morphology.

In our previous study, systematic mutagenesis of c-di-GMP-related genes in *S. meliloti* Rm2011 suggested *gdcP* (*SMc00074*) to be essential (Schäper *et al.*, 2016). As a first step towards functional characterization of this gene, we constructed a GdcP depletion strain. The *gdcP* gene is most likely co-transcribed with the preceding *rimJ* gene,

encoding a probable ribosomal-protein-alanine acetyltransferase (Fig. S1a). To uncouple transcription of *rimJ* and *gdcP*, and to place *gdcP* under the control of an IPTG-inducible promoter, the *lac*-T5 tandem promoter sequence was inserted between *gdcP* and *rimJ* without altering the *rimJ* open reading frame. Conditional GdcP depletion was then achieved by constitutively expressing the *lacI* repressor gene from vector pSRKGm in the strain Rm2011 GdcP^{dep}. Growth of this strain was strongly dependent on the presence of IPTG (Fig. 1a). While cells cultured in presence of IPTG showed wild-type-like growth and morphology, cells depleted for GdcP were inhibited in growth and appeared shorter than non-depleted cells (Fig. 1a). Electron micrographs revealed shorter cells with a wrinkly cell border, implying a loss of cell wall integrity (Figs. 1b & S14a). Moreover, cell wall synthesis appeared to be affected, as labeling of one cell pole and/or the division site with D-amino acid HADA, a marker for active cell wall synthesis (Kuru *et al.*, 2012), was detected for only about half of cells (Fig. 1c). By contrast, cells grown in presence of IPTG showed a characteristic HADA staining pattern at the growing pole as well as the mid-cell region of pre-divisional cells (Fig. 1c). These results suggest that GdcP is involved in cell growth and division by contributing to synthesis of new cell wall material in *S. meliloti*.

GdcP displays cell cycle-dependent dynamic localization.

To monitor the subcellular localization pattern of GdcP, an in-frame fusion of *gdcP* with *egfp* was generated at the native chromosomal location. Microscopy analysis of exponentially growing cultures revealed one GdcP-EGFP focus in every cell, localized either at one cell pole or at the mid-cell region of pre-divisional cells (Fig. 2a). HADA and GdcP-EGFP foci showed co-localization (Fig. 2a). Tracking GdcP-EGFP by time-lapse microscopy revealed a characteristic spatiotemporal subcellular localization pattern of the protein over the cell cycle. The polar fluorescence signal was detected during the entire phase of cell elongation (Fig. 2b). Fluorescence disappeared from the pole and appeared at the mid-cell region of pre-divisional cells shortly before separation of mother and daughter cells. GdcP-EGFP was detected at both newborn poles after completion of cell division. Protein localization studies were also performed in a strain producing ParB-mCherry, which allowed monitoring of chromosomal origins during chromosome partitioning (Frage *et al.*, 2016). While one ParB-mCherry focus stayed at the old pole, the other ParB-mCherry focus moved from the old pole to the opposite pole, which is the new pole of this parental cell and the future old pole of the emerging

daughter cell. GdcP-EGFP was observed to localize to the new pole (Fig. 2b). This evidenced GdcP polar localization to the growing cell pole.

We asked if disappearance of polarly localized GdcP and localization of this protein to the prospective division site occurred by movement of the fluorescent protein focus. Fluorescence microscopy at two-minute intervals of *S. meliloti* strain Rm2011 *gdcP-mCherry pleD-egfp*, carrying a *gdcP-mCherry* and a *pleD-egfp* translational fusion in place of the respective native chromosomal locus, ruled out this possibility. We observed fading of the polar and accumulation of the septal GdcP-mCherry fluorescent signals in pre-divisional cells, while no intermediate fluorescent foci were detected along the cell axis (Fig. 2c). This points either to polar GdcP degradation followed by septal placement of newly synthesized protein or release from the pole and free diffusion of this protein, relocalizing to the prospective division site. Previously, we found that PleD, an ortholog of *C. crescentus* PleD that localizes in its active form to the stalked cell pole where it acts in polar differentiation and stalk biogenesis (Paul *et al.*, 2004), temporarily localizes to the new pole in *S. meliloti* (Schäper *et al.*, 2016). As soon as the PleD-EGFP focus emerged at the growing cell pole, the GdcP-mCherry signal decreased and accumulated at the septum approximately six minutes later.

Essentiality of GdcP resides in its N-terminal part.

To unravel the functional relevance of the different domains of GdcP we characterized strains producing variants of this protein lacking one or more of its domains or carrying mutations in conserved motifs of either the GGDEF or the EAL domain. To this end, *gdcP* variants carried by the single-copy vector pABC2S-mob were ectopically expressed from the native *gdcP* promoter in the GdcP depletion strain Rm2011 GdcP^{dep}. For plasmid constructions we first determined the native *gdcP* promoter and its activity levels. At its native chromosomal locus, *gdcP* is most likely in an operon with *rimJ*. Therefore, a short genomic region upstream of *gdcP* as well as a longer region including the putative *rimJ* promoter and the whole *rimJ* coding sequence were tested for promoter activity using fusions to *egfp* (Fig. S1a). Since higher levels of *egfp* expression were observed in the case of the longer fragment (Fig. S1b), we used this DNA region as native *gdcP* promoter. To exclude possible non-desirable effects of an additional *rimJ* copy, a nonsense mutation was introduced 64 nucleotides downstream of the *rimJ* start codon yielding promoter construct P^*_{gdcP}.

A total of eleven different *gdcP* variants (Fig. 3a), either with or without *egfp* tag, were

generated and placed under the control of P^*_{gdcP} on pABCS2-mob. Furthermore, the *gdcP* variants were inserted into the low-copy vector pR_EGFP downstream of a constitutve synthetic promoter (P_{syn}) to achieve enhanced ectopic expression levels. *S. meliloti* strains were characterized for complementation of the cell growth and morphology defects of the GdcP depletion strain, and for subcellular localization of the GdcP variant-EGFP fusions.

Expressed ectopically from either P^*_{gdcP} or P_{syn} in Rm2011 GdcP^{dep}, *gdcP*$_{Wt}$ and *gdcP*$_{Wt}$-*egfp* fully complemented growth and morphology defects of this strain in medium without IPTG (103-106 % growth relative to cultures grown with IPTG and non-depleted for GdcP, normal cell morphology), in contrast to Rm2011 GdcP^{dep} harboring the empty vectors pABCS2-mob or pR_EGFP (16-19 % growth relative to cultures grown with IPTG and non-depleted for GdcP, altered cell morphology) (Figs. 3b-c & S2). Accordingly, localization of ectopically produced GdcP$_{Wt}$-EGFP was identical to the pattern observed for Rm2011 carrying the *gdcP-egfp* fusion at the native chromosomal location (Figs. 3d & 2). Neither mutations in the conserved motifs of GGDEF (RxxD to AxxA, GGDQF to GAAAF) and EAL (EAL to AAL) domains nor removal of the complete EAL domain of GdcP considerably affected the complementation of growth and morphology defects of Rm2011 GdcP^{dep}, although growth supported by *gdcP*$_{\Delta EAL}$-*egfp* and *gdcP*$_{AxxA}$-*egfp* was slightly reduced (Figs. 3b-c & S2).

The ability of *gdcP* variants to complement GdcP depletion was also tested in c-di-GMP^0 strain Rm2011 ΔXVI (Schäper *et al.*, 2016). In strain Rm2011 ΔXVI GdcP^{dep}, complementation of growth and cell morphology defects by different *gdcP* and *gdcP-egfp* variants was indistinguishable from the complementation phenotypes in Rm2011 GdcP^{dep} (Fig. S2). Taken together, these results suggest that the essential function of GdcP is probably independent of c-di-GMP and other components of c-di-GMP signaling.

Complete removal of GGDEF or both GGDEF and EAL domains from GdcP and GdcP-EGFP negatively affected the complementation of Rm2011 GdcP^{dep} growth and morphology defects when the corresponding gene variants were placed under control of P^*_{gdcP}, whereas P_{syn}-driven ectopical expression of these variants resulted in cell densities similar to the strain complemented with the native *gdcP* (Figs. 3b-c & S2). Although P^*_{gdcP}-driven expression of these variants did not rescue the cell morphology defects, the localization of EGFP-tagged GdcP variants, lacking the GGDEF domain

only or both GGDEF and EAL domains, was similar to the localization of $GdcP_{Wt}$-EGFP (Fig. 3c-d). Spatiotemporal localization of $GdcP_{\Delta EAL\Delta GGDEF}$-EGFP was analyzed by time-lapse microscopy using a strain carrying an in-frame fusion of the corresponding *gdcP* variant to *egfp* in the native chromosomal location. Consistent with the negative effect on culture growth, generation time of these cells doubled as compared to Rm2011 *gdcP-egfp* cells. The protein subcellular localization pattern was unaffected, however the foci showed weaker intensity, indicating reduced protein abundance (Fig. S3). Thus, $GdcP_{\Delta GGDEF}$ and $GdcP_{\Delta EAL\Delta GGDEF}$ are likely to be functional but less stable, as they support normal proliferation if produced at higher levels.

Deletion of the N-terminal domains 7TMR-DISMED2, 7TMR-DISM_7TM or PAS, alone or in combinations, strongly reduced the ability of GdcP to complement GdcP depletion phenotypes, irrespective of the applied expression system (Figs. 3b-c & S2). Cells expressing these *gdcP* variants appeared to be shorter, similar to the empty vector control (Fig. 3c). Furthermore, these GdcP variants, tagged with EGFP, lost the characteristic polar or septal localization (Fig. 3d). In the case of $GdcP_{\Delta 7TMR\text{-}DISMED2}$-EGFP and $GdcP_{\Delta 7TMR\text{-}DISMED2\Delta 7TMR\text{-}DISM\_7TM}$-EGFP, the EGFP signal was almost non-detectable, indicating very low protein abundance.

Taken together, these data indicate that the GdcP N-terminal part is required for protein localization and cell growth, whereas the C-terminal part, containing the GGDEF and EAL domains, is dispensable for the essential function of GdcP.

GdcP is an active c-di-GMP phosphodiesterase.

Although being dispensable for the essential function of GdcP, its GGDEF and EAL domains were analyzed for enzymatic activities and the ability to bind c-di-GMP *in vitro*. Purified His_6-$GdcP_{PAS\text{-}GGDEF\text{-}EAL}$ was able to hydrolyze [α-^{32}P]-c-di-GMP, whereas no cleavage product was detected when PDE active site mutant variant His_6-$GdcP_{PAS\text{-}GGDEF\text{-}EAL}$-AAL was applied to the assay (Fig. 4a). In a DGC activity assay using [α-^{32}P]-GTP as a substrate, His_6-$GdcP_{PAS\text{-}GGDEF\text{-}EAL}$-AAL was unable to synthesize c-di-GMP, in contrast to *C. crescentus* DgcA used as a positive control (Fig. S4a). The ability of GdcP to bind c-di-GMP was analyzed in a differential radial capillary action of ligand assay (DRaCALA). In this assay, the positive control *Myxococcus xanthus* His_6-DmxB produced the characteristic DRaCALA pattern, whereas His_6-$GdcP_{PAS\text{-}GGDEF}$ was not able to prevent the diffusion of [α-^{32}P]-c-di-GMP on the nitrocellulose membrane (Fig. S4b). Thus, GdcP from *S. meliloti* was considered

443 an active c-di-GMP PDE, whereas the GGDEF domain likely possesses neither DGC
444 activity nor the ability to bind c-di-GMP.
445 To evaluate c-di-GMP PDE activity of GdcP *in vivo*, we determined the c-di-GMP
446 content of Rm2011 GdcP^{dep}, complemented with single-copy pABCS2-mob-based
447 constructs expressing *gdcP*$_{Wt}$, *gdcP*$_{AAL}$ and *gdcP*$_{GAAAF}$ from *P*$_{gdcP}$*, grown without
448 IPTG to deplete native GdcP. The c-di-GMP content of cells expressing *gdcP*$_{Wt}$ and
449 *gdcP*$_{GAAAF}$ was similar, whereas expression of PDE active site mutant variant *gdcP*$_{AAL}$
450 resulted in a two-fold increase in c-di-GMP content (Fig. 4b). This provided evidence
451 for GdcP contributing to degrade c-di-GMP *in vivo*. To obtain an additional proof for
452 PDE activity of GdcP *in vivo*, we studied the effects of *gdcP* in a strain overproducing
453 the DGC SMc03178. In our previous study, we showed that IPTG-driven *SMc03178*
454 overexpression from plasmid pWBT resulted in a ~2,500-fold increase in cellular
455 c-di-GMP content, growth inhibition and cell elongation (Schäper *et al.*, 2016). Rm2011
456 *gdcP-egfp*, carrying a construct for taurine-inducible expression of *SMc03178* and
457 grown in presence of taurine, showed cell elongation and branching, while the
458 GdcP-EGFP signal was partially diffuse, although somewhat concentrated at cell poles
459 (Fig. S5). These effects were abolished in a strain overexpressing the GGDEF active
460 site mutant variant *SMc03178*$_{GGAAF}$ (Fig. S5). Rm2011 GdcP^{dep}, harboring pR-P$_{tau}$-
461 *SMc03178* and expressing *gdcP*$_{Wt}$, *gdcP*$_{AAL}$ and *gdcP*$_{GAAAF}$ variants from *P*$_{gdcP}$*, was
462 also inhibited in growth (Fig. S6). Notably, mutation of the EAL active site to AAL in
463 ectopically produced GdcP amplified the negative effect on growth, while mutation of
464 the GGDEF active site to GAAAF did not affect growth compared to wild-type GdcP
465 (Figs. 4c & S6). In addition, plasmids for constitutive expression of these three variants
466 were introduced into Rm2011 harboring pWBT-*SMc03178* and the phenotype of IPTG-
467 induced cultures was analyzed. The negative effect of overexpression of *SMc03178* was
468 partially relieved when *gdcP*$_{Wt}$ was co-overexpressed. Culture growth was partially
469 restored and cell elongation was strongly reduced, compared to the empty vector control
470 (Fig. 4d). This effect probably can be assigned to the enzymatic activity of the EAL
471 domain of GdcP, since co-overexpression of *gdcP*$_{AAL}$ did not alleviate the toxicity of
472 *SMc03178* overexpression (Fig. 4d). In contrast, the GGDEF domain active site mutant
473 GdcP$_{GAAAF}$ behaved identical to wild-type GdcP. Thus, PDE activity of GdcP enabled
474 partial growth rescue and therefore may contribute to controlling intracellular c-di-GMP
475 levels in the wild-type strain.
476

GdcP interacts with periplasmic putative metallopeptidase GdpM.

Proteins which are part of the cell division machinery occur in multi-protein complexes and protein-protein interactions are often required for their proper function (Goehring & Beckwith, 2005; Alexeeva *et al.*, 2010; Egan & Vollmer 2013). In order to find potential protein interaction partners of GdcP, we generated an in-frame fusion of *gdcP* to *3xflag* at the native chromosomal location and subjected the resulting strain to co-immunoprecipitation. This identified 27 candidates as potential interaction partners of GdcP (Table S3). Among these candidates, the hypothetical transmembrane protein SMc02432 (renamed growth zone dynamic putative metallopeptidase, GdpM) was considered promising since it was highly abundant and identified with most unique peptides. Co-immunoprecipitation using C-terminally 3xFLAG-tagged GdpM resulted in identification of GdcP, further suggesting direct interaction between both proteins (Table S4). Comparative sequence analysis revealed that both GdcP and GdpM are largely restricted to the Rhizobiales and three unrelated species from the Gammaproteobacteria and Actinobacteria (Fig. S7a). GdpM contains a C-terminal domain that is characteristic for members of the family of M23 zinc-dependent metallopeptidases (pfam01551). This domain is predicted to have hydrolytic activity with a range of specificities. Closer inspection of the C-terminal domain of GdpM (further referred to as LytM domain) revealed a conserved HxxxD motif (Fig. S7c), which is known to be required for zinc ion coordination and hydrolysis of glycine-glycine bonds by *Staphylococcus aureus* LytM (Odintsov *et al.*, 2004; Firczuk *et al.*, 2005; Spencer *et al.*, 2010). Analysis of the GdpM N-terminal portion did not yield any homology to proteins with known functions. However, the combined transmembrane topology and signal peptide prediction online tool PHOBIUS (Käll *et al.*, 2004) predicted a small region with high hydrophobicity forming a single transmembrane α-helix (AA_{32-57}) as well as localization of the C-terminus to the periplasmic space.

Periplasmic localization of GdpM was experimentally verified using protein fusions to the *E. coli* alkaline phosphatase PhoA missing its signal peptide. Since the PhoA enzymatic activity is restricted to the periplasmic space, it can be used to indicate proteins located in the periplasm. Production of either full length GdpM or the N-terminal portion $GdpM_{1-66}$ fused to $PhoA_{27-471}$ in both *S. meliloti* Rm2011 or *E. coli* S17-1 resulted in blue staining of agar cultures on medium containing PhoA substrate 5-Brom-4-chlor-3-indolylphosphate (BCIP) (Fig. S8). In contrast, fusion $GdpM_{60-646}$-$PhoA_{27-471}$, missing the predicted transmembrane α-helix of GdpM, did not

mediate blue staining. Thus, the C-terminal portion of GdpM following the N-terminal transmembrane α-helix localized to the periplasm in both *S. meliloti* and *E. coli*.

gdpM is essential in _S. meliloti_.

To study GdpM-dependent phenotypes, we aimed at construction of a *gdpM* knockout mutant. However, the attempts to generate this mutant failed, which suggests *gdpM* to be essential. Therefore, a GdpM depletion strain Rm2011 GdpM^{dep} was constructed. In this strain, the chromosomal *gdpM* was placed under the control of the IPTG-inducible *lac* promoter, whereas the *lacI* repressor gene was constitutively expressed from the vector pSRKGm. This strain was strongly impaired in growth in the absence of IPTG (Fig. 5a), which further supported essentiality of *gdpM*. Strikingly similar to cells depleted for GdcP, GdpM-depleted cells were shorter than non-depleted cells (Figs. 5a & 1a). Electron micrographs obtained for GdpM-depleted cells revealed regions of low electron density within the cells that might represent polyhydroxybutyrate (PHB) granules as part of a general stress response (Figs. 5b & S14b). Moreover, pulse-labeling of GdpM-depleted cells with HADA revealed a fluorescence focus at the prospective division site in only a minority of pre-divisional cells, whereas Rm2011 GdpM^{dep} grown in IPTG-containing medium displayed a wild-type like HADA staining pattern (Fig. 5c). These phenotypic similarities strengthened the hypothesis on a functional relation between GdpM and GdcP.

GdcP and GdpM temporarily co-localize during cell cycle.

To study the subcellular localization pattern of GdpM, we constructed a *gdpM-mCherry* fusion at the native chromosomal location of Rm2011. Microscopy of the resulting strain revealed predominantly diffuse fluorescence, whereas in some cells GdpM-mCherry localized at one pole and the mid-cell region of pre-divisional cells. Using time-lapse microscopy, we observed a dynamic GdpM-mCherry localization during cell cycle, reminiscent of the GdcP-EGFP pattern (Figs. S9a & 2b). Partial co-localization of both proteins over the cell cycle was detected using Rm2011 carrying both *gdcP-egfp* and *gdpM-mCherry* fusions at their native chromosomal locations (Fig. S9b). Foci formed by both protein fusions at the pole and the prospective division site overlapped with HADA-derived fluorescence signals (Fig. S9c). Strikingly, heterologous expression of *gdpM-mCherry* in *E. coli* S17-1 revealed GdpM-mCherry localization to

the cell poles and partly to the mid-cell region of pre-divisional cells (Fig. S9d). The cell cycle-dependent localization of GdcP and GdpM in *S. meliloti* again pointed to a functional relation between both proteins.

We also studied the co-localization of GdcP-EGFP and GdpM-mCherry in strains depleted for one of both protein fusions. Depletion of GdpM-mCherry in Rm2011 *gdcP-egfp* GdpM-mCherry^{dep} resulted in dispersed localization of GdcP-EGFP (Fig. S10a). Depletion of GdcP-EGFP in Rm2011 GdcP-EGFP^{dep} *gdpM-mCherry* resulted in increased GdpM-mCherry signals compared to Rm2011 *gdcP-egfp gdpM-mCherry* (Fig. S10a). Under depletion conditions, Rm2011 GdcP-EGFP^{dep} *gdpM-mCherry*, harboring the empty vector control of a complementing plasmid, showed three-fold higher GdpM-mCherry signal levels than the corresponding strain complemented with plasmid-borne $gdcP_{Wt}$ (Fig. S10b). Complementation of this strain with $gdcP_{AAL}$ reduced GdpM-mCherry signal levels to a similar extend, whereas complementation with the *gdcP* variants $gdcP_{\Delta GGDEF\Delta EAL}$ or $gdcP_{\Delta PAS}$ did not reduce the GdpM-mCherry signal to wild-type levels (Fig. S10b). These data suggest that GdcP may require the interaction partner GdpM for the polar localization. GdpM abundance may be affected by GdcP, while absence of GdcP may result in overproduction of GdpM.

Overexpression of *gdpM* compromises cell envelope integrity.

As a first step towards functional characterization of GdpM, we analyzed effects of *gdpM* overexpression. In TY medium, GdpM-overproducing Rm2011 showed wild-type like growth, whereas in LB medium, growth was severely impaired and cells appeared enlarged and spheric compared to the empty vector control (Fig. 6a). Electron microscopy of GdpM-overproducing cells revealed an enlarged periplasm and severe inner membrane invagination (Figs. 6b & S14c). HADA incorporation by Rm2011 overexpressing *gdpM* and grown in LB medium was strongly impaired, as only weak and dispersed fluorescence signals could be detected compared to Rm2011 harboring the empty vector control (Fig. 6c). Since decreased medium osmolarity can destabilize cells compromised in their envelope integrity (Rodríguez-Herva *et al.*, 1996; Palomino *et al.*, 2009), we hypothesized that *gdpM* overexpression may affect the cell envelope. In agreement with this assumption, increasing the NaCl concentration to 300 mM mitigated the *gdpM* overexpression-associated changes in morphology and growth, whereas addition of either $CaCl_2$ or $MgCl_2$ resulted in wild-type-like growth of GdpM-

overproducing agar cultures (Fig. S11).

To examine the role of the C-terminal LytM domain of GdpM, we generated GdpM variants containing either a single amino acid exchange in the putative zinc ion coordination motif HxxxD ($GdpM_{H510A}$) or a deletion of the complete LytM domain ($GdpM_{\Delta LytM}$). $GdpM_{H510A}$-overproducing cells were inhibited in growth when cultured in either TY or LB medium and showed similar morphologic changes as GdpM-depleted cells, indicating the exchange of H510 to alanine rendered the protein a dominant negative mutant (Fig. S12). In the case of $gdpM_{\Delta LytM}$, overexpression resulted in growth defects of cells cultured in LB medium, while cell enlargement was mitigated compared to $gdpM_{Wt}$-overexpressing cells (Fig. S12).

To obtain hints towards a putative GdpM metallopeptidase activity conferred by the LytM domain, wild-type *gdpM* and mutant variants were heterologously expressed in *E. coli.* Leakage of cytoplasmic proteins due to compromised cell envelope and cell lysis was detected as by Paradis-Bleau *et al.* (2014). Leakage of cytoplasmic β-galactosidase is detected by hydrolysis of the poorly membrane-permeable β-galactosidase substrate chlorophenol red-β-D-galactopyranoside (CPRG) resulting in a purple staining of the agar cultures. *E. coli* S17-1 overexpressing $gdpM_{Wt}$ showed pronounced staining compared to the empty vector control upon growth on CPRG-supplemented LB agar lacking NaCl (Fig. 6d). This result suggests destabilization of the *E. coli* cell envelope or increased cell lysis upon $gdpM_{Wt}$ overexpression. In line with this, *E. coli* S17-1 overexpressing $gdpM_{Wt}$ was affected in growth and pronounced cell lysis was observed in LB medium lacking NaCl (Fig. S13). By contrast, *E. coli* S17-1 overexpressing $gdpM_{H510A}$ and $gdpM_{\Delta LytM}$ showed a negative CPRG phenotype and no cell lysis, although $gdpM_{H510A}$ overexpression still inhibited *E. coli* growth (Figs. 6d & S13). Taken together, these results would be in agreement with a metallopeptidase activity of the LytM domain of GdpM targeting cell wall components *in vivo*.

GdcP and GdpM are important for cell wall integrity.

To test whether GdcP and GdpM are involved in cell envelope biogenesis, we profiled muropetides of *S. melioti* Rm2011 depleted for GdcP and GdpM. Muropeptide profiles of Rm2011 $GdcP^{dep}$ and Rm2011 $GdpM^{dep}$ grown in TY medium supplemented with IPTG were similar to those obtained for the Rm2011 wild-type (Fig. 7a). GdcP- and GdpM-depleted cells grown in absence of IPTG showed changes in relative abundances

of specific muropeptides, as in both strains penta peptides accumulated, whereas tetra-tetra and tetra-tetra-tetra peptides were less abundant compared to non-depleted cells (Fig. 7a). We also determined muropeptides in Rm2011 overexpressing $gdpM_{Wt}$ and $gdpM_{H510A}$. GdpM-overproducing cells accumulated penta and tetra-penta peptides compared to cells harboring the empty vector control, while overproduction of $GdpM_{H510A}$ showed similar but weaker changes in the muropeptide profiles (Fig. S15). The accumulation of penta peptides upon either depletion or overproduction of GdcP and GdpM point to impaired incorporation of new material into the growing sacculus and might involve indirect effects.

To gain further mechanistic insights in GdcP and GdpM functions in *S. meliloti*, purified His_6-tagged variants of both proteins were assayed for binding and hydrolysis of peptidoglycan (PG). His_6-$GdpM_{\Delta tm}$ was mixed with *S. meliloti* murein sacculi and sedimented by ultracentrifugation. The protein was exclusively recovered in the pellet fraction, whereas it remained in the supernatant without the addition of sacculi (Fig. 7b). By contrast, His_6-$GdcP_{7TMR\text{-}DISMED2}$ showed only small binding capacity in the same conditions, as in presence of sacculi the vast majority of protein remained in the supernatant (Fig. 7b). PG hydrolase activity of His_6-$GdpM_{\Delta tm}$ was assayed by incubation of the protein with various *S. meliloti* murein substrates followed by muropeptide profiling. Presence of His_6-$GdpM_{\Delta tm}$ did not cause evident changes in the muropeptide profiles, which remained also unchanged when His_6-$GdcP_{7TMR\text{-}DISMED2}$ was added to the reaction (Fig. 7b). Taken together, these results indicate GdpM to be a potent PG-binding protein, whereas hydrolytic activity towards PG was non-detectable *in vitro*. However, it can not be excluded that assay conditions were suboptimal or that an additional factor is required for stimulation of GdpM activity. The latter has been described for *S. aureus* LytM, whose activity is stimulated by proteolytic cleavage (Odintsov *et al.*, 2004; Firczuk *et al.*, 2005).

GdcP and GdpM functions are conserved in alpha-rhizobial species.

Comparative sequence analysis revealed conservation of GdcP and GdpM within the order Rhizobiales (Fig. S7). To test for functional conservation of GdcP among alpha-rhizobial species, we analyzed the subcellular localization pattern of *R. etli* and *A. tumefaciens* homologs RHE_CH00976 ($GdcP_{Re}$) and Atu0784 ($GdcP_{At}$) by generating in-frame fusions of the corresponding genes with *egfp* at their native chromosomal locations. Localization to one cell pole and the mid-cell region of

pre-divisional cells, similar to the subcellular localization pattern of *S. meliloti* GdcP-EGFP, was detected in the respective hosts (Fig. 8a). Pulse-labeling of these strains with HADA showed active cell wall synthesis at the sites where GdcP-EGFP foci were observed (Fig. 8a).

We also tested the ability of *A. tumefaciens* and *R. etli* GdcP and GdpM homologs to complement *S. meliloti* GdcP and GdpM depletion strains, respectively. For this purpose, *gdcP* and *gdpM* from *S. meliloti*, *R. etli* and *A. tumefaciens* were placed under the control of a taurine-inducible promoter on the low-copy plasmid pR-P_{tau} and introduced into the *S. meliloti* depletion strains. In strains grown in presence of taurine, *R. etli* and *A. tumefaciens* GdcP and GdpM fully complemented the growth and morphology defects of the respective *S. meliloti* depletion strains, similar to the *S. meliloti* homologs (Fig. 8b-c). In the absence of taurine, $gdpM_{At}$ did not efficiently reconstitute growth of Rm2011 $GdpM^{dep}$, suggesting partial functionality of $GdpM_{At}$ in *S. meliloti.*

Collectively, the similar subcellular localization pattern of GdcP homologs in *S. meliloti*, *R. etli* and *A. tumefaciens* as well as cross-complementation of *gdcP* and *gdpM* between these species provide evidence for functional conservation of both proteins in the Rhizobiales.

DISCUSSION

Bacteria which grow and divide face the challenge of maintaining their cell shape and passing it on to their progeny. Remodeling of the mesh-like PG sacculus is essential for this dynamic process. Insertion of new material into the growing sacculus and hydrolysis of old material have to be tightly coordinated in space and time to allow for safe growth and propagation. This requires robust mechanisms spatiotemporally controlling enzymatic activities of extracellular PG synthases and hydrolases, which are incorporated into large multi-enzyme complexes (Typas *et al.*, 2012). The molecular basis of these mechanisms is largely unknown and only few factors regulating these enzymes have been unraveled. In this study, we provide evidence for GdcP as the first member of the seven-transmembrane receptor family 7TMR-DISM to be required for proliferation of alpha-rhizobial species. GdcP dynamically localizes to sites of zonal cell wall synthesis and acts in concert with the putative metallopeptidase GdpM, suggesting a role of GdcP in cell growth and division.

GdcP primary function

The subcellular localization pattern of GdcP to sites of zonal cell wall synthesis was shown to be a common feature among the studied alpha-rhizobial species. Members of the order Rhizobiales, including *S. meliloti*, display growth at one cell pole as well as at the mid-cell region of pre-divisional cells (Brown *et al.*, 2012). In *A. tumefaciens*, the two division proteins FtsA and FtsZ likely contribute to polar growth by associating with the elongating cell pole and the septal site in pre-divisional cells (Zupan *et al.*, 2013; Cameron *et al.*, 2014). PG-synthesizing PBP1a as well as a Rhizobiales- and Rhodobacterales-specific L,D-transpeptidase, both contributing to zonal cell wall synthesis, also localize to the growing cell pole and pre-divisional site (Cameron *et al.*, 2014). The localization pattern of GdcP in *S. meliloti* and that of proteins associated with PG synthesis in *A. tumefaciens* is strikingly similar. This similarity suggests that the function of GdcP may be related to synthesis of new cell wall material during cell growth and division. A function of GdcP related to cell envelope biogenesis may also account for the inherence of its essentiality in the N-terminal part including periplasmic 7TMR-DISMED2 and cytoplasmic PAS domains.

Coordinating the PG synthesis machinery and directing it to sites of zonal cell wall synthesis is a prerequisite for maintaining cell shape after completion of cell division. Cell wall remodeling was studied mostly in rod-shaped *E. coli, C. crescentus* and *Bacillus subtilis,* all utilizing a laterally dispersed mode of PG synthesis (Brown *et al.*, 2011). In these organisms, the PG synthesis machinery associates with the cytoplasmic scaffold proteins MreB (elongasome) and FtsZ (divisome), both directing placement and activity of PG synthases from inside the cell. Members of the Rhizobiales lack the lateral PG synthesis scaffold MreB and other related proteins (Margolin *et al.*, 2009), suggesting the presence of alternative factors coordinating PG synthesis and hydrolysis during cell growth and division.

PG synthesis and hydrolysis were proposed to spatially and temporarily correlate in *E. coli* cells (Höltje, 1998; Egan & Vollmer, 2015). Cell wall hydrolases are involved in murein growth, maturation, turnover, recycling, and cleavage of the septum at cell division, while uncontrolled activities can cause cell lysis (Lee & Huang, 2013). These enzymes have various cleavage specificities and often require a PG-binding domain for activity (Buist *et al.*, 2008). Periplasmic interaction between GdcP and murein-binding putative metallopeptidase GdpM may provide a mechanism to control incorporation of new material into the growing sacculus of alpha-rhizobial cells. Identification of an

essential putative PG-hydrolyzing protein in *S. meliloti* was somewhat surprising considering the complexity of PG hydrolases described for other bacteria. For instance, bioinformatics search in closely related *A. tumefaciens* revealed eight genes encoding putative PG hydrolases, and the *E. coli* genome encodes as many as twelve known PG hydrolases with a periplasmic location (Vollmer & Bertsche, 2008; Cameron *et al.*, 2014). It is often difficult to assign a distinct function to a PG hydrolase or identify associated regulatory factors due to redundancies and multiple functions (Vollmer *et al.*, 2008; Lee & Huang, 2013). Nevertheless, several endopeptidases were described to play important roles in cell morphology and division. In *E. coli*, enzymatically inactive NlpD and EnvC are recruited to the septal site where they mediate cell wall hydrolysis by stimulating amidase activities (Uehara *et al.*, 2009, 2010). The three endopeptidases Spr, YdhO and YebA, which are redundantly essential, were shown to be required for incorporation of new murein during sacculus enlargement (Singh *et al.*, 2012). In *C. crescentus*, murein-binding endopeptidase DipM functions in PG remodeling upon cell division by localization to the site of constriction, which is dependent on the essential murein-binding protein FtsN (Möll *et al.*, 2010). Genomes of bacteria from the order Rhizobiales do not encode FtsN suggesting alternative mechanisms for directing PG remodeling enzymes to the septum. In the case of *S. meliloti*, GdcP may be a functional homolog of FtsN and regulate GdpM activity at sites of zonal cell wall synthesis.

Artificially increased GdpM levels caused severe morphological changes in *S. meliloti*, as cells were enlarged, coccoid and displayed invaginations of the inner membrane. Cell wall perturbations upon dysregulation of PG-modifying and -binding proteins are known to result in altered cell shapes. Control of PG hydrolase abundance has been described for functional endopeptidase MepS from *E. coli*, which is proteolytically degraded (Singh *et al.*, 2015). In spiral-shaped *Helicobacter pylori*, altered levels of PG hydrolase HdpA result in stocky, branched and cocci-shaped cells (Bonis *et al.*, 2010). Deletion of PG-binding protein CsiV, modulating PG biogenesis in *Vibrio cholerae*, results in a loss of rod shape (Dörr *et al.*, 2014). In *S. meliloti*, morphology defects of cells accumulating GdpM were partially rescued under high osmolarity conditions, further indicating dysregulation of PG biogenesis and cell wall integrity to be affected at elevated GdpM levels.

The mechanistic consequences and direction of signaling mediated by GdcP and GdpM interaction remain to be investigated in more detail. GdcP-GdpM interaction may

modulate perception of environmental stimuli by GdcP receptor domains or promote interactions with other proteins, catalytic activity and ligand binding of the intracellular signaling module. Alternatively, perception of signals from the cytoplasm might modulate accessibility of the interaction interface in GdcP receptor domains for either GdpM or ligands such as murein derivatives. Conservation of GdcP and GdpM in the order Rhizobiales suggests a common mechanism for cell envelope biogenesis in these organisms. The importance of the PG layer in these organisms has recently been demonstrated, as it has an essential role in differentiation during symbiosis (Gully *et al.*, 2016). GdcP and GdpM contribution to the interaction of alpha-rhizobial species with their leguminous plant hosts remains to be investigated.

GdcP accessory function

The relevance of GdcP to cell envelope biogenesis in combination with its ability to degrade c-di-GMP potentially implies a direct connection between cell wall remodeling and intracellular c-di-GMP signaling. In line with this, recent studies have described a link between c-di-GMP signaling and cell growth and division. In polarly growing *Mycobacterium smegmatis*, a strain lacking dually active DGC/PDE DcpA displayed cell elongation and multi-septation, presumably as a result of transcriptional upregulation of genes with functions related to cell wall processes. This suggested a role of c-di-GMP signaling in cell division and morphology (Gupta *et al.*, 2016). A link between PG remodeling and c-di-GMP signaling was also demonstrated for the cell division-related DGC YfiN from *E. coli*. Under envelope stress conditions, YifN binds to the cytoplasmic scaffold proteins FtsZ and ZipA likely in a c-di-GMP-bound state. This results in recruitment of the protein to the prospective division site and subsequent inhibition of septal PG synthesis (Kim & Harshey 2016). Inactivation of the EAL domain of GdcP from *S. meliloti* neither altered growth and cell morphology nor GdcP localization, indicating its PDE activity not to be important for its primary function. However, GdcP PDE activity counteracted artificially increased c-di-GMP levels by reducing the concomitant cell damage.

Polar and septal placement of c-di-GMP PDEs has previously been shown to serve as a mechanism for restricting signaling events to specific sites of *C. crescentus* cells. PdeA transiently localizes to the stalked cell pole and determines the swarmer cell-specific program (Abel *et al.*, 2011). Flagellum biogenesis at the swarmer cell pole requires dynamically localizing TipF, whose localization to the division plane is dependent on

cytokinesis (Huitema *et al.*, 2006). PDE activity of GdcP in *S. meliloti* may provide a mechanism for decreasing c-di-GMP levels to initiate downstream signaling events at either the growing cell pole or the mid-cell region of pre-divisional cells. Identification of c-di-GMP effectors and their target genes influenced by GdcP PDE activity would allow a better understanding of the c-di-GMP-related function of GdcP.

Deletion of the GGDEF domain of GdcP resulted in a reduced growth rate, although neither catalytic activity nor c-di-GMP binding could be demonstrated. Comparative sequence analysis revealed protein sequences homologous to *S. meliloti* GdcP and containing an intact A site in the GGDEF domain as in the case of *A. tumefaciens* GdcP, whose EAL domain also contains all conserved motifs indicating PDE activity (Fig. S7b). However, the functional consequences of a DGC activity in addition to the PDE activity of GdcP remain unclear, also because $gdcP_{Sm}$ and $gdcP_{At}$ complemented the phenotypes of GdcP-depleted Rm2011 in a similar manner (Fig. 8b-c). Our results suggest that the C-terminal part containing the GGDEF and EAL domains is dispensable for the essential function of GdcP. The GdcP GGDEF domain may modulate PDE activity of the covalently linked EAL domain. Such an example was described for PAS-GGDEF-EAL domain protein PdeA from *C. crescentus*, which contains a degenerate A site (GEDEF) and possesses no DGC activity, while the GGDEF domain is able to bind GTP and thus to regulate the PDE activity of the covalently linked EAL domain (Christen *et al.*, 2005). Moreover, PDE activities of BifA and RmcA from *P. aeruginosa* were shown to be stimulated depending on the A sites of the covalently linked GGDEF domains (Kuchma *et al.*, 2007; Okegbe *et al.*, 2017). Similar to GdcP from *S. meliloti*, DGC activity of BifA containing a GGDEF domain with a GGDQF motif was not detectable (Kuchma *et al.*, 2007).

GdcP PDE activity may also be modulated by the cytoplasmic PAS domain, which generally regulates the activities of covalently attached effector domains (Möglich *et al.*, 2009). Such a mechanism was identified for DosP from *E. coli*, as O_2-binding to a heme cofactor in the PAS domain results in increased PDE activity of the protein (Tanaka *et al.*, 2007). In *Acetobacter xylinum*, AxDGC2 regulates cellular c-di-GMP levels depending on the redox state of a flavin cofactor in the PAS domain, while the oxidized state promotes DGC activity (Qi *et al.*, 2009). The FAD-binding PAS domain of dual-function enzyme RmcA from *P. aeruginosa* supposedly influences the stimulating effect that the GGDEF domain has on the covalently linked EAL domain (Okegbe *et al.*, 2017). For the PAS domain of GdcP a putative heme pocket has been

817 predicted suggesting the protein might be able to sense redox states. A link between
818 redox signaling and cell envelope biogenesis has been reported for
819 gammaproteobacterial species, as the YfiBNR signal transduction system provides a
820 mechanism for inhibiting septal PG synthesis. Under reducing and envelope stress
821 conditions, redox sensor YfiR is released from the periplasmic PAS domain of the
822 membrane-standing DGC YfiN, which acts as a cell division inhibitor (Malone *et al.*,
823 2012; Kim & Harshey, 2016). Ligands that bind to the PAS domain of GdcP and their
824 possible contribution to the cell cycle-dependent localization of the protein remain thus
825 far unknown.
826

827 **ACKNOWLEDGEMENTS**

828 We thank Dr. Uwe Linne for support of MS-based protein identification; Prof.
829 Dr. Martin Thanbichler and Prof. Dr. Ulrich Koert for sharing HADA; Dr. Thomas
830 Heimerl for supporting assistance with transmission electron microscopy; Annette
831 Garbe for technical assistance with LC-MS/MS measurements; and Dr. Matthew
832 McIntosh and Dr. Marta Robledo for sharing plasmids pWBT and pR-P_{tau}, respectively.
833 We acknowledge financial support from the German Research Foundation
834 (Collaborative Research Centre 987), the LOEWE program of the State of Hesse
835 (Germany), and the Max Planck Society. *To be completed by HY and WV*
836

837 **REFERENCES**

838 1. Abel S, Bucher T, Nicollier M, Hug I, Kaever V, Abel Zur Wiesch P, Jenal U.
839 2013. Bi-modal distribution of the second messenger c-di-GMP controls cell fate
840 and asymmetry during the *Caulobacter* cell cycle. PLoS Genet 9:e1003744.
841 2. Abel S, Chien P, Wassmann P, Schirmer T, Kaever V, Laub MT, Baker TA, Jenal
842 U. 2011. Regulatory cohesion of cell cycle and cell differentiation through
843 interlinked phosphorylation and second messenger networks. Mol Cell 43:550-60.
844 3. Alexeeva S, Gadella TW, Verheul J, Verhoeven GS, den Blaauwen T. 2010. Direct
845 interactions of early and late assembling division proteins in *Escherichia coli* cells
846 resolved by FRET. Mol Microbiol 77:384-98.
847 4. Anantharaman V, Aravind L. 2003. Application of comparative genomics in the
848 identification and analysis of novel families of membrane-associated receptors in
849 bacteria. BMC Genomics 4:34.
850 5. Basu Roy A, Sauer K. 2014. Diguanylate cyclase NicD-based signalling
851 mechanism of nutrient-induced dispersion by *Pseudomonas aeruginosa*. Mol
852 Microbiol 94:771-93.
853 6. Beringer JE. 1974. R factor transfer in *Rhizobium leguminosarum*. J Gen Microbiol
854 84:188-98.
855 7. Bonis M, Ecobichon C, Guadagnini S, Prévost MC, Boneca IG. 2010. A M23B
856 family metallopeptidase of *Helicobacter pylori* required for cell shape, pole
857 formation and virulence. Mol Microbiol 78:809-19.

8. Bordeleau E, Brouillette E, Robichaud N, Burrus V. 2010. Beyond antibiotic resistance: integrating conjugative elements of the SXT/R391 family that encode novel diguanylate cyclases participate to c-di-GMP signalling in *Vibrio cholerae*. Environ Microbiol 12:510-23.
9. Brown PJ, de Pedro MA, Kysela DT, Van der Henst C, Kim J, De Bolle X, Fuqua C, Brun YV. 2012. Polar growth in the alphaproteobacterial order Rhizobiales. Proc Natl Acad Sci U S A 109:1697-701.
10. Brown PJ, Kysela DT, Brun YV. 2011. Polarity and the diversity of growth mechanisms in bacteria. Semin Cell Dev Biol 22:790-8.
11. Buist G, Steen A, Kok J, Kuipers OP. 2008. LysM, a widely distributed protein motif for binding to (peptido)glycans. Mol Microbiol 68:838-47.
12. Burhenne H, Kaever V. 2013. Quantification of cyclic dinucleotides by reversed-phase LC-MS/MS. Methods Mol Biol 1016:27-37.
13. Cameron TA, Anderson-Furgeson J, Zupan JR, Zik JJ, Zambryski PC. 2014. Peptidoglycan synthesis machinery in *Agrobacterium tumefaciens* during unipolar growth and cell division. MBio 5:e01219-14.
14. Chambonnier G, Roux L, Redelberger D, Fadel F, Filloux A, Sivaneson M, de Bentzmann S, Bordi C. 2016. The hybrid histidine kinase LadS forms a multicomponent signal transduction system with the GacS/GacA two-component system in *Pseudomonas aeruginosa*. PLoS Genet 12:e1006032.
15. Christen M, Christen B, Folcher M, Schauerte A, Jenal U. 2005. Identification and characterization of a cyclic di-GMP-specific phosphodiesterase and its allosteric control by GTP. J Biol Chem 280:30829-37.
16. Cowie A, Cheng J, Sibley CD, Fong Y, Zaheer R, Patten CL, Morton RM, Golding GB, Finan TM. 2006. An integrated approach to functional genomics: construction of a novel reporter gene fusion library for *Sinorhizobium meliloti*. Appl Environ Microbiol 72:7156-67.
17. Davies JA, Harrison JJ, Marques LL, Foglia GR, Stremick CA, Storey DG, Turner RJ, Olson ME, Ceri H. 2007. The GacS sensor kinase controls phenotypic reversion of small colony variants isolated from biofilms of *Pseudomonas aeruginosa* PA14. FEMS Microbiol Ecol 59:32-46.
18. Döhlemann J, Wagner M, Happel C, Carillo M, Sobetzko P, Erb TJ, Thanbichler M, Becker A. 2017. A family of single copy repABC-type shuttle vectors stably maintained in the alpha-proteobacterium *Sinorhizobium meliloti*. ACS Synth Biol 6:968-984.
19. Dörr T, Lam H, Alvarez L, Cava F, Davis BM, Waldor MK. 2014. A novel peptidoglycan binding protein crucial for PBP1A-mediated cell wall biogenesis in *Vibrio cholerae*. PLoS Genet 10:e1004433.
20. Egan AJ, Vollmer W. 2013. The physiology of bacterial cell division. Ann N Y Acad Sci 1277:8-28.
21. Egan AJ, Vollmer W. 2015. The stoichiometric divisome: a hypothesis. Front Microbiol 6:455.
22. Ernst OP, Lodowski DT, Elstner M, Hegemann P, Brown LS, Kandori H. 2014. Microbial and animal rhodopsins: structures, functions, and molecular mechanisms. Chem Rev 114:126-63.
23. Ferri L, Gori A, Biondi EG, Mengoni A, Bazzicalupo M. 2010. Plasmid electroporation of *Sinorhizobium* strains: the role of the restriction gene *hsdR* in type strain Rm1021. Plasmid 63:128-35.
24. Firczuk M, Mucha A, Bochtler M. 2005. Crystal structures of active LytM. J Mol Biol 354:578-90.
25. Frage B, Döhlemann J, Robledo M, Lucena D, Sobetzko P, Graumann PL, Becker

A. 2016. Spatiotemporal choreography of chromosome and megaplasmids in the *Sinorhizobium meliloti* cell cycle. Mol Microbiol 100:808-23.
26. Goehring NW, Beckwith J. 2005. Diverse paths to midcell: assembly of the bacterial cell division machinery. Curr Biol 15:R514-26.
27. Green MR, Sambrook J. 2012. Molecular cloning: a laboratory manual. 4th ed. Cold Spring Harbor Laboratory Press, Cold Spring Harbor, NY.
28. Gully D, Gargani D, Bonaldi K, Grangeteau C, Chaintreuil C, Fardoux J, Nguyen P, Marchetti R, Nouwen N, Molinaro A, Mergaert P, Giraud E. 2016. A peptidoglycan-remodeling enzyme is critical for bacteroid differentiation in *Bradyrhizobium* spp. during legume symbiosis. Mol Plant Microbe Interact 29:447-57.
29. Gupta KR, Baloni P, Indi SS, Chatterji D. 2016. Regulation of growth, cell shape, cell division, and gene expression by second messengers (p)ppGpp and cyclic di-GMP in *Mycobacterium smegmatis*. J Bacteriol 198:1414-22.
30. Henry JT, Crosson S. 2011. Ligand-binding PAS domains in a genomic, cellular, and structural context. Annu Rev Microbiol 65:261-86.
31. Höltje JV. 1998. Growth of the stress-bearing and shape-maintaining murein sacculus of *Escherichia coli*. Microbiol Mol Biol Rev 62:181-203.
32. Huitema E, Pritchard S, Matteson D, Radhakrishnan SK, Viollier PH. 2006. Bacterial birth scar proteins mark future flagellum assembly site. Cell 124:1025-37.
33. Käll L, Krogh A, Sonnhammer EL. 2004. A combined transmembrane topology and signal peptide prediction method. J Mol Biol 338:1027-36.
34. Khan SR, Gaines J, Roop RM, Farrand SK. 2008. Broad-host-range expression vectors with tightly regulated promoters and their use to examine the influence of TraR and TraM expression on Ti plasmid quorum sensing. Appl Environ Microbiol 74:5053-62.
35. Kim HK, Harshey RM. 2016. A diguanylate cyclase acts as a cell division inhibitor in a two-step response to reductive and envelope stresses. MBio 7.
36. Krol E, Becker A. 2014. Rhizobial homologs of the fatty acid transporter FadL facilitate perception of long-chain acyl-homoserine lactone signals. Proc Natl Acad Sci U S A 111:10702-7.
37. Kuchma SL, Brothers KM, Merritt JH, Liberati NT, Ausubel FM, O'Toole GA. 2007. BifA, a cyclic-Di-GMP phosphodiesterase, inversely regulates biofilm formation and swarming motility by *Pseudomonas aeruginosa* PA14. J Bacteriol 189:8165-78.
38. Kuru E, Hughes HV, Brown PJ, Hall E, Tekkam S, Cava F, de Pedro MA, Brun YV, VanNieuwenhze MS. 2012. *In situ* probing of newly synthesized peptidoglycan in live bacteria with fluorescent D-amino acids. Angew Chem Int Ed Engl 51:12519-23.
39. Kuru E, Tekkam S, Hall E, Brun YV, Van Nieuwenhze MS. 2015. Synthesis of fluorescent D-amino acids and their use for probing peptidoglycan synthesis and bacterial growth *in situ*. Nat Protoc 10:33-52.
40. Lee TK, Huang KC. 2013. The role of hydrolases in bacterial cell-wall growth. Curr Opin Microbiol 16:760-6.
41. Lori C, Ozaki S, Steiner S, Böhm R, Abel S, Dubey BN, Schirmer T, Hiller S, Jenal U. 2015. Cyclic di-GMP acts as a cell cycle oscillator to drive chromosome replication. Nature 523:236-9.
42. Malone JG, Jaeger T, Manfredi P, Dötsch A, Blanka A, Bos R, Cornelis GR, Häussler S, Jenal U. 2012. The YfiBNR signal transduction mechanism reveals novel targets for the evolution of persistent *Pseudomonas aeruginosa* in cystic fibrosis airways. PLoS Pathog 8:e1002760.

43. Margolin W. 2009. Sculpting the bacterial cell. Curr Biol 19:R812-22.
44. Möglich A, Ayers RA, Moffat K. 2009. Structure and signaling mechanism of Per-ARNT-Sim domains. Structure 17:1282-94.
45. Möll A, Schlimpert S, Briegel A, Jensen GJ, Thanbichler M. 2010. DipM, a new factor required for peptidoglycan remodelling during cell division in *Caulobacter crescentus*. Mol Microbiol 77:90-107.
46. Odintsov SG, Sabala I, Marcyjaniak M, Bochtler M. 2004. Latent LytM at 1.3A resolution. J Mol Biol 335:775-85.
47. Okegbe C, Fields BL, Cole SJ, Beierschmitt C, Morgan CJ, Price-Whelan A, Stewart RC, Lee VT, Dietrich LEP. 2017. Electron-shuttling antibiotics structure bacterial communities by modulating cellular levels of c-di-GMP. Proc Natl Acad Sci U S A doi:10.1073/pnas.1700264114.
48. Palomino MM, Sanchez-Rivas C, Ruzal SM. 2009. High salt stress in *Bacillus subtilis*: involvement of PBP4* as a peptidoglycan hydrolase. Res Microbiol 160:117-24.
49. Paradis-Bleau C, Kritikos G, Orlova K, Typas A, Bernhardt TG. 2014. A genome-wide screen for bacterial envelope biogenesis mutants identifies a novel factor involved in cell wall precursor metabolism. PLoS Genet 10:e1004056.
50. Paul R, Weiser S, Amiot NC, Chan C, Schirmer T, Giese B, Jenal U. 2004. Cell cycle-dependent dynamic localization of a bacterial response regulator with a novel di-guanylate cyclase output domain. Genes Dev 18:715-27.
51. Pierce KL, Premont RT, Lefkowitz RJ. 2002. Seven-transmembrane receptors. Nat Rev Mol Cell Biol 3:639-50.
52. Qi Y, Rao F, Luo Z, Liang ZX. 2009. A flavin cofactor-binding PAS domain regulates c-di-GMP synthesis in AxDGC2 from *Acetobacter xylinum*. Biochemistry 48:10275-85.
53. Robinson VL, Buckler DR, Stock AM. 2000. A tale of two components: a novel kinase and a regulatory switch. Nat Struct Biol 7:626-33.
54. Rodríguez-Herva JJ, Ramos-Gonzalez MI, Ramos JL. 1996. The *Pseudomonas putida* peptidoglycan-associated outer membrane lipoprotein is involved in maintenance of the integrity of the cell cell envelope. J Bacteriol 178:1699-706.
55. Roelofs KG, Wang J, Sintim HO, Lee VT. 2011. Differential radial capillary action of ligand assay for high-throughput detection of protein-metabolite interactions. Proc Natl Acad Sci U S A 108:15528-33.
56. Römling U, Galperin MY, Gomelsky M. 2013. Cyclic di-GMP: the first 25 years of a universal bacterial second messenger. Microbiol Mol Biol Rev 77:1-52.
57. Schäfer A, Tauch A, Jäger W, Kalinowski J, Thierbach G, Pühler A. 1994. Small mobilizable multi-purpose cloning vectors derived from the *Escherichia coli* plasmids pK18 and pK19: selection of defined deletions in the chromosome of *Corynebacterium glutamicum*. Gene 145:69-73.
58. Schäper S, Krol E, Skotnicka D, Kaever V, Hilker R, Søgaard-Andersen L, Becker A. 2016. Cyclic di-GMP regulates multiple cellular functions in the symbiotic alphaproteobacterium *Sinorhizobium meliloti*. J Bacteriol 198:521-35.
59. Schirmer F, Ehrt S, Hillen W. 1997. Expression, inducer spectrum, domain structure, and function of MopR, the regulator of phenol degradation in *Acinetobacter calcoaceticus* NCIB8250. J Bacteriol 179:1329-1336.
60. Singh SK, Parveen S, SaiSree L, Reddy M. 2015. Regulated proteolysis of a cross-link-specific peptidoglycan hydrolase contributes to bacterial morphogenesis. Proc Natl Acad Sci U S A 112:10956-61.
61. Singh SK, SaiSree L, Amrutha RN, Reddy M. 2012. Three redundant murein endopeptidases catalyse an essential cleavage step in peptidoglycan synthesis of

Escherichia coli K12. Mol Microbiol 86:1036-51.
62. Skotnicka D, Smaldone GT, Petters T, Trampari E, Liang J, Kaever V, Malone JG, Singer M, Søgaard-Andersen L. 2016. A minimal threshold of c-di-GMP is essential for fruiting body formation and sporulation in *Myxococcus xanthus*. PLoS Genet 12:e1006080.
63. Spencer J, Murphy LM, Conners R, Sessions RB, Gamblin SJ. 2010. Crystal structure of the LasA virulence factor from *Pseudomonas aeruginosa*: substrate specificity and mechanism of M23 metallopeptidases. J Mol Biol 396:908-23.
64. Sultan SZ, Pitzer JE, Boquoi T, Hobbs G, Miller MR, Motaleb MA. 2011. Analysis of the HD-GYP domain cyclic dimeric GMP phosphodiesterase reveals a role in motility and the enzootic life cycle of *Borrelia burgdorferi*. Infect Immun 79:3273-83.
65. Torres-Quesada O, Millán V, Nisa-Martínez R, Bardou F, Crespi M, Toro N, Jiménez-Zurdo JI. 2013. Independent activity of the homologous small regulatory RNAs AbcR1 and AbcR2 in the legume symbiont *Sinorhizobium meliloti*. PLoS One 8:e68147.
66. Tschowri N, Schumacher MA, Schlimpert S, Chinnam NB, Findlay KC, Brennan RG, Buttner MJ. 2014. Tetrameric c-di-GMP mediates effective transcription factor dimerization to control *Streptomyces* development. Cell 158:1136-47.
67. Typas A, Banzhaf M, Gross CA, Vollmer W. 2012. From the regulation of peptidoglycan synthesis to bacterial growth and morphology. Nat Rev Microbiol 10:123-36.
68. Uehara T, Dinh T, Bernhardt TG. 2009. LytM-domain factors are required for daughter cell separation and rapid ampicillin-induced lysis in *Escherichia coli*. J Bacteriol 191:5094-107.
69. Uehara T, Parzych KR, Dinh T, Bernhardt TG. 2010. Daughter cell separation is controlled by cytokinetic ring-activated cell wall hydrolysis. EMBO J 29:1412-22.
70. Vollmer W, Bertsche U. 2008. Murein (peptidoglycan) structure, architecture and biosynthesis in *Escherichia coli*. Biochim Biophys Acta 1778:1714-34.
71. Vollmer W, Joris B, Charlier P, Foster S. 2008. Bacterial peptidoglycan (murein) hydrolases. FEMS Microbiol Rev 32:259-86.
72. Zhan HJ, Lee CC, Leigh JA. 1991. Induction of the second exopolysaccharide (EPSb) in *Rhizobium meliloti* SU47 by low phosphate concentrations. J Bacteriol 173:7391-4.
73. Zupan JR, Cameron TA, Anderson-Furgeson J, Zambryski PC. 2013. Dynamic FtsA and FtsZ localization and outer membrane alterations during polar growth and cell division in *Agrobacterium tumefaciens*. Proc Natl Acad Sci U S A 110:9060-5.

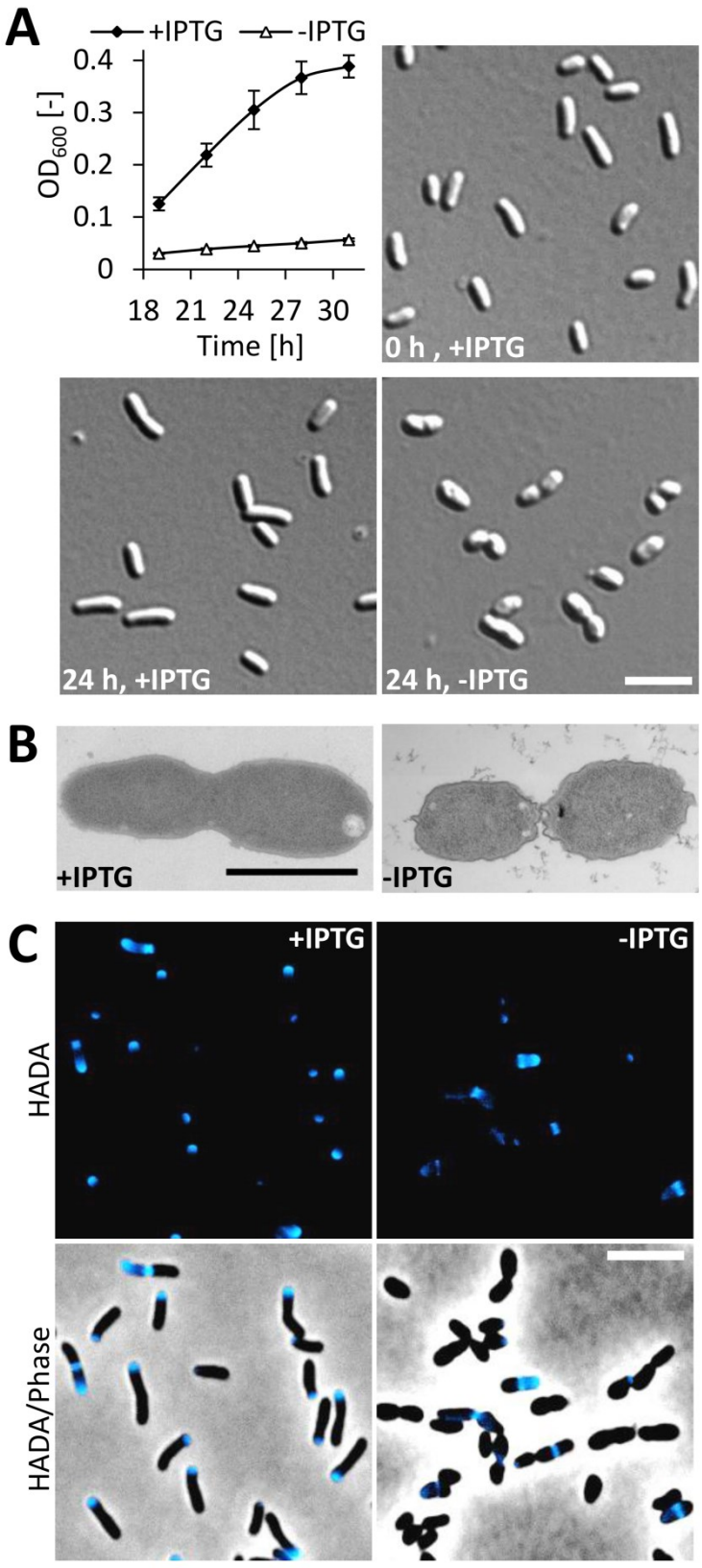

Figure 1. GdcP function is related to cell growth and division. (A) Growth of *S. meliloti* GdcP depletion strain Rm2011 GdcP^{dep} in TY medium in presence or absence of 0.5 mM IPTG. OD_{600} was recorded in three-hours intervals. Cell morphologies were assessed by DIC microscopy at the indicated time points. Error bars represent the standard deviation of three biological replicates. Bar, 5 µm. **(B)** Electron micrographs of Rm2011 GdcP^{dep} grown in TY medium in presence or absence of 0.5 mM IPTG for 24 hours. Bar, 1 µm. **(C)** Nascent peptidoglycan synthesis of Rm2011 GdcP^{dep} grown in TY medium in presence or absence of 0.5 mM IPTG for 24 hours. Cells were pulse-labeled with blue-fluorescent D-amino acid HADA for 3 min. Bar, 5 µm.

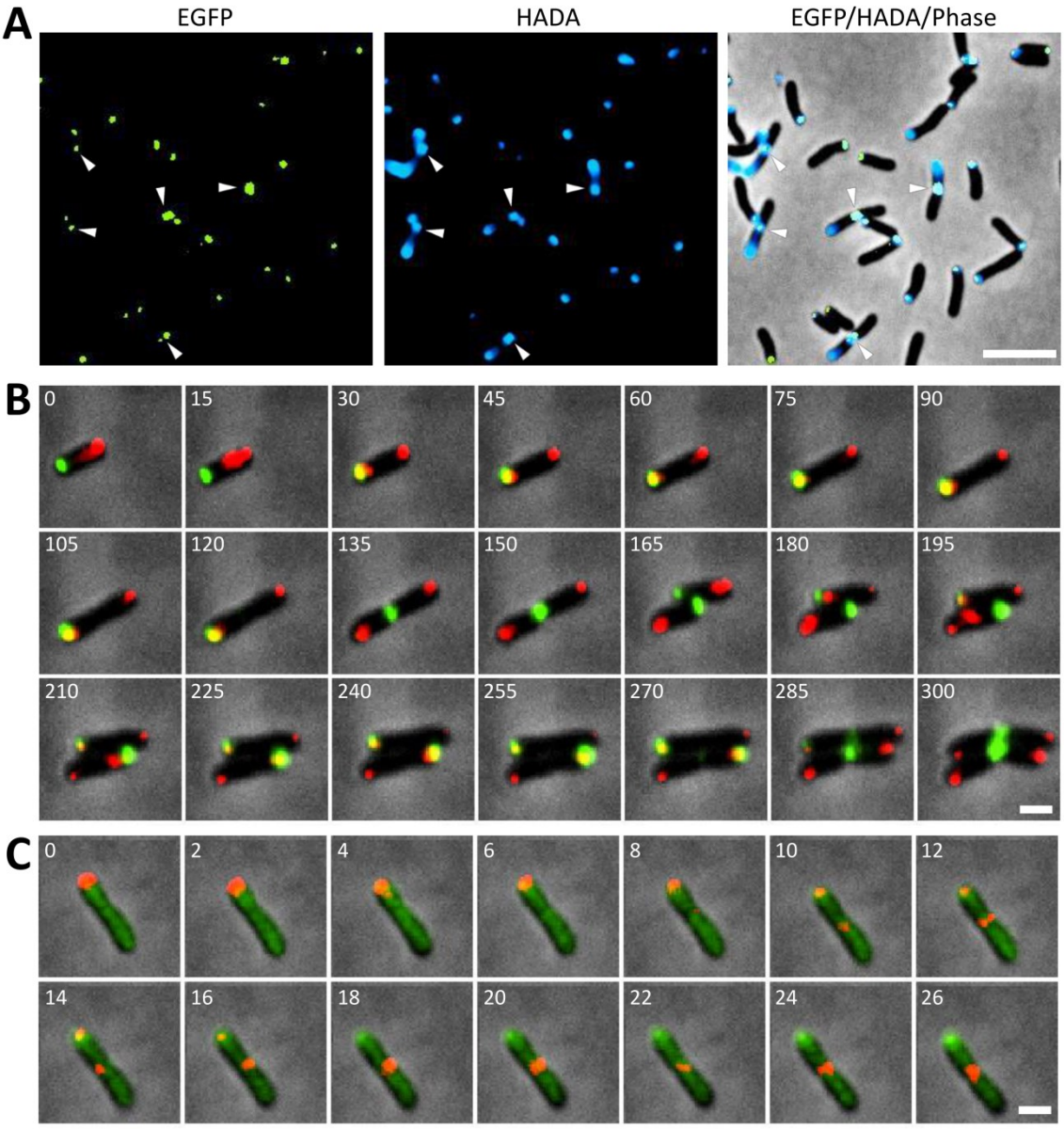

Figure 2. GdcP localizes to sites of zonal cell wall synthesis. (A) Fluorescence microscopic images of Rm2011 *gdcP-egfp* in the exponential growth phase. Cells were pulse-labeled with blue-fluorescent D-amino acid HADA for 3 min. Arrow heads indicate the mid-cell region of pre-divisional cells. Bar, 5 µm. **(B, C)** Time-lapse microscopy of (B) Rm2011 *gdcP-egfp* harboring pSRKGm-*parB-mCherry* and (C) Rm2011 *gdcP-mCherry pleD-egfp*. Time is given in minutes. Bars, 1 µm.

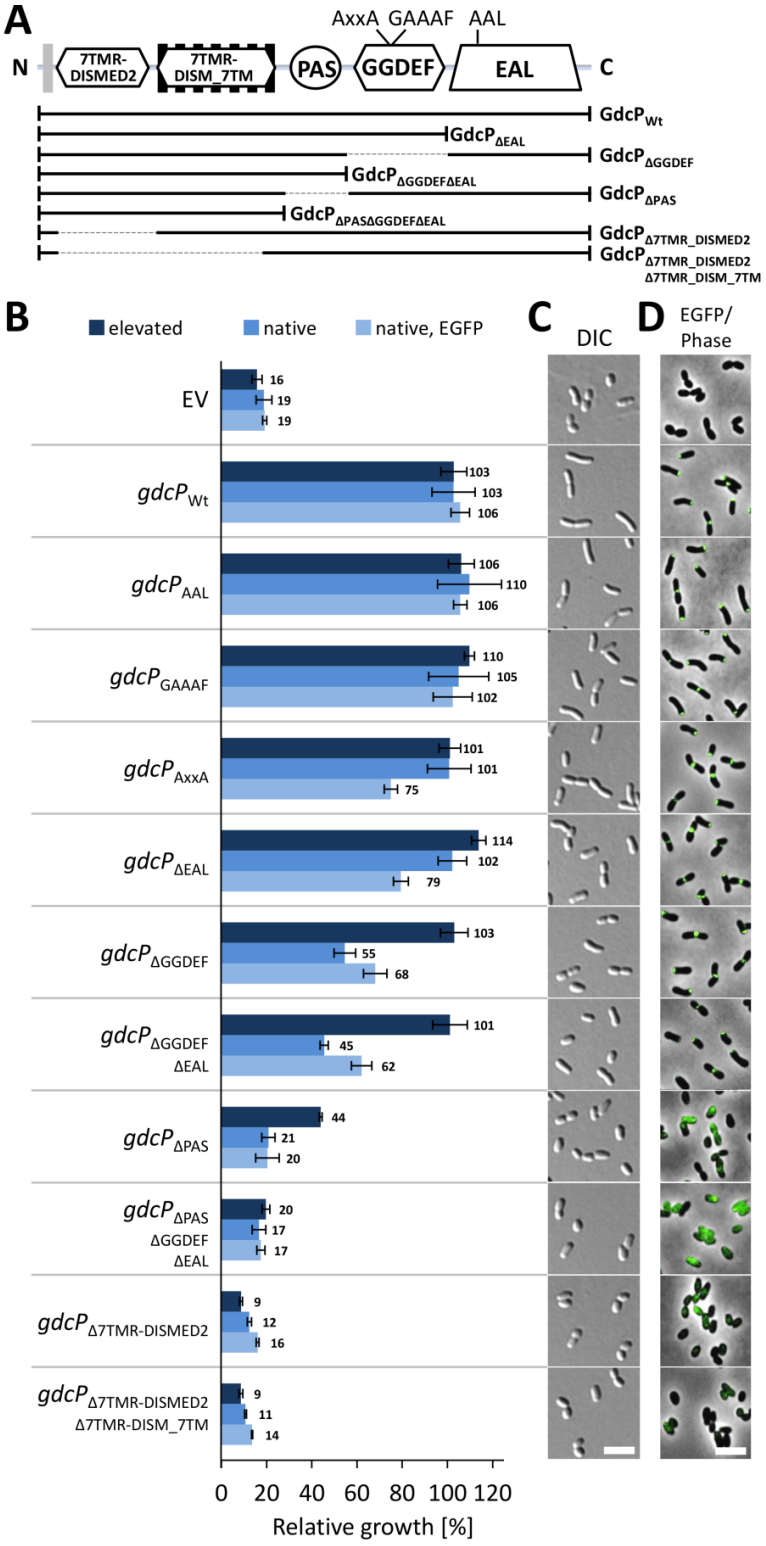

Figure 3. GdcP essentiality resides in its N-terminal part. (A) GdcP domain architecture with indications for generated mutant variants. **(B)** Complementation of the growth defect of GdcP depletion strain Rm2011 GdcP^{dep} by ectopic expression of non-tagged and *egfp*-tagged ('EGFP') wild-type *gdcP* and mutant variants from either P^*_{gdcP} (vector pABC2S-mob, transcription strength similar to the native level, 'native') or P_{syn} (vector pR_EGFP, elevated transcription strength compared to the native levels, 'elevated'). Relative growth was calculated as a ratio of OD_{600} values obtained for cultures induced for expression of the chromosomally encoded *gdcP* (grown with 0.5 mM IPTG) to the OD_{600} values of cultures non-induced for expression of this wild-type *gdcP* allele (grown without IPTG), 24 hours after inoculation. Error bars represent the standard deviation of three biological replicates. The absolute OD_{600} values are shown in Fig. S2. **(C, D)** Microscopic images of Rm2011 GdcP^{dep}, ectopically expressing the indicated (C) non-tagged and (D) *egfp*-tagged *gdcP* variants, acquired after 24 hours of growth without IPTG. Bars, 5 µm. EV, empty vectors pABC2S-mob and pR_EGFP.

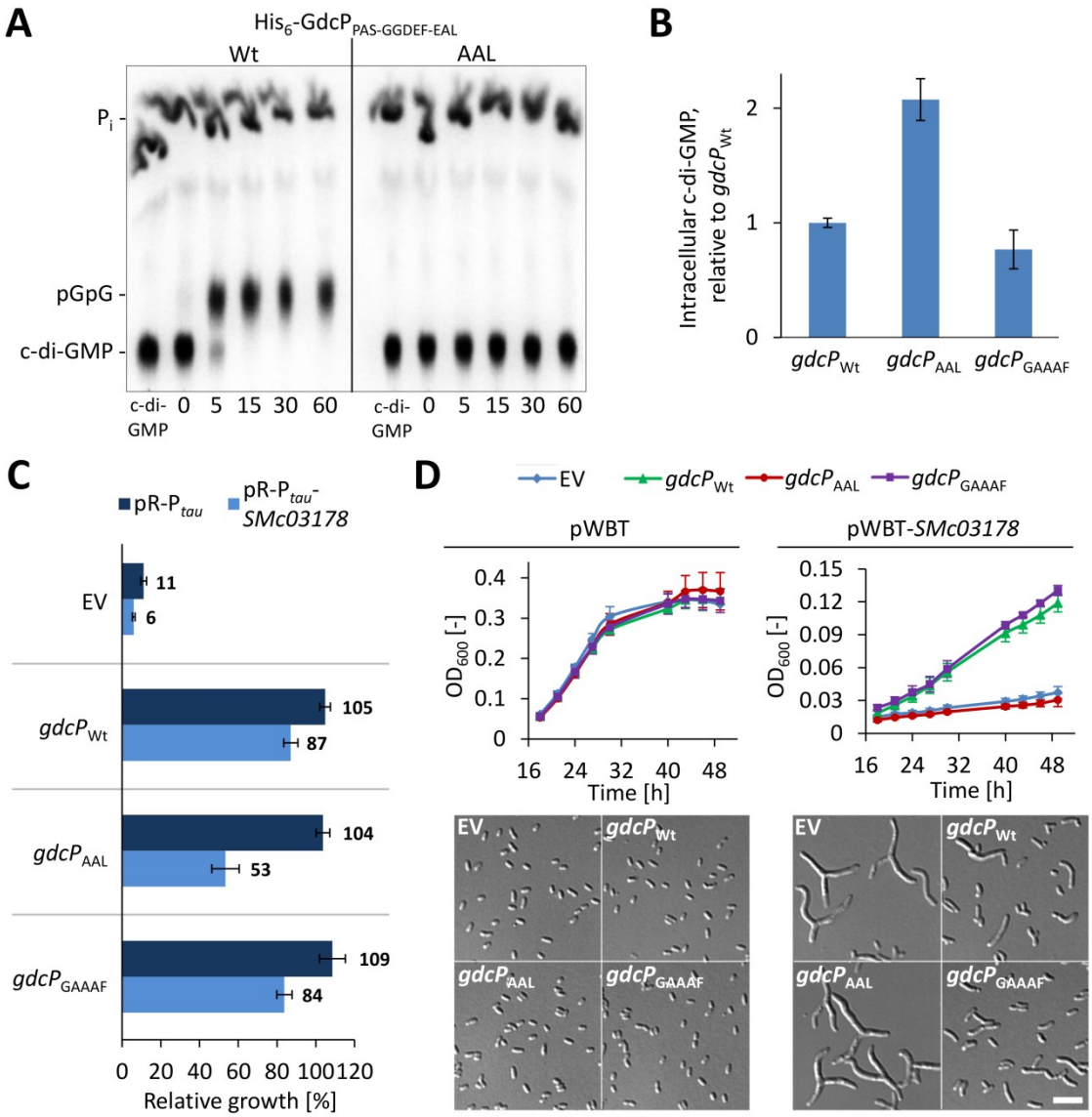

Figure 4. The EAL domain of GdcP shows PDE activity, which can counteract negative effects of very high c-di-GMP concentrations on growth and cell morphology. (A) Thin-layer chromatogram of PDE reactions with either purified His_6-$GdcP_{PAS\text{-}GGDEF\text{-}EAL}$ or His_6-$GdcP_{PAS\text{-}GGDEF\text{-}EAL}$-AAL and [α-^{32}P]-c-di-GMP. Reaction time is given in minutes. **(B)** c-di-GMP content of Rm2011 $GdcP^{dep}$, expressing the indicated *gdcP* variants from P^*_{gdcP}, grown in TY medium without IPTG for 24 hours and harvested in the exponential growth phase. Standard deviation was calculated from three biological replicates. **(C)** Complementation of the growth defect of GdcP depletion strain Rm2011 $GdcP^{dep}$, harboring either empty vector pR-P_{tau} or pR-P_{tau}-*SMc03178*, by ectopic expression of the indicated *gdcP* variants from P^*_{gdcP}. Relative growth was calculated as a ratio of OD_{600} values obtained for cultures induced for expression of the chromosomal *gdcP* allele (grown with 0.5 mM IPTG) or depleted for GdcP (grown without IPTG, non-induced for expression of the chromosomal *gdcP* allele), 24 hours after inoculation. Error bars represent the standard deviation of three biological replicates. The absolute OD_{600} values are shown in Fig. S6. EV, empty vector pABC2S-mob. **(D)** Growth in medium with 0.2 mM IPTG of Rm2011 ectopically expressing the indicated *gdcP* variants from P_{syn} (vector pR_EGFP) and harboring either empty vector pWBT or *SMc03178* overexpression plasmid pWBT-*SMc03178*. Error bars represent the standard deviation of three biological replicates. Microscopy was performed after 46 hours of culture growth. EV, empty vector pR_EGFP. Bar, 5 µm.

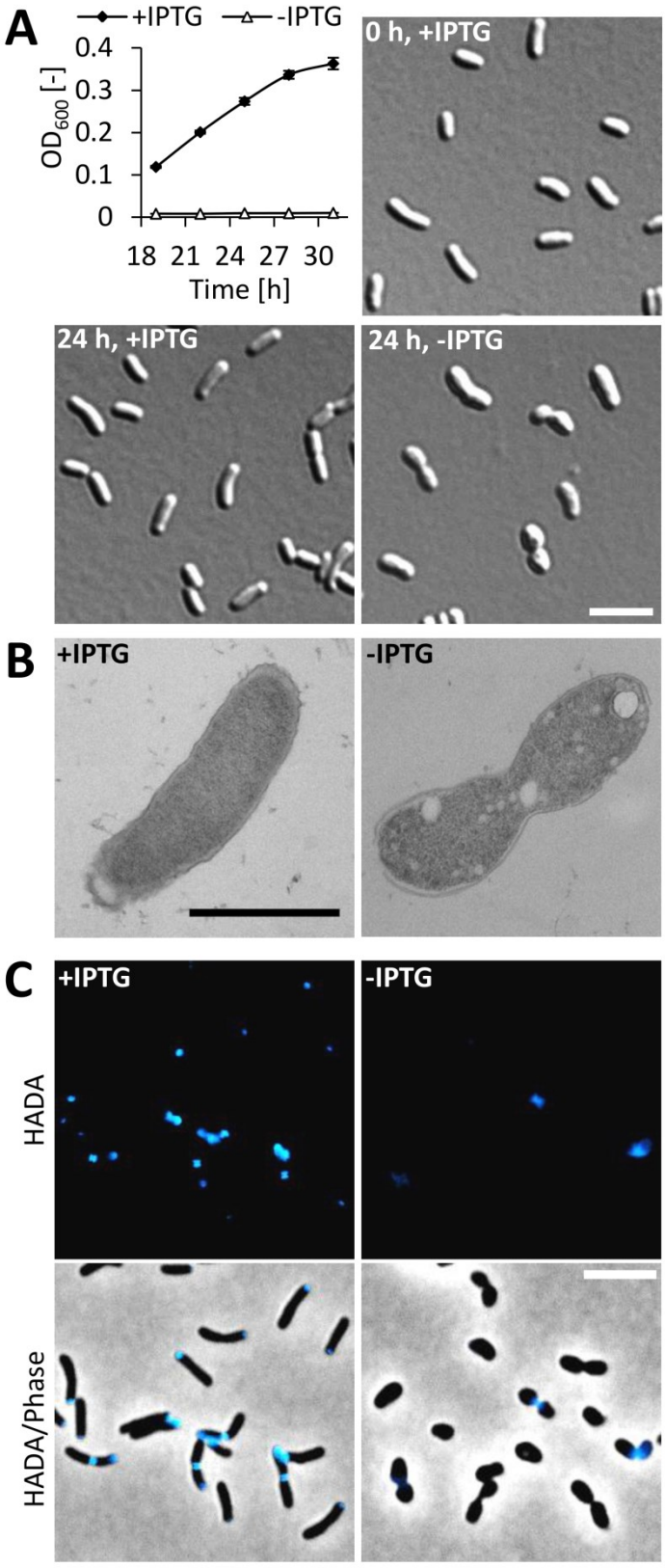

Figure 5. GdpM function is related to cell growth and division. (A) *S. meliloti* GdpM depletion strain Rm2011 GdpM^{dep} grown in TY medium with or without 0.5 mM IPTG. OD_{600} was recorded in three-hours intervals. Cell morphologies were assessed by DIC microscopy at the indicated time points. Error bars represent the standard deviation of three biological replicates. Bar, 5 µm. **(B)** Electron micrographs of Rm2011 GdpM^{dep} grown in TY medium in presence or absence of 0.5 mM IPTG for 24 hours. Bar, 1 µm. **(C)** Nascent peptidoglycan synthesis of Rm2011 GdpM^{dep} grown in TY medium in presence or absence of IPTG for 24 hours. Cells were pulse-labeled with blue-fluorescent D-amino acid HADA for 3 min. Bar, 5 µm.

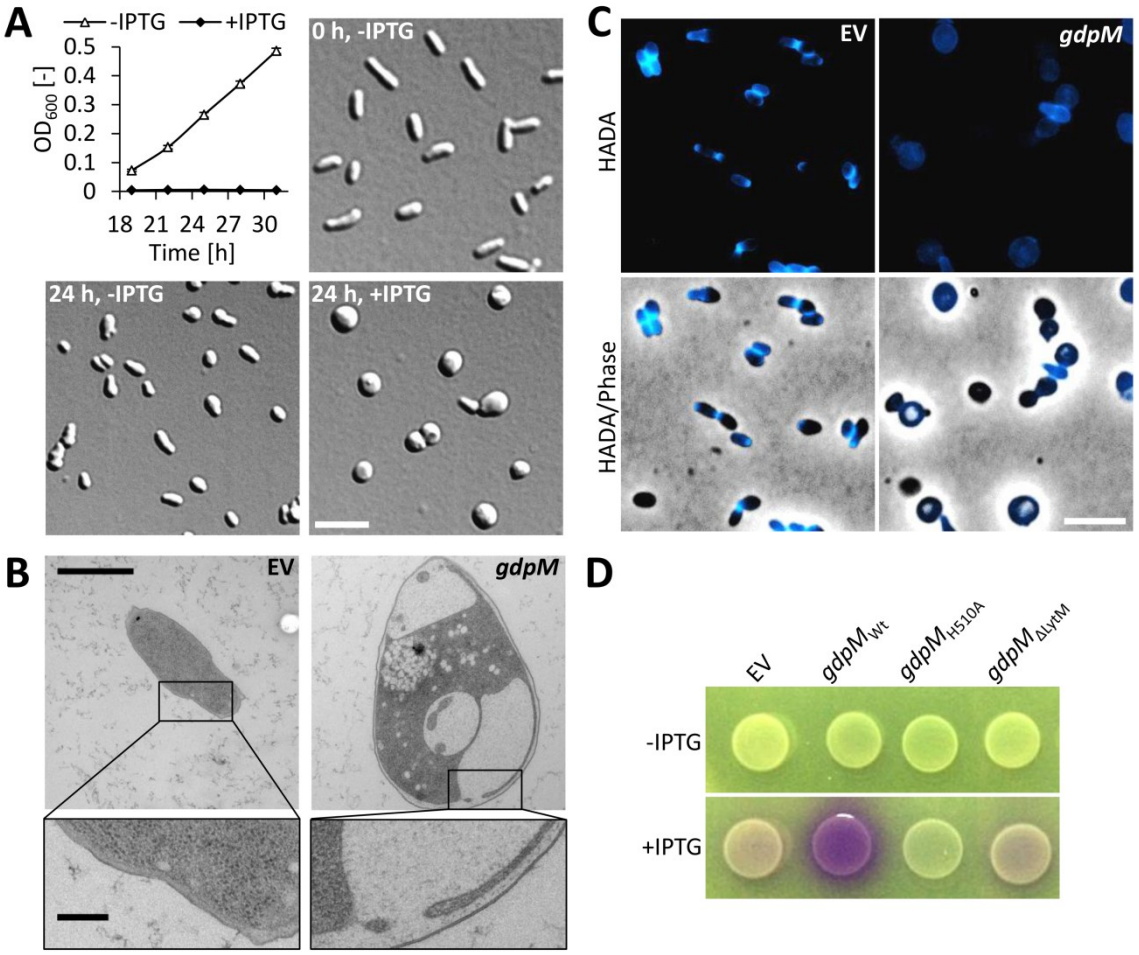

Figure 6. *gdpM* overexpression results in growth inhibition, altered cell morphology and cell envelope defects. (A) Rm2011 harboring *gdpM* overexpression plasmid pWBT-*gdpM* was grown in LB medium with or without 0.5 mM IPTG. OD_{600} was recorded in three-hours intervals and cell morphology was assessed by DIC microscopy at the indicated time point. Error bars represent the standard deviation of three biological replicates. Bar, 5 µm. **(B)** Electron micrographs of Rm2011, harboring either empty vector pWBT or pWBT-*gdpM*, grown in LB medium containing 0.5 mM IPTG for 24 hours. Bar, 1 µm. Bar(inset), 0.2 µm. **(C)** Nascent peptidoglycan synthesis of Rm2011, harboring either empty vector pWBT or pWBT-*gdpM*, grown in LB medium in presence or absence of 0.5 mM IPTG for 24 h. Cells were pulse-labeled with blue-fluorescent D-amino acid HADA for 3 min. Bar, 5 µm. **(D)** *E. coli* S17-1, harboring the indicated overexpression constructs, was grown on LB agar lacking NaCl, supplemented with or without 0.02 mM IPTG and containing 20 µg/mL CPRG at 30 °C. EV, empty vector pWBT.

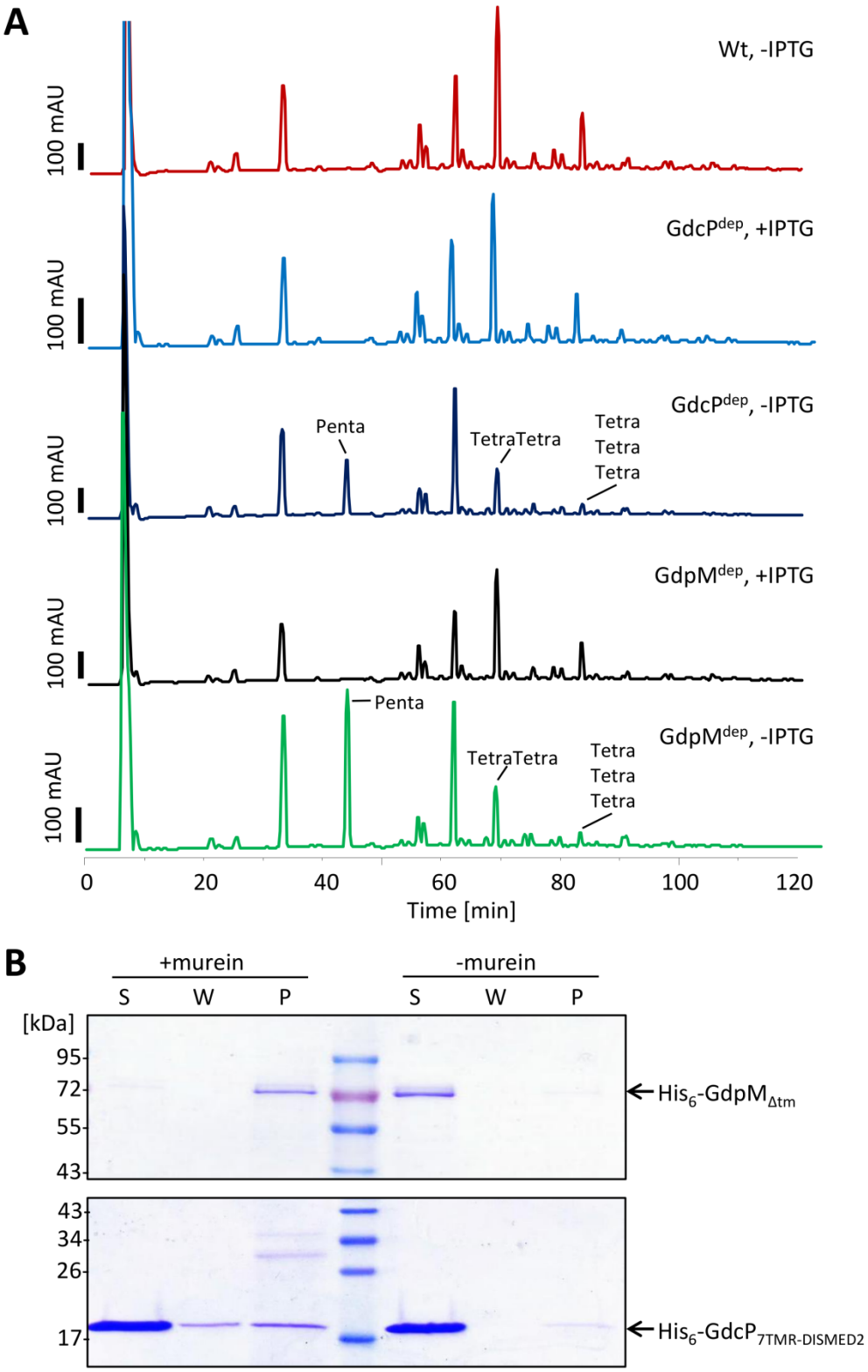

Figure 7. Relative abundances of muropeptides in the *S. meliloti* cell wall change upon depletion of GdcP and GdpM, while the latter binds peptidoglycan *in vitro*. (A) Rm2011 wild-type, Rm2011 GdcP^{dep} and Rm2011 GdpM^{dep} were grown in TY medium with or without 0.5 mM IPTG for 24 hours. Sacculi were isolated, treated with cellosyl and analyzed by HPLC. Differentially abundant peptides identified by mass spectrometry are indicated. Representative muropeptide profiles of two independent biological replicates per strain and growth condition are shown. **(B)** Peptidoglycan binding properties of GdpM and GdcP. 10 µg of either His$_6$-GdpM$_{\Delta tm}$ or His$_6$-GdcP$_{7TMR\text{-}DISMED2}$ were mixed with *S. meliloti* Rm2011 murein sacculi. Murein was collected by ultracentrifugation and washed once in binding buffer. The supernatant of the first centrifugation step (S), the supernatant of the washing step (W) and the resuspended pellet (P) were analyzed by SDS-PAGE and subsequent Coomassie blue staining. Control reactions were performed in the absence of murein sacculi.

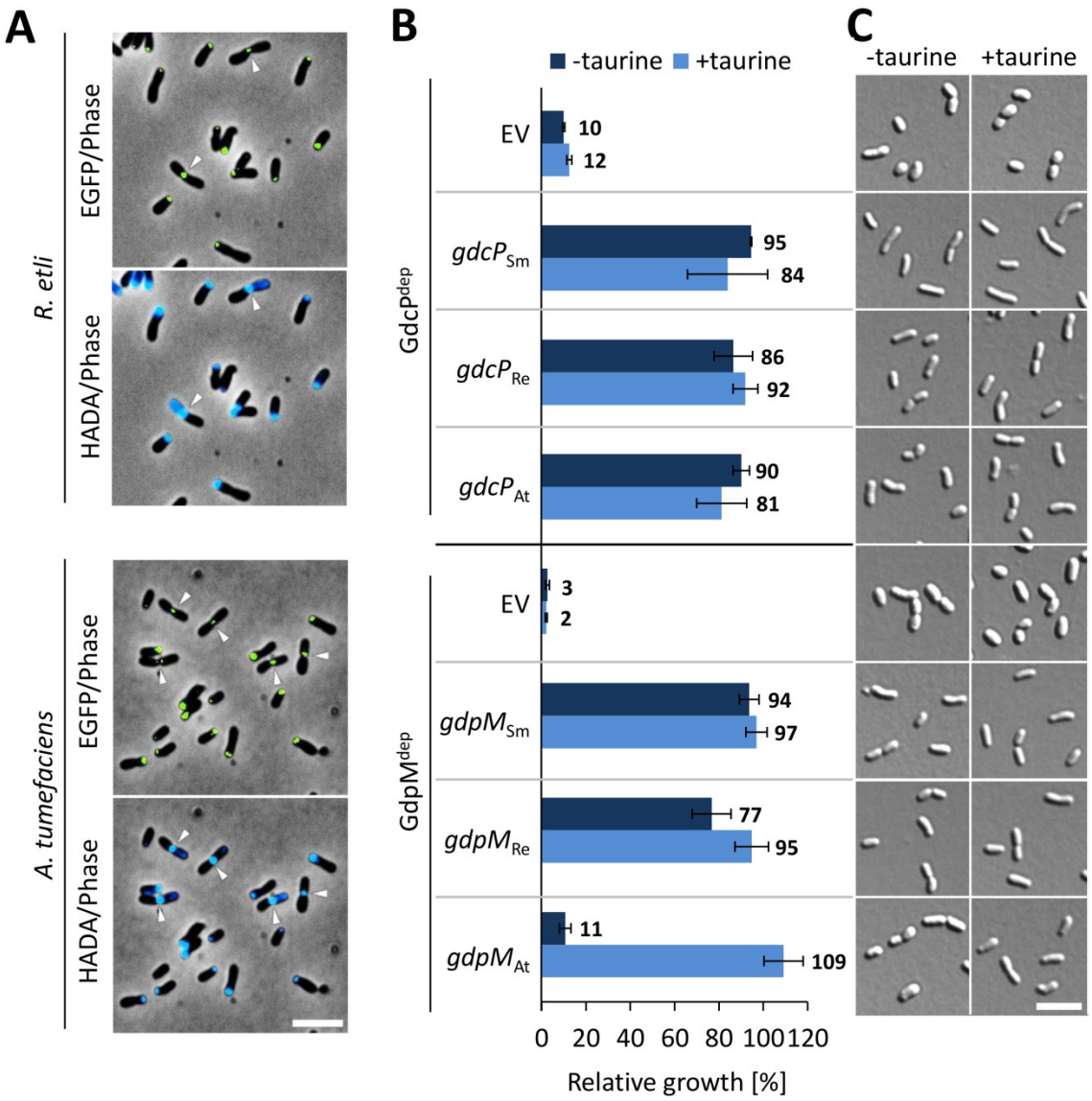

Figure 8. GdcP and GdpM homologs from related species are functional in *S. meliloti*. **(A)** Microscopic images of *R. etli* CFN42 *RHE_CH00976-egfp* and *A. tumefaciens* C58 *Atu0784-egfp* cells pulse-labeled with HADA for 3.5 and 2.5 min, respectively. Arrow heads indicate the mid-cell region of pre-divisional cells. Bar, 5 µm. **(B)** Complementation of the growth defect of GdcP depletion strain Rm2011 GdcP^{dep} and GdpM depletion strain Rm2011 GdpM^{dep} by ectopic expression of *gdcP*$_{Sm}$, *gdcP*$_{Re}$ or *gdcP*$_{At}$, and *gdpM*$_{Sm}$, *gdpM*$_{Re}$ or *gdpM*$_{At}$, respectively, from vector pR-P$_{tau}$ in presence or absence of taurine. Relative growth was calculated as a ratio of OD_{600} values obtained for cultures induced for expression of the chromosomally encoded *gdcP* and *gdpM* (grown with 0.5 mM IPTG) to the OD_{600} values of cultures non-induced for expression of the wild-type *gdcP* and *gdpM* alleles (grown without IPTG), respectively, 42 hours after inoculation. EV, empty vector pR-P$_{tau}$. Error bars represent the standard deviation of three biological replicates. The absolute OD_{600} values are shown in Fig. S17. **(C)** Microscopic images of *S. meliloti* strains indicated in panel B grown for 24 hours with or without taurine and in absence of IPTG. Bar, 5 µm. EV, empty vector pR-P$_{tau}$.

Supplementary Material:

A dynamic c-di-GMP phosphodiesterase is linked to alpha-rhizobial cell growth and division

Media

TY medium (5 g/L tryptone, 3 g/L yeast extract, 0.4 g $CaCl_2*2H_2O$).

LB medium (10 g/L tryptone, 5 g/L yeast extract, 5 g/L NaCl).

MOPS-buffered minimal medium (MM) (10 g/L MOPS, 10 g/L mannitol, 3.55 g/L sodium glutamate, 0.246 g/L $MgSO_4*7H_2O$, 0.25 mM $CaCl_2$, 2 mM K_2HPO_4, 10 mg/L $FeCl_3*6H_2O$, 1 mg/L biotin, 3 mg/L H_3BO_3, 2.23 mg/L $MnSO_4*H_2O$, 0.287 mg/L $ZnSO_4*7H_2O$, 0.125 mg/L $CuSO_4*5H_2O$, 0.065 mg/L $CoCl_2*6H_2O$, 0.12 mg/L $NaMoO_4*2H_2O$, pH 7.2).

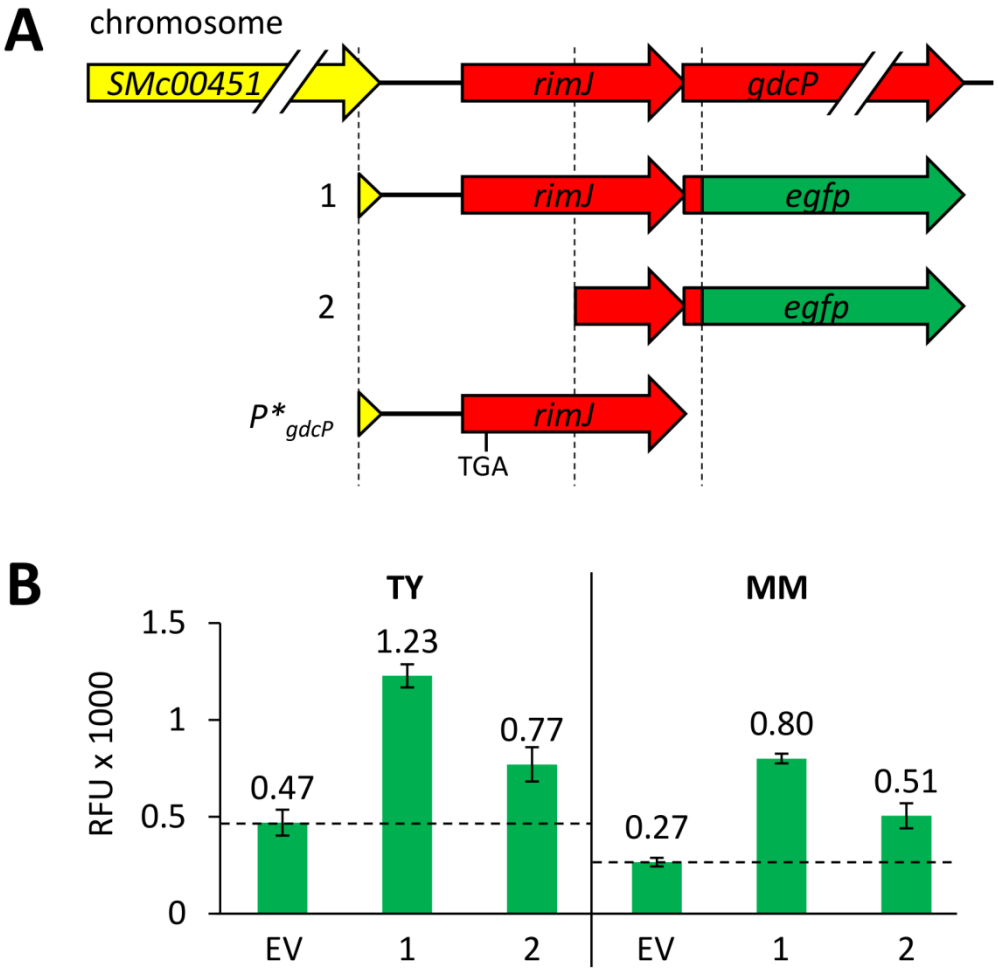

Figure S1. Determination of the *gdcP* promoter region. (A) *gdcP* upstream fragments including the first three codons of *gdcP* coding sequence were translationally fused to *egfp*. P^*_{gdcP}, containing a stop codon (TGA) inserted at position 64 of the *rimJ* coding sequence, represents the region taken for ectopic *gdcP* expression from vector pABC2S-mob. **(B)** Normalized EGFP fluorescence of Rm2011, harboring medium-copy plasmids carrying the translational fusions depicted in panel A, grown in TY and MM. Error bars represent the standard deviation of three biological replicates. EV, empty vector pSRKKm-EGFP.

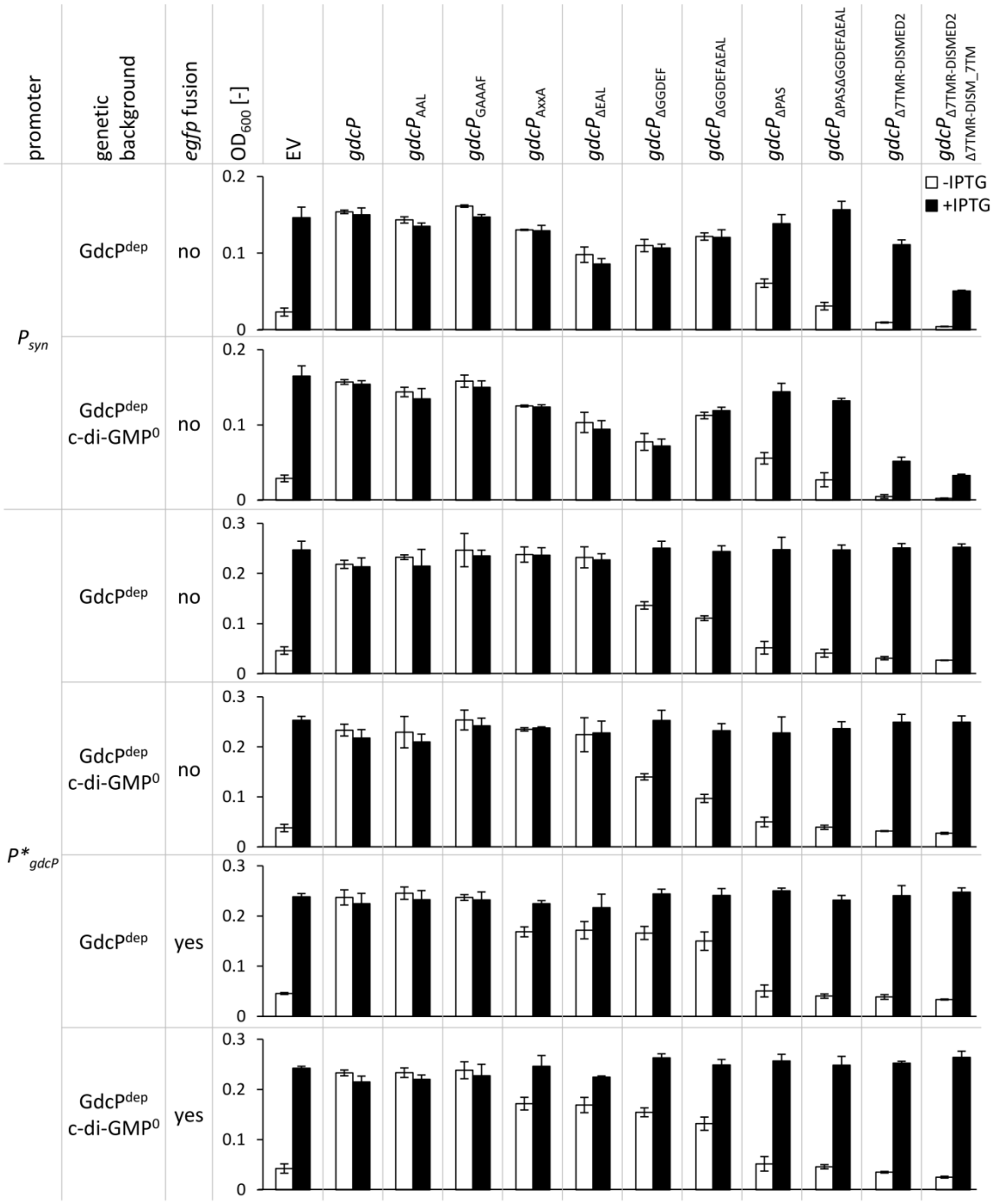

Figure S2. Complementation of GdcP-depleted *S. meliloti* by ectopic expression of various *gdcP* variants. Recorded growth of Rm2011 GdcP^{dep} and c-di-GMP^{0} strain Rm2011 ΔXVI GdcP^{dep}, ectopically expressing non-tagged and *egfp*-tagged *gdcP* variants from either P^*_{gdcP} (vector pABC2S-mob, transcription strength similar to the native level) or P_{syn} (vector pR_EGFP, elevated transcription strength compared to the native levels), grown in absence or presence of 0.5 mM IPTG. OD_{600} values were recorded after 24 hours of growth. Error bars represent the standard deviation of three biological replicates. EV, empty vectors pABC2S-mob and pR_EGFP.

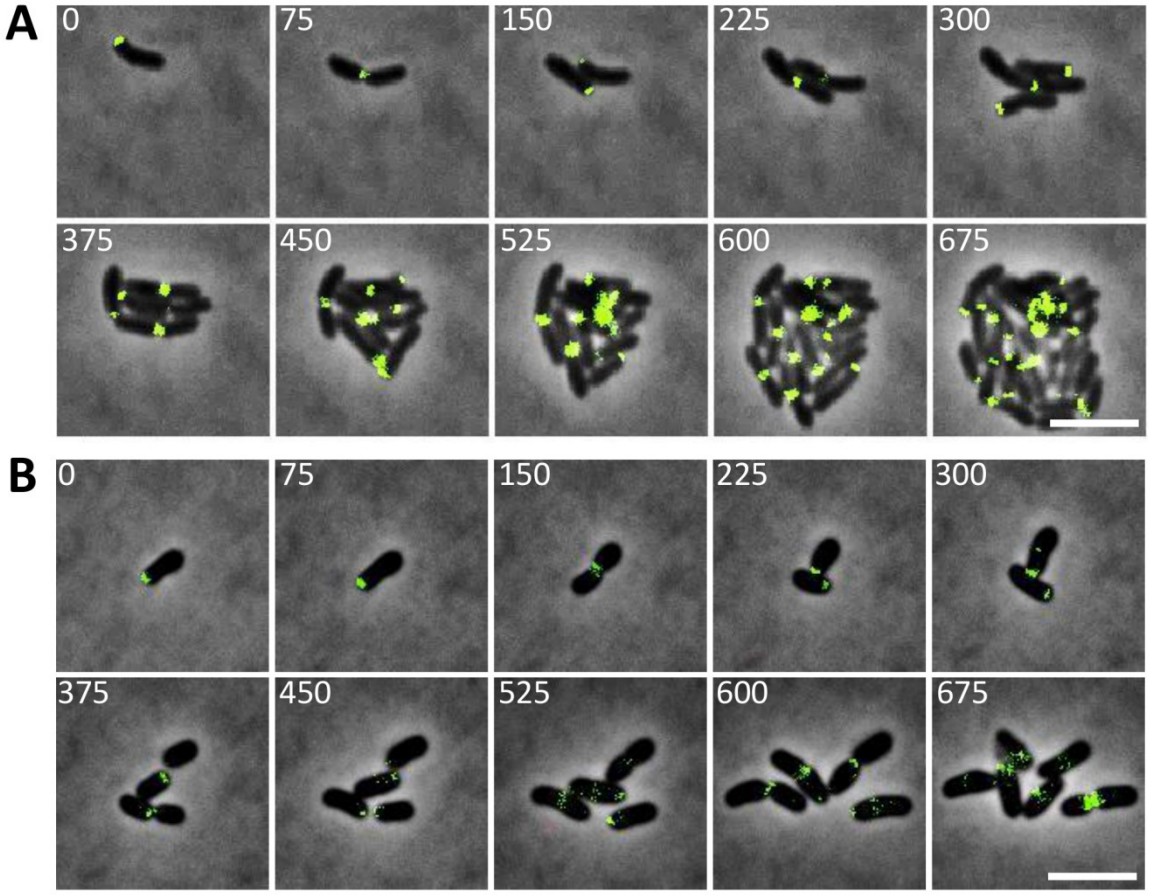

Figure S3. ***S. meliloti*** **cells expressing** ***gdcP*** $_{\Delta GGDEF\Delta EAL}$ ***-egfp*** **are shortened and show increased doubling time, while the protein fusion can be detected at the new pole and the mid-cell region of pre-divisional cells. (A, B)** Time-lapse microscopy of (A) Rm2011 *gdcP-egfp(Km)* and (B) Rm2011 *gdcP* $_{\Delta GGDEF\Delta EAL}$ *-egfp.* Time is given in minutes. Bars, 5 µm.

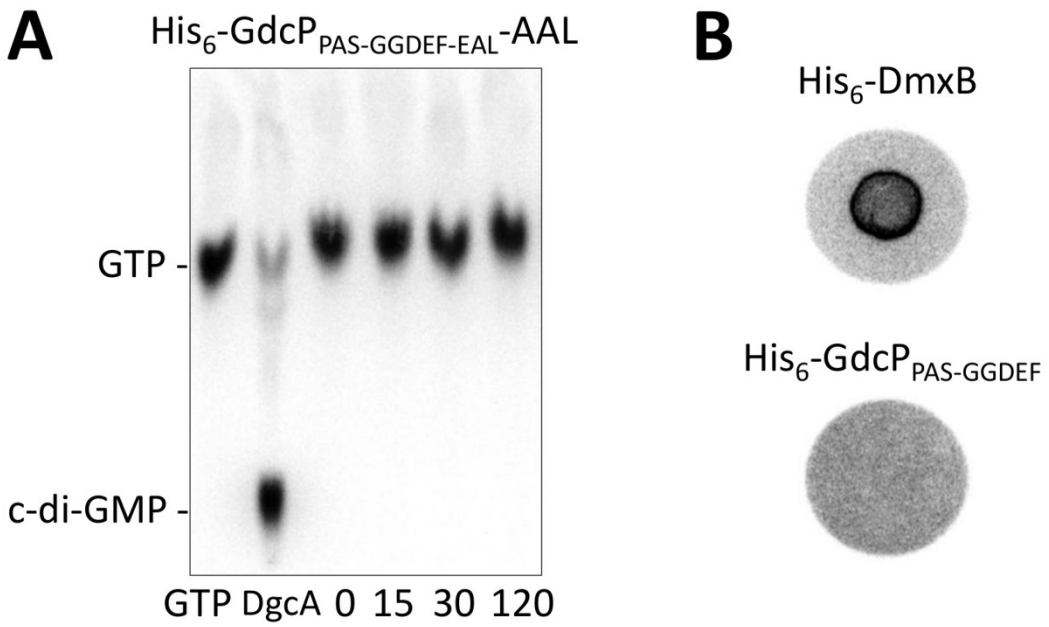

Figure S4. The GGDEF domain of GdcP is inactive and did not bind c-di-GMP *in vitro.* (A) DGC activity assay with purified His_6-$GdcP_{PAS\text{-}GGDEF\text{-}EAL}$-AAL and His_6-DgcA as positive control. Incubation time is given in minutes. **(B)** DRaCALA with purified His_6-$GdcP_{PAS\text{-}GGDEF}$ and His_6-DmxB as positive control.

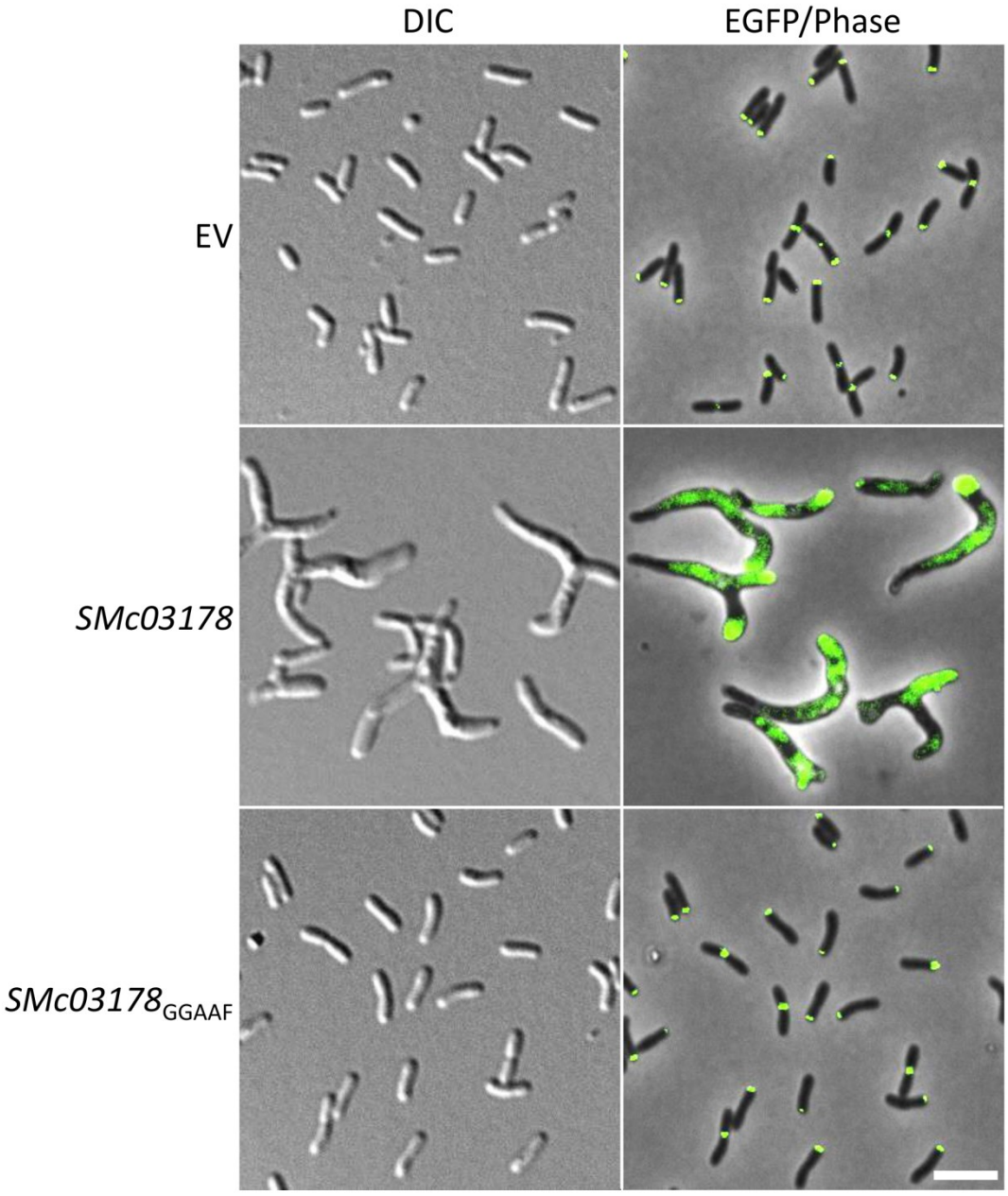

Figure S5. Cell morphology and GdcP localization are affected at very high c-di-GMP concentrations in *S. meliloti*. DIC and fluorescence microscopy of Rm2011, harboring either empty vector pR-P_{tau}, pR-P_{tau}-*SMc03178* or pR-P_{tau}-*SMc03178*$_{GGAAF}$, grown in liquid TY medium supplemented with 20 mM taurine. Bar, 5 µm. EV, empty vector pR-P_{tau}.

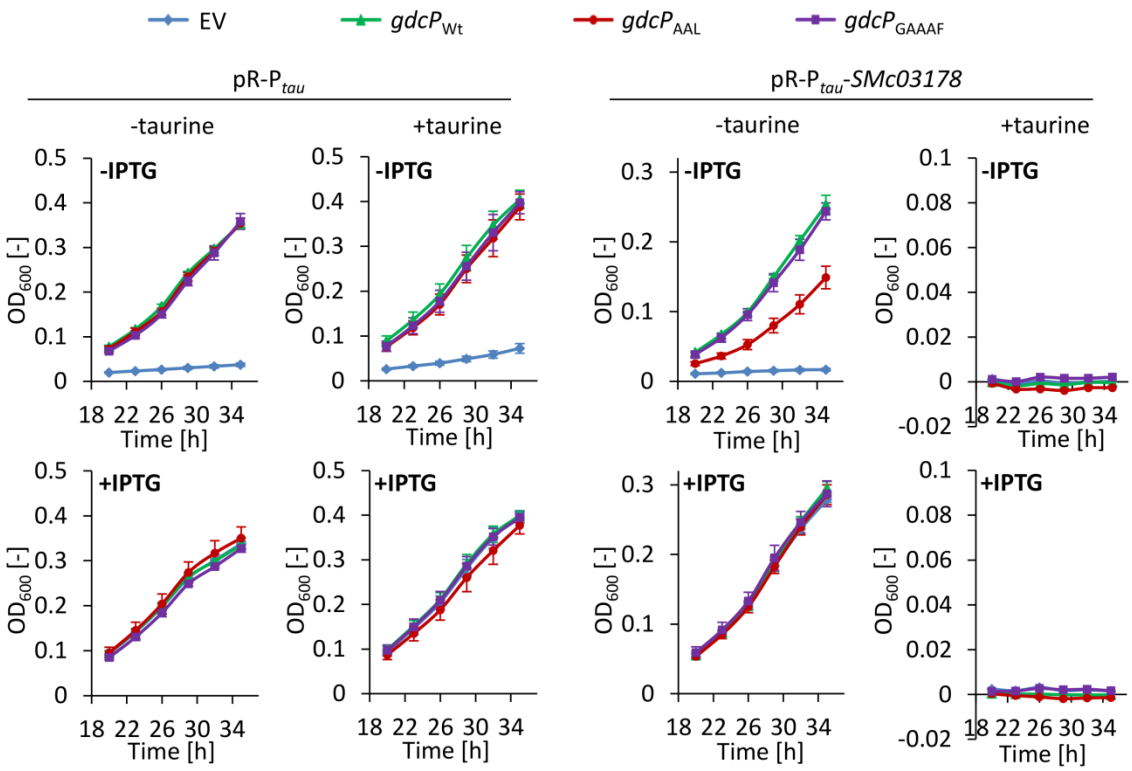

Figure S6. GdcP PDE activity counteracts negative effects of *SMc03178* overexpression on growth of *S. meliloti*. Complementation of the growth defect of GdcP depletion strain Rm2011 GdcP^{dep}, harboring either empty vector pR-P$_{tau}$ or overexpression construct pR-P$_{tau}$-*SMc03178*, by ectopic expression of the indicated *gdcP* variants from *P*$_{gdcP}$*. Error bars represent the standard deviation of three biological replicates. EV, pABC2S-mob.

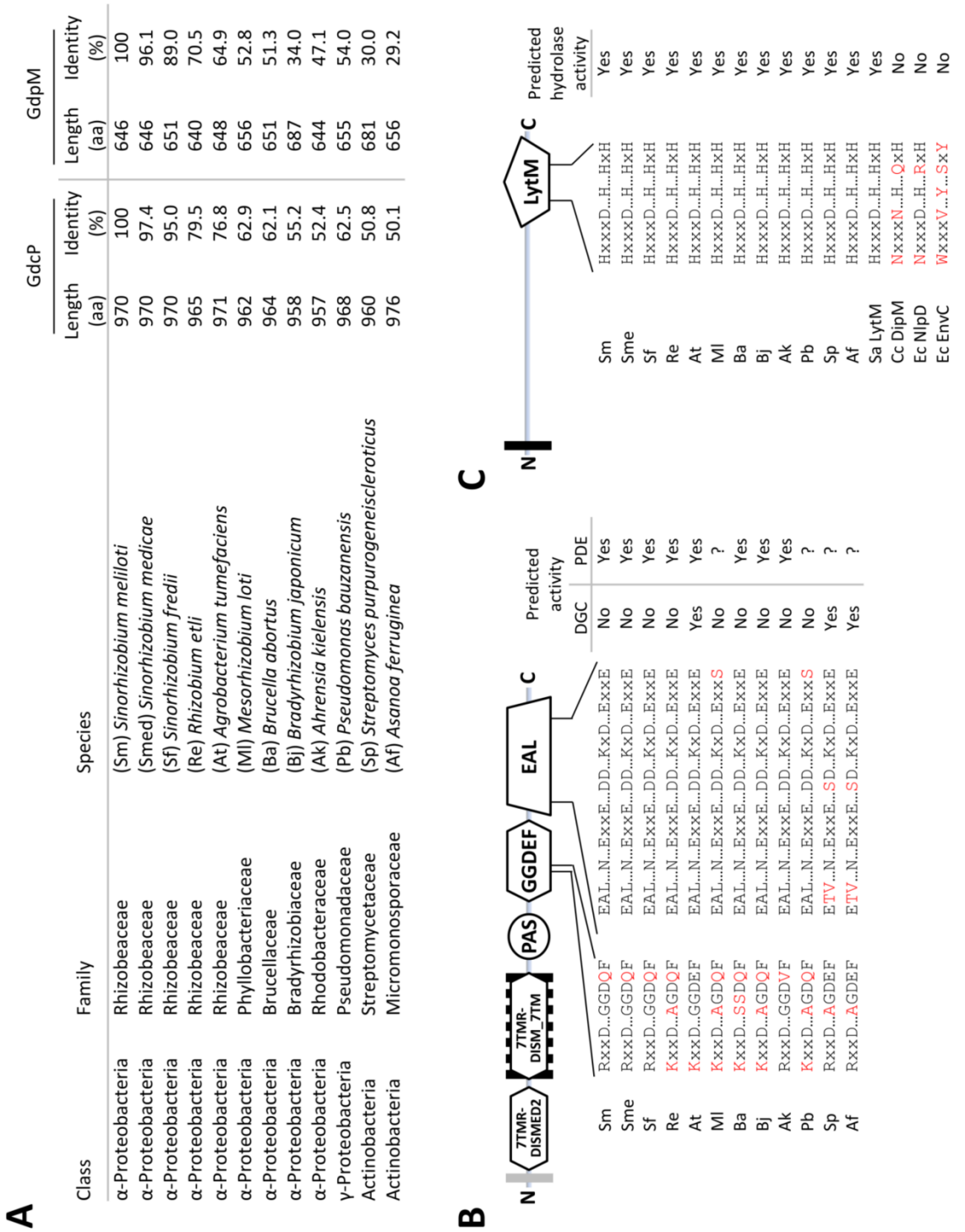

Figure S7. GdcP and GdpM are mainly conserved in related species from the order Rhizobiales. **(A)** BlastP search for GdcP and GdpM sequences revealed homolog proteins in the alphaproteobacterial order Rhizobiales (examples are listed) as well as in three species from the Gammaproteobacteria and Actinobacteria. **(B)** Multiple sequence alignment of GdcP homologs listed in panel A revealed conserved GGDEF and EAL domain motifs (Schirmer & Jenal, 2009; Römling *et al.*, 2013) required for DGC and PDE activity, respectively. Variations of the consensus sequence of GGDEF and EAL active sites are colored in red. **(C)** Multiple sequence alignment of GdpM homologs listed in panel A revealed conserved zinc ion coordination motifs previously identified for *Staphylococcus aureus* (Sa) LytM (Odintsov *et al.*, 2004; Firczuk *et al.*, 2005; Spencer *et al.*, 2010). *Caulobacter crescentus* (Cc) DipM (Möll *et al.*, 2010) and *Escherichia coli* (Ec) NlpD and EnvC (Uehara *et al.*, 2009, 2010) contain variations of the conserved motif, which are colored in red.

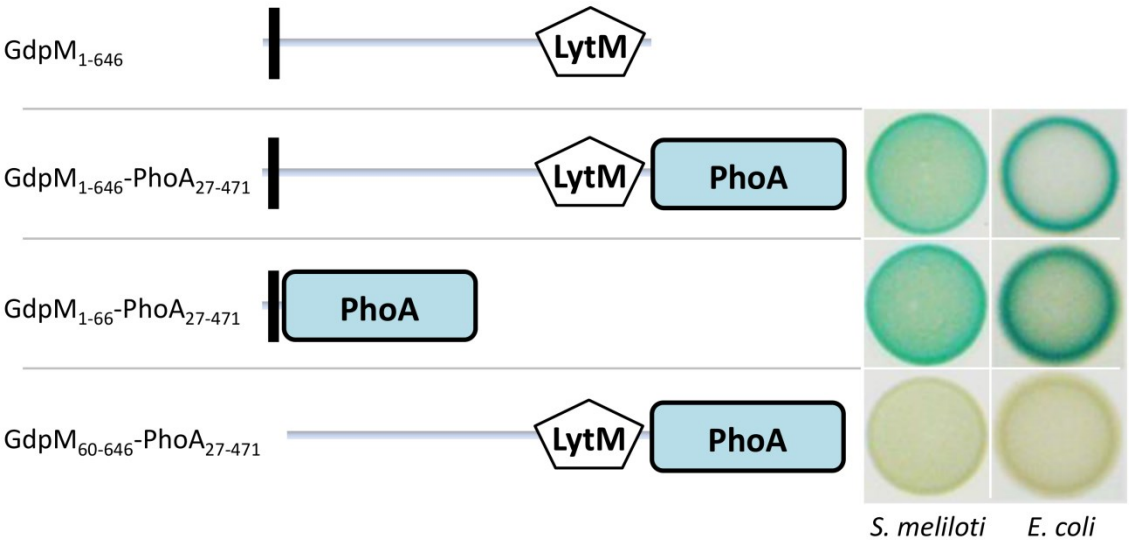

Figure S8. Putative metallopeptidase GdpM is localized in the periplasm. Detection of phosphatase activity indicating periplasmic localization. Protein fusions of full-length or truncated GdpM to $PhoA_{27-471}$ were produced in Rm2011 and *E. coli* S17-1 grown on medium supplemented with PhoA substrate BCIP.

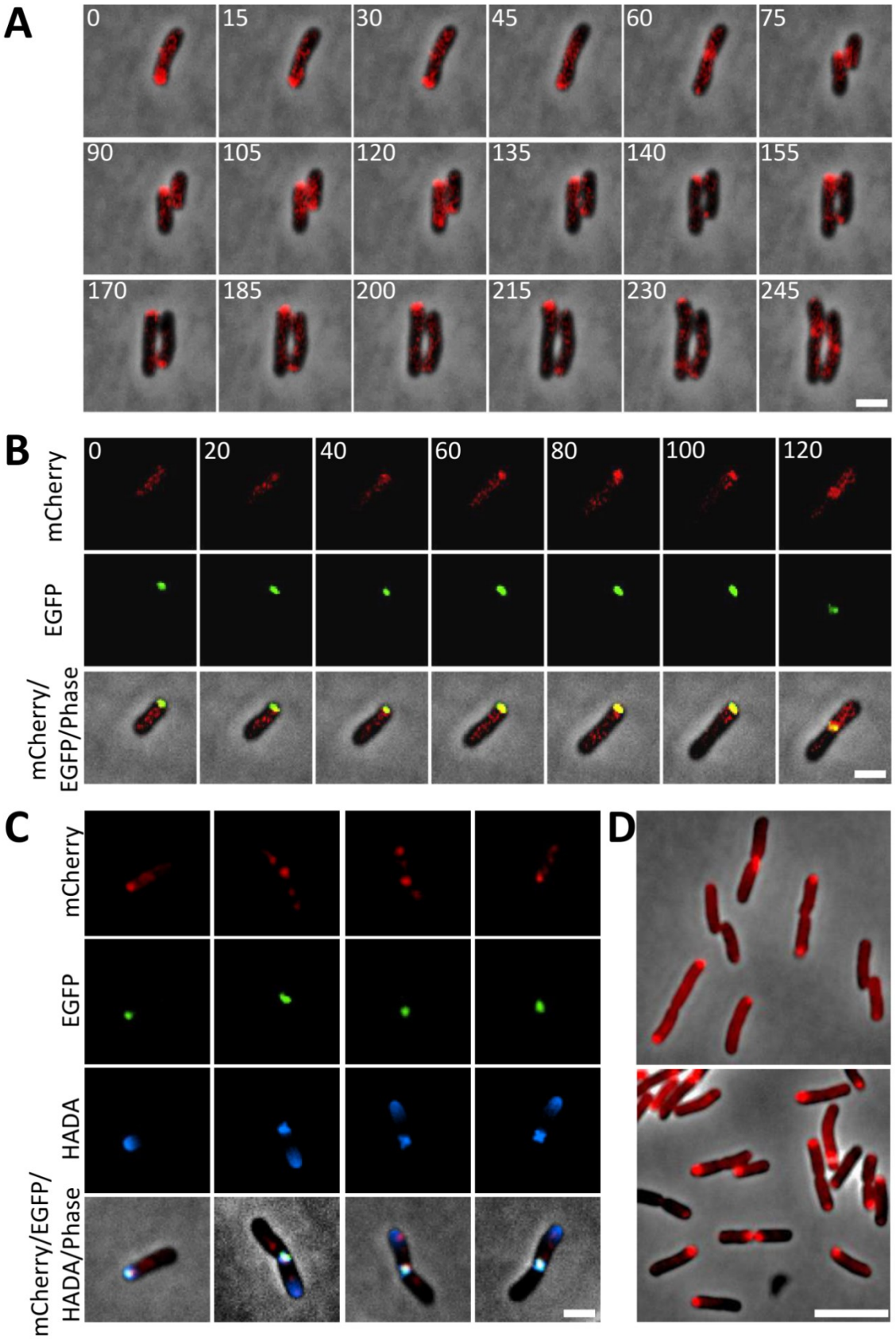

Figure S9. GdpM-mCherry and GdcP-EGFP display a similar subcellular localization pattern during the *S. meliloti* cell cycle. (A, B) Time-lapse microscopy of (A) Rm2011 *gdpM-mCherry* and (B) Rm2011 *gdcP-egfp gdpM-mCherry*. Time is given in minutes. Bars, 1 µm. **(C)** Nascent peptidoglycan synthesis of Rm2011 *gdcP-egfp gdpM-mCherry* exponentially growing in TY medium. Cells were pulse-labeled with blue-fluorescent D-amino acid HADA for 3 min. Bar, 1 µm. **(D)** Microscopic images of *E. coli* S17-1 harboring pSRKGm-*gdpM*-mCherry and cultured in LB medium containing 0.5 mM IPTG for three hours to exponential growth phase. Bar, 5 µm.

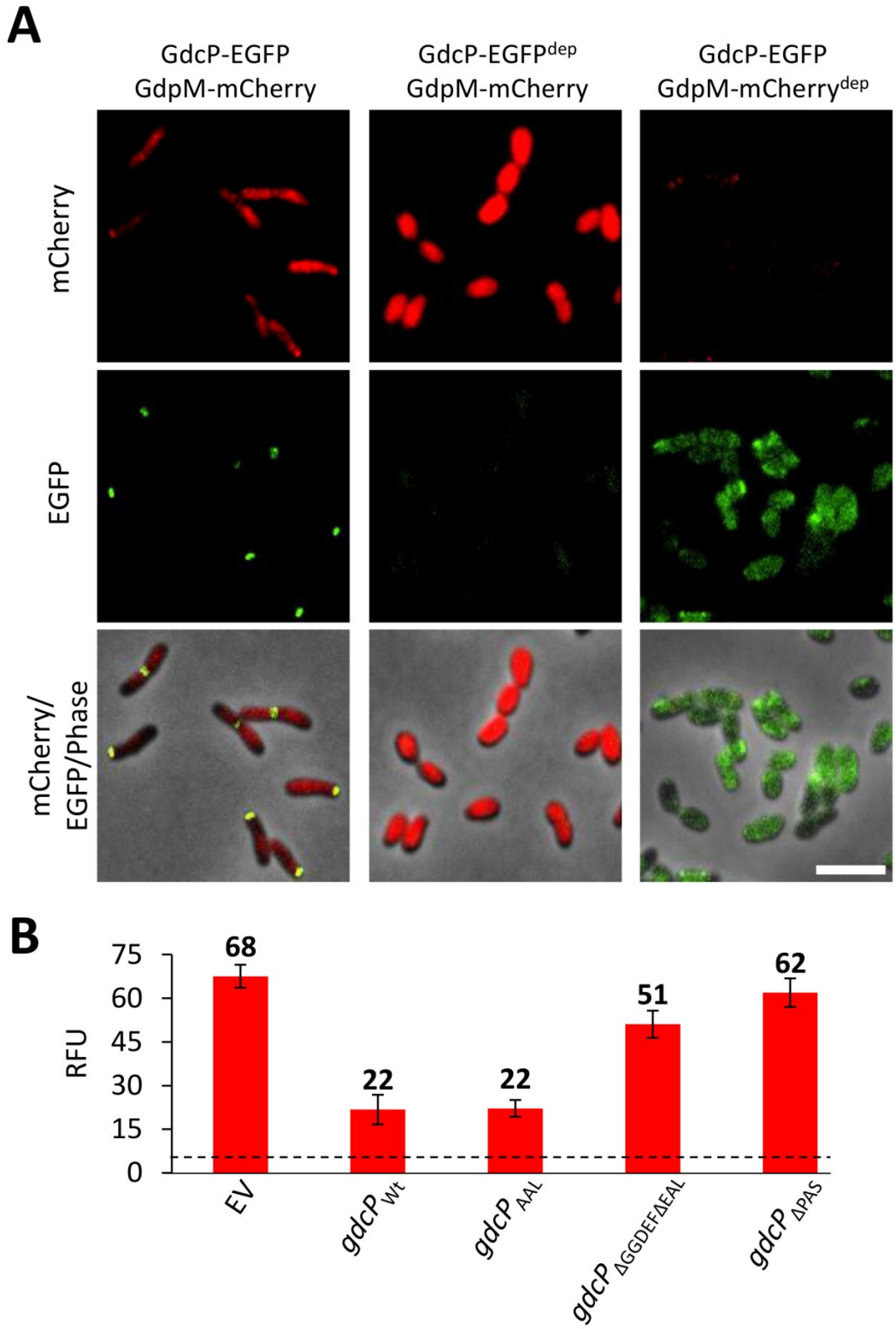

Figure S10. GdcP-EGFP polar localization and native GdpM-mCherry levels are dependent on presence of the interaction partners GdpM-mCherry and GdcP-EGFP, respectively. **(A)** Microscopic images of Rm2011 *gdcP-egfp gdpM-mCherry,* Rm2011 GdcP-EGFP^{dep} *gdpM-mCherry* and Rm2011 *gdcP-egfp* GdpM-mCherry^{dep} grown in TY medium without IPTG for 24 hours. Bar, 5 µm. **(B)** Normalized GdpM-mCherry fluorescence of Rm2011 GdcP-EGFP^{dep} *gdpM-mCherry*, ectopically expressing the indicated *gdcP* variants from P^*_{gdcP}, grown in TY medium without IPTG for 24 hours. Cells were washed and respuspended in 0.9 % NaCl prior to quantification of fluorescence signals. Dashed line indicates background fluorescence produced by Rm2011 GdcP^{dep} carrying no *mCherry* fusion. Error bars represent the standard deviation of three biological replicates. EV, empty vector pABC2S-mob.

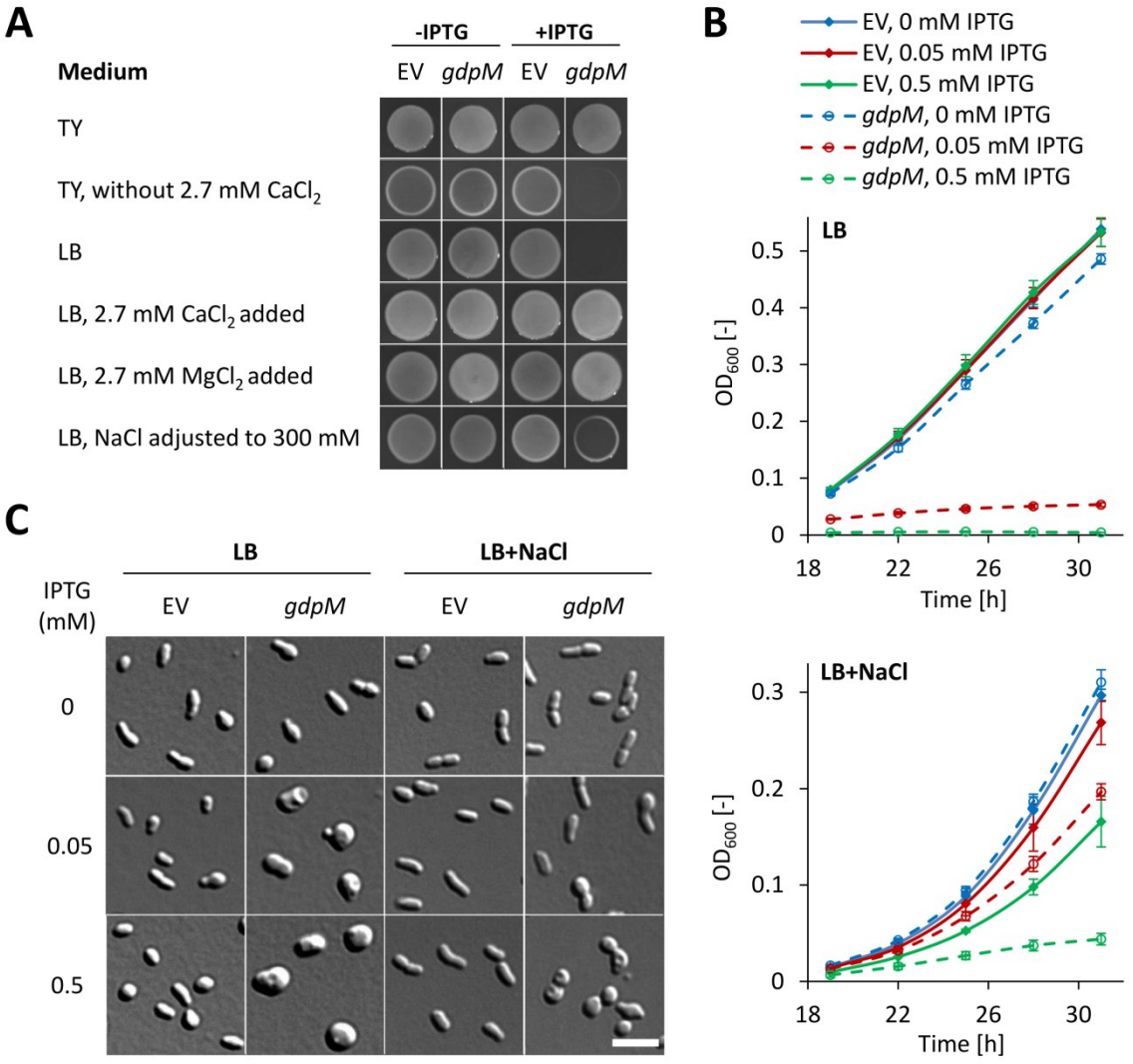

Figure S11. Growth inhibition and cell morphology defects upon *gdpM* overexpression in *S. meliloti* are dependent on medium composition. (A) Rm2011, harboring either empty vector pWBT or pWBT-*gdpM*, grown on solid LB and TY medium supplemented with NaCl, $CaCl_2$ and $MgCl_2$. 0.5 mM IPTG was added where indicated. **(B)** Strains described in panel A grown either in liquid LB medium or in LB medium containing 300 mM NaCl. IPTG was added at the indicated concentrations. OD_{600} was recorded in three-hours intervals. Error bars represent the standard deviations of three biological replicates. **(C)** Cell morphologies were assessed by DIC microscopy for liquid cultures described in panel B. Bar, 5 µm. EV, empty vector pWBT.

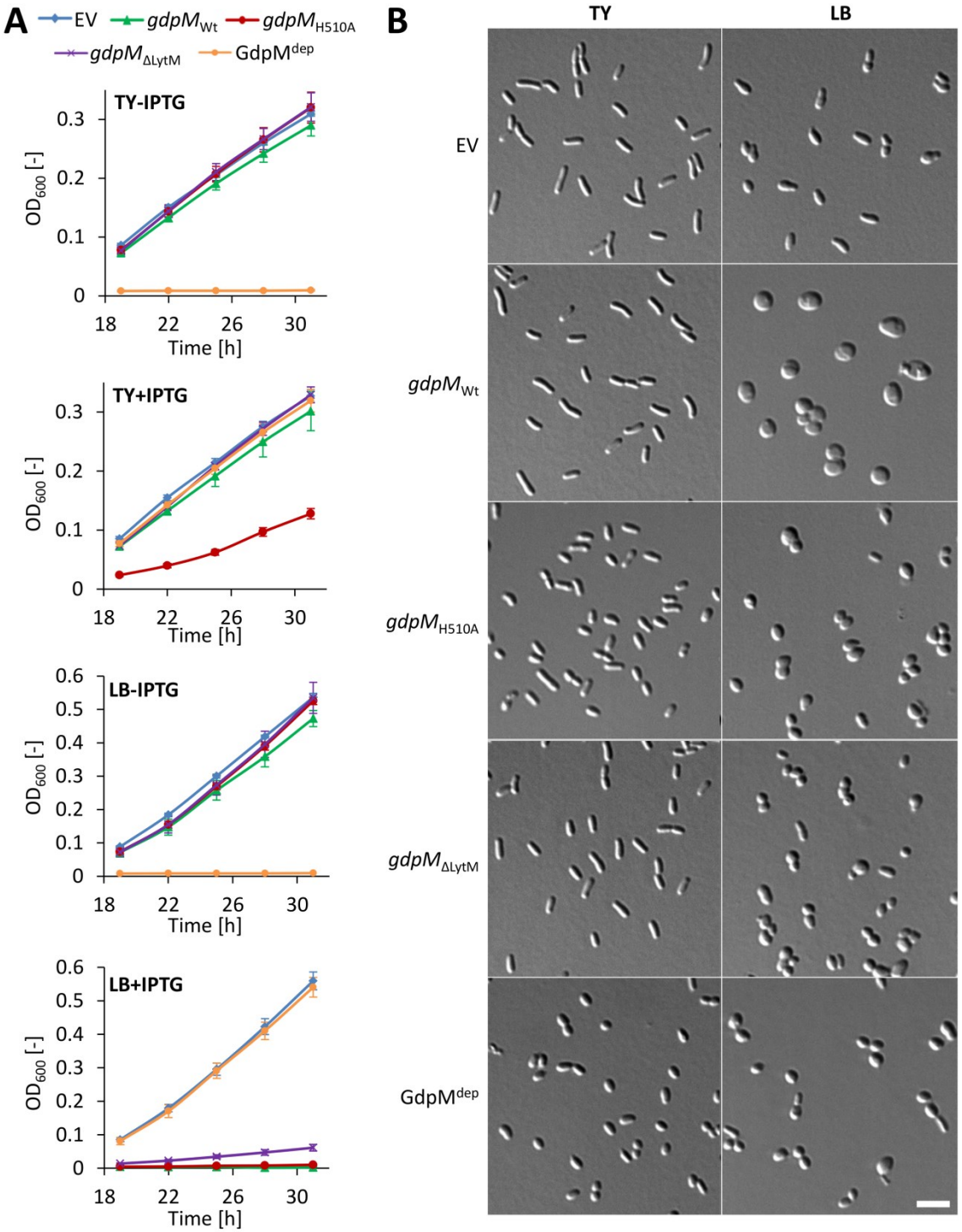

Figure S12. Growth inhibition and cell morphology defects upon overexpression of wild-type *gdpM* and mutant variants in *S. meliloti*. (A) Rm2011, harboring the empty vector pWBT, pWBT-*gdpM,* pWBT-$gdpM_{H510A}$ and pWBT-$gdpM_{\Delta LytM}$, and GdpM depletion strain Rm2011 $GdpM^{dep}$ grown in liquid TY and LB medium in presence or absence of 0.5 mM IPTG. OD_{600} was recorded in three-hours intervals. Error bars represent the standard deviations of three biological replicates. **(B)** Cultures described in panel A were analyzed by DIC microscopy after 24 hours of growth in the indicated medium. 0.5 mM IPTG was added to all cultures except for Rm2011 $GdpM^{dep}$. Bar, 5 µm. EV, empty vector pWBT.

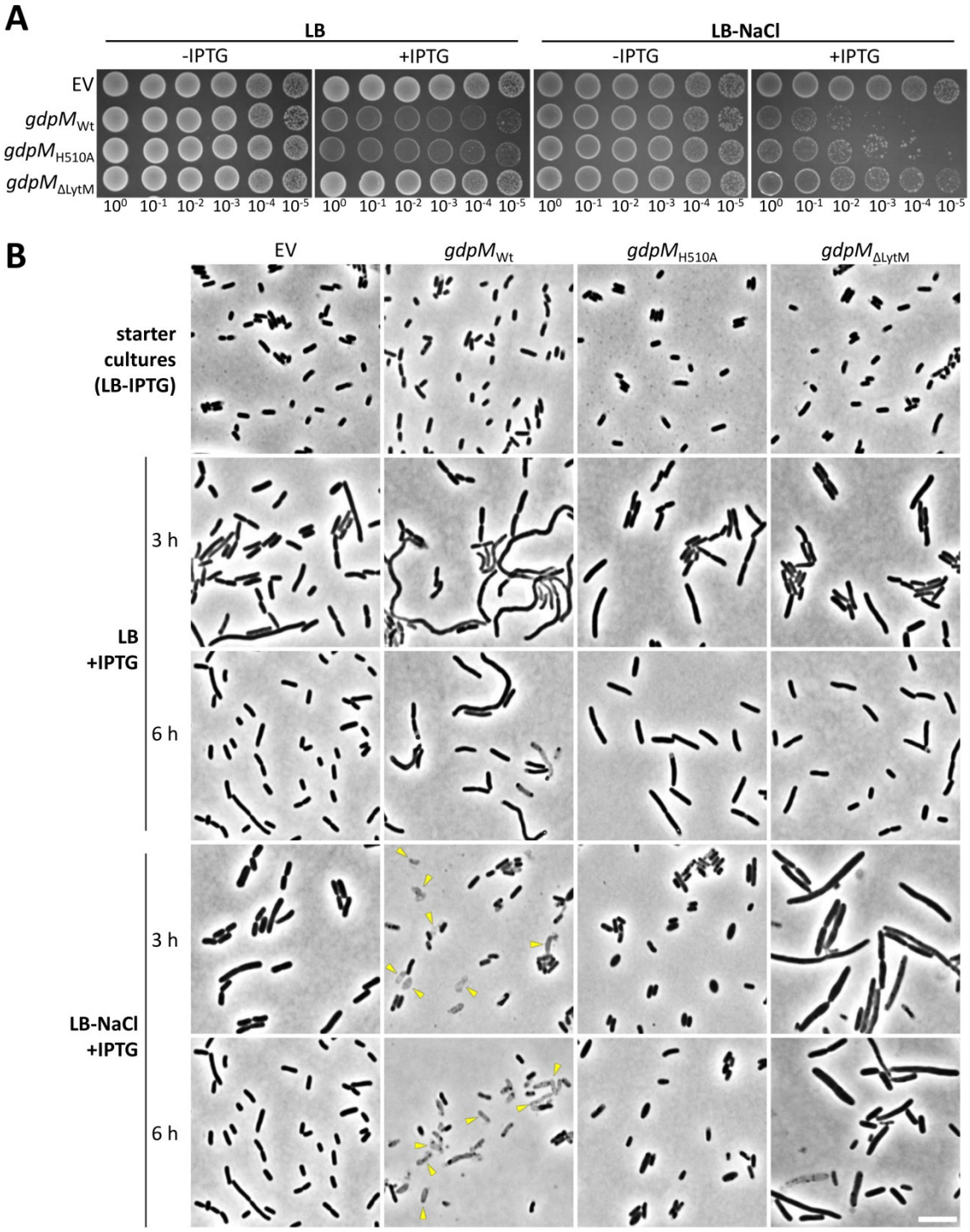

Figure S13. Growth inhibition and cell morphology defects upon overexpression of wild-type *gdpM* and mutant variants in *E. coli*. (A) *E. coli* S17-1, harboring the empty vector pWBT, pWBT-*gdpM,* pWBT-*gdpM*$_{H510A}$ and pWBT-*gdpM*$_{\Delta LytM}$, grown on solid LB medium with or without NaCl in presence or absence of 0.5 mM IPTG. Overnight cultures were OD_{600}-adjusted to 1 and spotted in serial dilutions. **(B)** *E. coli* strains described in panel A were grown in liquid LB medium with or without NaCl and containing 0.5 mM IPTG. Cells were analyzed by phase contrast microscopy at the indicated time points. Lysed cells are indicated by yellow arrow heads. Bar, 5 µm. EV, empty vector pWBT.

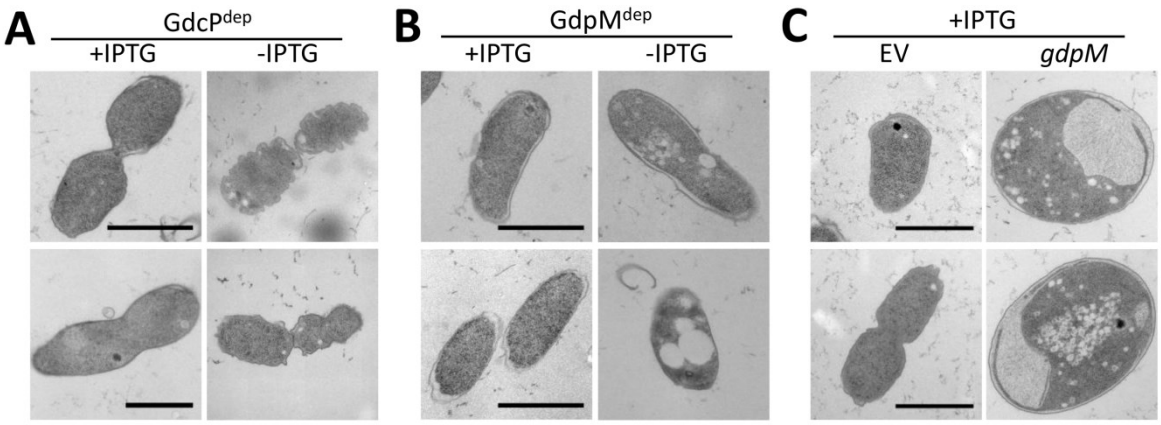

Figure S14. Electron micrographs of *S. meliloti* GdpM and GdcP depletion and overexpression strains. (A-C) Transmission electron microscopy revealed altered cell morphologies of (A) Rm2011 GdcP^{dep} grown in TY medium, (B) Rm2011 GdpM^{dep} grown in TY medium and (C) Rm2011, harboring either empty vector pWBT or pWBT-*gdpM*, grown in LB medium for 24 hours. 0.5 mM IPTG was added to the medium where indicated. Images in the same row of each panel are shown with identical scales. Bars, 1 µm. EV, empty vector pWBT.

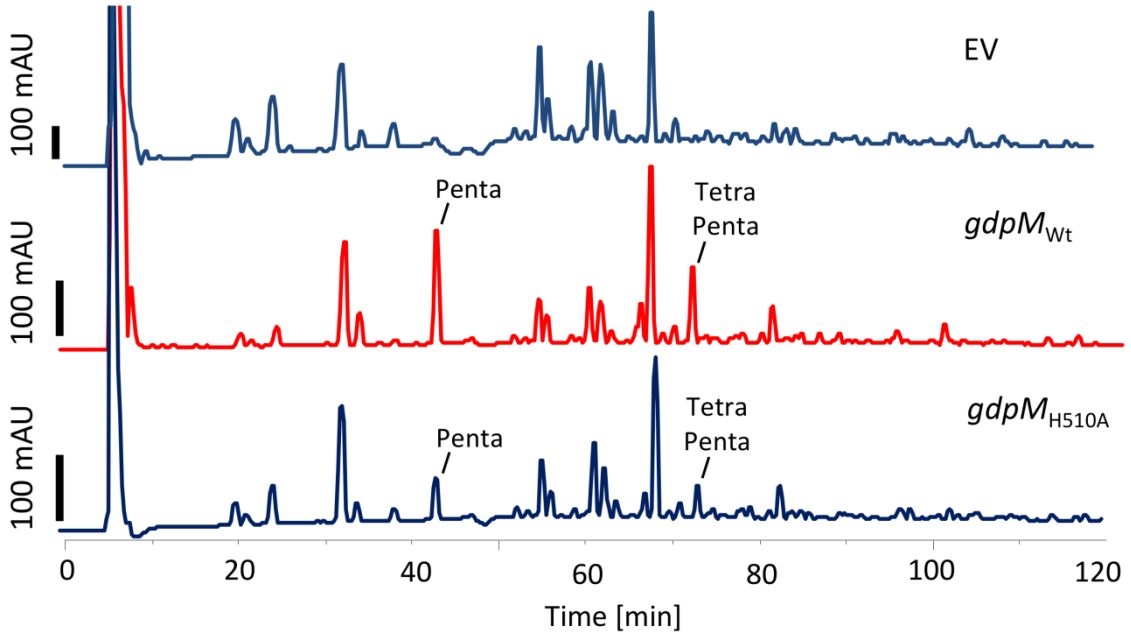

Figure S15. Relative abundances of muropeptides in the *S. meliloti* cell wall change upon overexpression of wild-type *gdpM* and mutant variant *gdpM*$_{H510A}$. Rm2011, harboring either empty vector pWBT, pWBT-*gdpM* or pWBT-*gdpM*$_{H510A}$, was grown in LB medium supplemented with 0.5 mM IPTG for 24 hours. Sacculi were isolated, treated with cellosyl and analyzed by HPLC. Differentially abundant peptides identified by mass spectrometry are indicated. Representative muropeptide profiles of two independent biological replicates per strain are shown. EV, empty vector pWBT.

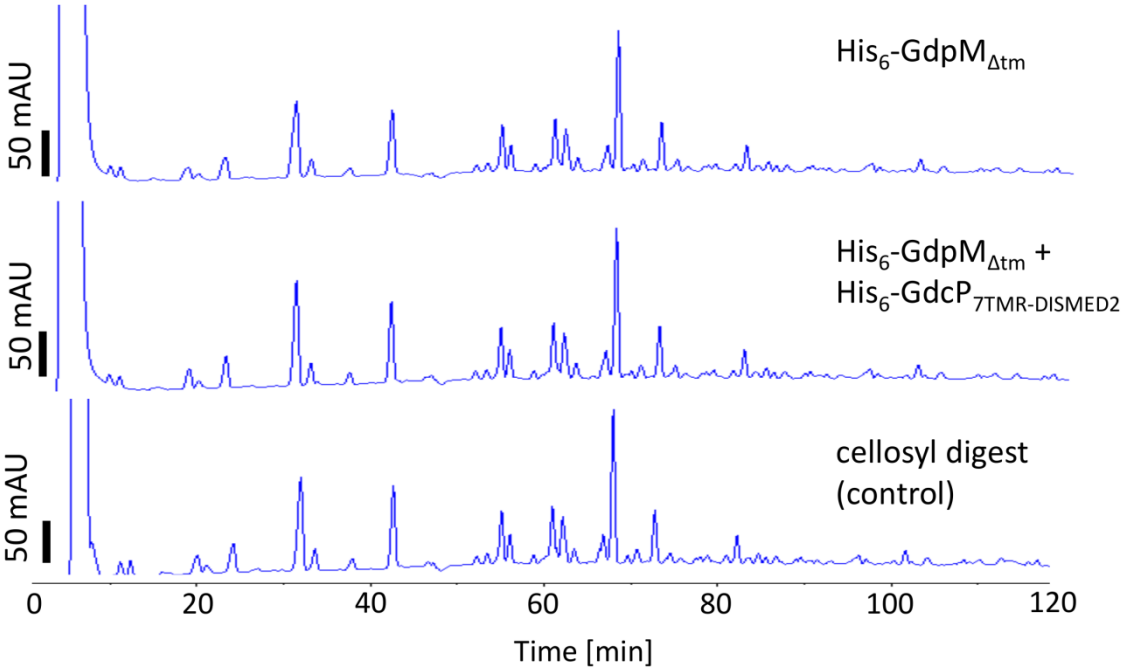

Figure S16. GdpM metallopeptidase activity towards peptidoglycan was absent. Metallopeptidase activity of His_6-$GdpM_{\Delta tm}$ in absence and presence of His_6-$GdcP_{7TMR\text{-}DISMED2}$ was analyzed by pre-incubation of the proteins with various *S. meliloti* PG substrates and subsequent determination of the murein peptide profiles. The control reaction was performed without any added protein.

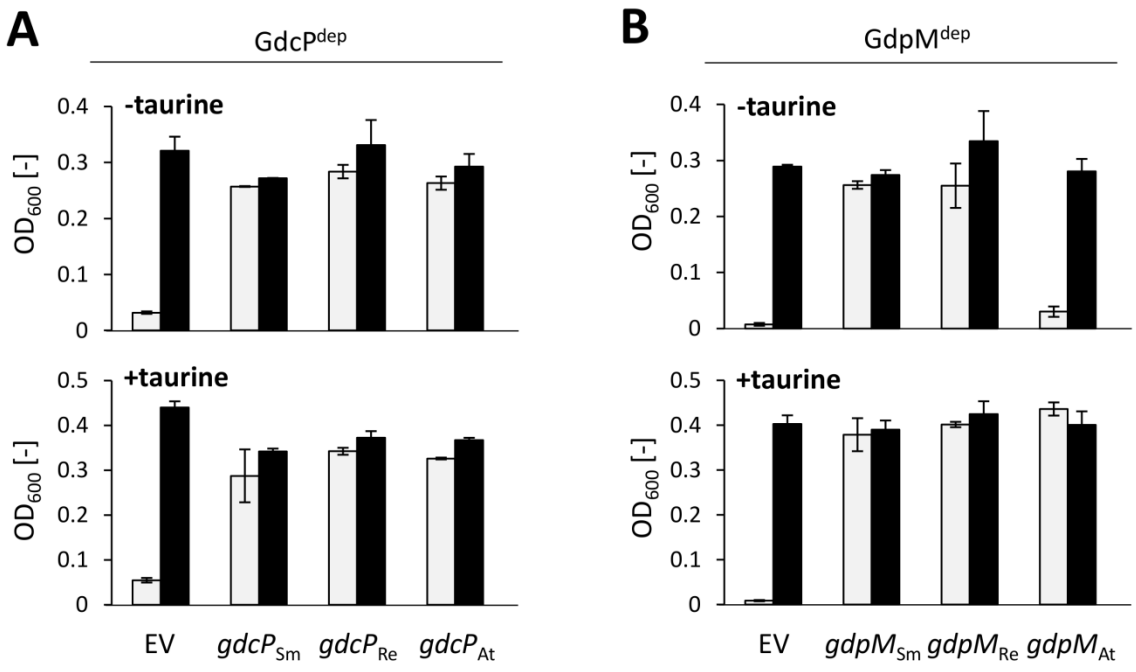

Figure S17. GdcP and GdpM are functionally conserved in alpha-rhizobial species. (A, B) Complementation of the growth defect of GdcP and GdpM depletion strains (A) Rm2011 $GdcP^{dep}$ or (B) Rm2011 $GdpM^{dep}$ by ectopic expression of $gdcP_{Sm}$, $gdcP_{Re}$ and $gdcP_{At}$ or $gdpM_{Sm}$, $gdpM_{Re}$ and $gdpM_{At}$, respectively, from vector pR-P_{tau} in presence or absence of taurine. OD_{600} was recorded after 42 hours of growth in TY medium either with (black bars) or without (white bars) IPTG. Error bars represent the standard deviation of three biological replicates. EV, empty vector pR-P_{tau}; Sm, *Sinorhizobium meliloti*; Re, *Rhizobium etli*; At, *Agrobacterium tumefaciens*.

Table S1. Strains and plasmids used in this study.

Strain	Properties	Reference
S. meliloti		
Rm2011	Wild-type, Str^r	Casse *et al.* (1979)
Rm2011 ΔXVI	Rm2011 containing 16 deletions for GGDEF domain encoding genes; c-di-GMP^0 strain	Schäper *et al.* (2016)
Rm2011 $P_{lac\text{-}T5}$-*gdcP*	Rm2011 *gdcP*::pK18mob2-$P_{lac\text{-}T5}$-*gdcP*, conditional GdcP depletion by introducing *lacI*, Km^r	This work
Rm2011 ΔXVI $P_{lac\text{-}T5}$-*gdcP*	Rm2011 ΔXVI *gdcP*::pK18mob2-$P_{lac\text{-}T5}$-*gdcP*, conditional GdcP depletion by introducing *lacI*, Km^r	This work
Rm2011 P_{lac}-*gdpM*	Rm2011 *gdpM*::pK18mob2-P_{lac}-*gdpM*, conditional GdpM depletion by introducing *lacI*, Km^r	This work
Rm2011 *gdcP-egfp*	Rm2011 expressing *egfp*-tagged *gdcP*, markerless insertion	This work
Rm2011 *gdcP-mCherry*	Rm2011 expressing *mCherry*-tagged *gdcP*, markerless insertion	This work
Rm2011 *gdcP-mCherry pleD-egfp*	Rm2011 *gdcP-mCherry pleD*::pK18mob2-*pleD*-EGFP, Km^r	This work
Rm2011 *gdcP-egfp(Km)*	Rm2011 *gdcP*::pK18mob2-*gdcP*-EGFP, Km^r	This work
Rm2011 $gdcP_{\Delta GGDEF\Delta EAL}$-*egfp*	Rm2011 *gdcP*::pK18mob2-$gdcP_{PAS}$-EGFP, Km^r	This work
Rm2011 GdcP-FLAG	Rm2011 *gdcP*::pG18mob2-*gdcP*-3xFLAG, Gm^r	This work
Rm2011 GdpM-FLAG	Rm2011 *gdpM*::pG18mob2-*gdpM*-3xFLAG, Gm^r	This work
Rm2011 *gdpM-mCherry*	Rm2011 expressing *mCherry*-tagged *gdpM*, markerless insertion	This work
Rm2011 *gdcP-egfp gdpM-mCherry*	Rm2011 *gdcP-egfp* expressing *mCherry*-tagged *gdpM*, markerless insertion	This work
Rm2011 $P_{lac\text{-}T5}$-*gdcP-egfp gdpM-mCherry*	Rm2011 *gdcP-egfp*::pK18mob2-$P_{lac\text{-}T5}$-*gdcP gdpM-mCherry*, conditional GdcP-EGFP depletion by introducing *lacI*, Km^r	This work
Rm2011 *gdcP-egfp* P_{lac}-*gdpM-mCherry*	Rm2011 *gdcP-egfp gdpM-mCherry*::pK18mob2-P_{lac}-*gdpM*, conditional GdpM-mCherry depletion by introducing *lacI*, Km^r	This work
A. tumefaciens		
C58	Wild-type, isolated from a cherry tree (*Prunus*) tumor	Hamilton & Fall (1971)
C58 *Atu0784-egfp*	C58 *Atu0784*::pK18mob2-$gdcP_{At}$-EGFP, Km^r	This work
R. etli		
CFN42	*R. etli* type strain, isolated from *Phaseolus*, Sm^r	Quinto *et al.* (1985)
CFN42 *RHE_CH00976-egfp*	CFN42 *RHE_CH00976*::pK18mob2-$gdcP_{Re}$-EGFP, Km^r	This work
E. coli		
BL21(DE3)	F$^-$ *ompT gal dcm lon* $hsdS_B(r_B^-m_B^-)$ λ(DE3 [*lacI lacUV5-T7p07 ind1 sam7 nin5*]) $[malB^+]_{K\text{-}12}(\lambda^S)$	New England Biolabs
DH5α	F$^-$ *endA1 glnV44 thi-1 recA1 relA1 gyrA96 deoR nupG purB20* φ80d*lacZ*ΔM15 Δ(*lacZYA-argF*)U169, hsdR17($r_K^-m_K^+$), λ$^-$	Grant *et al.* (1990)
S17-1	*E. coli* 294 Thi RP4-2-Tc::Mu-Km::Tn7 integrated into the chromosome	Simon *et al.* (1983)
Plasmids		
pABC2S-mob	variant of mobilizable *repABC*-based mini-replicon, single-copy in *S. meliloti*, Spec^r	Döhlemann *et al.* (2017)
pG18mob2	suicide vector, *lacZ*, *mob*, Gm^r	Schäfer *et al.* (1994)
pK18mob2	suicide vector, *lacZ*, *mob*, Km^r	Schäfer *et al.* (1994)
pK18mob2-EGFP	pK18mob2 carrying *egfp*, *lacZ*, *mob*, Km^r	N. Meier
pK18mobsacB	suicide vector, *lacZ*, *mob*, *sacB*, Km^r	Schäfer *et al.* (1994)
pK19mob2ΩHMB	integrative plasmid carrying a transcription-termination sequence, Km^r	Luo *et al.* (2005)
pR_EGFP	reporter fusion plasmid carrying P_{syn} for constitutive expression, Tc^r	Torres-Quesada *et al.* (2013)
pR-P_{tau}	pR_EGFP carrying the *tauA* promoter from *S. meliloti* in place of P_{syn}, Tc^r	M. Robledo
pSRKGm	pBBR1MCS-5-derived broad-host-range expression vector containing *lac* promoter and $lacI^q$, $lacZ\alpha^+$, Gm^r	Khan *et al.* (2008)
pSRKGm-*parB*-mCherry	pSRKGm carrying *S. meliloti parB* fused to *mCherry*, Gm^r	Schäper *et al.* (2016)
pSRKKm	pBBR1MCS-5-derived broad-host-range expression vector containing *lac* promoter and $lacI^q$, $lacZ\alpha^+$, Km^r	Khan *et al.* (2008)
pSRKKm-EGFP	pSRKKm carrying *egfp*, Km^r	Schäper *et al.* (2016)
pWBT	pSRKGm carrying T5 promoter, Gm^r	M. McIntosh
pWH844	expression vector carrying His6-tag coding sequence and T5 promoter, Amp^r	Schirmer *et al.* (1997)
pG18mob2-3xFLAG	pG18mob2 carrying *3xflag*, Gm^r	This work

Complementation and overexpression constructs		
pDJS31	pET24b(+) carrying *dgcA*^{Wt}, Km^r	Skotnicka *et al.* (2016a)
pDJS30	pET24b(+) carrying *dmxB*^{Wt}, Km^r	Skotnicka *et al.* (2016b)
pWBT-*SMc00074*	pWBT carrying *gdcP (SMc00074)* coding sequence	Schäper *et al.* (2016)
pWBT-*SMc03178*	pWBT carrying *SMc03178* coding sequence	Schäper *et al.* (2016)
pWH844-*SMc00074*$_{390\text{-}970}$	pWH844 carrying *gdcP*(AA$_{390\text{-}970}$)	Schäper *et al.* (2016)
pABC-*gdcP*	pABC2S-mob carrying 944 bp *gdcP* upstream fragment with a stop codon in *rimJ* coding region at position 64, *gdcP* coding region and *egfp*	This work
pABC-*gdcP*$_{\Delta 7TMR\text{-}DISMED2}$	pABC-*gdcP* containing *gdcP*(AA$_{49\text{-}183}$) deletion	This work
pABC-*gdcP*$_{\Delta 7TMR\text{-}DISMED2\Delta 7TMR\text{-}DISM\_7TM}$	pABC-*gdcP* containing *gdcP*(AA$_{49\text{-}363}$) deletion	This work
pABC-*gdcP*$_{\Delta 7TMR\text{-}DISMED2\Delta 7TMR\text{-}DISM\_7TM}$ -EGFP	pABC-*gdcP*$_{\Delta 7TMR\text{-}DISMED2\Delta 7TMR\text{-}DISM\_7TM}$ without *gdcP* stop codon	This work
pABC-*gdcP*$_{\Delta 7TMR\text{-}DISMED2}$-EGFP	pABC-*gdcP*$_{\Delta 7TMR\text{-}DISMED2}$ without *gdcP* stop codon	This work
pABC-*gdcP*$_{\Delta EAL}$	pABC-*gdcP* containing *gdcP*(AA$_{716\text{-}970}$) deletion	This work
pABC-*gdcP*$_{\Delta EAL}$-EGFP	pABC-*gdcP*$_{\Delta EAL}$ without *gdcP* stop codon	This work
pABC-*gdcP*$_{\Delta GGDEF}$	pABC-*gdcP* containing *gdcP*(AA$_{541\text{-}697}$) deletion	This work
pABC-*gdcP*$_{\Delta GGDEF\Delta EAL}$	pABC-*gdcP* containing *gdcP*(AA$_{541\text{-}970}$) deletion	This work
pABC-*gdcP*$_{\Delta GGDEF\Delta EAL}$-EGFP	pABC-*gdcP*$_{\Delta GGDEF\Delta EAL}$ without *gdcP* stop codon	This work
pABC-*gdcP*$_{\Delta GGDEF}$-EGFP	pABC-*gdcP*$_{\Delta GGDEF}$ without *gdcP* stop codon	This work
pABC-*gdcP*$_{\Delta PAS}$	pABC-*gdcP* containing *gdcP*(AA$_{423\text{-}524}$) deletion	This work
pABC-*gdcP*$_{\Delta PAS\Delta GGDEF\Delta EAL}$	pABC-*gdcP* containing *gdcP*(AA$_{417\text{-}970}$) deletion	This work
pABC-*gdcP*$_{\Delta PAS\Delta GGDEF\Delta EAL}$-EGFP	pABC-*gdcP*$_{\Delta PAS\Delta GGDEF\Delta EAL}$ without *gdcP* stop codon	This work
pABC-*gdcP*$_{\Delta PAS}$-EGFP	pABC-*gdcP*$_{\Delta PAS}$ without *gdcP* stop codon	This work
pABC-*gdcP*$_{AAL}$	pABC-*gdcP* containing E746A mutation	This work
pABC-*gdcP*$_{AAL}$-EGFP	pABC-*gdcP*$_{AAL}$ without *gdcP* stop codon	This work
pABC-*gdcP*$_{AxxA}$	pABC-*gdcP* R609A and D612A mutations	This work
pABC-*gdcP*$_{AxxA}$-EGFP	pABC-*gdcP*$_{AxxA}$ without *gdcP* stop codon	This work
pABC-*gdcP*-EGFP	pABC-*gdcP* without *gdcP* stop codon	This work
pABC-*gdcP*$_{GAAAF}$	pABC-*gdcP* containing G619A, D620A and Q621A mutations	This work
pABC-*gdcP*$_{GAAAF}$-EGFP	pABC-*gdcP*$_{GAAAF}$ without *gdcP* stop codon	This work
pR-*gdcP*	pR_EGFP carrying *gdcP* coding sequence and 114 bp *gdcP* upstream region	This work
pR-*gdcP*$_{\Delta 7TMR\text{-}DISMED2}$	pR-*gdcP* containing *gdcP*(AA$_{49\text{-}183}$) deletion	This work
pR-*gdcP*$_{\Delta 7TMR\text{-}DISMED2\Delta 7TMR\text{-}DISM\_7TM}$	pR-*gdcP* containing *gdcP*(AA$_{49\text{-}363}$) deletion	This work
pR-*gdcP*$_{\Delta EAL}$	pR-*gdcP* containing *gdcP*(AA$_{716\text{-}970}$) deletion	This work
pR-*gdcP*$_{\Delta GGDEF}$	pR-*gdcP* containing *gdcP*(AA$_{541\text{-}697}$) deletion	This work
pR-*gdcP*$_{\Delta GGDEF\Delta EAL}$	pR-*gdcP* containing *gdcP*(AA$_{541\text{-}970}$) deletion	This work
pR-*gdcP*$_{\Delta PAS}$	pR-*gdcP* containing *gdcP*(AA$_{423\text{-}524}$) deletion	This work
pR-*gdcP*$_{\Delta PAS\Delta GGDEF\Delta EAL}$	pR-*gdcP* containing *gdcP*(AA$_{423\text{-}970}$) deletion	This work
pR-*gdcP*$_{AAL}$	pR-*gdcP* containing E746A mutation	This work
pR-*gdcP*$_{AxxA}$	pR-*gdcP* containing R609A and D612A mutations	This work
pR-*gdcP*$_{GAAAF}$	pR-*gdcP* containing G619A, D620A and Q621A mutations	This work
pR-P$_{tau}$-*gdcP*$_{At}$	pR-P$_{tau}$ carrying *Atu0784* coding sequence	This work
pR-P$_{tau}$-*gdcP*$_{Re}$	pR-P$_{tau}$ carrying *RHE_CH00976* coding sequence	This work
pR-P$_{tau}$-*gdcP*$_{Sm}$	pR-P$_{tau}$ carrying *gdcP* coding sequence	This work
pR-P$_{tau}$-*gdpM*$_{At}$	pR-P$_{tau}$ carrying *Atu4178* coding sequence	This work
pR-P$_{tau}$-*gdpM*$_{Re}$	pR-P$_{tau}$ carrying *RHE_CH03752* coding sequence	This work
pR-P$_{tau}$-*gdpM*$_{Sm}$	pR-P$_{tau}$ carrying *gdpM* coding sequence	This work
pR-P$_{tau}$-*SMc03178*	pR-P$_{tau}$ carrying *SMc03178* coding sequence	This work
pR-P$_{tau}$-*SMc03178*$_{GGAAF}$	pR-P$_{tau}$-*SMc03178* containing D531A and E532A mutations	This work
pSRKGm-*gdpM*-mCherry	pSRKGm carrying *gdpM* fused to *mCherry*, Gm^r	This work
pSRKKm-*gdpM*$_{1\text{-}646}$-*phoA*	pSRKKm carrying *gdpM*(AA$_{1\text{-}646}$) fused to *phoA*$_{Ec}$(AA$_{27\text{-}471}$)	This work
pSRKKm-*gdpM*$_{1\text{-}66}$-*phoA*	pSRKKm carrying *gdpM*(AA$_{1\text{-}66}$) fused to *phoA*$_{Ec}$(AA$_{27\text{-}471}$)	This work
pSRKKm-*gdpM*$_{60\text{-}646}$-*phoA*	pSRKKm carrying *gdpM*(AA$_{60\text{-}646}$) fused to *phoA*$_{Ec}$(AA$_{27\text{-}471}$)	This work
pWBT-*gdcP*$_{AAL}$	pWBT-*SMc00074* containing E746A mutation	This work
pWBT-*gdcP*$_{GAAAF}$	pWBT-*SMc00074* containing G619A, D620A and Q621A mutations	This work
pWBT-*gdpM*	pWBT carrying *gdpM* coding sequence	This work
pWBT-*gdpM*$_{\Delta LytM}$	pWBT-*gdpM* containing *gdpM*(AA$_{480\text{-}646}$) deletion	This work
pWBT-*gdpM*$_{H510A}$	pWBT-*gdpM* containing H510A mutation	This work
pWH844-*gdcP*$_{7TMR\text{-}DISMED2}$	pWH844 carrying *gdcP*(AA$_{38\text{-}194}$)	This work
pWH844-*gdcP*$_{PAS\text{-}GGDEF}$	pWH844 carrying *gdcP*(AA$_{390\text{-}715}$)	This work
pWH844-*gdcP*$_{PAS\text{-}GGDEF\text{-}EAL}$-AAL	pWH844-*SMc00074*$_{390\text{-}970}$ containing E746A mutation	This work
pWH844-*gdpM*$_{\Delta tm}$	pWH844 carrying *gdpM*(AA$_{57\text{-}646}$)	This work
Promoter-*egfp* fusion plasmids		
pSRKKm-P$_{gdcP}$-*egfp*	pSRKKm-EGFP carrying *gdcP* upstream fragment	This work
pSRKKm-P$_{rimJ}$-P$_{gdcP}$-*egfp*	pSRKKm-EGFP carrying *rimJ* and *gdcP* upstream fragment	This work

Integrative plasmids		
pK18mob2-*pleD*-EGFP	pK18mob2-EGFP carrying 3' portion of *pleD*	Schäper *et al.* (2016)
pG18mob2-*gdcP*-3xFLAG	pG18mob2-3xFLAG carrying 3' portion of *gdcP*	This work
pG18mob2-*gdpM*-3xFLAG	pG18mob2-3xFLAG carrying 3' portion of *gdpM*	This work
pK18mob2-$gdcP_{At}$-EGFP	pK18mob2-EGFP carrying 3' portion of *Atu0784*	This work
pK18mob2-*gdcP*-EGFP	pK18mob2-EGFP carrying 3' portion of *gdcP*	This work
pK18mob2-$gdcP_{PAS}$-EGFP	pK18mob2-EGFP carrying internal portion of *gdcP*	This work
pK18mob2-$gdcP_{Re}$-EGFP	pK18mob2-EGFP carrying 3' portion of *RHE_CH00976*	This work
pK18mob2-P_{lac}-*gdpM*	pK18mob2 carrying 5' portion of *gdpM*	This work
pK18mob2-$P_{lac\text{-}T5}$-*gdcP*	pK18mob2 carrying T5 promoter, a Shine-Dalgarno sequence and 5' portion of *gdcP*	This work
pK18mobsacB-*gdcP*-EGFP	pK18mobsacB carrying 3' portion of *gdcP* excluding the stop codon, *egfp* and *gdcP* downstream fragment	This work
pK18mobsacB-*gdcP*-mCherry	pK18mobsacB carrying 3' portion of *gdcP* excluding the stop codon, *mCherry* and *gdcP* downstream fragment	This work
pK18mobsacB-*gdpM*-mCherry	pK18mobsacB carrying 3' portion of *gdpM* excluding the stop codon, *mCherry* and *gdcP* downstream fragment	This work
pK19mob2ΩHMB-*gdpM*	pK19mob2ΩHMB carrying internal portion of *gdpM*	This work

Table S2. Primers used in this study.

Primer	Sequence	Purpose
PrimJ_NotI_fwd	ATATGCGGCCGCTGAACGACATATTGTCCTCGCTGA	Construction of **pABC-*gdcP*$_{\Delta PAS\Delta GGDEF\Delta EAL}$-EGFP**; amplification of P*rimJ*-P*gdcP*-*gdcP*(AA_{1-414})
smc00074_1243_Van91I_rev	ATATCCAGCGCCTGGCGCTCGAGAT	
rimJ_51_stop_fwd	TGACATTATCTGCTCCGCCTCCC	Construction of **pABC-*gdcP*$_{\Delta PAS\Delta GGDEF\Delta EAL}$-EGFP**; *rimJ* stop codon insertion at position 64
rimJ_51_stop_rev2	GGGAGGCGGAGCAGATAATGTCACTGGCTGGCGATCTCGAC	
EGFP-Van91I-KpnI_fwd	ATATCCAGGCGCTGGCGCTGGGTACCAGCAAGGGCGAGGAGCTGTT	Construction of **pABC-*gdcP*$_{\Delta PAS\Delta GGDEF\Delta EAL}$-EGFP**; amplification of *egfp*
EGFP-ScaI_rev	ATATAGTACTTTACTTGTACAGCTCGTCCATGC	
EGFP-Van91I-Stop-KpnI_fwd	ATATCCAGGCGCTGGCGCTGTGAGGTACCAGCAAGGGCGAGGAGCTGTT	Construction of **pABC-*gdcP*$_{\Delta PAS\Delta GGDEF\Delta EAL}$**; amplification of *egfp*
smc00074_1243_Van91I_fwd	ATATCCAGGCGCTGGCGCTCAC	Construction of **pABC-*gdcP***; amplification of *gdcP*($AA_{415-970}$)
smc00074+stop_KpnI_rev	ATATGGTACCTCAAGCCCGCTTCATCAGCGGAAAT	
smc00074-nostop_KpnI_rev	ATATGGTACCAGCCCGCTTCATCAGCGGAAAT	Construction of **pABC-*gdcP*-EGFP**; amplification of *gdcP*($AA_{415-970}$)
smc00074GGDEF+stop_KpnI_rev	ATATGGTACCTCATTCGAGCTGTAGGCGGTCC	Construction of **pABC-*gdcP*$_{\Delta EAL}$**; amplification of *gdcP*($AA_{415-715}$)
smc00074GGDEF-nostop_KpnI_rev	ATATGGTACCTTCGAGCTGTAGGCGGTCC	Construction of **pABC-*gdcP*$_{\Delta EAL}$-EGFP**; amplification of *gdcP*($AA_{415-715}$)
smc00074PAS+stop_KpnI_rev	ATATGGTACCTCACAGAAGCGCGTTGTGCAA	Construction of **pABC-*gdcP*$_{\Delta GGDEF\Delta EAL}$**; amplification of *gdcP*($AA_{415-540}$)
smc00074PAS-nostop_KpnI_rev	ATATGGTACCCAGAAGCGCGTTGTGCAA	Construction of **pABC-*gdcP*$_{\Delta GGDEF\Delta EAL}$-EGFP**; amplification of *gdcP*($AA_{415-540}$)
smc00074_E>A-f	GCGGCCCTCATGCGCTGGGA	Generation of *gdcP*$_{AAL}$ (E746A)
smc00074_E>A-r	AGCGCATGAGGGCCGCGAAGCCGGCGATCTCGGCAT	
smc00074_GGDQF>GAAAF_f	GCCGCGGCCTTCGGCTTGATCCTCATGT	Generation of *gdcP*$_{GAAAF}$ (G619A, D620A, Q621A)
smc00074_GGDQF>GAAAF_r	AGGATCAAGCCGAAGGCCGCGGCGCCAAGACGCGCGAGCGT	
smc00074_Isite>AxxA_f	GCCCCGCAGGCCACGCTCGCGCGTCTTGGC	Generation of *gdcP*$_{AxxA}$ (R609A, D612A)
smc00074_Isite>AxxA_r	ACGCGCGAGCGTGGCCTGCGGGGCCAGAAGCCTGCGCAGGCG	
smc00074_GGDEF-del_f	GAGCCGTTCCGTCCGGCTTT	Generation of *gdcP*$_{\Delta GGDEF}$ ($\Delta AA_{541-697}$)
smc00074_GGDEF-del_r	GACGGAACGGCTCCAGAAGCGCGTTGTGCAA	
smc00074_PAS-del_f	ACCGAACAGCGCAATTCG	Generation of *gdcP*$_{\Delta PAS}$ ($\Delta AA_{423-524}$)
smc00074_PAS-del_r	TGCGCTGTTCGGTGGTATCGCCTGATCCCGTGA	
smc00074-full_-100_Bam_f	ATATGGATCCTGAGCGTGAAGGCTATTTGAGA	Construction of **pR-*gdcP***; amplification of *gdcP*(AA_{1-970}) including 114 bp upstream region
smc00074-full-Xba_r	ATATTCTAGATCAAGCCCGCTTCATCAG	
smc00074_EAL-del_Xba_r	ATATTCTAGATCATTCGAGCTGTAGGCGGT	Construction of **pR-*gdcP*$_{\Delta EAL}$**; amplification of *gdcP*(AA_{1-715}) including 114 bp upstream region
smc00074_GGDEF-EAL-del_Xba_r	ATATTCTAGATCACAGAAGCGCGTTGTG	Construction of **pR-*gdcP*$_{\Delta GGDEF\Delta EAL}$**; amplification of *gdcP*(AA_{1-540}) including 114 bp upstream region
smc00074_PAS-GGDEF-EAL-del_Xba_r	ATATTCTAGATCAGGTATCGCCTGATCCC	Construction of **pR-*gdcP*$_{\Delta PASGGDEF\Delta EAL}$**; amplification of *gdcP*(AA_{1-422}) including 114 bp upstream region
smc00074_DISMED2-del_f	GACGCCTACAAGGATACCGT	Generation of *gdcP*$_{\Delta 7TMR\text{-}DISMED2}$ (ΔAA_{49-183})
smc00074_DISMED2-del_r	TCCTTGTAGGCGTCCGCCGTGTCCTCGCGCGA	
smc00074_DISM-6TM-del_f	ACCGGTCAACTCGCCAAT	Generation of *gdcP*$_{\Delta 7TMR\text{-}DISMED2\Delta 7TMR\text{-}DISM\_7TM}$ (ΔAA_{49-363})
smc00074_DISM-6TM-del_r	CGAGTTGACCGGTCGCCGTGTCCTCGCGCGA	
smc03178-TIR-RBS_Bam_fwd	ATATGGATCCTGATTAACTTTATAAGGAGGAAAAACATATGTCCCCTCTGTCGCGCTTTCTC	Construction of **pR-P$_{tau}$-*SMc03178***; amplification of full length *SMc03178*
smc03178-Xba_rev	ATATTCTAGATCAGGCGGCGCGCCACCG	
smc03178_GGAAF_fwd	GCCGCCTTCGTCATCATTCGCGCAAGCG	Generation of *SMc03178*$_{GGAAF}$ (D531A, E532A)
smc03178_GGAAF_rev	CGCGAATGATGACGAAGGCGGCGCCGCCGATGCGGGCGAC	

smc00074-390_Bam_fwd	ATATGGATCCACCGTCATGCAGCACGCCTTTT	Construction of **pWH844-GdcP$_{PAS-GGDEF-EAL}$-AAL**; amplification of *gdcP*(AA$_{390-970}$)
smc00074_Sal_rev	ATATGTCGACTCAAGCCCGCTTCATCAG	
smc00074-715_Sal_rev	ATATGTCGACTCATTCGAGCTGTAGGCGGTCC	Construction of **pWH844-GdcP$_{PAS-GGDEF}$**; amplification of *gdcP*(AA$_{390-715}$)
smc00074-38_Bam_fwd	ATATGGATCCGAGCCGGTGAAGATCTCG	Construction of **pWH844-*gdcP*$_{7TMR-DISMED2}$**; amplification of *gdcP*(AA$_{38-194}$)
smc00074-194_+stop_SalI_rev	ATATGTCGACTCAGGTGAAGGCGTTGACGGTAT	
smc02432_57_Xho_fwd	ATATCTCGAGCTCGACGGCCGGCAGCAACT	Construction of **pWH844-*gdpM*$_{\Delta tm}$**; amplification of *gdpM*(AA$_{57-646}$)
smc02432_Pst_rev	ATATCTGCAGCTACTTGCTTGCGACCTCGTT	
smc02432-full-Xba-f	ATATTCTAGAATGAGCAGCGATAAGAACATGC	Construction of **pWBT-*gdpM***; amplification of *gdpM*(AA$_{1-646}$)
smc02432-full-Kpn-r	ATATGGTACCCTACTTGCTTGCGACCTCGTT	
smc00074-TIR-RBS_Bam_f	ATATGGATCCTGATTAACTTTATAAGGAGGAAAAACATATGCCCCTGACCCGTAAGC	Construction of **pR-P$_{tau}$-*gdcP*$_{Sm}$**; amplification of full-length *S. meliloti* Rm2011 *gdcP (SMc00074)*
RHE_CH00976-TIR-RBS_Bam_f	ATATGGATCCTGATTAACTTTATAAGGAGGAAAAACATATGCTGCCCAAGTCACCGT	Construction of **pR-P$_{tau}$-*gdcP*$_{Re}$**; amplification of full-length *R. etli* CFN42 *gdcP (RHE_CH00976)*
RHE_CH00976-full_Xba_r	ATATTCTAGATCAGGCCCTTTTCGTCAGCG	
Atu0784-TIR-RBS_Bam_f	ATATGGATCCTGATTAACTTTATAAGGAGGAAAAACATATGACCTACAATCACACTGCGCC	Construction of **pR-P$_{tau}$-*gdcP*$_{At}$**; amplification of full-length *A. tumefaciens* C58 *gdcP (Atu0784)*
Atu0784-full_Xba_r	ATATTCTAGATCAAGACGCCCGCTTCGT	
smc02432-full-X-r	ATATTCTAGACTACTTGCTTGCGACCTCGTT	Construction of **pR-P$_{tau}$-*gdpM*$_{Sm}$**; amplification of full-length *S. meliloti* Rm2011 *gdpM (SMc02432)*
RHE_CH03752-TIR-RBS_Xba_f	ATATTCTAGATGATTAACTTTATAAGGAGGAAAAACATATGATCCGCTCGCTGGGCAA	Construction of **pR-P$_{tau}$-*gdpM*$_{Re}$**; amplification of full-length *R. etli* CFN42 *gdpM (RHE_CH03752)*
RHE_CH03752-full_Xba_r	ATATTCTAGATTATTTGCTCGCCACCTGATCG	
Atu4178-TIR-RBS_Bam_f	ATATGGATCCTGATTAACTTTATAAGGAGGAAAAACATATGACTGCGGATCGCAATGT	Construction of **pR-P$_{tau}$-*gdpM*$_{At}$**; amplification of full-length *A. tumefaciens* C58 *gdpM (Atu4178)*
Atu4178-full_Xba_r	ATATTCTAGATCAGCGGCTCGCCACCTGAT	
Psmc00074_Hind_fwd	ATATAAGCTTCGGCGCTGCGCAGAACTG	Construction of **pSRKKm-P$_{gdcP}$-*egfp***
Psmc00074_Xba_rev	ATATTCTAGACAGGGGCATCAAAGGGGCAAAT	
PrimJ_Hind_fwd	ATATAAGCTTTGAACGACATATTGTCCTCGCTGA	Construction of **pSRKKm-P$_{rimJ}$-P$_{gdcP}$-*egfp***
Smc00074-C-SalI-fwd	ATATGTCGACTTTCCCTCGTATACCAGCCCA	Construction of **pK18mob2-*gdcP*-EGFP**
Smc00074-C-XbaI-rev	ATATTCTAGAAGCCCGCTTCATCAGCGGAA	
smc00074_1167_Hind_f	ATATAAGCTTACCGTCATGCAGCACGCCTTTT	Construction of **pK18mob2-*gdcP*$_{PAS}$-EGFP**
smc00074_1620_Xba_r	ATATTCTAGACAGAAGCGCGTTGTGCAA	
RHE_CH00976-C_Hind_f	ATATAAGCTTCAGCTCGAAACCGATCTGCG	Construction of **pK18mob2-*gdcP*$_{Re}$-EGFP**
RHE_CH00976-C_Xba_r	ATATTCTAGAGGCCCTTTTCGTCAGCGGAAA	
Atu0784-C_Sal_f	ATATGTCGACGCAAGGAGCTGTCCCTCGCCTAT	Construction of **pK18mob2-*gdcP*$_{At}$-EGFP**
Atu0784-C_Xba_r	ATATTCTAGAAGACGCCCGCTTCGTCGG	
smc02432_H510A_fwd	GCCACCGGCGTCGACTGGTCC	Generation of *gdpM*$_{H510A}$
smc02432_H510A_rev	GACCAGTCGACGCCGGTGGCCATGCGCGAGAAGCCGAGGATA	
Smc00074-C-KpnI-fwd	ATATGGTACCTTTCCCTCGTATACCAGCCCA	Construction of **pG18mob2-*gdcP*-3xFLAG**
gdpM1437-stop-r-Kpn	TTCCGGTACCTAGCGGATGCTCTTGCCGTCCTT	Generation of *gdpM*$_{\Delta LytM}$
mCh/egfp-Kpn-r	GTACGGTACCTTACTTGTACAGCTCGTCCATG	Construction of **pK18mobsacB-*gdcP*-EGFP/-mCherry**; amplification of 3' *gdcP* fused to *egfp*
smc00074-763-r-K_f	ATATGGTACCGGGCATCTGCCCCGTCAG	Construction of **pK18mobsacB-*gdcP*-EGFP/-mCherry**; amplification of *gdcP* downstream region
smc00074-763-r-S_r	ATATCCCGGGATGGCGAAAAACGTGCTG	
smc02432-C717-EcoRI-f	ATATGAATTCTTGGCAAGCAATGTCGACTT	Construction of **pK18mobsacB-*gdpM*-mCherry**; amplification of 3' *gdpM* fused to *mCherry*
smc02432-774-r-K_f	ATATGGTACCCCACACAGCAACGGTATCG	Construction of **pK18mobsacB-*gdpM*-mCherry**; amplification of *gdpM* downstream region
smc02432-774-r-S_r	ATATCCCGGGAGTACATGGAGAAGCATTCGGT	
SMc02432-326-HindIII_fwd	ATATAAGCTTGCGCGAGATCTCGATGCG	Construction of **pK19mob2ΩHMB-**

SMc02432-326-PstI_rev	ATATCTGCAGACGTCTGATGGTTGGCGG	***gdpM***
PT5-BamH-f	ATATGGATCCCATATGCTTTCGTCTTCACCTC	Construction of **pK18mob2-P*lac-T5*-*gdcP*** ; pWBT-*SMc00074* as PCR template
smc00074-N584-Hind_r	ATATAAGCTTACAGGGTGAAGGCGTTGA	
phoAEc+79-f-Xba	GTGTTCTAGACCTGTTCTGGAAAACCGGG	Amplification of $phoA_{Ec}(AA_{27-471})$
phoAEcstop-r-Kpn	TTCGGGTACCTTATTTCAGCCCCAGAGCGGC	
smc02432-full-N-f	ATATCATATGAGCAGCGATAAGAACATGC	Construction of **pSRKKm-*gdpM*$_{1-646}$-*phoA*** and **pSRKGm-*gdpM*-mCherry**; amplification of $gdpM(AA_{1-646})$
smc02432-C738-XbaI-f	ATATTCTAGACTTGCTTGCGACCTCGTT	
gdpM+198-r-Xba	GCCTCTAGACGGAATCGCCAGTTGCTGCCG	Construction of **pSRKKm-*gdpM*$_{1-66}$-*phoA*** ; amplification of $gdpM(AA_{1-66})$
gdpM+178-f-Nde	GCCTCATATGCGGCAGCAACTGGCGATTCCG	Construction of **pSRKKm-*gdpM*$_{60-646}$-*phoA*** ; amplification of $gdpM(AA_{60-646})$
Smc00074-seq-550	ACGCCTACAAGGATACCGTCA	$gdcP_{Sm}$ sequencing primer 1
Smc00074-seq-1146	ATCGTGCTCCTGATCGGC	$gdcP_{Sm}$ sequencing primer 2
Smc00074-seq-1780	ACAATGTCCTCATCGCGCT	$gdcP_{Sm}$ sequencing primer 3
smc03178-657	TCTTCGGCGACCCGGCAATCT	*SMc03178* sequencing primer 1
smc03178-1391	CGCTTCCTGGACCAGATTCT	*SMc03178* sequencing primer 2
smc02432_679	TTCTATGTCGACCCGCAAC	$gdpM_{Sm}$ sequencing primer
RHE_CH00976_seq-395	GAGCGAAGGCTTTGCGCT	$gdcP_{Re}$ sequencing primer 1
RHE_CH00976_seq-1141	CTGATCGGCTTCACCGTCAT	$gdcP_{Re}$ sequencing primer 2
RHE_CH03752_seq-361	AAGATGACGCTGGCCGCCAA	$gdpM_{Re}$ sequencing primer
Atu0784_seq-388	CAGCGCATCATCGCCATCA	$gdcP_{At}$ sequencing primer 1
Atu0784_seq-1141	GTGCTGATCGTGCTGCTGAT	$gdcP_{At}$ sequencing primer 2
Atu4178_seq-371	CTCACGTCAAGATTCCGCTG	$gdpM_{At}$ sequencing primer
PCR1	CGGGCCTCTTCGCTATT	standard sequencing primer 1
PCR2	TTAGCTCACTCATTAGG	standard sequencing primer 2
egfp_rev	ACTTCAGGGTCAGCTTGCCGTA	standard sequencing primer 3
405	GATCCGGCAAACAAACCACC	standard sequencing primer 4
456	CGCTCTCCTGAGTAGGACAAA	standard sequencing primer 5

Table S3. Co-immunoprecipitation revealed putative interaction partners of GdcP (SMc00074).

Accession	Description	Coverage	Unique Peptides	Peptides	PSMs	AAs	MW [kDa]
15964671	transmembrane signal peptide protein SMc00074	36.29	22	27	42	970	107.2
15966360	hypothetical protein SMc02432	54.64	18	22	25	646	69.7
15966480	hypothetical protein SMc00644	26.16	8	10	12	753	80.0
15964167	small heat shock protein	67.83	5	6	9	143	15.9
15965540;Q92PG9	30S ribosomal protein S4	36.59	5	5	9	205	23.5
15965409;Q92PS4	glucosamine--fructose-6-phosphate aminotransferase	23.36	5	8	14	608	65.8
15965119;Q92QG0	50S ribosomal protein L14	47.54	4	5	8	122	13.4
15965121;Q92QF8	50S ribosomal protein L5	32.43	4	4	8	185	20.9
2580515	citrate synthase	28.44	4	8	12	429	47.9
15965337	peptidyl-prolyl cis-trans isomerase B protein	38.46	3	4	5	169	18.6
15965395	signal peptide protein	33.01	3	5	6	209	22.5
15965248;Q92Q55	30S ribosomal protein S2	22.75	3	4	6	255	28.0
15965112;Q92QG7	50S ribosomal protein L2	22.66	3	3	8	278	30.4
15963759;Q92TE7	preprotein translocase subunit SecB	35.12	2	3	9	168	18.3
15965567	ferredoxin, 2FE-2S FDII electron transport iron-sulfur protein	30.19	2	2	2	106	11.4
15965311;P56898	single-stranded DNA-binding protein	26.44	2	3	5	174	19.0
15965105;Q92QH3	30S ribosomal protein S7	25.64	2	2	7	156	17.7
334320817	heat shock protein Hsp20	21.38	2	2	2	159	17.8
15965096	transcription antitermination protein NusG	37.50	1	3	4	176	19.9
15964367	translation initiation factor IF-1	30.56	1	1	1	72	8.3
15965730	dimethylamine corrinoid protein	25.00	1	2	2	232	25.5
15963996;Q92SW1	30S ribosomal protein S15	24.72	1	1	4	89	10.1
15966770	ABC transporter ATP-binding protein	24.72	1	4	4	356	39.7
8571395	NifU-like protein	23.81	1	1	1	63	6.7
334319033	electron transfer flavoprotein subunit alpha	23.46	1	7	8	567	59.4
384533786	hypothetical protein	22.61	1	2	2	261	29.3
8133104	NADP-dependent isocitrate dehydrogenase	21.78	1	4	4	404	45.2
15963984;Q92SX1	hypothetical protein SMc02906	21.50	1	1	2	107	11.6

Cell lysate of exponentially growing Rm2011 GdcP-FLAG liquid culture was cross-linked with 0.1 % formaldehyde for 15 min and applied to anti-FLAG antibody-coupled agarose. Enriched proteins were identified by mass spectrometry. Identified proteins for Rm2011 harboring the empty vector pWBT were removed from the obtained list of candidate interaction partners. MW, molecular weight.

Table S4. Co-immunoprecipitation revealed putative interaction partners of GdpM (SMc02432).

Accession	Description	Coverage	Unique Peptides	Peptides	PSMs	AAs	MW [kDa]
NP_386713.1	hypothetical protein SMc02432	57.28	23	23	62	646	69.7
NP_385024.1	transmembrane signal peptide protein SMc00074	17.11	11	11	11	970	107.2
NP_386833.1	hypothetical protein SMc00644	31.08	11	11	11	753	80.0
NP_385532.1	hypothetical protein SMc01011	15.41	4	4	4	331	34.8
NP_385748.1	signal peptide protein SMc00950	11.48	2	2	2	209	22.5
NP_385925.1	ubiquinol-cytochrome C reductase iron-sulfur subunit protein	7.81	1	1	1	192	20.5
YP_002122333.1	molecular chaperone GroES (plasmid)	15.38	1	1	1	104	11.4
NP_385964.1	hypothetical protein SMc00150	0.95	1	1	1	631	69.5
NP_387388.1	hypothetical protein SMc03899	30.12	1	1	1	83	9.8
NP_435918.1	NapC membrane-bound tetraheme cytochrome c subunit (plasmid)	10.73	1	1	1	233	26.1
NP_384173.1	ATP-dependent helicase	4.76	1	1	1	820	88.5
NP_435823.1	hypothetical protein SMa1065 (plasmid)	8.02	1	1	1	262	27.9
NP_437769.1	hypothetical protein SM_b21402 (plasmid)	11.63	1	1	2	387	39.1
NP_386896.1	hypothetical protein SMc04006	7.59	1	1	1	145	16.0
NP_386684.1	hypothetical protein SMc02351	18.06	1	1	1	155	17.1
NP_385170.1	DNA-directed RNA polymerase subunit omega	29.63	1	1	1	135	14.9
NP_386284.1	UDP-N-acetylmuramoyl-L-alanyl-D-glutamate synthetase	6.91	1	1	2	463	48.0

Cell lysate of exponentially growing Rm2011 GdpM-FLAG liquid culture was cross-linked with 0.1 % formaldehyde for 15 min and applied to anti-FLAG antibody-coupled agarose. Enriched proteins were identified by mass spectrometry. Identified proteins for Rm2011 harboring the empty vector pWBT were removed from the obtained list of candidate interaction partners. MW, molecular weight.

REFERENCES

1. Casse F, Boucher C, Julliot J, Michel M, Dénarié J. 1979. Identification and characterization of large plasmids in *Rhizobium meliloti* using agarose gel electrophoresis. Microbiology 113:229-242.
2. Döhlemann J, Wagner M, Happel C, Carillo M, Sobetzko P, Erb TJ, Thanbichler M, Becker A. 2017. A family of single copy repABC-type shuttle vectors stably maintained in the alpha-proteobacterium *Sinorhizobium meliloti*. ACS Synth Biol 6:968-984.
3. Firczuk M, Mucha A, Bochtler M. 2005. Crystal structures of active LytM. J Mol Biol 354:578-90.
4. Grant SG, Jessee J, Bloom FR, Hanahan D. 1990. Differential plasmid rescue from transgenic mouse DNAs into *Escherichia coli* methylation-restriction mutants. Proc Natl Acad Sci U S A 87:4645-4649.
5. Hamilton RH, Fall MZ. 1971. The loss of tumor-initiating ability in *Agrobacterium tumefaciens* by incubation at high temperature. Experientia 27:229-230.
6. Khan SR, Gaines J, Roop RM, Farrand SK. 2008. Broad-host-range expression vectors with tightly regulated promoters and their use to examine the influence of TraR and TraM expression on Ti plasmid quorum sensing. Appl Environ Microbiol 74:5053-5062.
7. Luo L, Yao SY, Becker A, Rüberg S, Yu GQ, Zhu JB, Cheng HP**.** 2005. Two new *Sinorhizobium meliloti* LysR-type transcriptional regulators required for nodulation. J Bacteriol 187:4562-4572.
8. Möll A, Schlimpert S, Briegel A, Jensen GJ, Thanbichler M. 2010. DipM, a new factor required for peptidoglycan remodelling during cell division in *Caulobacter crescentus*. Mol Microbiol 77:90-107.
9. Odintsov SG, Sabala I, Marcyjaniak M, Bochtler M. 2004. Latent LytM at 1.3A resolution. J Mol Biol 335:775-85.
10. Quinto C, De La Vega H, Flores M, Leemans J, Cevallos MA, Pardo MA, Azpiroz R, De Lourdes Girard M, Calva E, Palacios R. 1985. Nitrogenase reductase: a functional multigene family in *Rhizobium phaseoli*. Proc Natl Acad Sci U S A 82:1170-1174.
11. Römling U, Galperin MY, Gomelsky M. 2013. Cyclic di-GMP: the first 25 years of a universal bacterial second messenger. Microbiol Mol Biol Rev 77:1-52.
12. Schäfer A, Tauch A, Jäger W, Kalinowski J, Thierbach G, Pühler A. 1994. Small mobilizable multi-purpose cloning vectors derived from the *Escherichia coli* plasmids pK18 and pK19: selection of defined deletions in the chromosome of *Corynebacterium glutamicum*. Gene 145:69-73.
13. Schäper S, Krol E, Skotnicka D, Kaever V, Hilker R, Søgaard-Andersen L, Becker A. 2016. Cyclic di-GMP regulates multiple cellular functions in the symbiotic alphaproteobacterium *Sinorhizobium meliloti*. J Bacteriol 198:521-35.
14. Schirmer F, Ehrt S, Hillen W. 1997. Expression, inducer spectrum, domain structure, and function of MopR, the regulator of phenol degradation in *Acinetobacter calcoaceticus* NCIB8250. J Bacteriol 179:1329-1336.
15. Schirmer T, Jenal U. 2009. Structural and mechanistic determinants of c-di-GMP signalling. Nat Rev Microbiol 7:724-35.
16. Simon R, Priefer U, Pühler A. 1983. A broad host range mobilization system for *in vivo* genetic engineering: transposon mutagenesis in gram- negative bacteria, 1:784-791, Nature Biotechnology.
17. Skotnicka D, Petters T, Heering J, Hoppert M, Kaever V, Søgaard-Andersen L. 2016a. Cyclic di-GMP regulates type IV pilus-dependent motility in *Myxococcus xanthus*. J Bacteriol 198:77-90.

18. Skotnicka D, Smaldone GT, Petters T, Trampari E, Liang J, Kaever V, Malone JG, Singer M, Søgaard-Andersen L. 2016b. A minimal threshold of c-di-GMP is essential for fruiting body formation and sporulation in *Myxococcus xanthus*. PLoS Genet 12:e1006080.
19. Spencer J, Murphy LM, Conners R, Sessions RB, Gamblin SJ. 2010. Crystal structure of the LasA virulence factor from *Pseudomonas aeruginosa*: substrate specificity and mechanism of M23 metallopeptidases. J Mol Biol 396:908-23.
20. Torres-Quesada O, Millán V, Nisa-Martínez R, Bardou F, Crespi M, Toro N, Jiménez-Zurdo JI. 2013. Independent activity of the homologous small regulatory RNAs AbcR1 and AbcR2 in the legume symbiont *Sinorhizobium meliloti.* PLoS One 8:e68147.
21. Uehara T, Dinh T, Bernhardt TG. 2009. LytM-domain factors are required for daughter cell separation and rapid ampicillin-induced lysis in *Escherichia coli*. J Bacteriol 191:5094-107.
22. Uehara T, Parzych KR, Dinh T, Bernhardt TG. 2010. Daughter cell separation is controlled by cytokinetic ring-activated cell wall hydrolysis. EMBO J 29:1412-22.

Danksagung

Mein ausdrücklicher Dank gilt Frau Prof. Dr. Anke Becker für die Vergabe des spannenden Projektes und die Betreuung meiner Dissertation. Neben dem wissenschaftlichen Diskurs habe ich im Speziellen die mir gewährte Freiheit zur Umsetzung eigener Ideen geschätzt, die mir bei meiner beruflichen Weiterentwicklung geholfen hat.

Mein aufrichtiger Dank gilt Dr. Elizaveta Krol, die mich seit Beginn meiner Arbeit mit Rat und Tat unterstützt hat. Im Weiteren bedanke ich mich bei den restlichen Mitgliedern der AG Becker für eine durchweg angenehme Arbeitsatmosphäre. Hervorheben möchte ich hierbei Dr. Matthew McIntosh für seine nützlichen Tipps im Labor, Dr. Egidio Lacanna für hilfreiche Diskussionen zum Thema c-di-GMP und Bettina Happel für die mehrfachen Hilfeleistungen bei organisatorischen Angelegenheiten. Darüber hinaus bedanke ich mich bei den Kooperationspartnern für die produktive Zusammenarbeit bei gemeinschaftlichen Projekten, insbesondere bei Dr. Dorota Skotnicka und Dr. Wieland Steinchen für ihr Engagement bei der praktischen Umsetzung.

Mein herzlicher Dank gilt meinen Eltern Helmut und Helga für den familiären Rückhalt. Zuletzt bedanke ich mich zutiefst bei meiner Freundin Alexandra für ihr Verständnis und ihren Beistand als meine fortwährende Motivationsstütze.

Eidesstattliche Erklärung

Hiermit versichere ich, dass ich die vorliegende Dissertation mit dem Titel

„Roles of the second messenger cyclic di-GMP in environmental adaptation of *Sinorhizobium meliloti*“

selbstständig verfasst, keine anderen als die im Text angegebenen Hilfsmittel verwendet und sämtliche Stellen, die im Wortlaut oder dem Sinn nach anderen Werken entnommen sind, mit Quellenangaben kenntlich gemacht habe.
Die Dissertation wurde in der jetzigen oder einer ähnlichen Form noch bei keiner anderen Hochschule eingereicht und hat noch keinen sonstigen Prüfungszwecken gedient.

Marburg, den 28.06.2017

_____

Simon Schäper